Experiments in thin film deposition:
Plasma-based fabrication of Carbon Nanotubes and Magnesium Diboride thin films

Dirk Coetsee

Submitted in fulfilment of the requirement for the degree of Master of Science in Engineering

Date: 20/12/2004
Supervisor: Mr. A.L.L Jarvis **Co-supervisor**: Prof. T.B. Doyle

As the candidate's Supervisor I have/have not approved this thesis/dissertation for submission

Signature: **Name:** A.L.L. Jarvis **Date:** 5th April 2005

Acknowledgements

I am deeply indebted to a great many people without whom this work would have certainly been a dismal failure. On the technical side, I owe Tony Roos a thousand favours for the endless milling, turning, welding and machining he has done at short notice (not to mention for all the surfing tips...). Thanks must also go to Peter Siegling for all the glasswork. Divesh Maharaj and Gregory Moodley from electronic and chemistry stores have also done me innumerable favours by supplying me with the necessary equipment and chemicals to make things work. Chris van der Merwe and Mike Witcomb are also duly thanked for all the work they put into helping me with SEM and TEM use in the analysis stage of this project. And of course, I really do owe my supervisor, who for some reason let me often have my way in the course of this work and suffered the consequences...

As clichéd as it may be, my mother deserves a most special thank-you for tirelessly putting up with me (and feeding me) all this time. And of course, above all I thank God, truly. In the end, He bailed me out of trouble yet again.

One last thank-you to Goku, Gohan, Cloud and Yakumo Fujii for their incredible inspiration and determination. When the going gets tough, they grind the axe. When all is lost, they rise again.

The contribution of the National Research Foundation is gratefully acknowledged.

Abstract

A simple, low-cost plasma reactor was developed for the purpose of carrying out thin film deposition experiments. The reactor is based largely on the Atmospheric Pressure Nonequilibrium Plasma (APNEP) design with a simple modification. It was used in an attempt to fabricate magnesium diboride thin films via a novel, but unsuccessful CVD process where plasma etching provides a precursor boron flux. Carbon nanotubes were successfully synthesised with the apparatus using a plasma-based variation of the floating catalyst or vapour phase growth method. The affect of various parameters and chemicals on the quality of nanotube production was assessed.

Table of Contents

Table of Figures

1 Introduction

The work described in this dissertation is the product of a desire to grow high quality superconducting thin films of Magnesium Diboride (MgB_2). Simple in structure and both easy and cheap to obtain, Magnesium Diboride offers a good compromise between the complex, difficult-to-work-with high-Tc superconductors, and the simple, but difficult-to-cool low temperature superconductors. Not constrained by the weak-link effect and boasting a high critical temperature of 39K, MgB_2 shows much promise for application in the realm of superconducting magnets, wires and electronics. To date, however, only one method has succeeded in fabricating high quality epitaxial thin-films of this material. But this method requires the use of expensive and dangerous diborane gas. A search for alternatives to diborane as a boron flux precursor led to the development of a new method for the chemical vapour deposition (CVD) of MgB_2 thin films. The new method required the simultaneous development of plasma reactor for the purpose of etching boron. This dissertation describes the development of this plasma reactor, which is a modification of the Atmospheric Pressure Nonequilibrium Plasma (APNEP) design. It also describes the rationale behind and development of the new CVD method - which ultimately failed in producing the desired thin films.

The reactor built is quite versatile, however, and to this end it was used in the fabrication of carbon nanotubes via the floating catalyst approach. The remainder of the dissertation is devoted to a discussion of the nanotube synthesis method with a thorough analysis of the results obtained. It was found that hydrogen support gas was essential for good nanotube growth. In addition, a low concentration of ethanol as a carbon precursor did seem to be beneficial for creating a clean product, while the addition of thiophene seemed to have the effect of creating better uniformity in nanotube diameter.

2 Magnesium Diboride Thin Films

2.1 Introduction

Superconductivity has been an exciting area of research since the phenomenon was first discovered by Heike Kamerlingh Onnes in 1911. To this very day, almost a century later, new literature is constantly being published on both the theory and application of superconductors. Certain questions over theoretical aspects of the fundamental mechanism of superconductivity, specifically high temperature superconductors, remain unanswered after all this time. One exciting area of development is in the realm of superconducting electronics. Although certain more recent ideas such as quantum and biological computing are giving superconducting electronics stiff competition on the 'next big computing technology' front, it remains uniquely useful in certain niche applications.

In order for superconducting electronics to work and work well, thin films of superconducting material need to be manufactured to high standards. This is similar to how the semiconductor electronics industry could not progress well until high quality silicon wafers were fabricated. A major part of the work conducted in this dissertation involved an attempt to find a low-cost method of fabricating high quality Magnesium Diboride (MgB_2) thin films for this purpose.

Magnesium Diboride (MgB_2) was chosen for its unique compromise between simplicity of structure and superconducting critical temperature (T_c). In addition, at the start of this project it had only recently been discovered that MgB_2 was in fact a superconductor at the relatively warm temperature of 39 K (Nagamatsu et al., 2001) and thus there was considerable scope for novel research in this area.

This review seeks to provide an overview of Magnesium Diboride thin film fabrication methods with an explanation of how our own research fits in. To this end, it does not aim to be comprehensive in its assessment of superconductivity or superconducting applications as a whole.

2.2 Superconductivity

Superconductivity is a state of matter characterized by truly zero dc resistance. In addition, superconductors expel flux from their centres via the Meissner-Ochsenfeld effect. Superconductivity occurs in many compounds, including organic ones, but only when the sample is cooled to temperatures below a certain threshold called the critical temperature (*Tc*). In addition, once a sample is superconducting, the state may be destroyed by application of a current that is too high (the critical current) or an applied field that exceeds some minimum (the critical field). Both the critical current and field are functions of temperature.

A more interesting property of superconductivity is that it is a macroscopic manifestation of a quantum phenomenon. On a quantum level, electrons and phonons interact in such a way that electrons can pass through the sample unhindered. The electrons form into pairs which can all be described by a single wavefunction. This truly remarkable phenomenon is best described to date by the Bardeen-Cooper-Schrieffer (BCS) theory. BCS theory will not be covered in this dissertation. Although this theory does not seem to apply to all superconductors – most notably not those with particularly high *Tc*'s - it remains a monumental work in the description of this state.

Most conventional superconductors require very low temperatures to work. Pure elements need to be cooled typically to less than 10 K – sometimes less than 1 K. High Temperature

superconductors, which are copper oxide ceramics (often called cuprates), fare a little better and several will superconduct when cooled down to liquid nitrogen temperatures, making them far easier to use.

Quite obviously, the ability to carry current without resistance (at least for dc) is highly desirable in many power applications. Superconductors can allow for a 70% reduction in motor size while even gaining one or two percent in efficiency (Bretz, 2004). They could potentially save billions in losses for power supply companies. Furthermore, some superconductors are capable of carrying exceedingly high currents in high fields making them very useful for creating super-magnets. Superconductors have not, however, found expansive use in the mainstream particularly because of their need for such cold temperatures and expense in their fabrication and maintenance. However, they are an essential part of many high power magnets, some modern motors, MRI machines, and many niche applications.

Among the niche applications is the development of superconducting electronic devices. These are based on weak-links, called Josephson Junctions. They are the equivalent of the transistor in the superconducting world. Superconducting Quantum Interference Devices (SQUIDS), comprised of a pair of Josephson Junctions and a superconducting ring, are a class of superconducting electronic components that can be used to make the world's most sensitive detectors of magnetic flux. Superconducting electronics also holds the potential to make the world's most accurate A/D and D/A converters and electronic integrated circuits that are orders of magnitude faster than competing silicon solutions. In order for any of these applications to see more widespread use, it is important to find a superconductor that is easily useable at readily reachable temperatures.

2.3 Magnesium Diboride

2.3.1 Introduction

Though the intermetallic compound MgB_2 has been studied and used since the 1950's, it was only in 2001 that researchers discovered the compound was also a superconductor (Nagamatsu et al., 2001). In the three years since that original paper appeared, it has received a staggering number of citations as researchers around the world furiously worked to uncover the secrets of this compound. Interest in the superconductor was so high, in fact, that two months after the initial announcement, the American Physical Society arranged a special evening session for 1-minute announcements on progress in MgB_2 work. The session lasted till 1 a.m. High Tc Update, an internet source of information on high Tc superconductors, even added a special section just for this material (http://www.iitap.iastate.edu/htcu/39K.html). The frantic pace of that initial research has calmed down more recently, but interest in the properties of this superconductor and its application in the real world remain very high.

Initial interest revolved around the fact that MgB_2 transitions to a superconducting state at a very high temperature of 39K to 41K. This is very surprising for a simple, intermetallic compound where previous conventional superconducting record-holders had a *Tc* of only around 33K (Akimitsu and Muranaka, 2003). In addition, this *Tc* is at or beyond the theoretical limit for *Tc* predicted by the BCS model (reported as around 40K in Buzea and Yamashita, 2001). Immediately the race was on to find out if MgB_2 is an extreme form of BCS (phonon-mediated) superconductor, or if the mechanism for superconductivity were more exotic as in high-*Tc* cuprates.

Very early research on the subject seemed to suggest MgB_2 may well be an example of traditional phonon mediated or BCS superconductivity (e.g. Zhao, G., 2002; Bud'ko et al., 2001). Changing the isotope of Boron used in samples of MgB_2 to the lighter variant (B_{10}) would cause *Tc* to shift up by 1K. This so-called Isotope effect suggests the BCS mechanism is responsible for superconductivity in MgB_2. A very good review of the early work on this subject

has been written by Nguyen and Doan (2004) and Akimitsu and Muranaka (2003). It is generally accepted at this point, however, that MgB_2 superconductivity is a special case of phonon-mediated (BCS) superconductivity and that it actually possesses two energy gaps (Souma et al., 2004; Tajima et al., 2003).

In addition to the theoretical interest that the compound has generated due to the mystery of its high *Tc*, MgB_2 was considered extremely promising for various applications. This was primarily because it served as a happy medium between the low *Tc* BCS superconductors such as Niobium, and the high *Tc* cuprates such as Yttrium Barium Copper Oxide ($YBa_2Cu_3O_{7-delta}$). While low *Tc* materials are cheap and easy to work with, they typically need to be cooled with liquid Helium which makes them expensive and difficult to use in the real world. On the other hand, high *Tc* cuprates will superconduct when simply immersed in liquid nitrogen, but are complex, generally with poor mechanical properties (they are ceramics), and require the addition of expensive silver or complex texturing to overcome the weak-link effect when forming wires, tapes and so forth. In addition, although such materials are superconducting at liquid nitrogen temperatures, they typically need to be cooled to much lower temperatures to carry high enough currents and tolerate high enough fields to be very useful.

Enter MgB_2. Here is a compound that is simple in structure, cheap and easily available. In addition it has a *Tc* that is easily reachable by modern cryo-refrigerators. It furthermore exhibits no weak-link effect at its grain boundaries, has a reasonably large coherence length (especially compared to high *Tc* superconductors), and a high critical current (Buzea and Yamashita, 2001). The advantages of the material will be considered more fully in the next section. The main point is that MgB_2 has a host of advantages associated with it, and can be used at relatively accessible temperatures. It is a happy medium between low *Tc* and high *Tc* worlds with great promise. Thus from a theoretical and commercial perspective, MgB_2 is still a very hot topic.

2.3.2 Structure and Properties

This overview points out only the most basic and important properties of MgB_2 while the bulk of this review will concentrate primarily on thin film fabrication. For a very comprehensive review of the properties of MgB_2, the reader is encouraged to read Buzea and Yamashita (2001). Canfield and Bud'ko (2001) also provides a very accessible and interesting introduction to this material.

Magnesium Diboride consists of Boron layers having the honeycomb-like structure of graphite separated by hexagonal close-packed layers of magnesium. This is shown in the image below

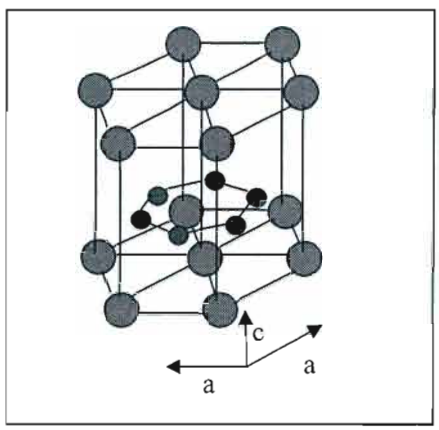

Figure 2-1: Hexagonal, graphite-like layers of Boron (small molecules) sandwiched between HCP magnesium.

This is commonly referred to as the AlB_2-type structure (Buzea and Yamashita, 2001).

Apart from its superconductivity at low temperature, MgB_2 is also a very good conductor of electricity. At 300 K the resistivity is only 9 to 10 μΩ.cm (Rowell, 2001). Other values reported are between 5 and 10 μΩ.cm for bulk samples at 300 K (Rowell et al., 2003). This resistivity drops with temperature readily to less than 1 μΩ.cm at 40 K. It is found also that resistivity can increase by an order of magnitude in certain polycrystalline samples – particularly many thin films – even though these samples will still have a good *Tc*. It is believed that this is because many MgB_2 samples either do not have densely packed grains, or the grains are insulated by impurities such as MgO (not fully connected) (Rowell et al., 2003). This leads to there being less total current-carrying area available for use. It also provides some degree of pinning and as such, thin films of MgB_2 typically have a higher upper critical field.

Grains boundaries do not appear to form weak-links[1] in MgB_2 giving it a major advantage over high *Tc* superconductors. In fact, so good is this property in MgB_2, that it is possible to prepare wires simply by densely packing MgB_2 powder into a tube, without any annealing or heat treatment whatsoever (Kumakura et al., 2001). This is very important from an economical standpoint and also theoretically quite interesting. The lack of weak links at boundaries makes MgB_2 highly promising for electronics applications as well.

MgB_2 is a Type-II superconductor which is characterised by two critical field limits. Thus, if a magnetic field is applied to it, at some point (critical field I or Hc_1) the magnetic field will penetrate it, but it will still be able to superconduct (except for within vortex regions where the magnetic flux penetrates). If the field is further increased, at the second critical field (Hc_2), superconductivity will cease. This means that it can potentially be used in applications that require a high magnetic field such as superconducting magnets.

In terms of superconducting properties, MgB_2 shows a wide variance of such parameters as critical current (Jc), critical field (Hc), critical temperature (*Tc*), coherence length and so forth in the literature. The differences stem from subtle variations in sample preparation and are strongly influenced by crystallinity and level of impurities. For example, in the thin film review later in this chapter, it shall be seen that slight loss of magnesium content or incorporation of oxygen impurities will rapidly diminish *Tc*. In addition, MgB_2 shows anisotropy in most of its properties although the degree of anisotropy is much less than for high *Tc* superconductors.

$Hc_2^{\parallel}$ (upper critical field for c plane orientation) values vary from 2.5 T to 36 T. The upper value is for 5% carbon doped MgB_2 thin films (AMES, 2004). Critical field of bulk, undoped samples tends to be lower (about 16 T). In fact, alloying of thin films (by systematic carbon doping) has produced MgB_2 films that show an $Hc_2^{\parallel}$ of 51 T at 4.2 K - an incredibly good value. Extrapolated to 0K, this would mean an $Hc_2^{\parallel}$ of 70 T which is a considerable improvement (Braccini et al., 2001) over the undoped sample. In general, thin film values tend to be higher than those in bulk samples with highly epitaxial, highly crystalline, low impurity film having an $Hc_2^{\parallel}$ of 29.2 T at zero field (Zeng et al., 2002).

Doping tends to diminish *Tc* by several Kelvin but is a necessary trade-off to make MgB_2 useful for wire and motor applications. Doping here referring to the systematic addition of impurities to create vortex pinning sites (by pinning the sites at which flux penetrates a Type-II superconductor, it is able to maintain its superconducting properties to higher applied magnetic fields).

---

[1] A weak link arises when two pieces of superconductor are separated by a physically small region. These are also called Josephson Junctions

This doubling or even tripling of Hc values by systematic doping is an important area of current research as it allows MgB_2 to become truly useful for cable, motor, and other power applications. In fact, MgB_2 wire can be made that exceeds the upper critical field of mainstay low *Tc* competitors like NbTi and Nb_3Sn at all temperatures (Madison, 2003). This is in addition to the fact that MgB_2 can be cooled using cheaper liquid Hydrogen or liquid Neon refrigerant (cheaper compared to liquid He required for many low *Tc* competitors). Furthermore, MgB_2 is cheaper to produce in wire form than its Niobium alloy competitors (Azom, 2003). Of course, for such applications, Hc_2 alone is not the last word on absolute usefulness of the material. But the fact that this parameter has been notably improved to competitive levels so soon after the inception of MgB_2 research is a promising development. It seems as if MgB_2 will certainly be very promising in magnetic applications such as MRI which could make MRI machines more affordable.

The low resistivity of MgB_2 is also an advantage for the production of wires. If at some stage a small part of the wire does become normal for whatever reason, it will not ohmically heat excessively causing a cascade failure of the whole wire. This is a problem especially associated with high temperature superconductors which are terrible conductors at room temperature.

Critical current is equally important in determining how useful MgB_2 can be for power applications. Early Jc values for MgB_2 were quite low at even modest values of applied field. This was considered a problem since it would fall off very quickly as field increased. Under self-field, Jc values are reasonably good on the order of 10^5 A/cm^2 (Canfield and Budko, 2001). However, by 2 T the value will have already decreased by at least an order of magnitude or even more depending on the temperature, form, and method of preparation. The value continues to fall off almost logarithmically. By contrast, competitors such as Nb_3Sn maintain their Jc's quite well in increasing field and start off with values above those of MgB_2. In spite of this, the higher operating temperature of MgB_2 makes it promising even compared to its higher Jc competitors. Doping has already allowed for considerable improvement in such properties. Notably, Wang et al. (2004) managed to improve self-field Jc to 1 MA/cm^2 for temperatures under 10 K in MgB_2/Cu tapes. There is much work to be done in this area, but the rate of improvement is quite rapid.

Coherence length[2] values vary a great deal in the literature: typically between 3.7 and 12.8 nm in the ab-plane and 1.6 and 5nm in the c plane (Buzea and Yamashita, 2001). This is long enough again that the grain boundaries do not form weak-links. There is no foreseeable barrier seen in making high quality superconducting circuits from MgB_2. These would not only operate at higher temperatures than the current Niobium standard, but at potentially higher speeds due to the large product of the critical current and normal resistance (Burnell et al., 2001). Although $YBa_2Cu_3O_{7\text{-delta}}$ (a typical high temperature superconductor) circuitry could operate at still warmer temperatures, the weak-link effect in that material complicates sample preparation substantially. In addition, MgB_2 has less anisotropy and a better coherence length than such materials (Malisa et al., 2004). Although Josephson Junctions and even SQUIDs have indeed been made from this material, the process is still in its infancy (e.g. Malisa et al., 2004; Tao et al., 2003).

It is interesting to note how systematic doping of films can radically improve MgB_2's basic properties. This is an important property of MgB_2 since it could not compete in terms of current carrying capability and magnetic field tolerance otherwise. As it stands, most authors agree that MgB_2 holds considerable promise insofar as it should allow for lower cost superconducting wire

[2] Coherence length is a fundamental characteristic of a superconducting material. Its definition is complex without a more thorough grounding in superconductivity, but essentially it can be considered as a measure of the scale over which variation of the level of superconductivity occurs. It relates fundamentally to the pairing of the electrons in the sample, mentioned earlier in this chapter.

and tape that is cheaper to cool. Likewise, it should provide for more accessible, faster superconducting electronics.

Our group was originally interested in MgB_2 for the purpose of electronics. To this end, high quality thin films would be needed. The following review focuses on how thin film fabrication is accomplished for this compound.

2.4 Thin Films

Thin film fabrication in MgB_2 has proved more difficult than many may have originally anticipated. In fact, only two methods thus far have succeded in growing high quality epitaxial films (Zeng et al., 2002; Bu et al., 2002). The problem is primarily due to the very high vapour pressure of magnesium relative to the very low vapour pressure of boron. In addition, it was found that magnesium and indeed Boron would readily react with oxygen creating impurities. This section provides an overview of the various methods that have been used to fabricate MgB_2 thin films over the past three years with an assessment of the relative merits of each. This assessment leads to the development of a new method for thin film fabrication that can overcome some of the obstacles observed. A truly excellent, lengthy review has recently appeared in the literature (Naito and Ueda, 2004) and the reader is highly encouraged to start any further reading on the subject there.

2.4.1 Types of methods

All methods for MgB_2 thin film deposition fall under one of five categories (Brinkman et al., 2003): (1) *in situ* deposition of Boron films followed by an *ex situ* anneal in Mg vapour; (2) *in situ* deposition of Mg-B (non-superconducting) films followed by a *ex situ* anneal in Mg vapour; (3) *in situ* annealing of Mg-B films; (4) *in situ* anneal of multilayer (alternating B and Mg) films; (5) *in situ* deposition with no anneal.

It is simpler, however, to class MgB_2 film deposition into one of two groups: one-step and two-step. Two-step methods include an annealing at one of the stages, which may be performed either *in situ* or *ex situ*. One problem with two-step methods is that for superconducting electronics (the primary future application of such thin film technology), multilayer films are highly desirable and an extra annealing step could ruin previously deposited layers and any electronics they may contain.

In assessing the merits of any particular method, we must consider not only the quality of its superconducting properties (high *Tc*, good *Hc*, *Jc* etc.) but also its physical properties: surface smoothness, grain connectivity, grain alignment, crystallinity and degree of epitaxy. In addition, the process by which a film is formed will dictate how useful it is in many applications.

The similarity of several of these methods is underpinned by the fact that Boron, when annealed in an Mg-rich environment, will readily absorb Mg to form MgB_2. This fact has been used to produce MgB_2 wires simply by annealing readily available boron fibres (Canfield et al., 2001) and gives a convenient route to MgB_2 thin film synthesis. It is much simpler to deposit a high quality Boron layer (or Mg-B, non-superconducting composite layer), by whatever means, and then simply convert it to MgB_2. The annealing process involves taking the Boron (or Mg-B) coated sample and encapsulating it in some refractory container (such as quartz or tantalum) together with some pure magnesium. Sufficient magnesium needs to be enclosed such that the vapour pressure of Mg remains high enough for the correct phase to form. The enclosure is heated typically at temperatures between 600°C and 900°C for 10 to 60 minutes (Ueda and Naito, 2002). Films prepared in this manner tend to have good superconducting properties on a par with bulk samples, but surface quality is often reduced in the annealing step (Brinkman et

al., 2003) leading to more surface roughness. In this regard, films that are formed by annealing an Mg-B composite layer fare a little better.

One-step methods (no *ex situ* annealing) would be advantageous from an economic standpoint, and particularly for multilayer electronics work. But films thus made typically have poor superconducting properties. This is most commonly as a result of Mg deficiency due to the volatility problem mentioned earlier. Oxygen contamination is also rife in the literature with virtually all films reported containing some degree of MgO contamination.

The standard methods used to fabricate thin films of MgB_2 are: Pulsed Laser Deposition (PLD), electron beam evaporation, thermal evaporation, sputtering, chemical vapour deposition, and molecular beam epitaxy (MBE). Some other methods such as ion beam implantation (Peng et al., 2003) and electrochemical synthesis (Pawar et al., 2002) have also been used. Of these, PLD, e-beam evaporation, thermal evaporation and sputtering are rather similar in their approaches and can be grouped under the category of physical vapour deposition (PVD). In these processes, atoms of the relevant species are removed from a solid, bulk precursor (either from one MgB_2 source or from two sources, one of Mg and one of B) into the vapour phase. Such atoms then move to a substrate where they ultimately combine (if necessary) with other elements, condense, nucleate and grow into a solid film. The actual physics of thin film deposition is reasonably complex and will not be covered in this dissertation. For an excellent source encompassing most modern methods, the reader is referred to Bunshah (1994).

2.4.2 Pulsed Laser Deposition (PLD)

Briefly, PLD involves striking a solid target with a high energy laser beam such that atoms near the surface of the solid evaporate. It is possible to tune the laser frequency to make it interact better with the relevant material, but in many cases (and certainly with MgB_2), UV frequency light is used.

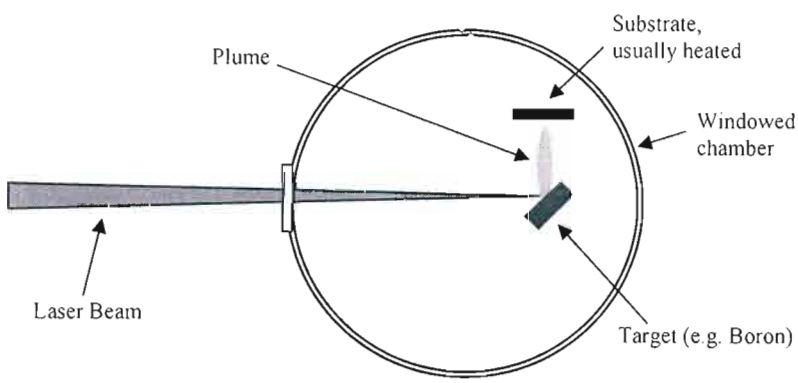

Figure 2-2: Basic PLD apparatus.

This has made excimer lasers extremely popular for the purpose. The light is focused into intense, short bursts to provide sufficient energy to cause ablation. A typical laser employed in MgB_2 deposition may have a wavelength of 248 nm, a pulse duration of 25 ns, and a repetition

rate of about 50Hz corresponding to 650 mJ per pulse (Mijatovic, 2004). An important fact is that at such short wavelengths, with such short pulses, penetration remains very close to the surface – on the order of 100 nm deep (Venkatesan and Green, 1996). Thus an intense amount of energy causes these atomic layers to vaporise with intense heat (several thousand K) assuring that all elements present are vaporised simultaneously. This causes rapid expansion of the vaporisation product into a visible, plasma plume, containing ions and electrons as well as simply atoms. Though conceptually simple, the physics of PLD is quite complex.

PLD was very popular in early MgB_2 thin film research (Wang et al., 2001; Ferdeghini et al., 2001; Berenov et al., 2001; Kang et al., 2001a). Perhaps this had to do with the fact that PLD had become an indispensably useful tool in the fabrication of complex High-*Tc* cuprates like YBCO. This popularity followed the discovery by Venkatesan and colleagues that using an excimer laser to evaporate matter from a bulk sample resulted in a nonequilibrium evaporation (Dijkkamp et al., 1987). That is to say, atoms at the target surface would all evaporate simultaneously when struck by an excimer laser. This as opposed to elements evaporating at different rates according to their vapour pressures as would occur in a normal evaporation process. Although lasers had been used for the purpose of thin film deposition even earlier than this, this insight was a revelation. It was particularly useful at the time since it allowed complex materials made from many elements (such as YBCO) to be transferred from a bulk sample to a thin film essentially preserving structure and stochiometry.

However, this fortuitous ability of PLD processes did not carry much weight when it came to MgB_2. In spite of its very simple structure, the high volatility of Mg (due to its very high vapour pressure) means that attempting to transfer MgB_2 to a substrate in this way will result in Mg deficient samples. For this reason, many of the early works cited above made use of a two-step method. PLD was first used to deposit thin, non-superconducting films – Boron (Wang et al., 2001) or Mg-B in a non-superconducting phase (Ferdeghini et al., 2001; Berenov et al., 2001). These films were then annealed *ex situ* in Mg vapour to convert them to MgB_2 as described earlier. Some groups did also try *in situ* annealing (Zhao et al., 2003a; Zeng et al., 2001). And even one-step deposition was attempted (Grassano et al., 2001). Thus the work with PLD gave experimentalists and theorists alike much information in the early days of MgB_2 research.

Results were quite mixed. Even groups using the same method (e.g., two-step *ex situ* anneal) tended to produce samples with different characteristics. The following table summarises some important aspects of work done in PLD to this date. The critical field values reported are extrapolations to 0 K. Resistivity is reported for the sample just before transition.

Group	Method	*Tc*	Hc_2^{perp} (T)	$Hc_2^{\parallel}$ (T)	ρ (μΩ.cm)	*Jc* (A/cm^2)	Notes
Ferdeghini et al. 2001	Mg-B precursor layer annealed *ex situ*	31.4K	14.6	26.4	100	-	Samples showed good crystallinity and were largely c-oriented on MgO
Wang et al. 2001	B precursor layer annealed *ex situ*	38.6K and 38.1K	-	-	-	-	Good morphology with large grains on Al_2O_3 and MgO substrates
Berenov et al. 2001	Mg-B precursor annealed *ex situ*	29.2K – 34K	-	-		$3x10^4$ – $2.7x10^5$ @ 20K, 0T	O contamination, often Mg deficient. Several conditions attempted
Grassano et al. 2001	One-step, no anneal	25K	-	-	-	-	Significant O contamination, low deposition temperature
Zhao et al., 2003a	Mg-B precursor with *in situ* anneal	17-28K[3]	-	-	-	10^5 @ 5T, 5K	Large transition width, various annealing methods attempted
Zeng et al, 2001	Mg-B precursor with *in situ* anneal	32K				$1.34x10^6$ @ 7.5K, 0T	Small grain size, low temperature
Kang et al., 2001b	B precursor with *ex situ* anneal	39K	-	-	4.7 @290K	$6x10^6$ @ 5K, 0T	Very well oriented on MgO and Al_2O_3 substrates. 0.7K transition width. Excellent all-round

Table 2-1: Comparison of parameters for several PLD created thin films

The above table is by no means exhaustive, but is indicative of much that was learned in the early days of MgB_2 thin film deposition. The bulk of the work was accomplished via the two-step, *ex situ* anneal method. This method tended to give the highest quality samples with the best properties. Most notably, Kang et al. (2001b) showed early on that it was possible to create films in this way that had properties meeting or exceeding those of the best bulk samples. A short while later, the same group reported very highly oriented films grown on r-cut sapphire by the same method. The films had an onset *Tc* of 39.2K, a transition width of only 0.15K (smaller is better) and a 300K resistivity of 10.4 μΩcm. Jc was very high at 16 MA/cm^2 for 15K. In contrast to this, many groups using similar methodology obtained very poor results. The

[3] *Tc* values for Zhao et al., 2003a, are for onset only. Transition to superconducting state had a wide width (over 10K) and *Tc* offset was typically as low as 5 to 10K

primary problem, mentioned earlier, tended to be oxygen contamination. Even trace amounts of oxygen in the apparatus would show up, typically reducing *Tc*. Not only did Mg react readily with oxygen, but the Boron did as well. For this reason, purity of reactants and excellent vacuums became paramount.

It was confirmed in most of these early works that the grain boundaries were indeed not weak links. However, the substantial difference among many observed resistivity values was attributed to grain connectivity and possibly inter-grain impurities as mentioned earlier. This meant that making dense, highly oriented films was still very important.

Process parameters within the PLD apparatus also varied from group to group. It was found that, depending on pressure and gas (usually Argon) used within the chamber, the colour of the plume from an ablated MgB_2 target would change from green to blue. The superconducting phase would be formed with the blue plasma, not the green. It was thought early on that the green colour was indicative of oxygen contamination (Grassano et al., 2001). However, later this colour was attributed to the form of the magnesium in the plume (neutral Mg I being green and ionic Mg II being blue) (Mijatovic, 2004). The addition of Hydrogen (typically at 4%) to the chamber in addition to the usual argon also increased the range over which the blue plasma would form. Hydrogen is especially useful because of its ability to getter oxygen that would otherwise be present. Without hydrogen, UHV conditions (less than 10^{-9} torr) are typically necessary to prevent oxygen contamination from being a problem. Even so, oxygen contamination during annealing can frequently hamper results. An interesting side-effect of increased contamination, and suppressed *Tc*, is a greater flux-pinning effect resulting in high Hc values (Zhao et al. 2003b). This is already indicative of how the critical field of MgB_2 can be dramatically enhanced through careful doping.

Works that attempted *in situ* annealing and one-step synthesis invariably gave poor results. Here, not simply oxygen contamination, but Mg deficiency proved a great problem. Nevertheless, such processes remained important since they would be very useful in the field of superconducting electronics. Zhao et al. (2003a) carried out a study on *in situ* annealing conditions varying such parameters as rate of heating, duration of annealing and final temperature. They observed that the MgB_2 phase would form better if the film was heated at a lower temperature for a long time before using a higher temperature. They also observed that a higher ambient pressure during annealing was very important (since this would keep Mg vapor more confined to the surface). The trouble, of course, is that high temperatures are necessary for good crystallinity. However, as soon as temperature increases, Mg begins to vaporize at an ever increasing rate.

Mijatovic at al. (2002) attempted to overcome this problem by continuing to ablate the Mg target during annealing to create a high Mg flux. Their results still showed suppressed *Tc* which they attributed largely to oxygen contamination and small grain size. Annealing was still not nearly as thorough (due to low temperatures used) as in the *ex situ* approach and crystallinity was indeed very poor.

Another recent attempt to overcome this problem involved the use of a tri-layer system and optional metal cap (Uchiyama et al., 2004). By depositing first a layer of MgB_2 (non superconducting, yet to be annealed) then depositing on top of that a layer of Mg, and then a layer of B, a tri-layer system was formed. By making sure that the more volatile element (Mg) was capped with the element with the lower melting point (B), it was surmised that more of the Mg could be retained. Annealing was still carried out in the lower temperature regime (around 500-660°C). Annealing was also carried out at very low pressures (10^{-7} torr HV or 20 torr O_2 atmosphere) which was probably not advantageous. In spite of this, *Tc* was relatively good for *in situ* work at around 30K. Crystallinity was still somewhat predictably poor, however, due to low annealing temperatures. An inconel (Ni-Cr-Fe alloy) plate could be optionally added to cover the tri-layer system, further improving local Mg vapour pressure. The fact that annealing

in an O_2 atmosphere (20 torr) did not hamper results illustrated that the Boron cap did provide some shielding.

PLD continues to receive much attention. However, this review illustrates clearly that it is not a method which allows for optimal *in situ* or one-step deposition of MgB_2 films. PLD still has some advantages over certain other evaporation methods – most notably the wide range of process parameters over which it is useable and the large number of parameters that may be altered independently. Although good films could be made this way using *ex situ* annealing, it was left to other methods of thin film deposition to solve the one-step problem. Perhaps most importantly, early PLD work did show how sensitive MgB_2 deposition was to oxygen impurity levels and how even films with almost no crystallinity could achieve superconductivity – albeit with a reduced *Tc*.

2.4.3 Sputtering, e-beam evaporation and sublimation

Due to the fact that sputtering, e-beam evaporation and thermal evaporation are all really examples of PVD and thus largely similar in many ways to PLD, they are considered together. These methods vary primarily in the means by which the solid precursor is evaporated.

The most simple method involves resistive heating, leading to evaporation of the solid. MgB_2 (or Mg and B separately) would be loaded onto heaters of some description (typically molybdenum or tantalum boats) and heated to raise their vapour pressures. Ideally, the ambient pressure would be low enough that the solids would sublime and the dissociated atoms could have a long mean-free path. The atoms typically have a lobe-shaped evaporation profile, with the highest density of evaporant located directly above the source (Bunshah, 1994).

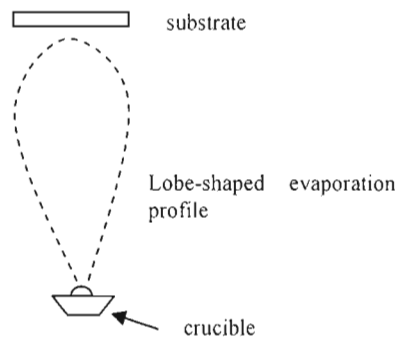

Figure 2-3: Resistive heating - the most simple form of PVD.

To this end, obtaining smooth films will often require some sort of complex motion imparted to the substrate holder (Bushnah, 1994). However, it is difficult to imagine a more simple means of deposition. Very soon after the announcement of MgB_2's superconductivity, Plecenik et al. (Plecenik et al., 2001) had already synthesized very high quality films using this simple method. A thin film of Boron, *ex situ* annealed in Mg vapour gave a film with a *Tc* of roughly 39K. It was also attempted to make films in this manner by simultaneous evaporation of Mg and B from two resistive heaters. Such films were then either *ex situ* annealed in an argon atmosphere, or *in situ* annealed in vacuum at low temperatures (around 600°C versus 800°C for the ex situ sample). The co-deposited films had better surface morphology, but at the expense of superconducting properties. Given the review of PLD work above, such results are predictable. Similar work was attempted by Paranthaman et al. (2001). Their *ex situ* anneal approach gave a similarly high *Tc* even though crystallinity was poor. In spite of the simplicity of these methods, they have not proved particularly popular in research.

Electron beam evaporation sources have the advantage of very high power density and wide range of control over evaporation rates (Bunshah, 1994). Electrons are accelerated at high kV (typically up to 40kV) to impinge on a crucible containing the substance to be evaporated. Electron guns can take many forms such as work accelerated (the target is on the anode) or self-accelerated (the electrons pass through the anode and are propelled towards the target). Good control over evaporation rates is advantageous in a process where the evaporation rates of the constituent materials is so different as in MgB_2. However, in light of the evidence above, there is no good reason to expect e-beam evaporation would fair particularly better than other process. It is certainly less costly than PLD in terms of startup costs, however. Indeed, early experiments by Moon et al. (2001) produced thin films comparable to the best of the PLD results using the standard two-step, ex-situ anneal starting with a Boron precursor layer. It was found that depositing Boron onto room temperature substrates gave superior results.

More recently, Shimakage et al. (2003, 2004) combined e-beam and thermal evaporation methods. The electron beam was used to evaporate the harder Boron with its very low vapour pressure, and resistive heating was used to simultaneously evaporate a pure magnesium source at an ambient pressure of about 10^{-5} Pa. The group found that by precisely varying the evaporation rate of the two materials and controlling the substrate temperature, it was in fact possible to deposit films that would superconduct with no need for further annealing. In fact, substrate temperature during deposition was kept under 300°C and yet it was still possible to obtain films with a *Tc* of 34.5K and a 0.9K transition width (a sharper transition width implies a better sample). This is quite remarkable considering the poor results of such processes in PLD experiments. Very good results were achieved at a substrate temperature of 290°C. At this temperature, the Mg would sublime since its vapour pressure would be well above the chamber base pressure. Thus there was no danger of Mg excess and so long as a sufficient B flux was maintained, MgB_2 would form. The films showed low crystallinity due to the low substrate temperature, and it was necessary to control evaporation rate with extreme precision (figures were quoted to within 0.1nm/s). Nevertheless, this is a promising route and makes considerable sense in terms of the thermodynamic considerations presented later in this review.

Sputtering is possibly the most complex of the methods in terms of the apparatus used. A very good description can be found in Rossnagel et al. (1990, ch. 6). Sputtering is essentially the process of bombarding a surface with highly energetic ions. Ions, created in a plasma or glow discharge, are accelerated by some or other means towards a target (in this case, the B, Mg, or MgB_2 precursor. Upon striking the target, the ions will dislodge atoms from its surface.

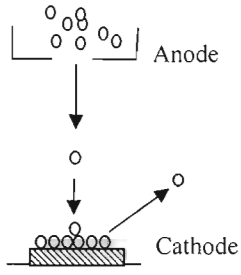

Figure 2-4: Basic sputter process. Ions (white) are accelerated towards a substrate on the cathode which dislodge surface atoms (grey).

To this end, sputtering is a somewhat different process from the other two, involving a momentum transfer. Nevertheless, the process does result in evaporation and can be used to produce very high quality films. Magnetron sputtering is a variation on the basic theme where magnetron plasma sources are used. Plasma sources will not be discussed in this review and the reader is once again referred to Rossnagel et al. In a magnetron source, the addition of magnets

in a particularly clever manner can enable higher density plasmas to be created by trapping electrons and causing them to circulate. This translates into higher deposition rates.

Sputtering is the method used by one of only two groups to report quality epitaxial growth (Bu et al., 2002). The method once again employed the typical two-step *ex situ* anneal with a pure Boron precursor layer. The group obtained truly epitaxial layers, with good characteristics. However, *Tc* was slightly suppressed (35K) due to slight impurities or defects. Magnetron Sputtering has also been the source of many attempts at an entirely *in situ* process (Lee et al., 2003; Ohkubo and Akinaga, 2004; Akinaga et al., 2003; Saito et al., 2002). Akinaga's group (Ohkubo and Akinaga, 2004; Akinaga et al., 2003) and Saito et al. (2002) succeeded in making superconducting MgB_2 films with no annealing whatsoever (one-step). Akinaga's group sputtered Mg targets containing small chunks of Boron. They managed to deposit onto substrates with the very low temperature of 100°C, while still producing superconducting MgB_2. In spite of this, the *Tc* was greatly suppressed and the films obviously of poor quality in terms of crystallinity. By contrast, Saito et al. used separate targets of Mg and B in a considerably more complex system. The Mg flux was maintained at around 400 nm/min and the B flux at around 6 nm/min. Using higher substrate temperatures of 200°C to 250°C, they managed to produce films with much better crystallinity and *Tc*'s up to 28K.

2.4.4 Chemical Vapour Deposition (CVD)

CVD varies from PVD primarily insofar as the precursors are introduced in the gas phase. By applying energy to the gas in some form (typically heating, or via plasma dissociation), the gas is caused to dissociate, yielding up the desired constituent. For example, diborane (B_2H_6) may be disassociated in the presence of heat to yield Boron and Hydrogen. The Boron atoms diffuse to the substrate surface where they adsorb, form nucleation sites, and ultimately grow into a thin film. The hydrogen by-product is pumped away.

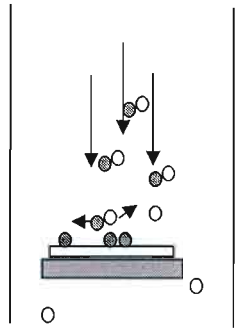

Figure 2-5: Basic CVD process. Molecules of an incoming gas stream are dissociated to yield up a desired product (represented by dark grey circles).

CVD is conceptually quite simple and in practice, relatively easy to implement. In addition, it provides for many control parameters (gas flow rate, pressure, temperature, method of dissociation, gas mix etc.) and has the ability to make an extremely pure product. It can take place at much higher pressure than many PVD processes (although low pressure is of course still quite possible) and it is not as dependent on line-of-sight path between source and substrate as is PVD. A very good reference on the basics and thermodynamics of CVD has been written by Pierson, H. (1999).

Little pure CVD work has been done in the realm of MgB_2 with the exception of hybrid physical-chemical vapour deposition, described later. Fu et al. (2002) and Wang et al. (2003) used Diborane (B_2H_6) gas to deposit Boron thin films via CVD. These films were then annealed as usual in the two-step *ex situ* anneal process. The films were of good quality (*Tc* of 37.5K, *Jc*

of 2.6 x 10^7 A/cm^2 in zero field at 15K), but not particularly notable in any way as compared to the bulk of the literature.

2.4.5 Molecular Beam Epitaxy (MBE)

MBE has become a very popular method of creating advanced epitaxial films in the semiconductor industry. In this method, 'beams' of molecules are directed onto a substrate resulting in layer-by-layer growth on an atomic scale. Typically, multiple molecular sources are used which can be shuttered on and off very quickly. This allows complex systems to be built up one atomic layer at a time. Multiple beams can be used simultaneously to grow compound materials.

Because the system used beams of molecules transported along a trajectory towards the substrate, it is imperative that pressures be extremely low (typically in the UHV range at under 10^{-9} torr) to allow for a good mean free path. The beam generators, known as effusion cells, typically make use of evaporated solids as in PVD, but their construction is rather complex. In fact, MBE is a highly complex and sophisticated method of thin film growth both in terms of the underlying physics and the apparatus used. In spite of this, the ability to grow thin films one atomic layer at a time with intricate control over molecular composition is invaluable. It is possible, for example, to precisely sandwich GaAs between AlAs layers providing multiple layers with different band gaps. A good introduction to the basics of MBE can be found in Rinaldi, 2002.

Applied to MgB_2, MBE has been marginally successful. Ueda and Naito (2001) created as-grown (*in situ* with no annealing) MgB_2 films very early on after the MgB_2 discovery. They found that superconducting films would only form for substrate temperatures between 150 and 320°C. They managed to obtain films with a *Tc* of 36K and a transition width of only 1K which is certainly very impressive for early as-grown work. Poor crystallinity was again the problem plaguing this method. In 2002, van Erven et al. succeeded in growing more highly crystalline films by this method. It was still necessary to use a lower substrate growth temperature than other methods employ (250°C) and very precise control over the relative B:Mg flux rates was required. That said, MBE is a method that excels in such precise control. They also noted that oxygen contamination was a big problem even with very high (10^{-10} torr) vacuums. Furthermore, the growth was not adsorption controlled, meaning that the amount of Mg incorporated into the films (relative to boron) was not automatically controlled as it is with certain semiconductor materials. Making the Mg flux too high would result in Mg rich films. Adsorption-controlled growth is considered more in the thermodynamic section below.

2.4.6 Other methods

Most of the work done in thin film deposition makes use of one of the methods described above, or the HPCVD method described later in this chapter. In addition, there have been sporadic attempts by certain groups to make MgB_2 using less mainstream approaches. Peng et al. (2003) directed a boron ion beam at a magnesium ribbon to implant boron ions in the magnesium surface. The superconducting state did form, but the quality was very poor. A group at Shivaji University in India (Jadhav and Pawar, 2003) managed to grow films via the exceedingly simple process of electrochemical deposition onto silver substrates. The films did require post annealing, but only at low temperature (300°C for 90 minutes). Films managed a *Tc* of 38.5K at best and were reasonably smooth. None of these more unique methods seem to have ever caught on in the community, however, and the bulk of thin film deposition work seems to be done by some form of PVD, or HPCVD which will be described shortly.

2.4.7 Thermodynamics of the MgB2 system.

Although Oxygen contamination is a great nuisance in film deposition, it is seen from the above review that across the board, magnesium volatility is the real problem. On the one hand, films need to be deposited at high temperature to ensure good crystallinity and adequate formation of the correct, superconducting phase. On the other hand, increasing the temperature universally results in Mg loss, unless it is done via *ex situ* anneal where it is possible to maintain a very high Mg vapour pressure by placing sufficient Mg in a sealed container. Very early on in MgB_2 thin film research, the problem was thoroughly treated by a group at Pennsylvania State University in several works (Xi et al., 2002; Liu et al., 2001). These papers have become fairly seminal in current thought on MgB_2 thin film deposition. In these works, the group calculated the phase diagrams of the MgB_2 system for various vapour pressures of Mg.

In the system, in addition to MgB_2, Mg (solid, liquid and vapour), solid Boron, MgB_7, and MgB_4 may exist at any one time. It would be desirous in forming MgB_2 films to keep temperature and pressure at such a level that only the MgB_2 and gas Mg phases are present. Within such a window, not only would MgB_2 be stable, but no excess Mg or B would form either. An example of a phase diagram is showed below.

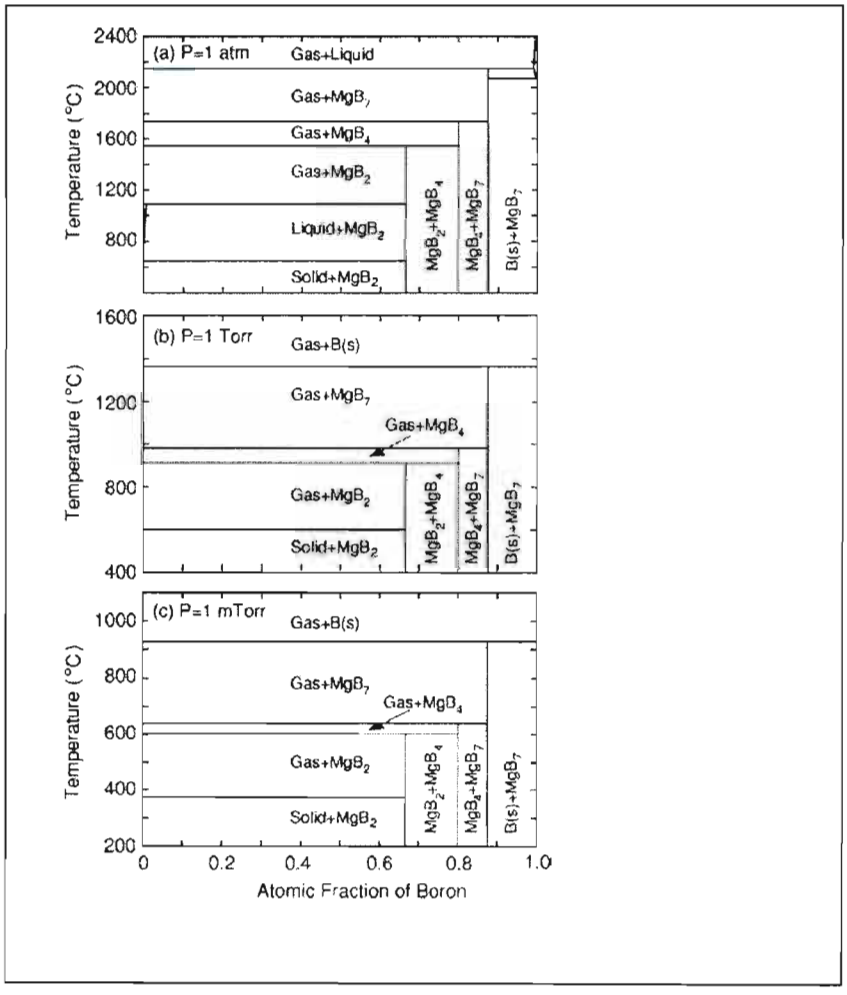

Figure 2-6: Phase diagrams of MgB2 system for different pressures (Liu et al., 2001).

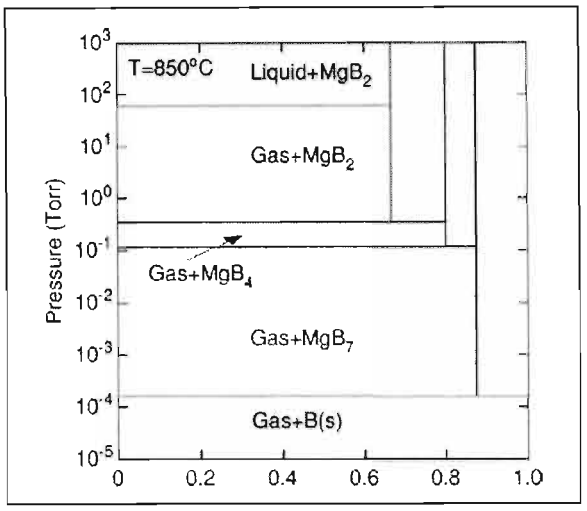

Figure 2-7: States of MgB2 system for temperature of 850°C (Liu et al., 2001).

In each phase diagram, the fraction of Boron relative to Magnesium makes up one axis. The pressure is the Mg vapour pressure and the atomic fraction of Boron determines the Boron vapour pressure or flux ratio required. For example, at 1 torr, to remain in the "gas + MgB_2" window, temperature needs to be below about 900°C and above about 600°C, and atomic fraction of Boron must be less than about 0.667 (Mg:B ratio must be above stochiometric 1:2). Typically, however, the charts would be used by selecting a desired temperature and finding the Mg pressure and B atomic fraction window. It is also important to maintain temperature below the decomposition temperature of MgB_2.

The high volatility of Mg actually allows for automatic composition control (self-limiting adsorption of Mg) if deposition occurs in the Mg (gas) + MgB_2 window (Naito and Ueda, 2004). This means that Mg will combine with B in the required ratio is the correct conditions are met and any excess will not form a solid. This makes control of the relative flux rates considerably simpler.

The Penn State grouped calculated that for optimum epitaxy, MgB_2 should be grown at temperatures of around 1080°C (Liu et al., 2001). The phase diagrams show that for MgB_2 to be stable at this temperature, an Mg partial pressure of at least 11 Torr is required. This is out of the range of many common, low pressure techniques.

The revelations of this work explain many of the results observed in thin film work then and since. However, they make it seem more simple to produce MgB_2 than it actually can be. For example, Naito and Ueda (2004) note that for an Mg pressure of 10^{-4} – 10^{-6} torr, MgB_2 should form at a substrate temperature of 400°C. However, in this case, Mg will tend to re-evaporate from the surface before it has been able to combine with boron. The diagrams only illustrate that MgB_2 will be stable, but do not take the kinetics of the system into consideration. Mg tends to re-evaporate very easily above 300°C (Xi et al., 2003). In addition, it has been shown that MgB_2 decomposes less easily than predicted in the model (Fan et al., 2001).

This work does not only explain why decomposition was so prevalent and why *in situ* films tended to be Mg deficient, but it also explains why some *in situ* and one-step methods succeeded: they generated sufficient Mg flux relative to Boron flux in a growth window where MgB_2 was stable. However, other products may have formed and crystallinity was often poor. This was why such precise control over the relative flux rates of Mg and B was required in the MBE method.

2.4.8 Hybrid Physical Chemical Vapour Deposition (HPCVD)

The same group that uncovered the thermodynamics of the system used their results to produce what remains to date the only method to produce near-perfect epitaxial films (Zeng et al., 2002; Xi et al., 2003; Progrebnyakov et al., 2003). Essentially the method used a gas-phase Boron precursor (Boron CVD) and a solid-phase magnesium precursor (Mg PVD).

A substrate is placed in a quartz tube reactor on a graphite susceptor and surrounded by chips of solid Mg. The susceptor is then heated to the relevant deposition temperature (optimally 720°C in Progrebnyakov et al., 2003). Heating too much would not only risk decomposition, but it would increase the reaction between substrate and film. The Mg chips near the substrate ensure a high local Mg vapour pressure. Diborane is introduced from the top of the reactor and dissociates in the presence of the heated substrate to yield Boron. Diborane is introduced at 1000 ppm in H_2. The H_2 provides for excellent gettering of stray oxygen, resulting in oxygen-contamination free films (with the exception possibly of a thin layer of MgO on the surface of Al_2O_3 substrates due to substrate-film reaction). SiC substrates and Al_2O_3 substrates were found to give excellent results.

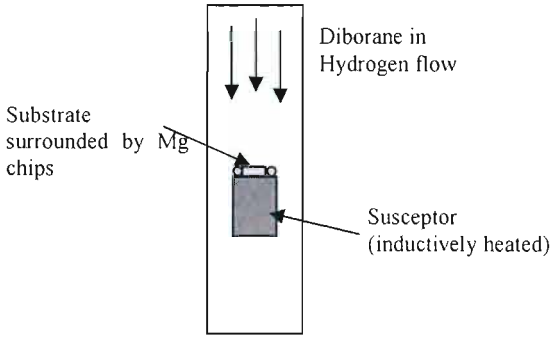

Figure 2-8: Basic schematic of HPCVD experiment.

Using this method, it was possible to grow large-grained, smooth (25-40 Å surface roughness) epitaxial films with a *Tc* of 41.7K and a sharp superconducting transition of 0.1K. These are certainly the best reported results available. Jc was 120 MA/cm^2 and $Hc_2^{\parallel}$ 29.2T. These films remain unique in their quality.

Also, the importance of a high hydrogen flow rate cannot be overemphasized. The gettering action of hydrogen proves far more effective in keeping oxygen contamination to a minimum than using extremely good vacuums.

2.5 Experimental - The basic premise

The idea to get involved in MgB_2 thin film work grew out of casual reading on the subject during lulls in other work that was continuing at the time (see Appendix). MgB_2 films were desired, but diborane gas proved ridiculously expensive owing to the fact that it had to be

specially imported into the country and could not be transported on a plane (due to its hazardous nature). In addition, B_2H_6 is highly poisonous and explodes spontaneously in moist air, making it a less-than-desirable gas to work with.

Nevertheless, there was a great desire on our part to produce films such as those made in the HPCVD method. The basic premise was reasonably simple: keep a high local Mg vapour pressure near the surface of a heated substrate as in the HPCVD method, but come up with another way of introducing a Boron flux.

2.6 Alternatives

There was no other suitable gas to be used as a precursor for the Boron CVD aspect of the HPCVD method. Other Boron precursors tended to be similarly hazardous, hard to get, and often contained unsuitable elements that would create impurities (e.g. BCl_3). Thus it was necessary to find some other way of creating a Boron flux.

2.6.1 Evaporation

PVD of the Boron was another option. Indeed, Shimakage et al. (2003,2004) have shown that dual-PVD is a viable option by simultaneously evaporating Boron and Mg at precisely controlled rates. They did manage to produce as-grown films, but their films were of poor quality and their method quite complicated, relatively speaking. In addition, simple resistive heating (or even electron beam heating) at an ambient pressure of 100 torr (the minimum used by the HPCVD group) would be quite difficult. The vapour pressure of Boron is very low indeed. At 2300°C, its vapour pressure is still only around 3 mTorr which would be completely overwhelmed by the ambient gas. Realistically, Boron would need to be heated to over 3000°C in a crucible that would itself not provide much contamination – perhaps tantalum. This is far from impossible, but does not seem an elegant solution.

2.6.2 PLD

An interesting option would be to use PLD to ablate the Boron into the hydrogen air stream. PLD does indeed work at higher pressures. If the Boron plume were ejected into a rushing stream of hydrogen gas, this would surely provide some Boron flux. The rest of the HPCVD experiment could remain the same.

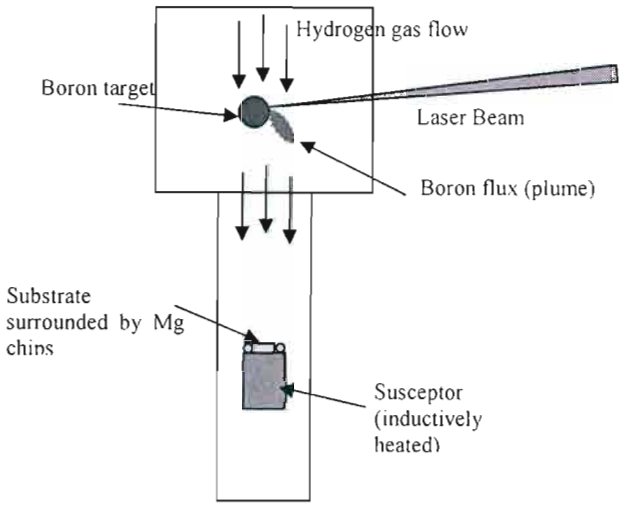

Figure 2-9: Possible alternative to diborane source for B flux.

Some time after this, it was mentioned that a group at Cambridge was trying to produce a variation on the HPCVD method using PLD. This is encouraging, since it means we were probably not too far off the mark. However, we did not pursue this idea primarily because using a laser would make the process very expensive. One uncertainty in this method is the degree of vaporization of the Boron source at the higher pressures (100 torr) required for the HPCVD-type method to work. It would probably require high power and very good focusing to achieve a good Boron flux. Perhaps a free electron laser would be most suitable. This remains a possible, but expensive and complex solution.

2.6.3 Plasma processes

Sputtering is not an alternative at the required pressures. However, its more passive cousin, chemical etching, may be more promising. Chemical etching takes place in a plasma environment. Active species in the plasma combine with surface particles of the substance to be etched. For example, in the semiconductor industry, chlorine gas is decomposed in a plasma reactor to form chloride ions and atomic chlorine. These active species will readily adsorb onto the surface of a silicon wafer where they react and form a new, gaseous product. The gas then desorbs from the surface and escapes via the vacuum system. This is illustrated diagrammatically in the following figure:

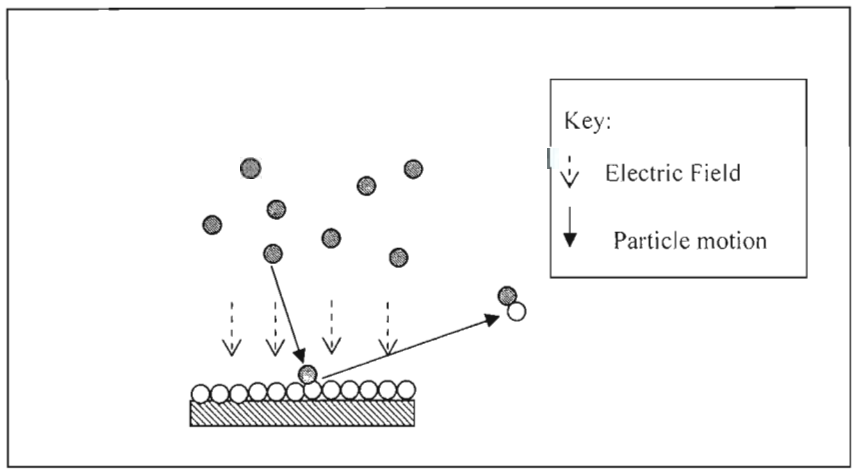

Figure 2-10: Basic process of etching. Active species in the plasma (dark grey circles) move to the substrate surface where they attach chemically to surface atoms of the substrate (light circles). The resulting molecule will ultimately be disposed of via the vacuum.

Typically, the gaseous product is pumped away and expelled. However, why may it not be used instead? The idea to use etching to create a Boron flux came primarily from the work of Reinke et al. (2000). In this work, a hydrogen plasma was used to etch a cubic Boron Nitride (cBN) thin film. cBN is the second hardest material known to man, beaten only by diamond. Yet it was etched chemically in hydrogen plasma at a rate of 0.65 nm/min (in 22 torr pressure) which is actually quite high (relative to thin film deposition rates). What is more, there was no preferential etching of either boron or nitrogen. The question then became that if cBN could be etched thus, then why not pure boron? And if boron could be etched, then the exhaust from the etching apparatus should contain a Boron flux which could be used to supply boron to the substrate in the HPCVD type of setup. Since etching can occur at high pressure (in fact, increased pressure should typically improve etch rate), it should be quite suitable for this purpose. So long as a suitably cheap and easy-to-make plasma source could be found, this technique could possibly be successful.

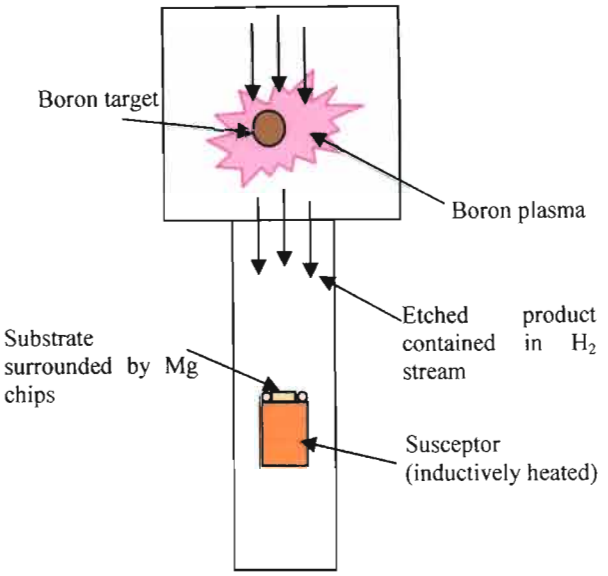

Figure 2-11: Showing idea behind plasma etch route to Boron flux generation.

2.6.4 Heat Pipe

A variation of the thermal evaporation theme was also considered: heat pipes. Heat pipes were originally encountered when looking for a way to create an environment where the Mg vapour pressure could be precisely known and controlled. A great resource is available from Stellenbosch University's Laser Research Institute website (LRI, 2001 in the bibliography). The following figure shows how a basic heat pipe may be used to create a stable Mg environment:

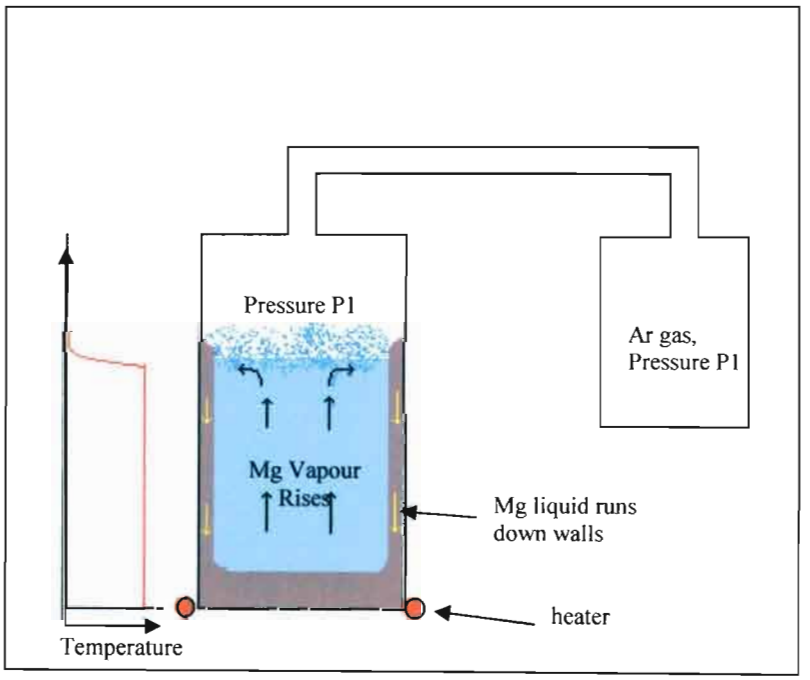

Figure 2-12: Basic operation of heat pipe oven. Redrawn from (LRI, 2001). Liquid Mg is shown in grey, Mg vapour is shown in light blue.

Mg solid is heated in the cylinder on the left. As it is heated, Mg vapour starts to rise. Eventually, an equilibrium is reached where the rate of evaporation and condensation is

constant. Mg vapour that slowly rises will reach a point where it condenses and runs down the walls of the chamber to return to the heated region. At this point, the Mg vapour pressure is equal to P1, the pressure of the external Argon gas. Because the Mg vapour is continuously rising, impurities are forced out. There is a narrow mixing zone between the two gases.

Because a liquid-gas phase equilibrium is reached, temperature and vapour pressure become precisely linked. Vapour pressure is directly dependent on temperature (as opposed to volume) in a closed environment. Thus the temperature of the pipe is uniquely determined by pressure P1, which can be easily controlled, and vice versa. The temperature is constant over the Mg gas region.

This makes heat pipe ovens very useful as isothermal ovens with precise temperature control. For our purposes, it makes a useful environment generator where the vapour pressure of Mg can be precisely controlled and known. In addition, the Mg environment becomes very clean. The trouble is, how to introduce Boron?

In fact, several schemes exist for mixing gases within heat pipe ovens. One, again proposed on the LRI webpage at Stellenbosch, involves a cross-concentric heat pipe oven. In this apparatus, a heat pipe is placed within another oven (which could be made from another heat pipe).

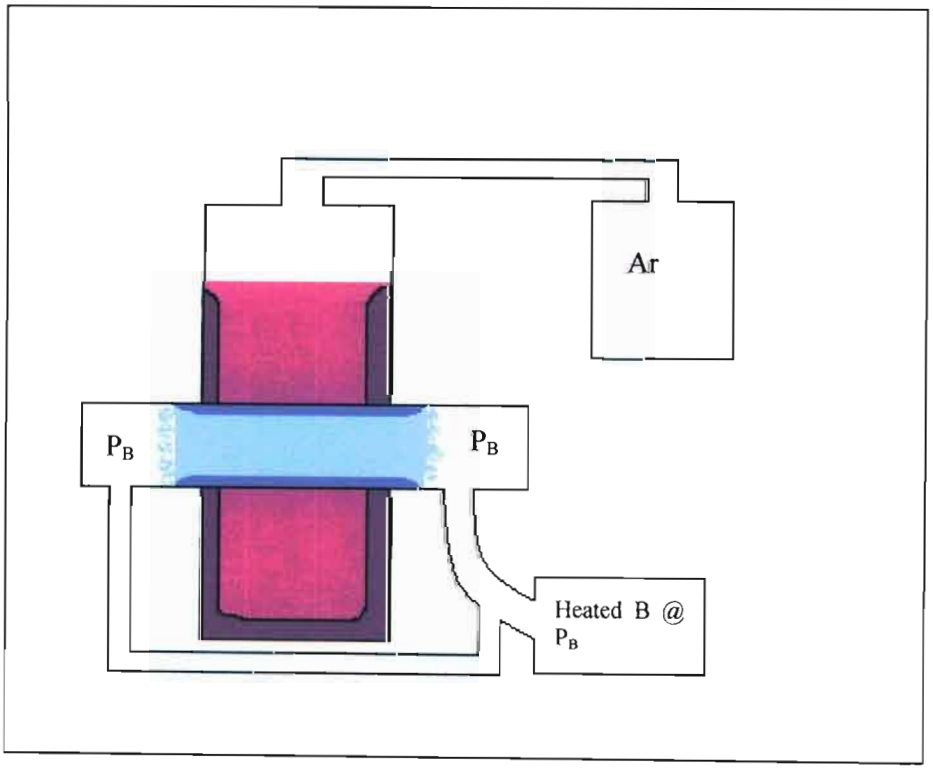

Figure 2-13: Cross-concentric heat pipe oven. Mg liquid is shown in darker blue. Mg vapour is shown in lighter blue. The purple represents a different metal in the outer heat pipe.

In the cross-concentric heat pipe, the central heat pipe bisects the larger outer heat pipe, which really serves the purpose of an oven to control the temperature of the inner heat pipe precisely. The vapours of Boron and Mg will mix in the light blue section. The advantage is that the vapour pressure of Mg is precisely controlled by the outer oven, and the vapour pressure of B is precisely controlled by its own, separate heating source. Other, schemes for multi-element heat pipes have been proposed (Vidal and Hessel, 1972, Bednarska et al., 1996).

This remains a uniquely interesting solution because of the precise, independent control afforded over Mg and B vapour pressures. However, it suffers again from the problem that Boron needs to be heated a great deal to produce any reasonable vapour in such a system. This would mean that part of the system at least would need to be made from expensive Tantalum.

2.7 Conclusion

To this day, the HPCVD method remains the only MgB_2 thin film production method capable of such high quality, epitaxial films. We were quite eager to attempt to duplicate this feat without diborane gas. MgB_2 deposition should be relatively simple provided that the correct thermodynamic window for its production can be maintained. Although at one stage it was desired to try multiple paths to this route, in the end there was only time and budget for one attempt. To this end, we decided to try and plasma etch the boron to obtain the necessary B flux in the hydrogen stream. This method might not seem like the simplest, but there are several advantages to taking this route:
1) It has the potential to be quite cheap if a cheap plasma source can be found;
2) To the author's knowledge, creating a flux of a desired species in this way has not been tried. This makes it potentially valuable and scientifically interesting. Should it work, it could be a very useful technique in general since one negative aspect of general CVD is that suitable precursors are not always available.
3) Using a plasma has other potential advantages. Firstly, the laboratory could use a good, high pressure plasma source in any event. Secondly, changes in the methodology could allow the same apparatus to be used for plasma-enhanced CVD experiments. It is worth nothing that PECVD of any nature has not yet been tried in MgB_2 thin film deposition.

The next chapter surveys suitable plasma sources considered for use in this system.

3 Plasma Sources

Based on conclusions drawn in the literature review on MgB_2 thin film deposition, the next step involved acquiring an adequate plasma source to suitably etch the boron precursor. This review is intended to provide a brief overview of plasma sources in general, followed by a survey of some likely candidates. Plasma processing and plasma physics are complicated and extensive topics and as such this review intends to provide an overview deep enough only for the purposes of the discussion at hand. For an excellent text on plasma fundamentals as applied to film processing, the reader is referred to Rossnagel, Cuomo and Westwood (1990).

3.1 Plasmas

3.1.1 Introduction

A plasma is a gas that has been by some means dissociated into some or all of its constituent parts: atoms, molecules, ions and electrons. Not all plasmas are created equal, with some containing more ions (strongly ionised plasmas) and some containing mostly neutral particles (weakly ionised). In plasmas where that are mostly ionised (such as the sun), one finds a good degree of thermal equilibrium between ions and electrons. In weakly ionised plasmas, the electrons tend to have a very high temperature, while the ions remain relatively cool. These are termed nonequilibrium plasmas and most common laboratory plasma generators produce these types of plasmas. Since most of the energy is contained in the electrons – which are incredibly small – such plasmas do not cause much heating in objects they come into contact with. Thermal (or equilibrium) plasmas, on the other hand, have a greater degree of equilibrium between ion and electron energies and are quite capable of inducing considerable heating.

Typically one refers to the electron temperature of a plasma for the sake of comparison. Process plasmas (used in most materials science processing) have an electron temperature of around 1 to 10 electron Volts (eV). One electron Volt is equivalent to approximately 11600 K (Rossnagel, Cuomo and Westwood, 1990, pp. 15). This does not of course mean that the plasma gas temperature is 11600 K since the ion temperature is considerably lower. By contrast, magnetic fusion reactors operate at temperatures of nearly 10^6 eV.

It is estimated that plasmas make up 99% of the visible universe (Wikipedia, Plasma). Even on earth they are quite common with a flame being an example of a type of plasma.

3.1.2 Some basic properties

Again, this review does not seek to be a physics lecture but offer some basic plasma concepts by way of introduction.

The most startling and obvious characteristic of plasmas is of course the fact that they emit vibrant glows. The reason for this is that electrons are constantly excited and then decay back to lower energy levels, emitting photons in the process. This effect is incredibly useful in diagnostics since each element will emit a specific wavelength – the foundation of spectroscopy.

In addition, a plasma will react to an imposed charge or electric field in order to diminish the effects of that charge or field. This is the phenomenon of Debye shielding. One consequence of this is that plasmas are always charge neutral on average. This is termed 'quasineutrality'. If there were any region of excess positive or negative charge, a field would be set up which

would counteract the effect. For this reason, electric fields are not useful for containing plasmas and magnetic fields are used primarily for this purpose.

The most useful aspect of plasmas for the purposes of this thesis has already been mentioned: the generation of active species. Since electrons are moving about furiously within a plasma, there are numerous collisions between electrons and molecules. When this happens, two main reactions may occur (Rossnagel, Cuomo and Westwood, 1990, pp. 35): 1) dissociation, where the molecule is broken up into its constituent atoms or 2) dissociative ionisation ($e^- + AB \rightarrow A^+ + B + 2e^-$ where AB is the molecule). The products of such dissociations can themselves be further ionised or dissociated by electron bombardment. Note that recombination is a constantly occurring process as well which is why, of course, without the application of power a plasma will quickly revert to a normal gas.

This active species generation is what makes a plasma so suitable for chemical etching (described in the previous chapter) where active species combine with surface atoms of a material to form a new gas product. The resulting product then desorbs from the surface and is pumped away. Of course, it is possible that the surface may be modified instead of etched (no desorption) which is another use of plasma processing: surface activation or modification. Etching by plasmas is known as 'dry' etching as opposed to wet etching where the substance to be etched would be placed in a solution of some sort. It is also often called chemical etching.

In most reactors, there is a natural acceleration of ions towards the substrate due to electric fields which form about the substrate. This enhances the speed of the reaction. It is possible, however, to deliberately accelerate the ions using dedicated means to do so. If ions are accelerated fast enough, they strike the surface of the substrate with sufficient kinetic energy to physically knock substrate particles off the surface. This is a type of billiard-ball effect. In this case, the etching is typically termed 'sputtering' as mentioned in the previous chapter. This is a physical, not chemical process. Sputtering is typically a low pressure process since ions would need to have considerable mean free path to be accelerated sufficiently.

3.2 Sources

To break a gas up in this manner will obviously require the input of energy. Many schemes have been developed for the generation and then application of such energy. A dc or ac power supply will typically be coupled to a gas chamber through an antenna, electrodes, a coil, or electrostatic plates. Frequencies of the power source vary all the way from dc up to the microwave range.

For the purposes of this research , two basic requirements had to be met: 1) the source and reactor had to be as low-cost as possible, 2) the source and reactor had to be easily obtainable and simple to set up. The constraints were limitations imposed primarily by budget and time. Keeping the apparatus simple and low-cost would in addition have the advantages of making any results obtained particularly accessible and more useful. Furthermore, if complex and expensive equipment were used, the method would have no advantage over the simpler and already-proven HPCVD method.

Expense and difficulty in implementation will be incurred mainly in obtaining a suitable power supply, or often in constructing a suitable reactor chamber (or both). An added constraint was imposed by the intended use of the apparatus: to etch Boron or MgB_2 at high pressure. A large number of common laboratory plasma sources are useable only at very low pressures – typically less than a torr. In fact, a very old Plasmaprep 100 barrel etcher was accessible for use, but could only operate at sub 1 torr pressures.

The added pressure constraint automatically ruled out a large number of the more common plasma sources such as the typical parallel plate barrel etcher. What follows is an overview of several plasma sources that were considered.

3.2.1 Capacitively-coupled, 13.56 MHz RF sources

Most common laboratory plasmas are either of the barrel type or parallel-plate type as illustrated below:

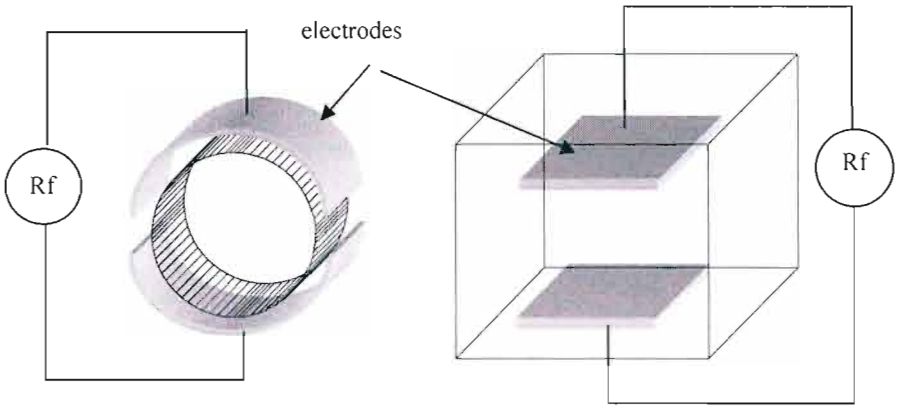

Figure 3-1: Barrel type (left) and parallel-plate (right) etchers.

Owing to the ubiquitous nature of such sources, these types of reactors were considered first. The parallel-plate structure is also commonly used with a simple dc source. However, dc sources are considered inferior primarily because they are less efficient and require a net conducting current to sustain the plasma which makes them less suitable for processing insulating materials. Commercial RF sources such as that used in our own PlasmaPrep 100 tend to use a frequency of 13.56MHz. The frequency is assigned by the United States Federal Communications Commission (FCC) and is not based on design parameters. Both RF and dc plasma apparatus of this nature work at very low pressures which makes them unsuitable for the task at hand. They are also characterised by low ion density and low ion-to-neutral ratio (Popov, 1995).

3.2.2 Inductively Coupled Plasma (ICP)

The RF inductively-couples plasma, however, has long been used at pressures up to atmospheric. They are high temperature (7000 K – 8000 K heavy particle temperature) sources that are used in such applications as vaporisation and even fusion. Not very complex in construction and known for high efficiency, such a plasma source was always going to be an option.

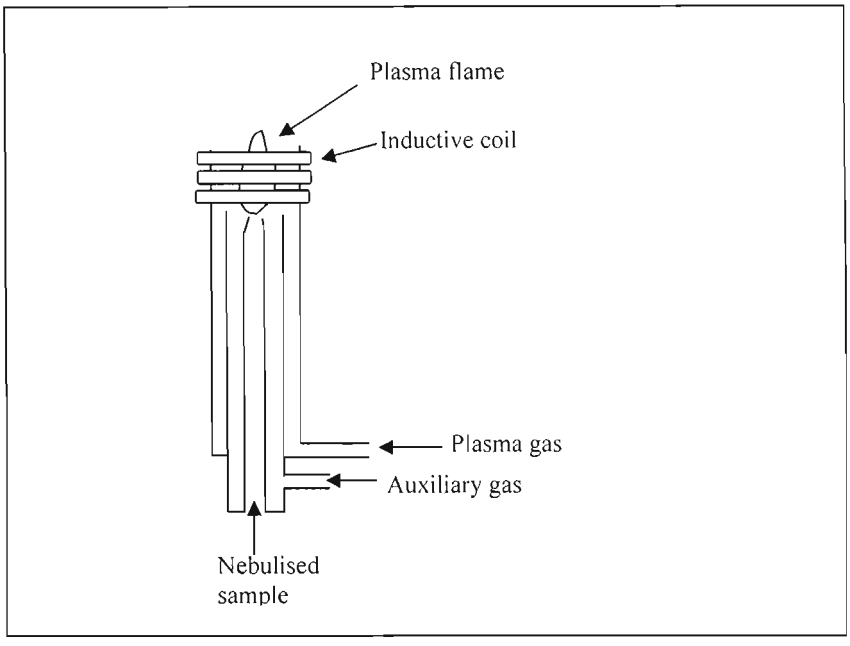

Figure 3-2: Basic torch used in ICP-Mass Spectroscopy (Thomas, 2001).

One of the most common uses for ICP today is in spectroscopy. A sample to be scanned is nebulised and then injected into the stream of an ICP torch. The plasma is sufficiently hot and dense to quickly vaporise the target. The wavelength of the photon emissions as the electrons decay to lower energy levels allows the sample to be identified via spectroscopy.

From the above figure it is clear that an ICP is made to work by applying a suitable power supply to a coil. Such a torch would be quite successful for the task at hand. There are two problems, however, which make it largely unsuitable: it requires a 600 W-1800 W (Timmermans and van der Mullen, 2003), high frequency power supply and quartz glass tubes. Quartz seems quite popular and common in certain countries but in South Africa at least is a very expensive commodity that needs to be imported. The power supply presented something of a problem as well. Although it could realistically be built, this would make the final apparatus less easily accessible and cheap. In addition, the torch needs very high power to run on any gas other than argon which would further add to cost and difficulty since it was desirable to use hydrogen in these experiments.

The ICP torch does however remain a uniquely suitable apparatus for the present task.

3.2.3 Torche à injection axiale (TIA)

The TIA is a plasma torch based on a microwave power source (Moisan et al., 1994). Like the ICP, it can be used right up to atmospheric pressure and is very hot (1000 K - 4000 K heavy particle temperature according to Timmermans and van der Mullen, 2003). Unlike the ICP, the power source, being a microwave magnetron, is compact and relatively simple to acquire.

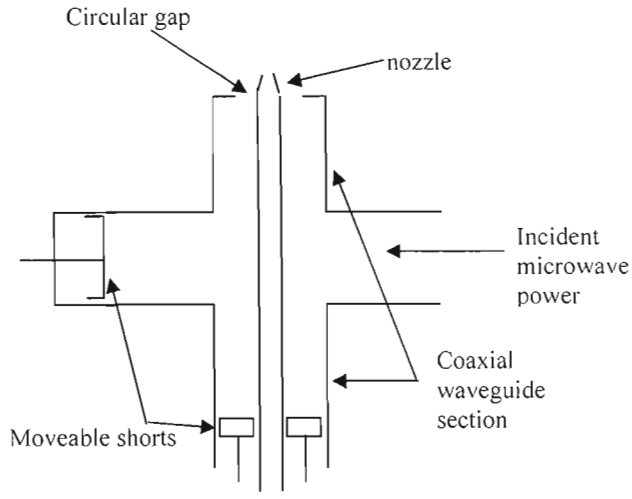

Figure 3-3: Basic design of TIA apparatus. The horizontal section is made of rectangular waveguide while the vertical section is coaxial.

As can be seen in the above figure, the TIA is made of two intersecting waveguides: a rectangular section that runs horizontally, and a coaxial section that runs vertically. Moveable shorts are in place to allow for tuning and the plasma itself forms at the very nozzle of the device. The apparatus essentially converts the TE_{01} mode running in the rectangular waveguide to the TEM mode in the coaxial section.

The TIA system is quite promising for the given application. However, it is more complex to build and set up than some alternatives especially owing to the rather complex tuning mechanism. Furthermore, microwave waveguide components such as directional couplers and circulators are quite expensive. Also, the entire outer waveguide section of the coaxial part would need to be enclosed in an air-tight chamber for thin film deposition. These are small problems, granted, but simplicity was key and it will be seen shortly that more promising alternatives existed. The TIA was certainly one of the most promising candidates but for its rather tedious construction. The TIA also requires a fairly high power supply (300 - 2000 W depending on gas and pressure).

3.2.4 Microwave Plasma Torch (MPT)

In fact several microwave-induced plasma torches have been designed over time all of which have similar characteristics. The Surfatron (not considered as a candidate, see Hubert et al., 1978) and TIA are examples of these. A more recent version improved on older designs to offer better stability and lower power consumption while allowing for simple construction (Bilgic et al., 1998). The result is shown in the figure below:

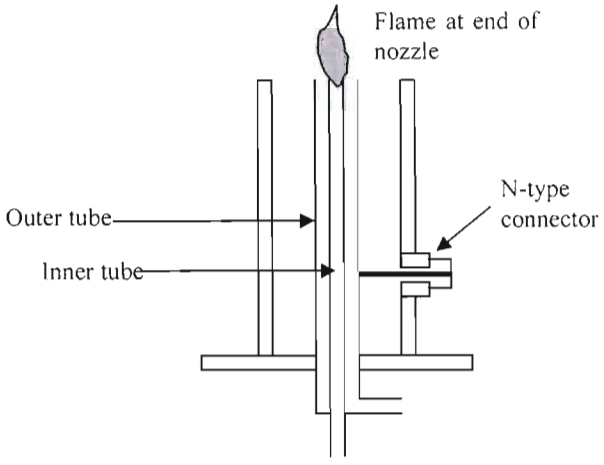

Figure 3-4: Design of the microwave plasma torch of Bilgic et al. (1998)

It can be seen from the above image that the MPT is not completely dissimilar from the TIA. The primary difference is that input power is coupled in through a coaxial line feed, and the tuning mechanism is simplified. On the whole, the setup is easier to construct and in addition, needs less power to run (50 W - 300 W vs. 300 W - 2000 W for the TIA). Yet this solution remained more complex in construction and therefore less accessible than certain other options. There is no doubt the electronic engineering workshop could have built such apparatus to the required specifications, however. A more subtle problem is that while magnetrons are quite easily available owing to the ubiquitous presence of microwave ovens, these magnetrons output their power into rectangular waveguides, not coaxial ones. It is again not a terrible difficulty to design and construct a mode converter and tuner (this would be expensive to purchase), but then complexity would increase unnecessarily.

3.2.5 Corona Discharge

Corona discharges are discharges created by dielectric breakdown due to intense field strength. These happen quite naturally, particularly around sharp points where electric field is intensified.

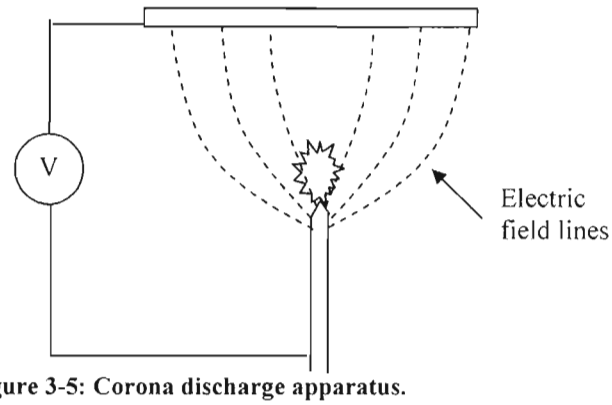

Figure 3-5: Corona discharge apparatus.

Corona discharge is reasonably simple to set up. However, it strikes one as being a less versatile source than many considered here. In addition, it does require a considerably high voltage power supply (several kilovolts, depending on gas and pressure) to work well which can be difficult to acquire or build. Its only real advantages are that is does indeed work at atmospheric

pressure and has a very simple structure. In addition, the plasma is usually very small extending only about 0.5 mm away from the point which is not desirable.

3.2.6 Dielectric Barrier Discharge (DBD)

A DBD consists of two electrodes, at least one of which will have its surface coated with a dielectric. There are several variations on this theme (e.g., Klages et al., 2000), but the basic concept is illustrated below.

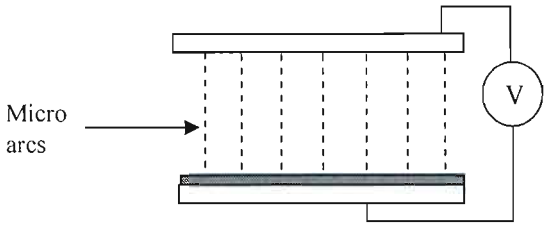

Figure 3-6: Dielectric Barrier Discharge.

A voltage of around 20KV is applied to a gap several millimeters wide existing between two plates. (Schutze et al., 1998). The plasma is actually composed of thousands of micro arcs that rapidly form and extinguish, lasting for about 10-100 ns each.

This apparatus is an interesting choice and not without its merits. However, it still requires the high KV power supply which would need to be built. This is not a huge obstacle, but the system has little unique or exciting to offer in the face of its competition and it simply did not seem worth the effort and time.

3.2.7 Atmospheric Pressure Plasma Jet (APPJ)

Although the TIA, MPT and even ICP already discussed could be quite feasibly called atmospheric pressure plasma jets, the APPJ is a different and rather interesting device. It is a rare device insofar as while it can indeed create a plasma all the way up to atmospheric pressure, the plasma maintains its nonequilibrium state (Schutze et al., 1998). This means that the heavy particles (ions etc.) within the plasma remain relatively cool. In fact, the gas temperature remains in the region of 25°C to 200°C – this compared to many thousands of degrees for thermal plasma torches. This makes the APPJ uniquely suited to treating a wide variety of surfaces that would otherwise be easily destroyed by plasma torches. It can, for example, 'burn' (etch) a surface clean at very low temperatures.

The APPJ is rather simple in construction consisting of two concentric, cylindrical electrodes through which the gases flow. 13.56MHz RF power is applied to the inner electrode at 50 to 500W (Jeong et al., 1998)

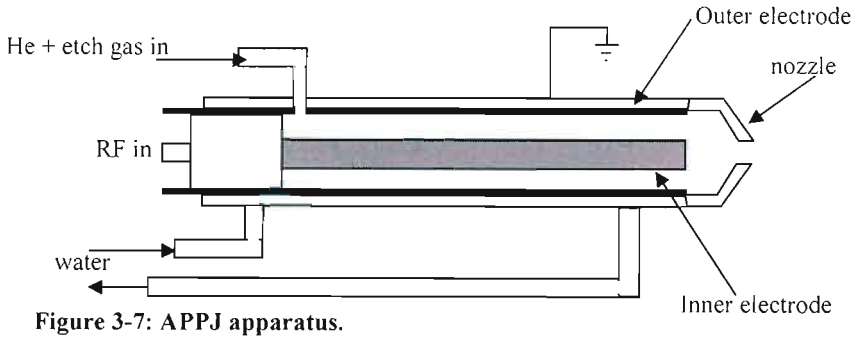

Figure 3-7: APPJ apparatus.

The APPJ requires that 99% of the process gas used is He, which is a significant drawback in this application. Nevertheless, the small 1% that remains is enough to carry out a chemical etching process (Jeong et al., 1998). In fact, using a cold plasma such as this would allow for the determination of just how successful chemical etching of Boron or MgB_2 really is since there would be no thermal evaporation.

In spite of this, the RF power supply would need to be built or acquired at some expense and it seemed as if a thermal plasma torch, which is simpler in construction and has the added advantage of thermally processing the Boron, would be a better option.

3.2.8 Thermal Plasma Torch – tube in waveguide

There are several variations on this theme, but the basic apparatus involves a refractory, dielectric tube (such as quartz or cubic boron nitride) intersecting a waveguide (Hadidi and Woskov, 1999; Moon and Choe, 2002).

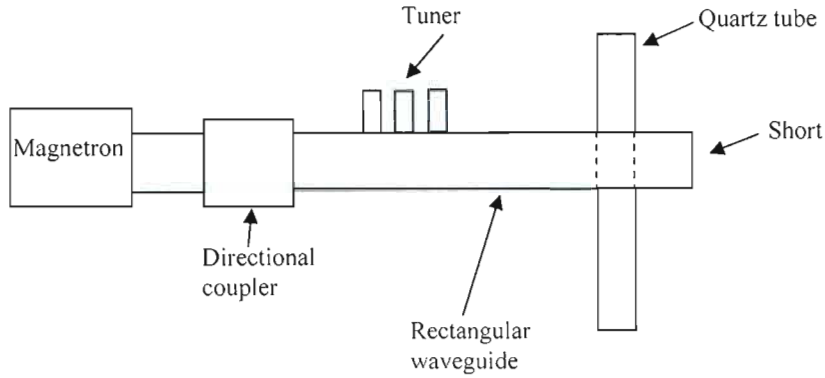

Figure 3-8: Basic implementation of microwave plasma torch by tube-in-waveguide method.

In the above figure, the tuner is used to ensure maximal coupling of energy and the directional coupler sends any returning waves to a dummy load. The tube is placed a quarter wavelength back from the waveguide short to ensure maximum E field strength. This is a very thermal plasma like most atmospheric plasma torches (the hot point of the flame was measured at 3200 K by Moon and Choe, 2002). What is more, atmospheric operation, at least for argon loads, is achievable with a very standard microwave magnetron operating at less than a kilowatt. In different implementations of this basic design (see for example, Woskov and Hadidi, 2002 versus Moon and Choe, 2002) there can be variations in the actual nature of the plasma flame. Moon and Choe observed filaments in the tube which converged to a point and then formed a flame, while in the work of Woskov and Hadidi, the filaments and convergence were not apparent. This is really not an important point, however, as the basic method would certainly serve the purposes of this experiment. Furthermore, since the plasma is produced directly in a quartz (or BN) tube, it is easy to link to a vacuum system and deposition chamber as desired.

This is certainly a very attractive option hindered only by the ridiculous price tag attached to commercial waveguide components. The magnetron could theoretically be taken from a conventional microwave oven, but a tuner, directional-coupler and even basic waveguide would set a small research lab back thousands of dollars. The waveguide could be quite easily made in the local workshop, but designing and building tuners and couplers is something of a chore. A further hindrance is the high cost of the refractory tubing once again. In addition, microwave oven magnetrons are not continuous wave and so their power supplies would need to be smoothed. Again, these are not insurmountable problems, and had a better method not been discovered, the tube in waveguide plasma torch was the number one contender for this project. Its suitability to the project and otherwise simple construction made it a very attractive option.

3.2.9 Microwave plasma Jet with nozzle

This is similar to the MPT discussed earlier and also to the tube-in-waveguide torch discussed above. A number of microwave-based approaches were looked at owing to their efficiency, simplicity, and the ubiquitous nature of cheap, powerful microwave power supplied courtesy of domestic ovens. The difference between the systems discussed so far and this one is that microwave power is coupled to the plasma through a rectangular waveguide (like the tube-in-waveguide approach) but then a tunable nozzle is used to focus the Electric-field at a particular point (Al-Shamma'a et al., 2001). The diagram below will make this more clear.

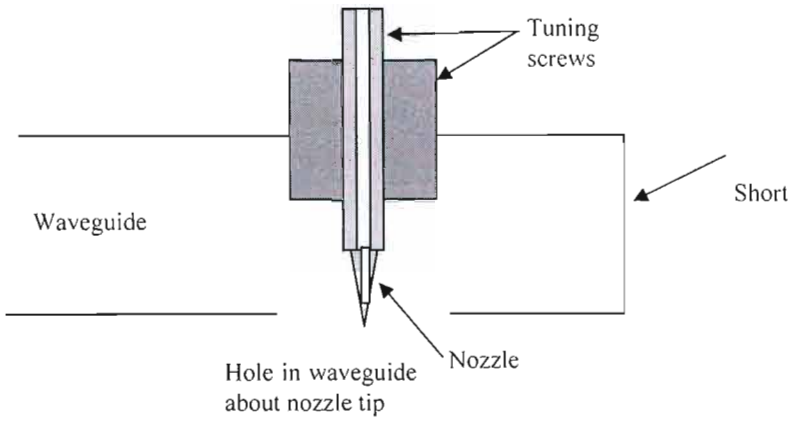

Figure 3-9: Nozzle-in-waveguide plasma torch design.

Again the nozzle is placed a quarter-wavelength back from the short where the E-field is a maximum. Through proper tuning by moving the tuning screws in the above diagram, the E-field is concentrated such that breakdown occurs and a plasma results.

The advantages of this system are that no refractory tube is needed. The nozzle may in fact be made out of an ordinary metal such as copper since the plasma forms beyond the nozzle tip and so the tip remains relatively cool.

However, for the purposes of the work in this thesis, the apparatus is a little less suitable than the tube-in-waveguide approach. This is primarily because the tube-in-waveguide allows for the plasma to be contained in an airtight tube easily connected to a deposition system. Doing the same with the above apparatus is more difficult. In addition, the nozzle method is more tedious and difficult in construction and tuning and still suffers from the drawbacks of requiring expensive waveguide equipment.

3.2.10 Fused Hollow Cathode (FHC)

Barankova and Bardos at the University of Uppsala, Sweden, published a series of papers on a rather novel plasma source called the Fused Hollow Cathode (Barankova and Bardos, 2000a; Bardos et al., 1998). Hollow cathodes are nothing new. They have been used for some years as a way to increase the rate of processing achieved in plasma processes (for example, a faster etching rate). Briefly, a hollow cathode means having at least two surfaces at the same electrode potential (the cathode potential) facing each other and being in close proximity to one another. A tubular cathode could also serve this purpose:

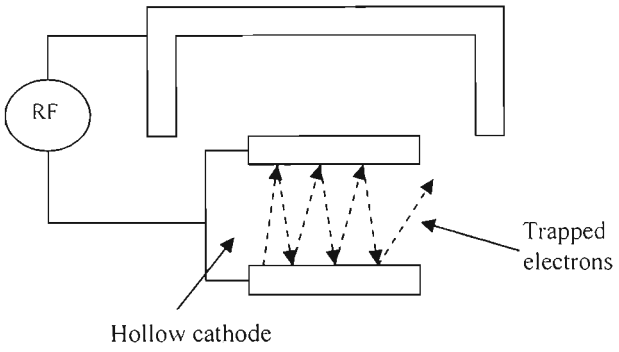

Figure 3-10: A type of hollow cathode configuration (Rossnagel, Cuomo and Westwood, 1990).

Not only are the reactants physically contained between the hollow cathode surfaces, but electrons are found to oscillate rapidly between the surfaces, increasing ionization. The major benefit to be gained from hollow cathode is this immense increase in ionization. The total plasma density increases by two or three orders of magnitude (Bardos et al., 1998)

However, typical hollow cathode setups still tend to work at relatively low pressures, unsuitable for our means. Nevertheless, the microhollow cathodes employed by Barankova and Bardos are quite capable of operation right up to atmospheric pressure. These cathodes are small needle-like tubes about 0.1mm to 0.4mm in diameter. In fact, microhollow discharges capable of working up to atmospheric pressure have been around for a while and were originally powered with a dc source (El-Habachi and Schoenbach, 1997; Stark and Schoenbach, 1999). The authors noted that for a hollow cathode to operate effectively, pressure scales inversely with diameter. To this end it was estimated that holes of diameter 0.1 mm and below would allow for atmospheric operation. Electrodes were made from 0.1 mm molybdenum foils separated by 0.2 mm mica spacers with a 0.1 mm gap separating the two cathodes.

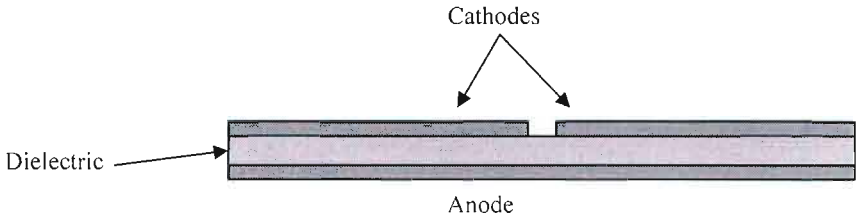

Figure 3-11: Early dc microhollow cathode (El-Habachi and Schoenbach, 1997).

Barankova and Bardos made use of RF instead of dc as a power source which allowed for easier ignition and greater thermal and operational stability (Barankova and Bardos, 2000a). One major advantage of the hollow cathode structure is that it is always a nonequilibrium plasma (El-Habachi and Schoenbach, 1997). One disadvantage is that the plasma emission is so small in extent that it can only be used to process small surfaces.

Barankova and Bardos overcame this by creating arrays of microhollow cathodes which they dubbed "Fused Hollow Cathodes" (Barankova and Bardos, 2000a, 2000b). The exact geometry can take several forms, one of which is shown below (Barankova and Bardos, 2000b).

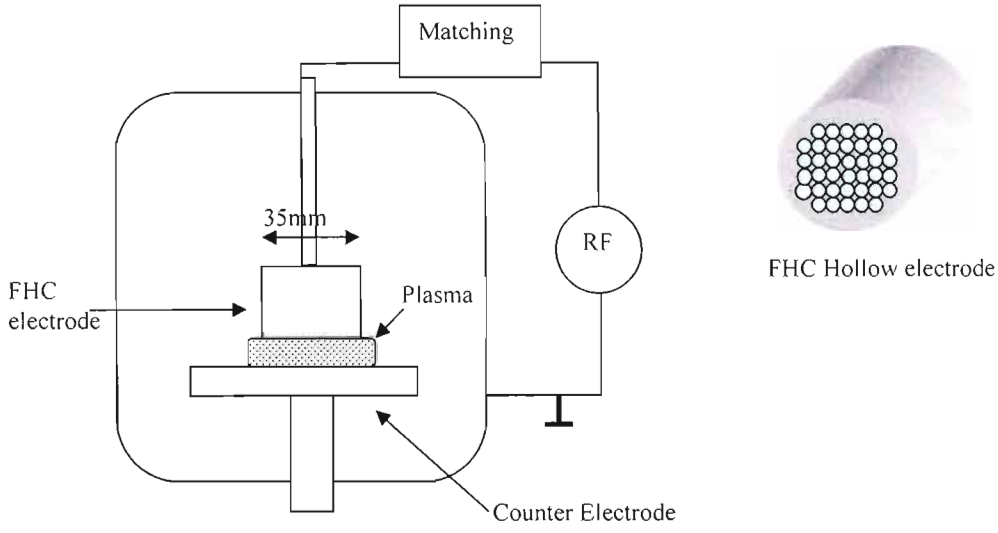

Figure 3-12: A type of FHC setup. Gas is blown through the FHC head which is also the cathode.

The electrode in the above example is essentially a fusion of many sub-mm hollow cathode tubes into one solid electrode. The micro-plasma generated by each will merge into one plasma of a larger surface area at the counter electrode. In addition to the low heat generation, the plasma used very little power, on the order of tenths of Watts per square cm (Barankova and Bardos, 2000b).

The system is remarkable in its achievements and incredibly valuable for all its simplicity. In the end, it was abandoned in favour of a more thermal, more accessible option. Nevertheless, it would be interesting to actually build an FHC at some stage as it provides perhaps the best example of a large-scale, atmospheric pressure, nonequilibrium plasma that is still reasonably simple to build.

3.2.11 Atmospheric Pressure Nonequilibrium Plasma (APNEP)

The APNEP is another plasma generated by a microwave magnetron. What separates the APNEP from other implementations of atmospheric microwave plasmas is its absolute simplicity. Recall that the most important parameters in this search were accessibility and cost. For this reason, figures such as ionization density, electron temperature and even power have not been considered important. Most of the plasmas mentioned thus far in any event are capable of high processing rates regardless of ionization density because of the high gas pressures and therefore large number of active species present.

The APNEP is so simple that it is almost remarkable somebody managed to patent it (Duan, 1999). It involves placing a containing reactor of some refractory dielectric inside a multimode microwave cavity. A multimode cavity is the same type of applicator used in common domestic microwave ovens: an applicator designed to support multiple modes for a given frequency range. So, essentially, an APNEP involves placing a dielectric reaction chamber (to contain the gases) inside a microwave oven.

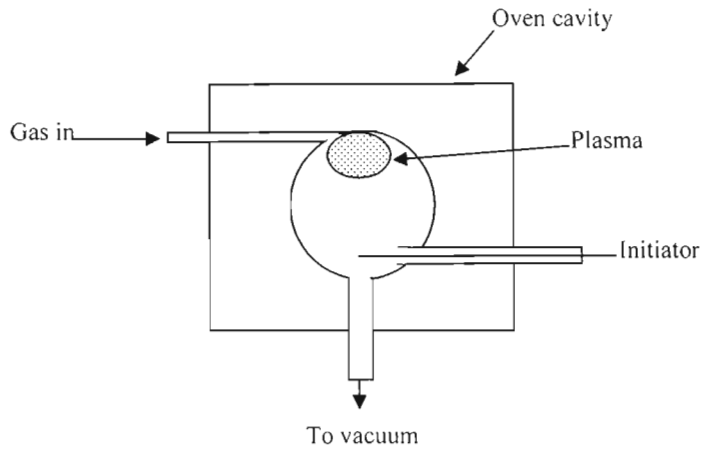

Figure 3-13: Basic APNEP apparatus. A quartz reactor is placed within a microwave multimode cavity. The initiator is used to ignite the plasma.

Of course, domestic microwave ovens are typically not very well designed having many hot and cold spots (true multimode applicators should have a relatively smooth electric field distribution, especially when loaded). In addition, they are not powered using a continuous wave generator, but rather make use of a half-wave rectified source (a voltage-doubler). Nevertheless, the APNEP will run perfectly well inside a commercial microwave oven and in fact is commonly used in such a form. It differentiates itself from other microwave plasma sources by being the first that is readily achievable using such cheap equipment (Shenton et al., 2002).

One problem is ignition. For example, were one to put a glass sphere into a microwave oven and switch the oven on, nothing would happen. The patent puts great focus on methods to cause the plasma to ignite. One way is to insert a sharp conducting object, which can then be removed (to prevent contamination). Electric fields are concentrated at the tip of the initiator which causes the plasma to ignite at atmospheric pressure. Once initiated, the plasma may be sustained without need for the initiator. The plasma will tend to float upwards till it reaches the top of the reactor as shown in the figure above.

Another method to initiate the plasma would be to evacuate the reactor until breakdown occurs. Once the discharge is initiated, pressure can be increased once again without extinguishing the plasma since a discharge path now exists.

Although the plasma is nonequilibrium by virtue of the microwave source (microwaves operate at such high frequencies that electrons are forced to oscillate with furious energy), the degree of nonequilibrium is quite poor at high pressure and the plasma is actually very hot. The temperature has been quoted as 2000°C (Shenton and Stevens, 1999). The degree of nonequilibrium is improved at low pressures.

This is the only potential drawback of using this equipment: a refractory reactor, such as one made of quartz, would negate all the advantages gained in such a cheap and simple setup.

However, the apparatus would generate plasmas in high flow rates (up to 600 l/min according to Shenton and Stevens, 1999) using a large variety of gases and the thermal component could only help in releasing boron from the solid precursor. The apparatus could also be used for PECVD purposes (Duan, 1999). The absolute simplicity and seeming flexibility of such apparatus made it a top contender for this project.

3.2.12 Persistent Ionisation in Air (PIA) in a microwave oven

The idea to create plasmas in the air using microwave ovens is actually not very new. A casual search on the internet will reveal several websites detailing experiments which involve doing just that (see, for example (Naudin, 2000)). Note that these sites are all made by hobbyists or laymen – not scientists. It is considered a well-known and 'fun' experiment to place, for example, a burning candle in a microwave oven and then apply power.

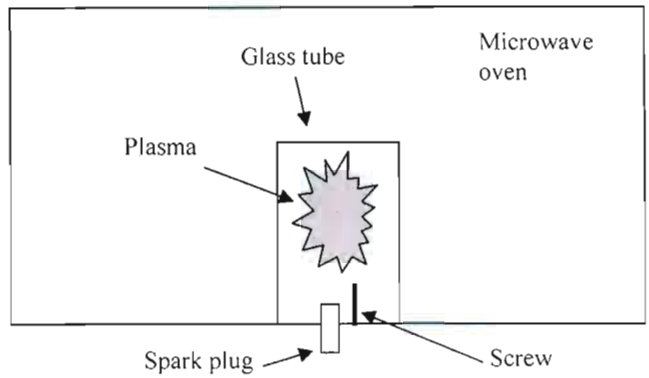

Figure 3-14: An implementation of the basic plasmoid experiment (Brandenburg and Kline, 1998).

In the above image, the screw may be replaced by a lit toothpick or thin pencil-lead (graphite) depending on where one looks on the Internet. This will be called the aerial in this discussion. The aerial concentrates the field and causes dielectric breakdown of the ambient gases (typically air). A spark plug was added in the above system to help initiate the plasma. By photoionising some of the air in the vicinity of the aerial, the required E-field strength to cause breakdown is lessened (Brandenburg and Kline, 1998). However, placing a lit toothpick under a bowl works equally well.

What results when power is applied is often called a 'plasmoid' or "artificial plasma" (Naudin, 2000) by the various people who produce such a thing. It is meant to be related to ball lightning in the way it manages to contain itself (Brandenburg and Kline, 1998). However, some dispute this.

Knowing that microwave ovens will readily feed plasmas as in the APNEP apparatus above, it becomes easy to see that this will work simply because after any sort of breakdown (e.g., arc or corona discharge) the microwave power will feed the plasma and make it grow. The plasmoid disconnects from the aerial that created it and floats its way to the upper wall.

Of course, a little ball of plasma that quickly rises to the top of the oven and dissipates is not of much use. However, it may be contained using suitable glassware.

It is interesting to note that, according to the above sources, the plasmoid will spin around in a so-called "vortex" and therefore, surprisingly, not melt through the containing glass. Our own experiments with such plasmoid confirmed this. Brandenburg and Kline even used Plexiglass in their experiments, which softens at a much lower temperature than Pyrex. Some casual experimenters on the web think that this means the plasma is cool (which technically would make it a plasma having a high degree of nonequilibrium). This, however, was shown to most certainly not the case in our own experiments.

In spite of all the fancy names, the plasmoid really is a plasma which simply has peculiar dynamics. It could certainly be useful in the task at hand with the exception that everything would need to be sealed in an airtight container as in the APNEP above. It must be noted that most research on these plasmoid experiments was conducted some time after work on our own

plasma apparatus had already begun (with the exception of the paper by Brandenburg and Kline, 2000). The method was largely dismissed in the early stages of this work since according to Brandenburg and Kline, it appeared that the plasmoid could be quite difficult to stabilise and thus was considered less suitable than the APNEP which is very similar. However, using a spherical container, J. Naudin (Naudin, 2000) found stability to be quite robust.

3.2.13 Summary

This review touches only on several of the more promising sources that were investigated. There is a wide array of high pressure plasma sources in the literature. Many were dismissed quickly because of cost or complexity in construction.

Of the many types of generators reviewed, the APNEP and tube-in-waveguide were deemed the most suitable for this purpose. They met the primary criteria of accessibility, simplicity and low-cost. It is with some regret that one source alone need be chosen since it would be interesting to attempt to use, for example, an FHC, cold plasma source as well as a torch, thermal source and compare results. The tube-in-waveguide apparatus had been used previously to etch cubic Boron Nitride with no preferential etching of either B or N by Reinke and Oelhafen (2000) making it a very promising candidate. However, it was deemed more expensive and difficult to implement than the APNEP. Although much of the waveguide apparatus could be designed and machined in the local workshop, this still made it a less accessible option since other groups may not be prepared to do the same. It was very important to come up with a process that could be easily mimicked.

In this regard, the APNEP system was simply unbeatable. Furthermore, it was so easy to test that it would be possible to get started right away. One drawback was that a glassblower would be needed to fabricate the reactor. This is not considered a major hurdle though. Although the reactor designed for these experiments was custom-made, it may even be possible to use an assemblage of standard laboratory glassware. Any pyrex container with an inlet pipe, and outlet pipe, and some access port (such as a stopper) that allows samples to be placed inside would be suitable.

One other hurdle was the requirement that the reactor be made from a refractory dielectric such as quartz. Since it was not necessary, however, for the plasma to be used right up to atmospheric pressure (even 100 torr should be sufficient based on HPCVD work discussed earlier in this dissertation), there was the possibility that simple pyrex could be used. If this were the case, this system simply could not be beaten for low cost, simplicity and accessibility.

The next chapter details the implementation of this APNEP system in our laboratory and the numerous revisions and additions that were required.

4 Development of the Plasma Apparatus

4.1 Introduction

The previous chapter discusses various high pressure plasma generation schemes. It was decided after a lengthy review to attempt to reconstruct an Atmospheric Pressure Nonequilibrium Plasma (APNEP) system. Not only is the system suitable for the task at hand and flexible, but it is simple in construction and cheap to implement requiring only a microwave oven and suitable glassware.

Having decided to use the APNEP system, it remained necessary to determine how this basic idea could be used for the task of MgB_2 thin film deposition. Furthermore, it was imperative to overcome the requirement that the reactor itself be made from quartz. In fact, solving both of these problems proved more difficult and laborious than anticipated. The evolution of the design is documented in this chapter.

4.2 Initial attempts

Creativity took a back seat in the early stages of this design process as it was decided to simply try and implement the design for the reactor as illustrated in the patent application itself (Duan, 1999). The initial design was constructed as in the image below:

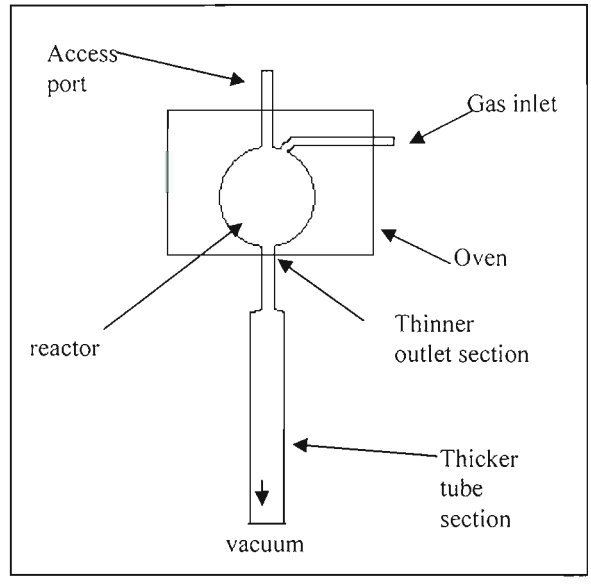

Figure 4-1: First APNEP design based largely on patent for APNEP.

The reactor itself was a 500 mL round flask to which a 10 mm outer diameter (OD), 120 mm long gas inlet pipe was attached. Another 15 mm inner diameter (ID) pipe was attached to the very apex of the sphere. This was 300 mm long and allowed various objects to be lowered and immersed in the plasma (such as initiators or samples). The lower, thicker (40 mm ID, 750 mm long) pipe was used to evacuate the chamber. This was connected to the reactor itself through a thinner, 15 mm ID pipe of length 140 mm. The glass was 2 mm walled, Schott™ Borosilicate.

The thicker pipe did not join directly to the chamber since it needed to pass through the door of the microwave oven. A hole of 44 mm in a microwave oven door is a major radiation hazard. Thus the thinner pipe was introduced between the 44 mm pipe and the 500 mL reactor so that a

smaller hole could be used. The wavelength in the microwave oven is around 12 cm, and thus a 17 mm hole is largely invisible.

The thicker pipe needed to be of such a large diameter in order to allow a substrate heater and substrate to fit inside. This would be where deposition would take place. The MgB_2 thin film deposition experiment was briefly discussed in the MgB_2 literature review and is based largely on the work of Zeng et al. (2002). To reiterate, the basic idea was that boron or MgB_2 would be placed in the plasma reactor. The sample would be etched by the plasma and the resulting boron flux in the gas stream would travel downstream to the heated substrate surface. Magnesium would be heated at the substrate surface producing a high local magnesium vapour pressure. The Boron should combine with the magnesium and form magnesium diboride. This is basically the HPCVD method of Zeng et al. (2002) with the exception that the Boron flux is created by the plasma and does not come from dissociated Diborane gas. The final experiment was envisaged to look as in the following diagram:

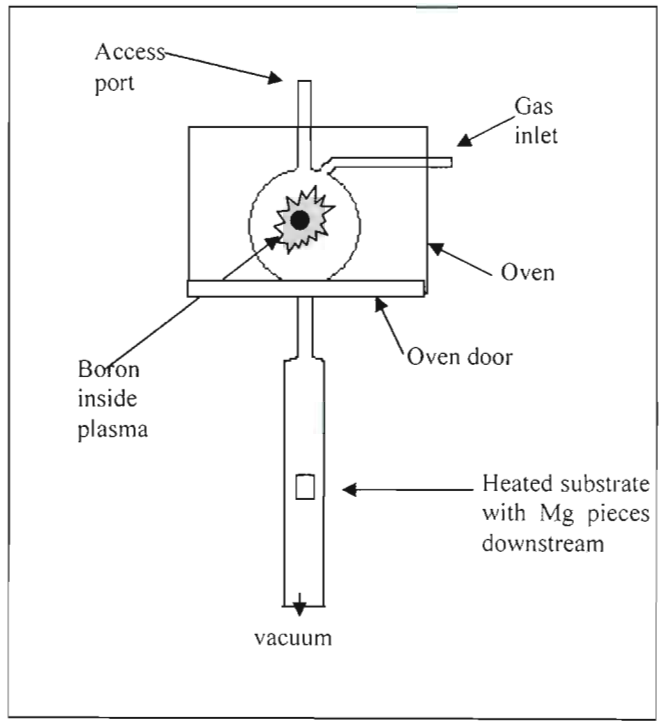

Figure 4-2: First APNEP system would be used to deposit MgB2.

In addition, a mercury manometer was attached to the 44 mm OD tube through high temperature, 8 mm hose to measure the pressure. Realistically, we would like to recommend that others who try to recreate this work use instead a capacitive manometer or some other electronic gauge since the hazards of using mercury proved a terrible nuisance.

The upper part of the glass (reactor, gas inlet and access port) were designed to fit into the microwave oven such that the oven door faced the floor. In order for the access port, inlet pipe and outlet pipe to pass through the oven walls and doors, holes needed to be punched in the screening metal. The radiation leakage from these holes was checked with a microwave oven leakage detector and found to be minimal. The holes were either 16 mm in diameter or 20 mm in diameter.

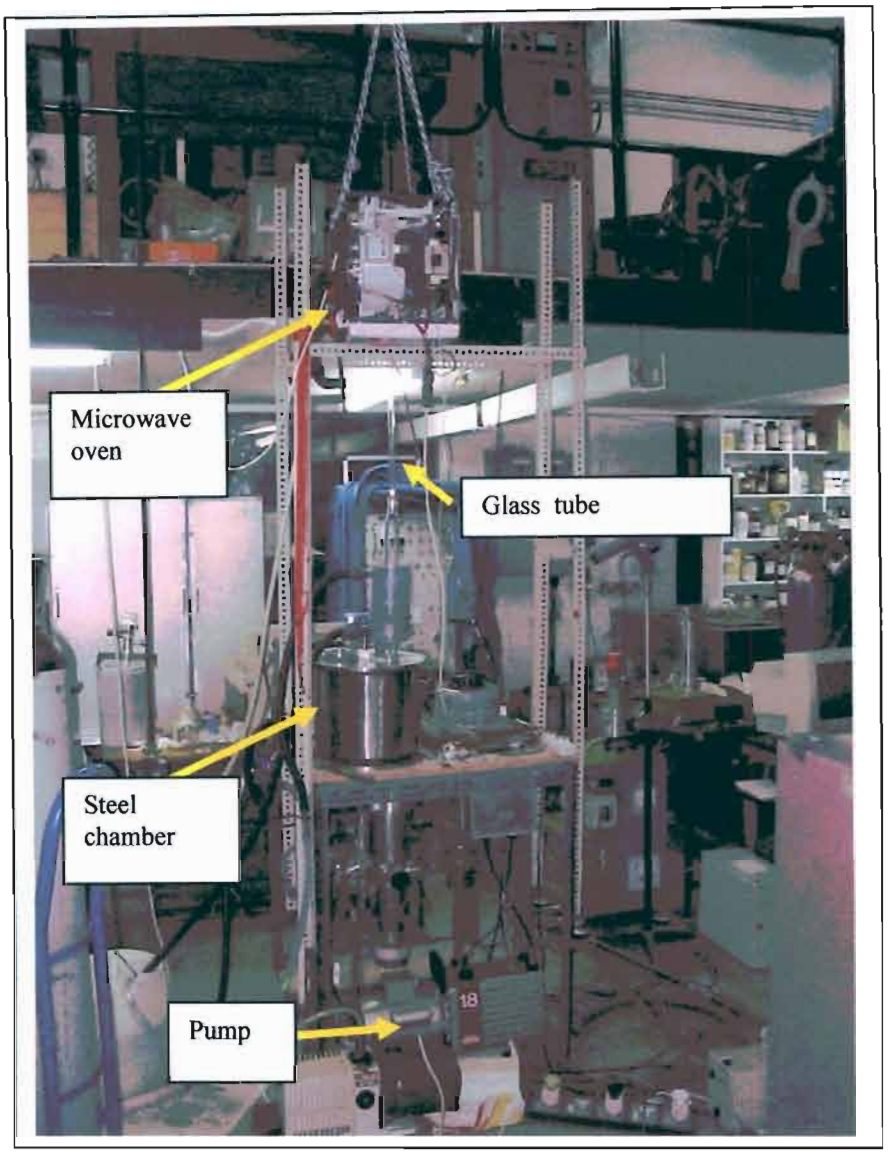

Figure 4-3: Stand for microwave oven with vacuum chamber below.

The oven itself was supported on a frame quite high in the air as shown in figure 4-3.

The microwave oven could be raised or lowered conveniently with a crane to which it was permanently attached.

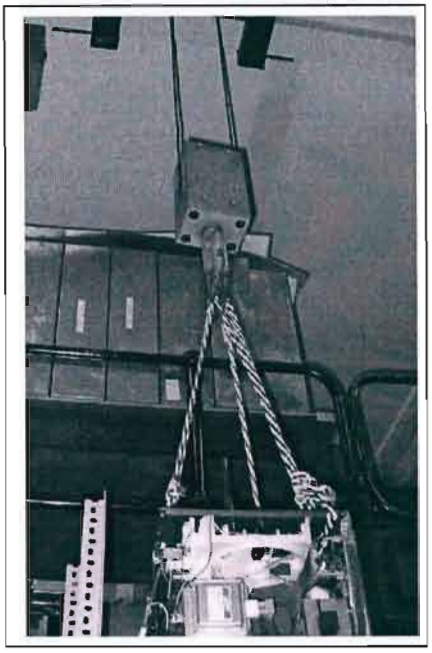

Figure 4-4: Crane supporting microwave oven.

The stainless steel, cylindrical chamber below the oven in the image was a vacuum deposition chamber that had been used in the laboratory before. Because the thicker tube of the glass chamber could be made to fit into it conveniently, it was used as a means to attach the rotary pump (shown in the image). This is completely nonessential and was done simply because it was available and already connected to the rotary pump complete with pressure gauge.

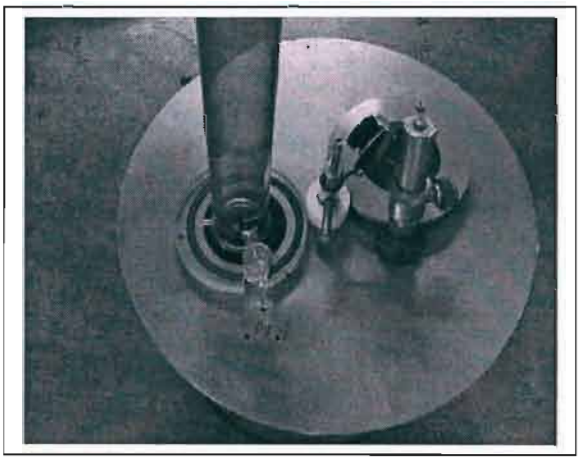

Figure 4-5: The lower section of the glass tube could be made to easily fit into a stainless steel vacuum chamber which was already attached to rotary pump and vacuum gauge.

The rest of the apparatus shown in the image will be discussed in more detail later in this chapter. For now it is the evolution of the glass chamber itself that is important. Before returning to that thread, another view of the microwave oven is shown here.

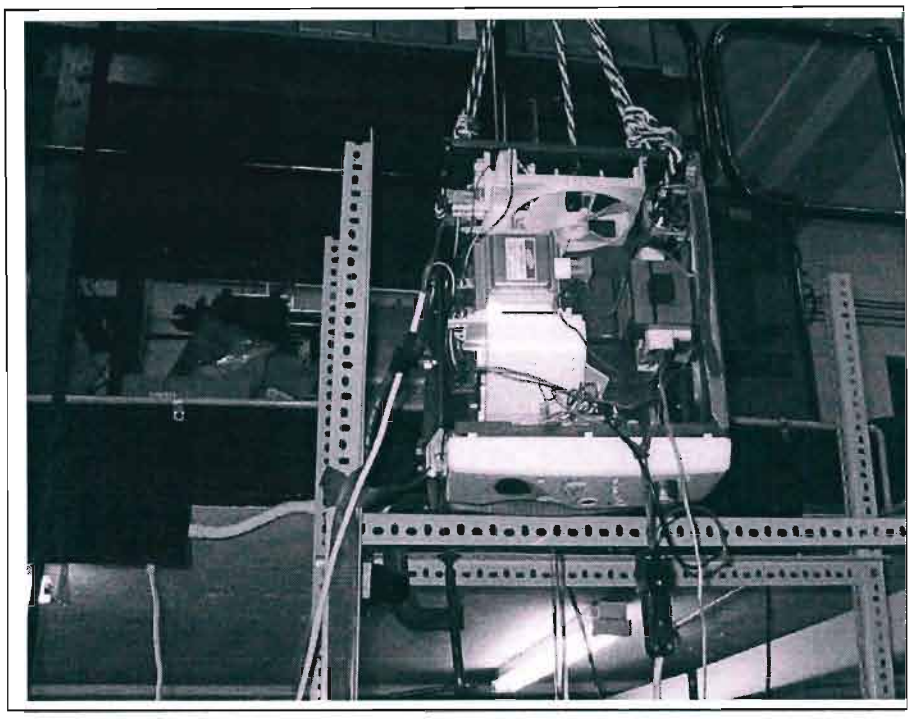

Figure 4-6: Another view of microwave oven. The controls visible were easily accessible from below.

This original glass reactor was far too unwieldy to be used with ease and was broken in short order. Inserting it into the microwave oven and setting everything up was an incredibly difficult task for one person to do. The microwave oven needed to be raised on the crane, then chamber needed to be very carefully inserted into the oven. This was quite difficult to do since it did not fit in directly. The access pipe first needed to be threaded through a hole punched in the top of the microwave (the side opposite the door), and then the gas inlet had to be threaded through a similar hole in the side. Next, the thicker pipe was inserted into the stainless steel chamber. Finally the oven would be lowered and the door sealed. These few words do not express how absolutely difficult it was to perform this operation without breaking anything. What is worse is that every time a sample needed to be changed the reverse process had to take place and then everything had to be done all over again. The probability of smashing glass was extremely high.

4.3 Mark II

Thus it was decided at a very early stage to split the chamber into two: 1) The upper reactor, gas inlet, access port and thin outlet pipe, and 2) the lower thick tube. The two parts were joined using a silicone bush compression fitting.

This made things considerably simpler. The thicker tube would now be permanently connected to the rotary pump through the stainless steel chamber and left in place. Only the upper chamber need be raised, lowered and moved around. Since it was so much shorter and lighter, this presented far less of a problem. In addition, previously the microwave oven door had been cut to allow the 44 mm OD tube to pass through it and then sealed up again (to stop microwave leakage) around the thinner section of tube. This meant the door was permanently attached to the apparatus. This was no longer a problem since now the upper chamber could be threaded through a small hole in the door with ease and without leakage

Figure 4-7: Two halves of the new chamber. The lower, thicker half is dark with a coating from an experiment.

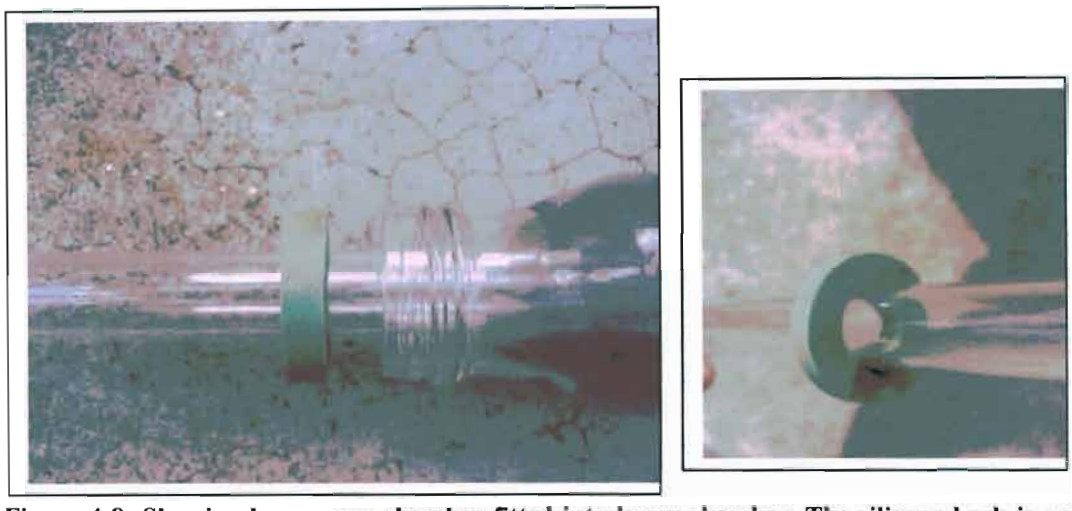

Figure 4-8: Showing how upper chamber fitted into lower chamber. The silicone bush is green in colour.

The plasma was ignited by evacuating the chamber to a point where ignition became spontaneous. This typically happened at around 20 torr. A large, deep purple plasma filled the entire reactor and the inlet and outlet pipes as well. The following image shows such a plasma:

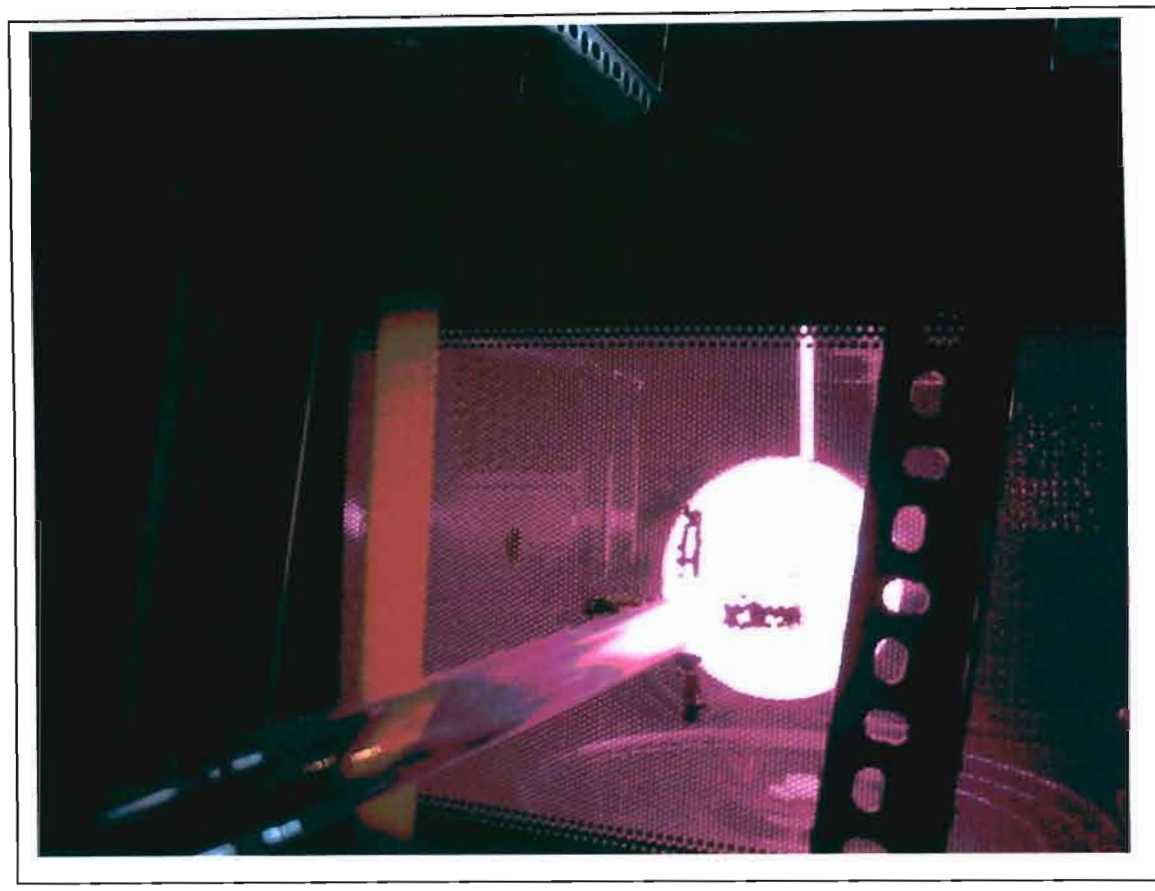

Figure 4-9: Showing low pressure plasma after evacuation and ignition. The purple colour was always present when the chamber was evacuated to low (<20 torr) pressures regardless of what gases had been flowing through before.

Recall that it was decided that hydrogen would make a good etchant. If hydrogen gas were introduced slowly while the rotary pump remained running, the purple colour would remain. As the flow rate was turned up, the pressure began to increase. Increasing pressure caused the plasma to shrink, since there is finite power available. Eventually the purple would become a bit deeper in colour as well. The plasma would slowly shrink to a very small ball (though it was not really spherical). This small plasma would stick to the glass – always in a particular spot, which must be a microwave hotspot – and then rapidly melt its way through[4]. This happened at pressures as low as about 40 torr. Below this, the plasma could run indefinitely. Thus two more problems were immediately apparent. Firstly, it requires much more power to maintain a hydrogen plasma all the way to atmospheric pressure and 1000 W would not be sufficient. This is possibly something that should have been investigated before work began. The fact is that it takes more energy to dissociate hydrogen than, for example, Argon. Comparing the two, hydrogen atoms are strongly bonded to other hydrogen atoms while Argon is a monoatomic gas. When dissociating hydrogen, extra energy needs to be input to the system to overcome the strong H-H coupling (4.52 eV) followed by further ionisation reactions. In argon, there is no inter-atomic-coupling to overcome and the argon atoms are merely ionised. This also means that hydrogen plasma delivers more heat upon impact with a surface (through recombination) than an argon plasma would (England, 2004). Experimentation showed that 1000 W was sufficient to ionise air and argon plasmas all the way to atmospheric pressure. Secondly, it was now apparent

[4] Note that the ability of a plasma to heat an object depends on energy density i.e. temperature and density. As the density of the plasma increases with increasing pressure, the thermal non-equilibrium between electrons and heavy particles diminishes resulting in a highly thermal plasma that can eat through glass.

that pyrex would not suffice for higher pressures unless the plasma could be kept away from the walls somehow. The experiment of Zeng et al. (2002) which we were trying to mimic used much higher pressures (100-700 torr) and thus it was very necessary to remedy this problem in order for the apparatus to be useful.

4.4 Plasma localisation

It was clear that the small plasma ball would always move to the same place on the glass and then 'eat' its way through. It did not float up, as may be expected, but formed on the side of the chamber instead. It was decided that this happened because of hotspots (areas of peak E-field intensity) inside the microwave oven. Domestic microwave ovens are not very well-made multimode cavities and have numerous spots where the E-field is higher than others. A complex standing wave pattern forms inside of them. So, one option would be to improve this characteristic. This is not necessarily a solution, however, since the plasma may still simply float upwards and eat through the top of the chamber. A more concrete means of confinement was needed. Magnetic or electrostatic confinement, however, would be very difficult owing to the microwave oven container (magnets and electrostatic plates could not be placed in the oven) and would complicate the system making it far less simple that intended.

One interesting idea that could be the missing piece was the plasmoid literature discussed previously. Brandenburg and Kline (1998) managed to confine a plasma at atmospheric pressure in a microwave oven using nothing but lowly plexiglass (polymethylmethacrylate which melts at 150°C). Further research at this point on the internet showed that many people, such as J. Naudin (Naudin, 2000) had created 'plasmoids' in microwave ovens as fun, do-at-home experiments. This has already been discussed in the plasma sources literature review. The main point is that these plasmoids were always contained in nothing better than pyrex (although often there were warnings to stop the experiment after a few seconds before the glass got too hot).

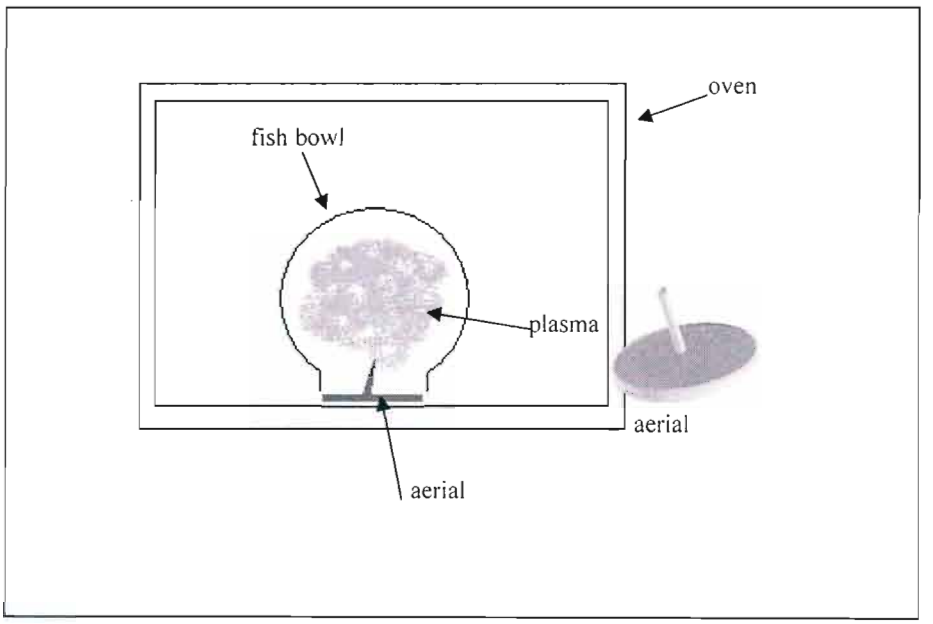

Figure 4-10: One of Naudin's experiments (Naudin, 2004). A small antenna maintains the plasma.

Clearly, somehow, these plasmas by did not cause glass to melt. Either this is because of the vortex motion attributed to them, or else they were cooler plasmas. One of the setups used by Naudin (Naudin, 2004) was particularly interesting insofar as the plasma seemed very stable and fully contained – i.e. it did not hit the top of the container or any of the walls.

The aerial or antenna used in the image above consisted of a 60 mm diameter metal sheet disc with a 30 mm long, thin sharpened graphite rod extending from it. The dimensions were chosen so as to form a quarter-wave antenna (the wavelength in the oven being roughly 12 cm). When this aerial was placed in a microwave hot-spot, it would quickly cause a breakdown which would be fed by the microwave energy to create a plasmoid. The plasma would swirl about the glass surface with a strong vortex motion. The spherical shape of the glass was reported as being important for this effect to occur.

The experiment turned out to be difficult to reproduce. The hardest part is finding a hotspot that will cause the aerial to ignite. If the plasma did ignite, then the plasma would indeed swirl around quickly in a vortex motion, but it stayed very close to the glass and the glass would get incredibly hot very quickly. A student trying some of these experiments at the time reported he had managed to get the plasma to concentrate away from the glass as desired, but this effect did certainly not seem easy to reproduce and we were unable to determine why. The glass would always get very hot during experiments, but did not melt.

Instead of switching over to such a plasmoid-based system, however, it was decided that our implementation of the APNEP could instead rather be changed by simply inserting an aerial into the reactor. It was found that thin metal aerials such as one made from 0.2 mm diameter tungsten wire would arc at their tips when placed in the oven. On the other hand, thicker, less sharp aerials (such as one made from 2 mm diameter molybdenum) would not cause any arcing and would not even be capable of allowing for spontaneous ignition of the plasma. Obviously this is related to the strength of the E-field as concentrated at the tip of the antenna.

Thus it seemed feasible that by placing a 2 mm diameter molybdenum antenna inside the APNEP reactor, the electric field would concentrate at its tip, but arcing would not occur. Arcing would not be desirable since it would cause the antenna to vaporise more quickly. If a slightly thicker aerial could indeed concentrate the E-field at its tip appropriately, then as the plasma shrinks, it should hopefully concentrate there rather than at some random hotspot. This seemed the simpler solution.

To accomplish this, it would be necessary to re-design the chamber (upper part). This was not unwelcome since the method of loading samples into the chamber via the access port had proved cumbersome and tricky.

4.5 Mark III

It was decided that the new chamber should be largely spherical to possibly promote the confinement effect reported by J. Naudin (Naudin, 2004). To further cool the glass, the input gas pipe and output vacuum pipe were attached to the bulb tangentially to encourage gas to swirl about the walls. The chamber comprised a round-bottomed flask, inverted so the neck faced downwards. The neck could be vacuum-sealed with a ground-glass stopper. The aerial and its base could then be placed on the stopper. The following images should make this clear

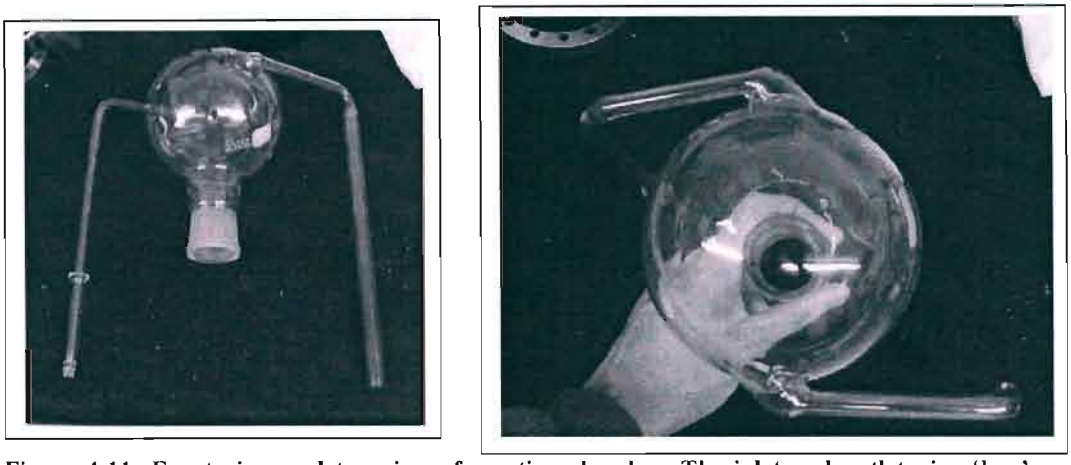

Figure 4-11: Front view and top view of reaction chamber. The inlet and outlet pipe 'legs' are attached tangentially and the ground-glass stopper faces downwards towards the microwave oven door.

The flask was 1L in volume. The outlet pipe was made of a 10 mm OD, 100 mm long, horizontal section which turned a 90° bend and widened into a thicker 16 mm OD vertical section. The vertical section extended downwards for 270mm. The inlet pipe similarly rose vertically for 270 mm and then turned 90° to extend another 100 mm horizontally. It was entirely 10 mm OD. Both pipes were attached to the spherical flask tangentially. The neck of the round-bottomed flask was 20 mm in diameter.

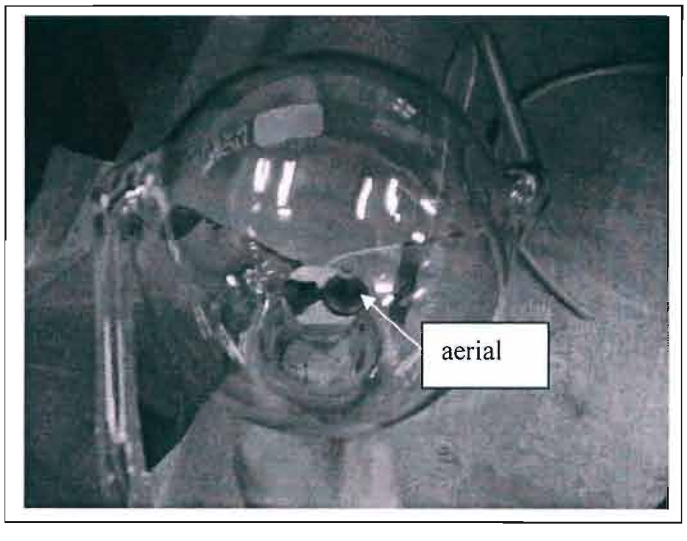

Figure 4-12: Aerial inserted in chamber. It rests atop the stopper.

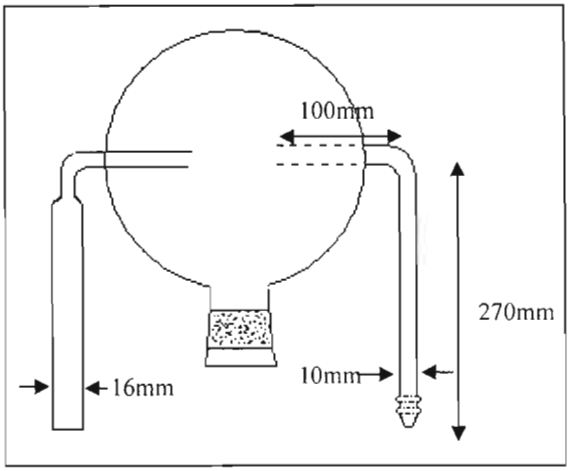

Figure 4-13: Schematic representation of chamber.

The inlet pipe was finished in a ribbed hose attachment.

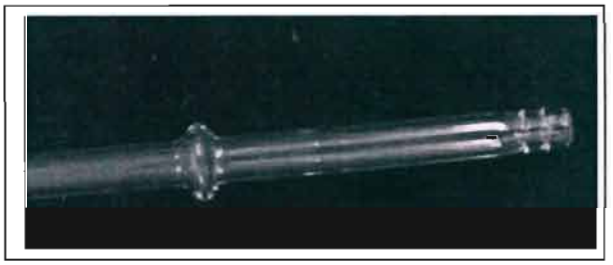

Figure 4-14: 'Ribbed' hose attachment at end of inlet pipe. The widened region visible is to prevent the entire inlet pipe from sliding through a hole punched in the microwave oven door.

The tangential attachment of the pipes actually proved quite useful. One version was made with direct, perpendicular attachments and it was found that the fast rushing air would cause the plasma to flicker terribly and could even affect stability.

The new design meant that now holes need only be punched in the microwave oven door, not in the walls of the oven as previously required. In addition, these holes were negligibly small. A section of the inlet pipe was widened as shown in the above figure. This acted as a stopper to prevent the inlet pipe from being pulled entirely through the door.

Earlier experiments with a plasmoid apparatus had shown that designing a quarter-wave antenna with the dimensions given by Naudin (60 mm diameter base and 30 mm high tip) was actually nonessential. A half-wave antenna (60 mm) with no base work identically, and in fact, the aerial could be just about any height (5cm, 4cm, etc.). Ignition seemed more a function of sharpness of the tip and location in the oven. To this end, the author believes that the quarter-wave antenna was actually simply a sharp point to focus the electric field and any sharp tip would do, in spite of much suggestion to the contrary. This allowed the base to be shrunk to 18 mm in diameter so that it could fit in the neck of the round-bottomed flask. The length of the aerial was kept at roughly 30 mm.

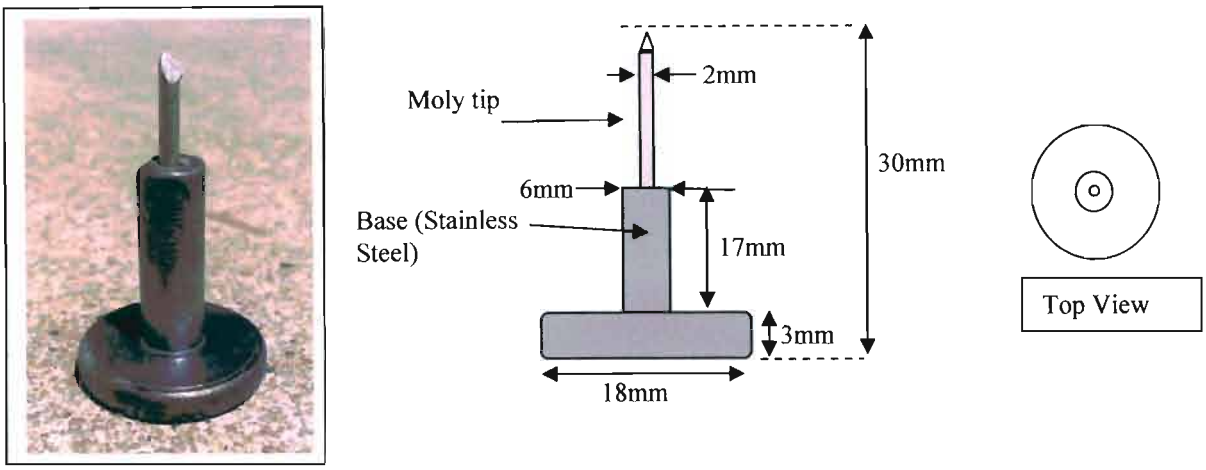

Figure 4-15: Early aerial used to localize the antenna.

The aerial used consisted of a stainless steel base (brass was also used early on) with a molybdenum tip. The molybdenum was cut from a 2 mm rod and sharpened. The base was 3 mm thick and 18 mm in diameter, with a thinner protruding section 6 mm in diameter and 17 mm high. It was milled out of one piece. A 2 mm hole was drilled in the protruding section of the base into which the molybdenum tip was added. The total height was typically about 30 mm from bottom of base to tip or molybdenum. However, as pointed out, this was nonessential and it was more important to ensure that the tip was near a microwave hotspot.

Indeed, this experiment proved a success and the hydrogen plasma was seen to slowly shrink until it sat as a small wisp on the aerial tip.

Figure 4-16:Small hydrogen plasma located at the aerial tip. This was a particularly hot, higher pressure plasma. At lower pressures, the colour is purple and the aerial does not glow such an intense bright orange/white.

However, this was not the end of the various problems. The plasma would often form both at the tip of the aerial and at the base. This was noticed as a side-effect during plasmoid tests as well, where the base would tend to try and arc to the microwave floor. It makes sense, however,

since the E-field would be concentrated at all sharp points. In fact, considering the aerial as a dipole antenna, both ends would contain a maximum field concentration. It was decided therefore to try and round the sharp edges of the base and this did seem to alleviate the problem. It was now possible to make the plasma form entirely at the tip of the aerial. However, at times it would still form around the bottom of the base, eating the glass stopper. For this reason, a glass stand was added to the stopper which would melt preferentially without any dramatic consequences. The stopper neck was also widened to allow aerials with more stable, wider bases to be used.

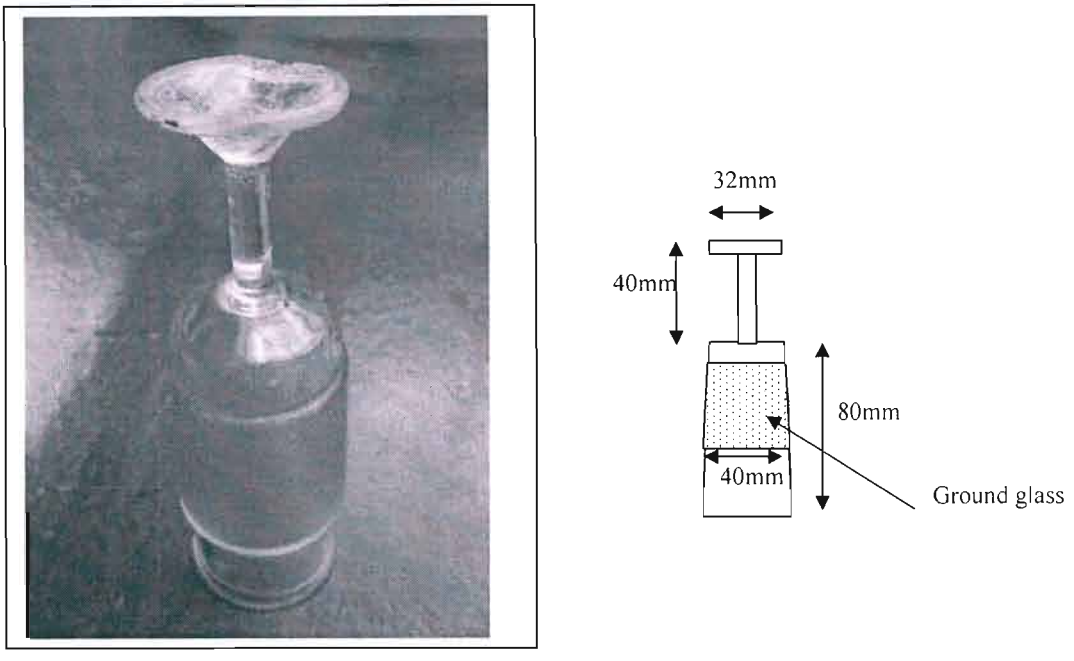

Figure 4-17: A well-used stopper with attached stand. The aerial is placed atop the stand.

It was found that as pressure increased, the plasma would eventually move up to the aerial tip alone. This makes sense as well since at higher pressures, only the stronger E-field will matter. This means that for a given aerial configuration, there was a minimum pressure below which the plasma could not be operated for fear of the glass stopper melting (since the plasma would exist at the aerial base). However, if the pressure went too high then the plasma would be extinguished. Thus the apparatus operates over a narrow window which for the configuration of aerial shown above is about 80 torr to 200 torr in hydrogen flow.

It must be pointed out here that these results pertain to a hydrogen plasma only. Other plasmas, such as Argon, retain their volume and do not shrink to a small ball as the pressure increases. Hydrogen remains uniquely difficult to dissociate. The author lacked the courage and financial backing to test whether a high pressure argon plasma, which filled the whole chamber, would melt the walls or not. It certainly was sustainable for several tens of seconds. In addition, by mixing argon with hydrogen, higher pressures could also be reached. Air would also dissociate right up to atmospheric pressure.

4.6 More localisation and sample loading

In an effort to improve the consistency of operation and the pressures that could be reached while providing a convenient means to load a sample into the plasma, various aerial configurations were tested. The most simple advancement involved sharpening the molybdenum tip to needle-like keenness over a 15 mm section at the top. This did, in fact, allow somewhat higher pressures to be achieved. It must be noted, that when the plasma was small and

concentrated on the tip of the aerial in this fashion, it was extremely hot. The molybdenum tip would glow a brilliant, bright orange and the entire microwave oven would eventually get quite hot to the touch. At higher pressures, above about 140 torr, the whole aerial base would glow very brightly. Alumina melts at about 2045°C and thin alumina rods were melted by such plasmas. In spite of this, the borosilicate reactor never melted (borosilicate is realistically useable up to about 500 to 600°C in a vacuum).

It was interesting to note that aerial position within the chamber had a far more prominent affect than aerial length. The best results (in terms of reachable pressure) were obtained when the aerial tip was near a microwave hotspot. Moving the aerial more than a few centimetres in any direction would alter the stability. This is a nuisance which would possibly be solved with a more truly multimode oven.

It was intended that samples to be etched would be placed in the plasma by sliding a thin alumina tube over the aerial base upon which a piece of Boron or MgB_2 could be placed:

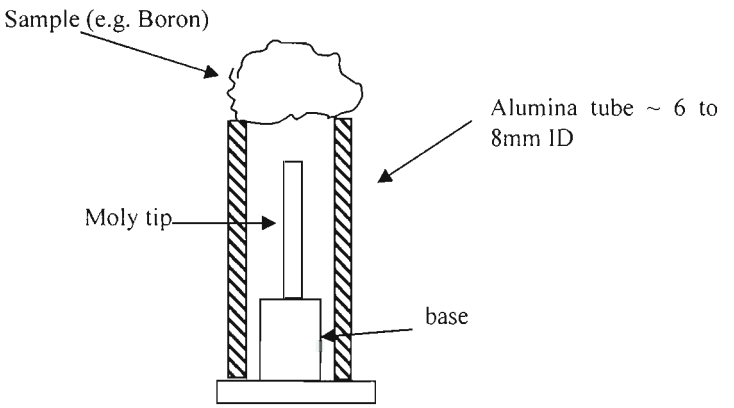

Figure 4-18: Early means of loading sample to be etched into chamber.

One problem with this setup was potential oxygen or aluminium contamination from alumina heating or etching. The molybdenum (Mo) antenna could also add a level of contamination. However, crystalline Boron has a vapour presser of around 10^{-2} torr at 2000°C while Mo has a vapour pressure on the order of 10^{-5} torr. Of course, since it is a plasma process, there is a possibility that etching could increase the flux of Mo in the air stream. But Mo is relatively inert to hydrogen according to most sources (such as (Rembar, metals) in the bibliography) and information on its hydride is quite scarce. Alumina could pose a greater problem, however, especially as a source of oxygen contamination.

Another aerial tried looked as shown in the figure below:

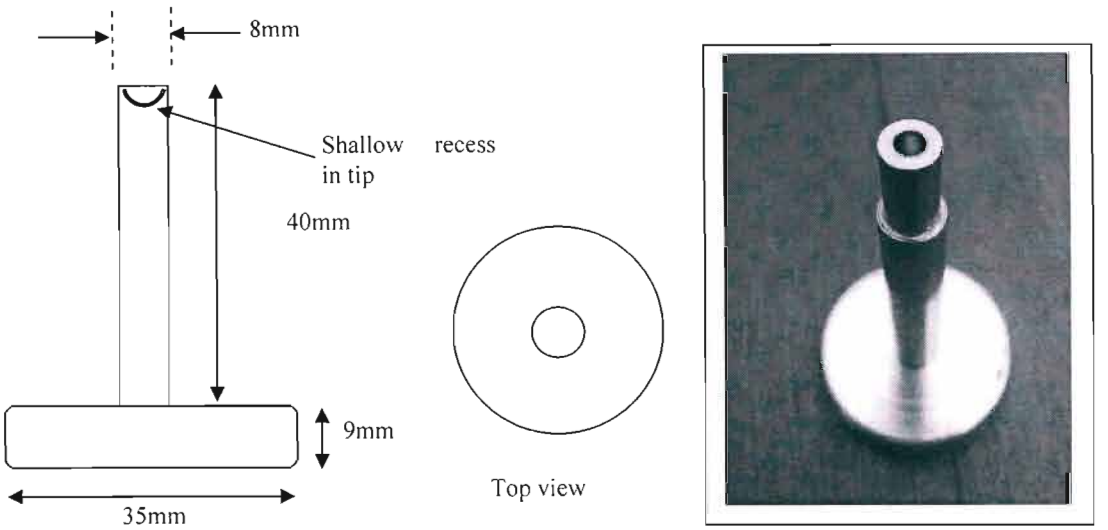

Figure 4-19: A different aerial tried, characterized by a large base and hollow top.

The idea behind this aerial was that the sample (B or MgB_2) could be placed directly in the aerial tip (where the plasma forms) in the small recess drilled out of it. In the case of MgB_2, the sample actually forms part of the aerial since it is conductive. The tip remained relatively sharp on the edges around the tip and could thus still support a high E-field. The big, thick base was primarily decided upon as a means of keeping the aerial from falling over. It was also an experiment to see how a larger base would affect the problem of base-supported plasmas.

The large base proved a big problem. Not only did it absorb considerable heat energy, eventually causing the stopper-holder to crack, but it would always support a strong plasma right up to the highest useable pressures, even though its edges were rounded. This would lead us to possibly question if sharpness alone is the criteria for E-field intensity and perhaps the aerial really does need to be designed as an aerial. Proper design using finite element analysis may be a future option. The evidence against this is that, for example, the initial aerial would work equally well for various lengths. If it truly was working as a dipole antenna or quarter-wave antenna, then it would be very sensitive to length.

In any event, the large base of the above design was scrapped, but the upper section retained. Thus the aerial became a long, 44mm rod, 8mm in diameter, with a hollowed out recess in its tip. To prevent it from falling over, the aerial needed to be mounted in some dielectric material. Soapstone or alumina (or both) were frequently used for this purpose. This allowed direct sample loading and prevented alumina from being immersed in the plasma. Nevertheless, reactive species are not confined to the glow region of the plasma and thus contamination is still a potential problem, but less so than before. The above aerial was made from stainless steel (316 grade) which was determined to be less of a contamination threat since at worst, the metals comprising the steel would form hydrides near the surface. Later experimentation proved that the heat was sufficient to cause vaporisation of the stainless steel and thus a molybdenum version is more prudent, if more expensive.

Another version of the same aerial was made with a much smaller base (27 mm diameter and 3 mm high). This worked very well insofar as it would seldom support a plasma at its base.

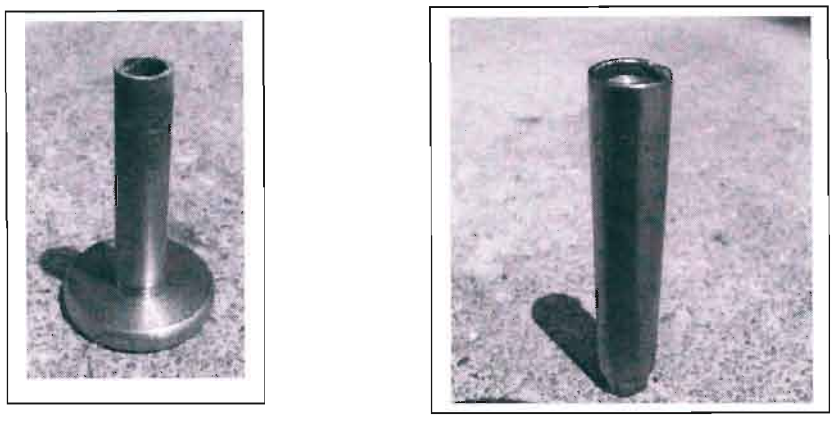

Figure 4-20: Aerial with smaller base and hollow top (left) and aerial with no base (right).

A similar aerial tried was made from thinner rod and with a small hole, not a large recess in its tip.

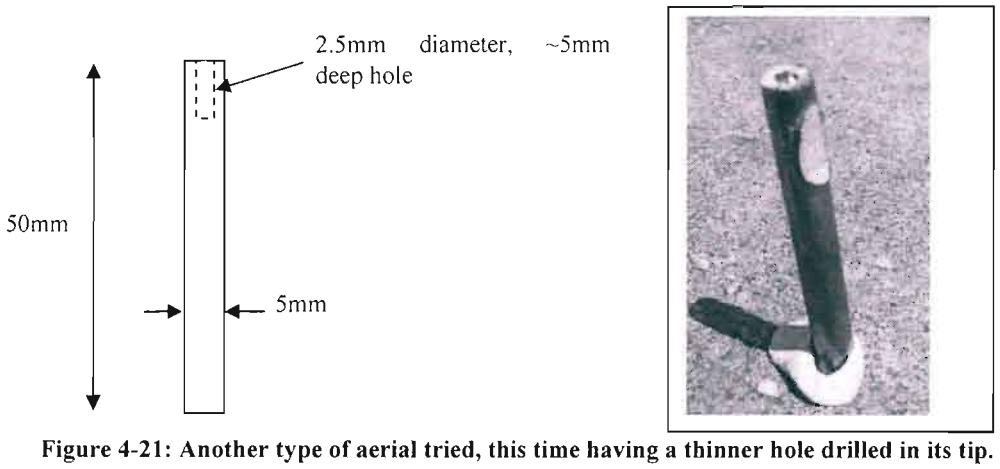

Figure 4-21: Another type of aerial tried, this time having a thinner hole drilled in its tip.

The edges at the bottom of this aerial were often rounded to prevent E-field concentration. The aerial was made from Mo, which has an incredibly low vapour pressure, although a stainless steel version (304 grade) with a 6 mm diameter was also made.

The idea was to insert a 'match-stick' pressed sample of MgB_2 into the hole in the tip:

Figure 4-22: MgB2 "matchstick" inserted into aerial tip, and matchstick pellets used.

The matchstick was pressed from commercial MgB_2 powder (Alfa Aesar, stock number 88149) using a hydraulic press (25MPa).

The total height of the aerial would then be around 60 mm making it a real dipole, ½ wavelength antenna. Again, however, this was not deemed essential.

With all of the above antennas, supporting a plasma at the base was still a possibility. If we consider them as dipole antennas, then it makes sense that the breakdown would occur at each end. However, it was possible to prevent this from happening reasonably often, but not every time.

Cup-type aerials made from stainless steel tube, sealed off at the bottom, were also tried:

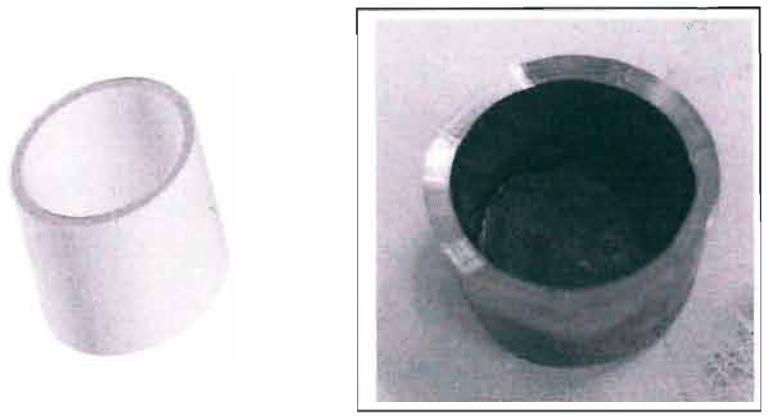

Figure 4-23: Another type of aerial tried. It was essentially nothing more than a 19 mm OD stainless steel tube (304 grade) sealed off at the bottom.

A 12 mm high and ~35 mm high aerial were tried. The longer aerial tended to work better. The idea was that a sample could easily be placed in the aerial, which was really a crucible. Although such a sample may not be inside the glow region of the plasma, it should still be exposed to considerable active species and be quite hot. The upper edge of the tube was sharpened to enhance E-field concentration. The aerial proved as capable as the others in terms of its ability to stabilise the plasma and confine it to a particular area. It also was far less likely to support a plasma at its base. However, these were not used in any actual experiments with MgB_2.

4.7 Other apparatus

Thus a chamber had been developed which could support a plasma at the required pressures. Several other additions to the basic apparatus were made in order to allow experiments to proceed.

4.7.1 Substrate Heater

The basic experiment required a heated substrate downstream of the reactor, inside the larger tube. Zeng et al. (2002) had used a SiC coated graphite susceptor which was inductively heated. We decided to opt for simpler resistive heating. Molybdenum wire of diameter 0.8 mm was wound into a tight, flat, "pancake" coil. The diameter of the coil was kept to roughly 20 mm.

Figure 4-24: Photo of one of the molybdenum coils made.

The ends of the coil wire were attached to stainless steel rods which supplied the current. A voltage was applied to the coils by means of a 1.12 KVA, 80 A, 14 V step-down transformer. The transformer was connected to the mains through a variac so that voltage (and hence current) to the coil could be altered smoothly. The transformer output connected to the heater coil through two stainless steel, threaded rods which were held in a vertical position by mild steel stands.

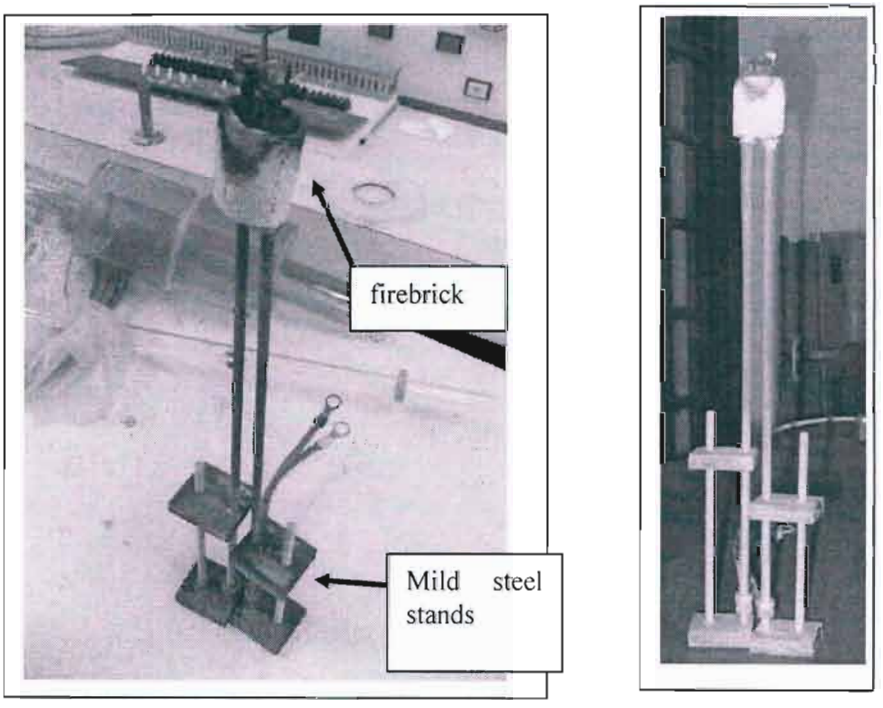

Figure 4-25: Stainless steel rods supported by mild steel stands. The coil is placed at the top of the rods.

The stainless steel rods are 6 mm in diameter so as to have minimal resistance. They rise 40 cm high. Bolts passing through the floor of the stainless steel chamber provide electrical connection between the outside of the chamber (open air) and the inside (vacuum). The vacuum is maintained with Teflon washers. Stainless steel hexagonal nuts clamp the coil to the ends of the stainless steel rods.

In order to prevent the heat of the coil from dissipating excessively down the stainless steel rods, a thin molybdenum disc of roughly 25 mm diameter is placed below the coil, above the tops of the rods. It is insulated from the rods themselves using a 'firebrick' chalk-like spacer. The spacer and molybdenum heat shield are held in place using a firebrick cylinder.

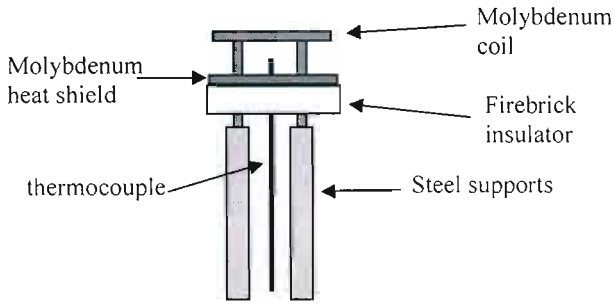

Figure 4-26: Schematic of molybdenum heat shield supported on firebrick. This prevented excess heat from spreading to the steel supports.

The firebrick cylinder also surrounds the coil. It does not provide any real heat insulation, however.

By varying the voltage applied to the coil, the temperature can be smoothly changed. Typically the coil is heated to temperatures between 600°C and 1100°C. Temperature is measured by way of a type-K thermocouple which is held in position just below the coil itself. A hole is drilled in the molybdenum heat shield, insulator and firebrick sheath to allow the thermocouple to pass through.

Recall that it is desirable to place atop the substrate heater not only the substrate to be heated, but also some solid magnesium. Heating the magnesium raises the local magnesium vapour pressure, allowing MgB_2 to be formed.

Magnesium filings (99.98%) were purchased from Sigma Aldrich to supply the magnesium vapour. Filings are considerably cheaper than magnesium ingots. To prevent them from blowing away in the hydrogen gas flow, the filings were compacted into small, 13 mm discs, typically 1 mm to 3 mm thick. The filings were compacted using the same hydraulic press mentioned previously using a cylindrical compactor.

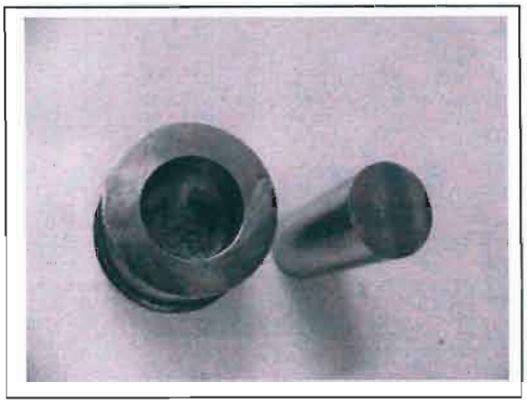

Figure 4-27: Die pieces used to press magnesium disc-shaped pellets.

The compacted discs could still be blown away, however, and thus they were inserted into a thin, stainless steel (grade 316) holder. The holder was a disc, 16 mm in diameter and 2 mm thick. A 13 mm diameter circle was milled out of the centre to accommodate the magnesium discs to a depth of 1.2 mm.

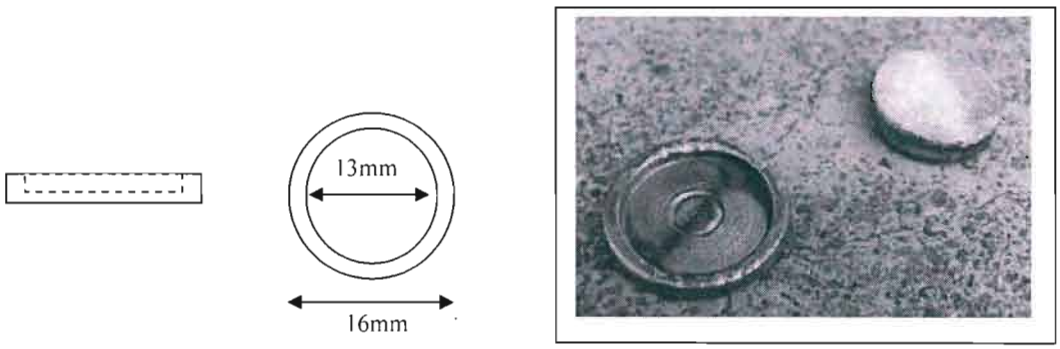

Figure 4-28: Magnesium disc and holder.

The substrate, which was typically a small piece of alumina film 0.7 mm thick and roughly 3 to 5 mm across, was placed directly atop the magnesium disc.

4.7.2 Cooling

If the coil were to be heated to such high temperatures as 1000°C, then the borosilicate tube surrounding it was in danger of softening or at least cracking after many heat/cool cycles. 600°C was the maximum realistic working temperature of the borosilicate, and although the coil was not touching the glass, and the low pressure and flowing gas would provide some isolation and cooling, it was decided that extra cooling of the glass walls would be desirable.

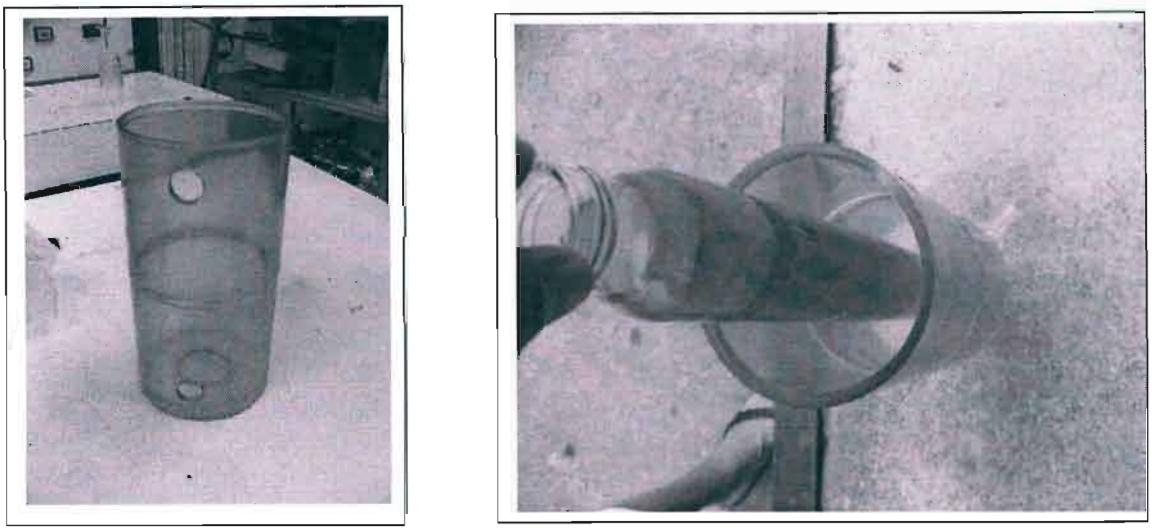

Figure 4-29: Showing photo of PVC tube that was used to cool glass.

To this end, a transparent, light blue PVC tube was placed around the borosilicate glass tube. The PVC tubing was 11 cm OD and its walls were 5 mm thick. The height of the tube was 21cm. The top of the tube was left open, while the bottom was sealed with a 10 mm thick Perspex disc which was machined to fit tightly into the PVC tube and then made water-tight with silicone. A hole was cut in the Perspex bottom, 44.5 mm in diameter. An o-ring was fitted into the centre of this hole to provide a watertight seal to the 44 mm glass tube.

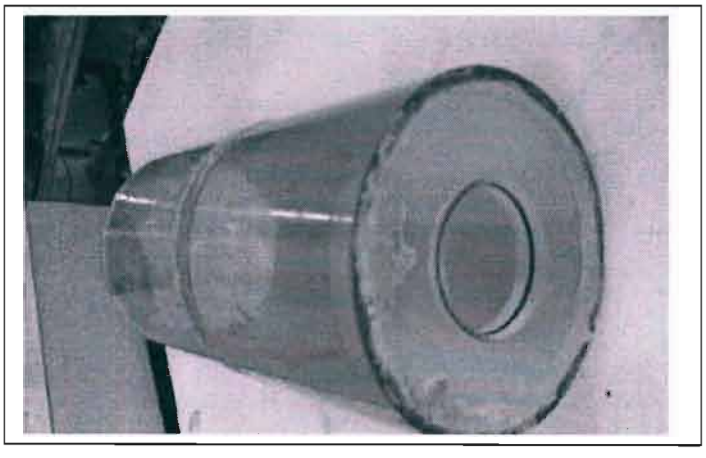

Figure 4-30: Photo of Perspex disc with o-ring inside.

Thus the entire PVC tube could be filled with water. To prevent this water from overheating, it was constantly recycled from a 25 litre drum. A standard garden submersible pump would pump water from the 25 litre drum through clear hose (PVC). The clear hose was connected to more easily flexible 'concertina' hose (the kind used in most vacuum cleaners) which attached to the blue PVC tube through a hole cut in its side, near the top.

Water was allowed to flow out of the PVC tube through another hole, situated near the bottom of the cylinder. The flow rate could be controlled with a PVC ball-valve tap. Water leaving the

cylinder ran down more concertina hose back into the 25 L drum. This cooling solution allowed the coil to be run to temperatures as high as 1200°C for very long periods (many hours).

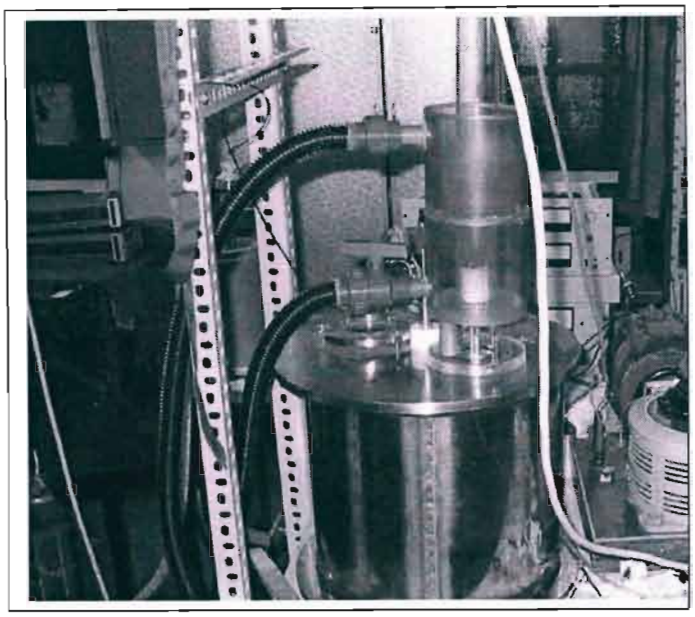

Figure 4-31: Cooling system. Water is piped in through the upper tube and released through the lower. The concertina hose is black in colour.

4.7.3 Microwave Power Control

The power is supplied to the magnetron of the microwave oven through a step up transformer, the primary of which is typically connected to the mains.

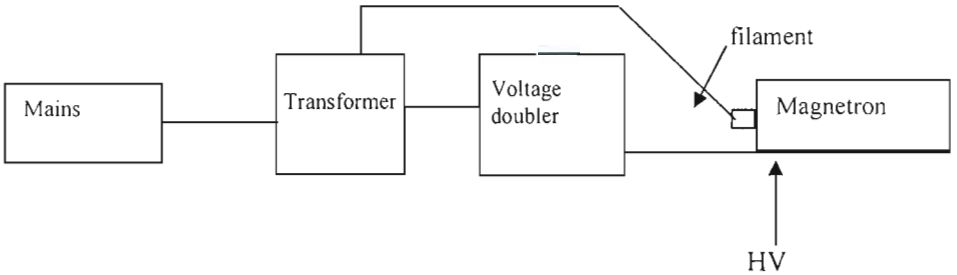

Figure 4-32: Schematic of power supply system to a commercial microwave magnetron.

The transformer steps the mains up to roughly 2 kV, from where it passes through a voltage double (which also serves as a half-wave rectifier) to provide a 4 kV, half-wave rectified waveform to the HV side of the magnetron. The filament of the magnetron is powered from a tap on the transformer at about 3 V. By inserting a variac between the mains and the transformer primary, the voltage to the magnetron can be changed. This allows for smooth output power control. It must be noted that domestic microwave ovens do not vary their power levels smoothly. Power is rather controlled by pulsing the magnetron on and off for variable duty cycles. When the magnetron is on, it is always operating at full power. Certain domestic ovens such as some Panasonic varieties ("over-the-range" models) do actually vary power smoothly. However, these are expensive and in fact unavailable in South Africa.

The variac does change the filament voltage as well, and thus has a finite extent of control. However, this solution was found to work quite adequately for our needs and it was found

during experimentation that there was seldom a need to change power in any event since hydrogen took so much power to dissociate.

4.7.4 Second Magnetron

Because the plasma was so small under hydrogen flows at higher pressures, it was decided to add a second magnetron to the oven. An entire new oven is not an expensive item. A 900 W oven was bought for only R500, from which the magnetron and attaching waveguide were duly cut. The 4 kV power supply was also removed to be used again. The waveguide was then reattached to the Samsung 1000 W microwave oven we had been using. It was attached quite simply by riveting and then welding it to the wall opposite the door. There was some concern over how well this would work since microwave coupling can be a tricky business. However, the attaching waveguide was designed (by the manufacturers) to open up directly into a very similarly-sized cavity, and thus it would theoretically work.

Using multiple magnetrons actually has the effect of smoothing the E-field distribution inside a multimode oven (Metaxas and Meredith, 1983). It was of concern, however, that this would mean the hot spots would move, making the already-designed aerials less effective.

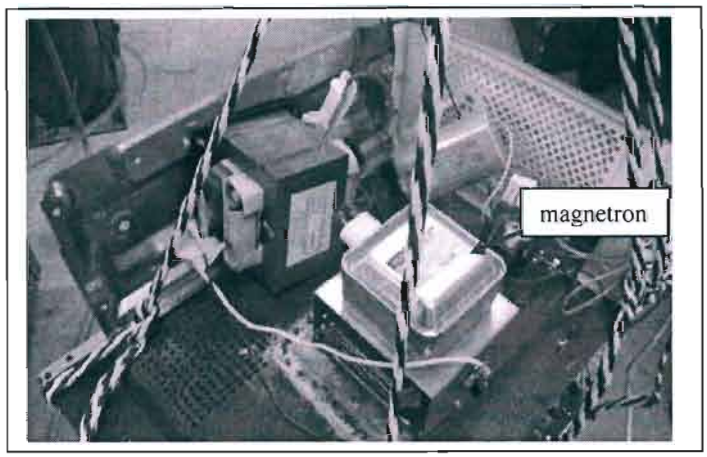

Figure 4-33: Extra magnetron with cooling fan and associated power supply.

The extra magnetron did indeed provide a helpful power jolt, raising total applied power to a theoretical 1900W. Power level was estimated by measuring how long it took to heat a litre of water to a specific temperature and it seemed as though power was actually close to 1500W. When the second magnetron was switched on, the hotspots did indeed move and it was found that a plasma would be more easily supported closer to the top of the chamber (i.e., closer to the second magnetron). In addition, an odd effect was that the second magnetron provided considerable increase in volume of the plasma at lower pressures, but at higher pressures this effect was barely noticeable. Using both sources did provide a way to make a truly intense plasma using a mixture of argon and hydrogen. However, in the end the second magnetron was seldom used in real experiments, but it remains a very cheap way of easily adding extra power. Adding even more magnetrons should smooth the E-field further. However, considering the poor design of the average cavity it is uncertain if this will really happen.

4.8 Conclusion

The apparatus evolved to its present form over some time as problems were systematically encountered and overcome. In the end a system was arrived at which allowed for the creation of a plasma in hydrogen at pressures as high as about 200 torr. Using argon mixtures, a plasma

could be sustained up until atmospheric pressure. The plasma was successfully contained away from the borosilicate chamber walls by the addition of an aerial into the chamber. This allowed low-cost borosilicate glassware to be used for the reactor vessel instead of considerably costlier quartz.

In the end a complete system was built up including substrate heater and glass-cooling solution which allowed the MgB_2 experiments described in the next chapter to be carried out. The design and implementation of this apparatus constituted a significant part of this work.

5 Experimental: Thin Film Deposition

5.1 Introduction

This chapter describes various experiments performed and results obtained for the MgB_2 deposition experiment outlined previously in this dissertation. The experiments were unsuccessful and abandoned to focus on the more promising nanotube work. To this end, this chapter serves only to document the process.

5.2 Early work

Before an aerial had been installed in the chamber to localise the plasma, a few experiments were carried out at low pressure (typically 20 torr). It was quickly determined that these processes would simply not suffice. Briefly, pure boron crystals (Alfa Aesar, 99.5%) or MgB_2 'matchstick' pellets were loaded into the original plasma chamber from above.

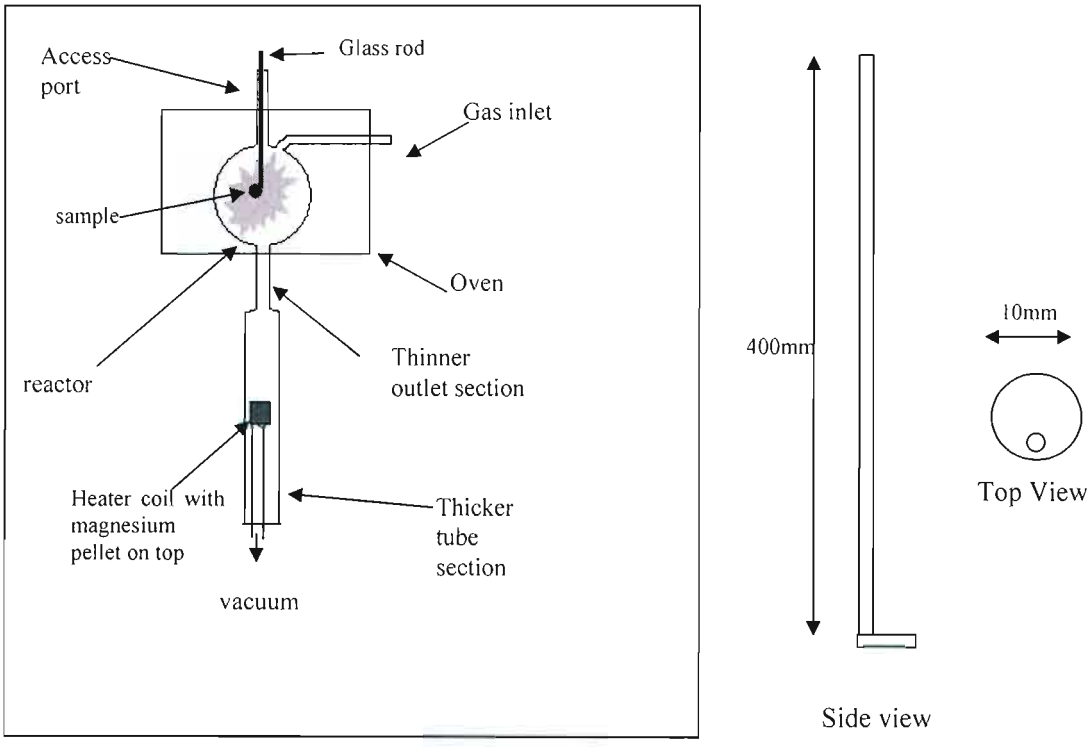

Figure 5-1: Early samples were loaded into chamber, with sample holder (borosilicate) on right.

The matchstick pellets were produced by pressing commercial MgB_2 powder (Alfa Aesar) into a 2 mm wide, 2 mm high, 10 mm long cavity using a hydraulic press.

Figure 5-2: MgB2 'matchstick' pellets. Each is 2x2x10 mm.

The vacuum was provided via an Edwards 18 rotary pump. There was no means to measure hydrogen flow rate, but it was exceedingly low (and at times nonexistent) in these experiments owing to the fact that even a mild pressure increase to about 40 torr would melt the chamber.

In spite of the very low pressure (typically less than 1 torr to a few torr), when Boron was loaded into the chamber, it would glow a bright orange after a time indicating that at least the plasma was having a heating effect. The glass walls tended to heat up to about 200 to 300°C at these low pressures. The microwave was always run at 1000 W (full power).

When an MgB_2 sample was introduced, the plasma in the immediate vicinity of the MgB_2 would glow a bright green. Following observations from the PLD papers discussed in the review on MgB_2 thin film deposition, this was believed to be the colour of magnesium plasma. This was at least evidence that some Mg vapour was finding its way into the gas stream. The colour would slowly fade and then disappear as Mg content was lost.

However, there was no point in continuing these experiments if pressure could not be raised and this was made the first priority. After plasma confinement had been achieved by using a molybdenum aerial, experiments continued.

5.3 First attempts

It was decided that it would be difficult and unwise to attempt to conduct the whole experiment from the start. This is because it could be that a suitable Boron flux was created, but there were problems with the Mg vapour and substrate control leading to no MgB_2 deposition. There would be no way of telling at which end the problem occurred. Thus some method was needed to determine if boron or MgB_2 would etch, and if the etch rate were sufficient.

Unfortunately, this is quite difficult to do. Boron is a notoriously difficult element to detect owing to its light mass. *In situ* spectroscopy would have been ideal, but was not possible. It was considered that we could weigh samples before and after etching, but this is not a good route to follow. First of all, it is useless for MgB_2 since there will definitely be Mg loss due to thermal processes regardless of how well the etching may work. Secondly, considering the rates of etching reported in the literature (0.65 nm/minute of cubic Boron Nitride by Reinke et al., 2000) and the lightness of boron atoms, this did not seem feasible for pure Boron either.

It was decided that we should attempt boriding of a suitable metal. Metals like tungsten will form borides in the presence of Boron when heated to high temperatures (over 1000°C). Thus, if we could form WB on a tungsten wire (or MoB on a molybdenum wire), we would know that thin films could be deposited.

The apparatus already allowed for a coil to be heated in the reactor exhaust stream, so the only difficulty was in suitably loading the sample to be etched. The various means of loading a sample into the chamber were discussed in the previous chapter. At first the sample was placed at the end of an alumina tube which encased the top part of the aerial:

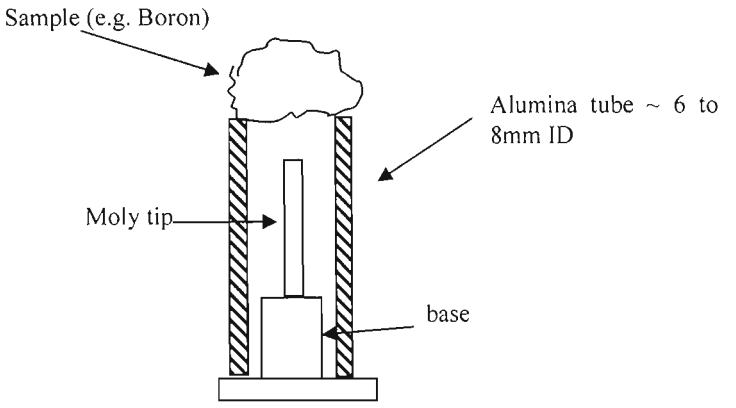

Figure 5-3: Early samples were loaded.

However, it seemed that this would cause oxygen contamination. This was suspected because of changes in the plasma colour when it came into contact with alumina (it turns orange) and the fact that white deposits could be found on the MgB_2 samples: the colour of MgO.

It is because of this that the stainless steel or molybdenum aerials with hollow tips were developed, as discussed in the previous chapter. However, a white coating could still be seen on samples. It is suspected that in these instances the coating may actually be evaporated metal since oxygen contamination should be quite low.

The system was evacuated to under 10 torr at which point the plasma could spontaneously ignite. The microwave power was always 1000 W. After this, hydrogen flow rate was gradually increased until the purple plasma shrank to be situated at the tip of the aerial. This typically happened at 80-100 torr although pressures of up to 200 torr were usually reachable.

Again it was observed that MgB_2 samples surrounded themselves with a green plasma within the larger, purple, hydrogen plasma. At times, a pale blue plasma could be observed, though this was rare. As discussed in the literature review, pale blue was considered to be indicative of a different Mg species and the colour change occurs with pressure change (in PLD). The blue plasma was seldom observed. Boron crystal samples would glow brightly from heating.

No boron was ever detected on a heated coil, even by Inductively Coupled Plasma Mass Spectroscopy (ICP-MS). This was discouraging, but it was decided that the problem could be that it was more difficult to boride such a wire than expected, perhaps because of rising air caused by the high heat of the coils.

5.4 Second Attempts

It was decided then to try the full experiment in spite of the earlier decision not to do so. Boron should react easily with Mg vapour and thus even if superconducting MgB_2 did not form, it should be possible to detect the presence of Boron somewhere, in some concentration.

Mg filings (99.98%, Sigma Aldrich) were pressed into a 13 mm diameter disc, 1 to 3mm high as described in the previous chapter. Such a disc would be placed in a stainless steel holder as pictured below.

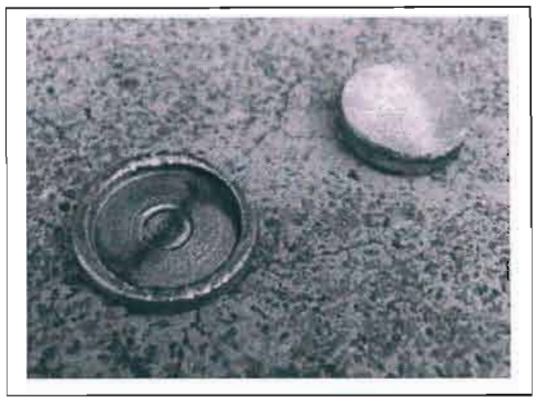

Figure 5-4: Stainless steel holder (left) and pressed magnesium disc (right).

The holder was placed directly on top of the coil, with no electrical insulation, and a small piece of alumina substrate, roughly 4 mm x 4 mm was placed on top of it. Figure 5-1 schematically illustrates the final setup, aspects of which were illustrated clearly in the previous chapter.

After loading an MgB_2 sample for etching into the plasma chamber by means of a hollowed aerial, the chamber was evacuated and the plasma ignited. Again, hydrogen flow rate was slowly increased so as to stabilise the plasma at the aerial tip at around 80-100 torr. At this point the MgB_2 sample would react violently for a short time, letting off a bright glow. This lasted very briefly and is thought to probably be due to violently evaporating magnesium. After a few seconds, a stable, green glow formed around the MgB_2 sample within the purple of the hydrogen plasma. This would last for some time, but would eventually diminish as the sample became Mg deficient.

After the plasma had been shrunk to be situated at the tip, current through the substrate heater coil was slowly increased by increasing the voltage supplied to the step-down transformer. This process continued until temperature of the coil stabilised to 700°C to 1000°C, depending on the experiment. Several temperatures were tried. It was simple to maintain a constant temperature without a need for any sort of control system as long as flow rate was not altered. It is important to heat the coil after the hydrogen is already flowing because the flow rate affects the coil temperature. In addition, if magnesium is heated in a high vacuum, it will very quickly coat all the walls of the apparatus.

It was found that a black powder was deposited on the walls of the thick section of the reactor. The deposit began in the region surrounding and below the coil, and slowly extended right up the length of the glass. This was an indication that the flow rate and pressure were too low for the substrate temperatures. Indeed, lowering the pressure and flow rate would result in a very quick deposition of magnesium all over the chamber while if pressure was increased the spread would be very slow. In spite of this, for relatively high flow rates, boron should mix with the magnesium in the deposition somewhere if the etch rate were high enough (the coating of the wall could take several minutes). This powder was analysed using ICP and found to be mostly magnesium, with negligible Boron content (in the parts per million range). There was oxygen contamination, and contamination from iron (from the aerial) along with other trace impurities. In fact, trace impurities that had no place in the reactor were detected in levels exceeding the boron concentration. This was disappointing. The total concentration of impurities generated in the chamber significantly outweighed the concentration of boron – which for all intents and purposes was not present.

The experiment was re-run using different pressures and temperatures, but never met with any success.

5.5 Discontinuation

At this point, time was quite limited and much remained to be done in other areas of this project. To this end, this line of experimentation was abandoned in favour of the more promising nanotube work.

Even though parameters such as pressure and flow rate were hardly optimised to the point where thin film deposition should have been possible, the complete lack of a boron deposit was indicative of the fact that the boron etch rate was simply too low to make the process viable. Even a few percent of boron present in some product would have been hopeful.

It remains uncertain as to exactly why these experiments met with such a decided lack of success. Based on the literature, and indeed, simply considering the thermal nature of the plasma, it is only reasonable to conclude that some boron should come off the sample.

It is hypothesized that in fact boron was indeed removed. However, the vapour pressure of boron is very low even at the high temperatures of the plasma (only $1x10^{-2}$ torr at 2027°C according to [USC, 2004]) and the etch rate is probably also much lower than we would have hoped for. To this end, the small boron flux would have been completely overwhelmed in the high ambient pressure and would probably have almost entirely been deposited in the glass tubes on its way to the substrate.

Realistically, there does not seem to be a simple solution to this problem. Merely moving the substrate and its heater closer to the chamber does not seem the route to go since it is unlikely it could be moved close enough. The only possible solution is to perhaps put the substrate directly inside the plasma reactor, but just beyond the glow region, above the aerial. The following image shows this setup:

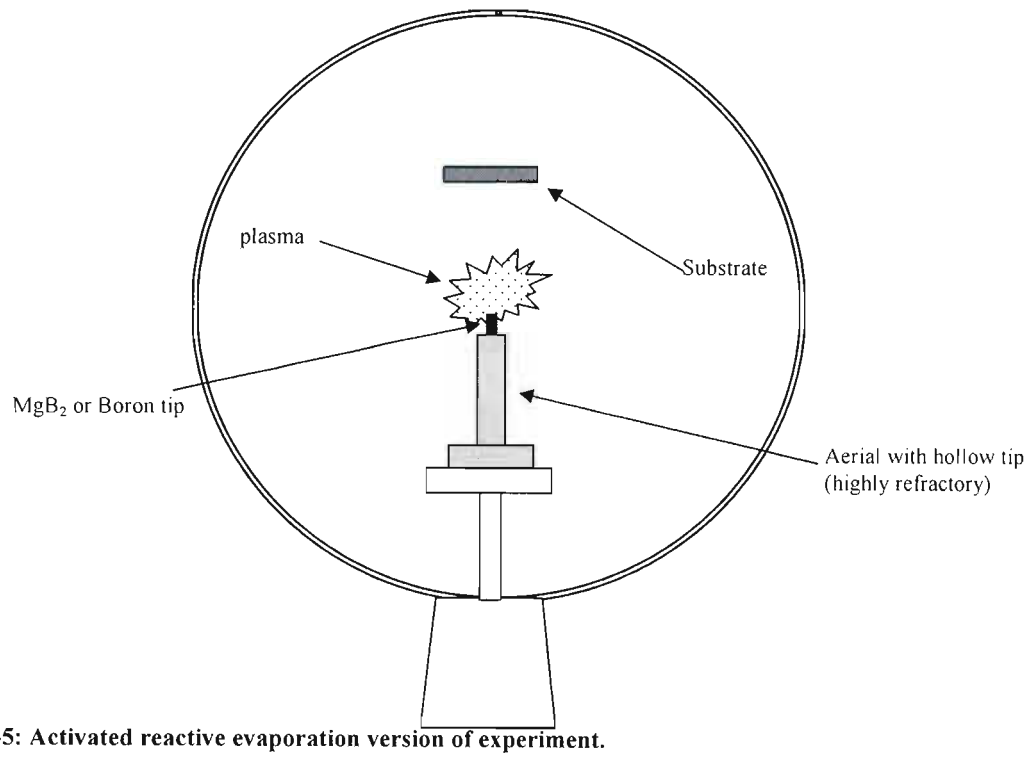

Figure 5-5: Activated reactive evaporation version of experiment.

This is an example of what is termed activated reactive evaporation (ARE) – a variant on plasma enhanced chemical vapour deposition where vapour from a heated sample is activated (broken into ions and active species) by passing it through a plasma.

Later experiments showed that we could make the plasma hot enough to soften alumina, which melts at around 2000°C. The addition of argon could allow for even hotter plasmas. Thus thermal evaporation of boron is possible. The antenna/sample holder would need to be made out of a suitable substance with an even lower vapour pressure and higher melting point than boron such as tantalum. It would be more prudent, however, to make the entire aerial out of MgB_2, which is a good conductor. This would eliminate impurities from the aerial as it stands now.

Nevertheless, this does not seem a promising route since the substrate temperature cannot be independently controlled inside the microwave oven. The whole experiment would also be difficult to setup and it is unlikely that film quality would be high. The method certainly would have no real advantage over the HPCVD method on which our original idea is based.

There were other ideas, such as generating diborane gas from the reaction of HCl and MgB_2, going back to the heat-pipe method, or some other dual PVD approach. However, in the end this whole line of work was dropped to concentrate on other projects. It would be interesting to see in the future if a high enough Boron flux could ever be generated this way, but this seems unlikely.

6 Carbon Nanotubes

6.1 Introduction

Even the most non-'tech-savvy' of people at the time of writing will have heard the now ubiquitous catch-phrase 'nanotechnology'. At the present time, nanotechnology is considered by many to be the gateway to the next great industrial revolution. Though some consider the great claims of the nanotechnology industry proponents a little far-fetched, by-and-large it is being taken quite seriously indeed. In 2000, the White House nearly doubled its nanotechnology R&D investment to half a billion dollars. This year (2004), President Bush increased that same investment to some $3.7 billion dollars. It is beyond the scope of this document to review the nanotechnology industry and its promise as a whole. However, it is worth at least considering this great promise to understand why methods for the production of carbon nanotubes have fostered such great interest since its inception.

Nanotechnology can quite broadly be defined as technology relating to the production or use of devices on a nanometer scale. The initial idea has been attributed to the great physicist Dr. Richard Feynman in a seminal speech in 1959 (Feynman, 1959). Here Feynman proposed the miniaturization of machines, devices and computers down to near-atomic scales. The central theme of his vision that created the early excitement about nanotechnology involves countless nanoscale factories, which use nanomachines to build complex products and materials – including more nanomachines.

The actual major developments of nanotechnology are decades away (at least) and are the stuff of Isaac Asimov's dreams: nano-scale robots or production lines that can build up remarkable materials one atom at a time, or even live in your body keeping it strong and well; fibers stronger than hardened steel but light as cotton; gene-therapy and drug delivery systems that can target the most lethal of ailments with endless precision and efficiency; and of course – a roll-back of Moore's Law well into the next century. Quantum computing, space-elevators, micro-batteries and materials with unheard of properties: one wonders at times reviewing such literature where the fiction ends and the science begins. However, it is relatively safe to say that the science of manufacturing devices on an atomic scale will certainly have a large impact on our lives although most probably not in the near future.

Within the realm of nanotechnology, Carbon Nanotubes (CNTs) have received considerable interest over the last decade. These tiny, 'one-dimensional' rolls of graphitic carbon have become something of a subset of nanotechnology. It is envisioned that nanotube-based products will be a booming industry by itself in years to come, but for now at least they are decidedly interesting for their chemical, electrical and physical properties.

6.2 Discovery

The excitement about the future of nanotechnology really gained momentum with the discovery first of fullerenes in 1985 (Smalley et al., 1985) and then of carbon nanotubes in 1991 (Ijima, 1991). Although Ijima is often credited with the discovery of nanotubes, they were in fact noticed in the 1970's by Morinobu Endo as part of his PhD studies at the University of New Orleans in France (Dresselhaus et al., 1998).

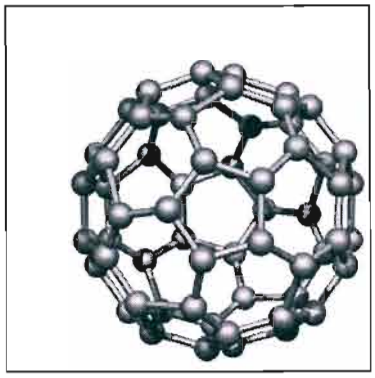

Figure 6-1: C60 'buckyball'.

Fullerenes are large, closed, ball-like cages of carbon atoms. Harold Kroto, Robert Curl and Richard Smalley were awarded the 1996 Nobel Prize in chemistry for their discovery (Smalley et al., 1985). Fullerenes are made up of pentagonal or heptagonal rings (unlike graphite with its hexagonal rings). They are seen to possess a number of unusual properties. For example, they can be made to superconduct, semiconduct, insulate or conduct by appropriate doping. Superconductivity is achieved by the addition of 3 alkali atoms per C_{60}. They can even be doped to exhibit ferromagnetic properties. In addition, it was discovered that other atoms could be trapped within these cages. Research in fullerenes garnered much support with many groups looking for new and different types of fullerenes. Carbon nanotubes were in essence born of this research, being produced in arc-discharge apparatus designed for fullerene synthesis. They can in fact be considered a one-dimensional form of fullerenes. The phrase 'one-dimensional' (Hamada et al., 1992) refers to the remarkable aspect ratio of these structures, which typically possess a diameter of only a few nanometers and a length of several microns. In addition, their walls are a single atomic layer thick.

6.3 Structure and Chemistry

A single-walled carbon nanotube (SWNT) is essentially a rolled up sheet of graphitic carbon. Such a graphene sheet, with its honeycomb structure, is shown in figure 6-2, where carbon atoms populate the hexagon vertices.

These are the same sheets of which graphite is composed. However, in graphite, the sheets are stacked one atop the other and held together by van der Waals forces. The Carbon atoms themselves are joined within each sheet by sp^2 bonds which are much stronger even than the sp^3 bonds enjoyed by diamond. It is for this reason that nanotubes are uniquely strong.

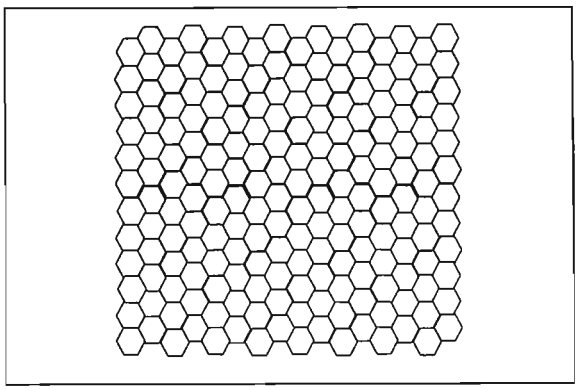

Figure 6-2: Showing hexagonal structure of graphene sheet. A carbon atom occupies each vertex.

By rolling the sheet up, a tube results. In order to form a tube that "fits" or seals properly at both ends, it is possible to roll the graphene sheet up along several discrete axes. Some examples are shown below.

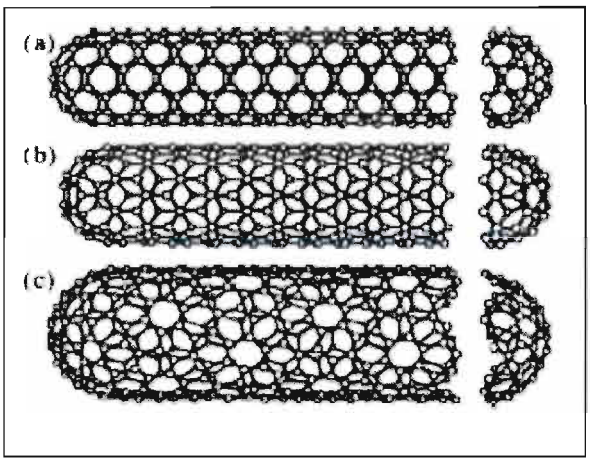

Figure 6-3: Showing nanotubes of different chiralities: (a) armchair, (b) zigzag and (c) chiral (Daresselhaus et al., 1995).

The nanotubes in the above figure contain a "cap" at either end. In fact, caps may or may not form at the end of carbon nanotubes depending on the process used and typically will only form on one end. If caps do form, they have the typically fullerene structure (i.e. composed of carbon hexagons and pentagons) and appear as half-fullerenes.

It is not immediately obvious as to about which axes the tubes may successfully be curled. In fact, three types of nanotubes are possible. These are termed "armchair", "zigzag" and "chiral". The following figures taken from a special issue of the journal *Carbon,* help explain the different possibilities (Dresselhaus, 1995)

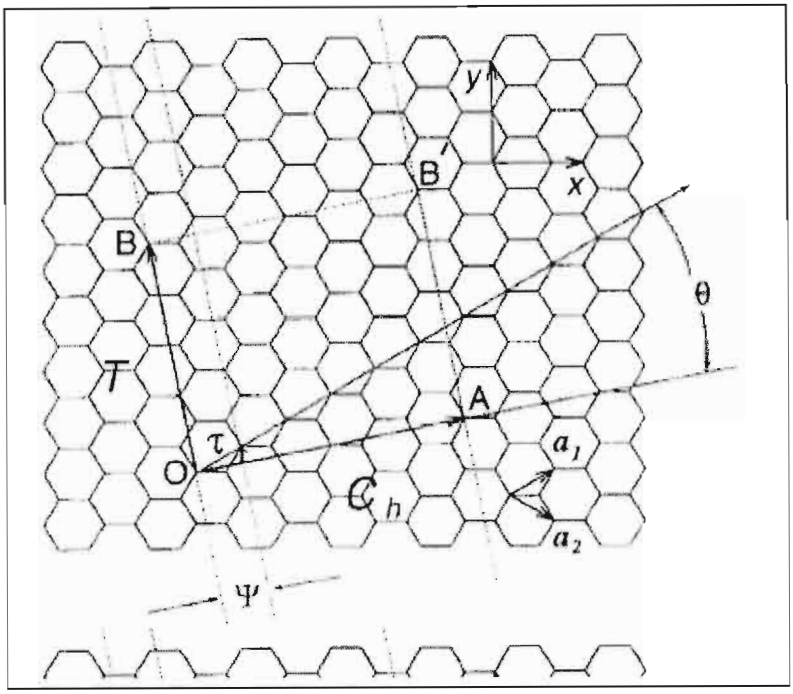

Figure 6-4: Showing definition of honeycomb unit vectors a_1 and a_2, the chiral vector C_h and its associated angle θ (Dresselhaus, 1995).

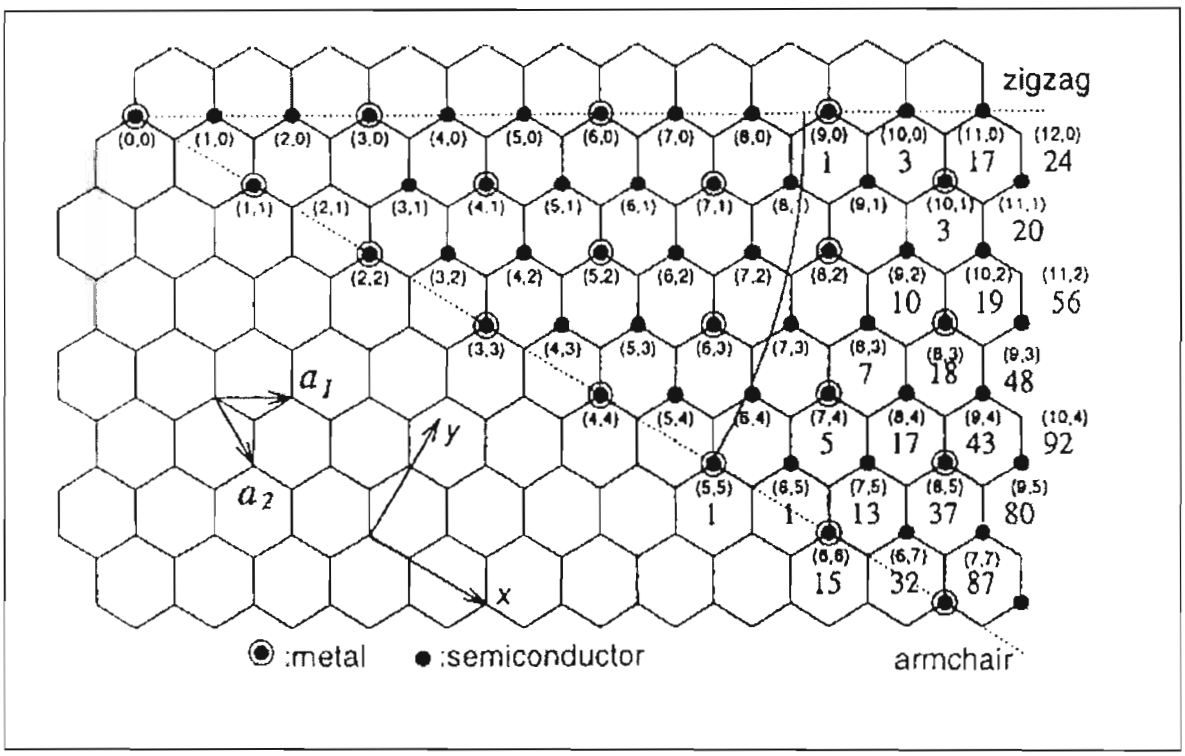

Figure 6-5: Showing all possible chiralities of single-walled nanotubes (Dresselhaus, 1995).

The chiral vector (C_h) points between two carbon atoms. The first carbon atom (at the base of the vector) is the origin, and the second is the termination. The graphite plane is rolled up such that the termination carbon atom touches the origin carbon atom. Thus the length of C_h determines the circumference of the nanotube and the axis of the nanotube runs perpendicular to it.

It can be seen that the angle of the chiral vector is specified in terms of the lattice directions a_1 and a_2 such that $C_h=\boldsymbol{n}a_1 + \boldsymbol{m}a_2$. The direction of a_1 is defined as the "zigzag" direction. If $\theta = 0°$ then the nanotube is termed "zigzag". If $\theta = 30°$ then the nanotube is termed "armchair". Anything between the two is called "chiral". All nanotubes formed have a chiral angle between zero and 30 degrees. The diameter of the tube is once again determined by the distance between the source and termination carbon atoms and n and m are always integers.

The chirality is important because is determines many properties of the nanotube. Most importantly, together with the nanotube diameter, it determines whether a nanotube is conducting or semiconducting. Figure 6-5 above shows how armchair tubules are uniquely conducting, while chiral and zigzag nanotubes may or may not be depending on n and m.

Multi-walled nanotubes (MWNTs) are simply nanotubes within nanotubes. That is, they are concentric cylinders of rolled-up graphene sheets.

6.4 Properties

6.4.1 Electrical

It has been noted that nanotubes may be conducting or semiconducting depending on the chiral angle and diameter. It has been shown in fact that nanotubes are metallic when $n=m$ or $(n-m)=3i$ where i is an integer (Daenen et al., 2003). The difference is related to the differing bandgaps. This allows nanotubes to be used in semiconducting devices as well as simply to carry electricity. The electrical properties of nanotubes are also influenced by applied fields (Kalaugher, 2004). In fact, semiconducting devices such as diodes (Kalaugher, 2004) and transistors (Kalaugher, 2003) have already been fabricated from nanotubes. Nanotubes are even capable of demonstrating superconductivity (Tang et al., 2001).

6.4.2 Mechanical

Nanotubes are very flexible and have a very high Young's modulus along their axis. The on-axis Young's modulus was predicted by Ruoff et al. (1995) as 1060 GPa, five times that of steel. However, in 1996 the value was measured as 1.8 TPa (Schewe and Stein, 1996). Much controversy has raged over the exact modulus with theory and different measurements often conflicting. For a good review the reader is invited to visit and excellent introduction at Michigan State University's website (Adams, 2004). It is generally accepted that the modulus is around or just exceeding 1 TPa but may depend on wall thickness and chirality.

In addition, the tensile strength is reported as high as 63 GPa (Wikipedia, Nanotubes), where steel's is a mere 0.4 GPa. Nanotubes are also found to harden into a new form of carbon more like diamond when pressurized (Ball, 2004).

The incredible strength of these devices coupled with their known ability to bend and obvious low density make them very attractive for various construction problems and personal-protection such as bullet-proof armour.

6.4.3 Heat conduction

In addition, nanotubes are great conductors of heat (1800-6000W/m/K) (Adams). CVD diamond previously had the highest known isotropic thermal conductivity at 2000 W/m/K (Diamond, 2004). It is well-known that graphite and diamond are both excellent conductors of heat as well. However, in solid graphite, the heat conduction is slow through the c-axis (i.e., between layers). Since nanotubes lack this weakness, their very high thermal conductivity is predictable (Ruoff and Lorents, 1995).

6.4.4 Summary

Nanotubes are exciting not only for their potential applications, but also for their interesting physical properties and chemistry. Much research is still underway to discover the secrets of these tiny tubes from theoretical and experimental standpoints even while other researchers struggle to use already-known properties to manufacture interesting devices.

6.5 Applications

A myriad of applications have been dreamed up for carbon nanotubes and it would simply not be possible to list them all in this brief review. Obvious applications include highly efficient, smaller, or higher speed transistors and diodes. Nanotubes can allow for higher bandgaps, better current carrying capacity, and theoretically faster switching times than silicon counterparts (1THz is estimated – Dume, 2004). They also allow for further reduction in size without tunnelling posing a problem (as it soon will in current MOS semiconductor technology). Some of the more interesting or promising applications are added here for interest's sake.

6.5.1 Bullet Proof Vests

Threads of nanotubes have already been created with a toughness of 570 Joules per gram which is three times that of spider silk (the toughest known natural material (Dalton et al., 2003)). This is just the first step, however, since the threads are actually simply nanotube composites. Li et al. (2004) also succeeded in spinning pure nanotube threads, but nobody has yet made single nanotubes long enough to be used in textiles. If a vest could be woven out of pure nanotubes (not bundles of short tubes or composites), it would be stronger than Kevlar while remaining even lighter.

6.5.2 Memory

A company named Nantero has already made nonvolatile memory using carbon nanotubes. For a good report, the reader is referred to TechWorld (TechWorld, 2004). The RAM, called NRAM contains nanotubes which are moved by an applied charge so that they either touch, or do not touch a conducting substrate. After the application of charge, the move is permanent until a new charge is applied. Thus the memories are in fact mechanical in construction. Not only does the use of nanotubes allow for incredible density, but the RAM is faster than SRAM, and should consume less power than DRAM in its final form, without requiring refreshing - all this in addition to being nonvolatile. It is truly the Holy Grail of RAMs and a good example of early nanotechnology.

6.5.3 Field Emitters

Nanotubes make excellent Field Emitters primarily because they are have a high aspect ratio, small radius of curvature at their tips, high stability and high mechanical strength (Saito and Uemura, 2000). This makes them excellent for SEM application in particular where final spot size is a function of source size. Saito and Uemura have long since succeeded in making cathode ray tube elements and vacuum-fluorescence display panels using MWNT field emitters. Nanotubes can even be made to emit light, making them the world's smallest LED's (SpaceDaily, 2004).

6.5.4 Visible light aerial

In addition to being able to emit light, nanotubes can act as aerials to visible light wavelengths. Furthermore, these antennas are polarized (Schewe and Stein, 2004; Wang et al., 2004). This could allow for highly efficient solar energy conversion, or even be used to receive modulated laser beam signals for data transfer.

6.5.5 Energy Storage

Nanotubes, like fullerenes, are capable of storing molecules inside themselves and on their surfaces. It is thought that they would make excellent storers of hydrogen for fuel-cells. The idea is that adsorption of hydrogen into nanotubes and onto their surfaces allows for more compact and safe storage of hydrogen than currently possible. However, reports on the capacity and abilities of CNTs in this area are mixed and this is still very much an active area of research. Figures quoting hydrogen uptakes between 4.2% and 65% (of nanotube weight) have been reported (Guay et al., 2004) Owing to the revolutionary impact hydrogen fuel-cells are expected to make, this is a very active area of nanotube research. Recent works, however, have called the abilities of nanotubes in this area into question (Guay et al., 2004).

6.5.6 Motor Shaft

Since nanotubes are both incredibly small and incredibly strong, they make excellent parts for proposed nano-machines. Researchers at Berkeley have already made a nanoscale motor, merely 500 nm across. That is small enough to be mounted on the back of a virus. The shaft of the motor is made from a multi-walled nanotube about 5 to 10 nm across. The rotor is made of gold and is a few hundred nanometers across. The rotor is attached to the outer tube of the MWNT which has been made to rotate freely about the inner tubes as a frictionless bearing. The motor itself is nothing short of remarkable and evidence not only of the potential usefulness of nanotubes, but of the potential veracity of the great claims of nanotech proponents. (Berkeley, 2003; Fennimore et al., 2003).

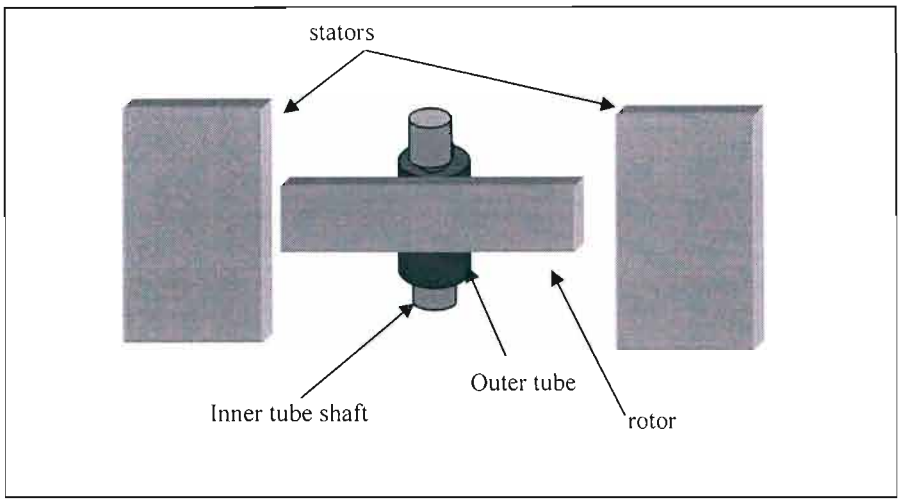

Figure 6-6: Basic schematic, not to scale, of nanotube motor construction.

6.5.7 Summary

This is just a brief look at the properties and potential applications of carbon nanotubes. A quick search on the internet search engine Google will reveal that almost every day new applications are dreamed up and advancements are made in nanotube science. Given the level of interest in the academic community and (more importantly) the level of funding worldwide, nanotube research and nanotechnology research is progressing at a remarkable rate. The rest of this review will concentrate on methods of nanotube fabrication which is the focus of this dissertation.

6.6 Synthesis

In order for the future of nanotube technology to remain bright, several hurdles need to be overcome. One of these is obviously a method for the low-cost creation of large quantities of nanotubes. The matter is complicated by the large variety of nanotubes that a given process might create. Again, nanotubes may vary in conductivity, diameter, number of walls, crystallinity, chirality and so forth. Thus product selectivity can be as important as yield.

There has been considerable work in the field to try and develop new fabrication processes. However, most nanotube synthesis methods developed thus far are variations of one of three fundamental processes: arc discharge, chemical vapour deposition and laser ablation. There are in addition several less common methods such as solvothermal synthesis (Zhang et al., 2004). Each method has its own particular advantages and disadvantages. It may well be, in fact, that no method wins out in the end as the 'ultimate' nanotube fabrication method, but rather that one or other method would be more suitable for a particular application. For example, there are times when yield is more important than quality and selectivity which would favor an arc discharge or vapour-phase method, and then there are times when the reverse is true. The remainder of the chapter provides an overview of these three basic processes with a more detailed look at the seemingly endless variations that have been proposed in the literature.

6.7 Arc Discharge

This is the method by which Ijima produced nanotubes in his seminal work (Ijima, 1991). Over time, many variations have been attempted and refinements have been made, but the essential process remains unchanged: a large current is made to arc between two graphite electrodes separated by a small gap. As the process continues, the anode is consumed and a deposit forms on the cathode and inside the chamber. The extreme temperature of the inter-electrode plasma causes carbon sublimation. The anode would be in some way doped with a metal catalyst if SWNT rather than MWNT were desired. Doping is covered more fully in the next section of this review.

Methods of arc discharge synthesis are distinguished by their apparatus (such as electrode design and electrode spacing) and their process conditions (ambient gas composition, gas pressure, catalyst composition etc.). A typical process would use such parameters as an Argon or Helium environment (50 to 700 mbar is suggested as a typical range by Daenen *et al., 2003, pp. 9)*, a gap on the order of a millimeter and currents of 50 to 100 amps. However, it is easy to see that such parameters can be toyed with endlessly and indeed much effort has been expended in this pursuit by various researchers. By changing the process parameters one finds deviation in the nanotube yield, the nanotube type (single-walled versus multi-walled), the production rate and purity. The arc discharge is known to be a method resulting in production of large quantities of soot, or amorphous carbon (and catalytic materials in the case of SWNT production). Recent efforts have been towards improving this negative aspect since the arc method remains a uniquely low-cost, simple, and rapid method for nanotube synthesis (see, for example, Zhao & Liu, 2004). In spite of any drawbacks, the arcing method tends to produce some of the most well graphitized nanotubes available owing to the very high temperature of the arc plasma. Figures quoted in the literature tend to suggest a temperature of around 4000 K (Tang et al. 2000). In order to give a better understanding of the processes involved as well as a richer grasp of the large number of variations available, some specific examples of both MWNT and SWNT synthesis by the method of arc discharge will now be given.

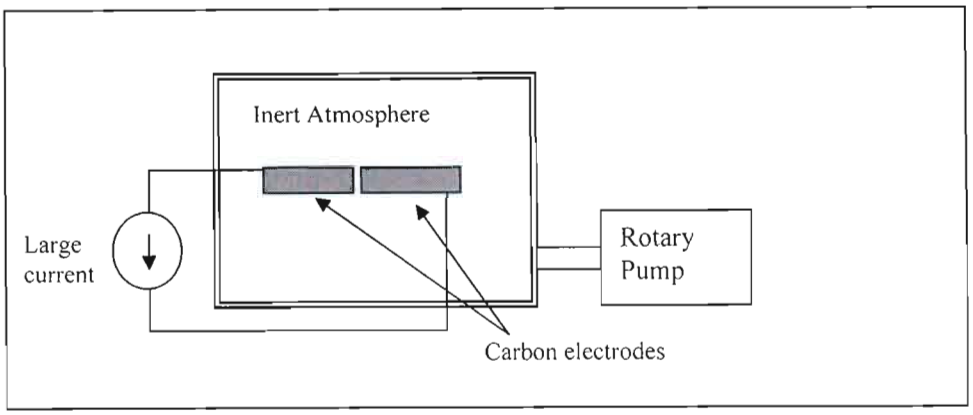

Figure 6-7: Basic arc discharge process.

6.7.1 Addition of catalyst

In order to make SWNTs, the anode is always doped with a metal catalyst. This is often achieved by drilling a hole into the anode and filling it with a mixture of metal catalyst and graphite powders. Many different metals are found to work in this process, the most common being Ni, Co, Mo and Fe. MWNTs are typically also formed. Sometimes, "webs" tend to grow at various places around the chamber containing fullerenes, graphitic sheets, amorphous carbon, and some SWNTs.

A large number of catalysts and combinations of catalysts have been tried, including Y, Ru, Mn, B, Co/Pt, Co/Fe, Ni/Fe and many others. Given the massive variety of catalysts tried and still wider variety of process conditions between researchers, it is obvious that results vary a great deal in the literature.

6.7.2 Optimisation of process parameters

Much effort in recent times has gone into improving the quality and purity of the yield of these processes. Although methods exist and are still being developed to purify the end product, these typically affect the quality of the nanotubes and in addition make up an extra processing step. A comprehensive, quantitative study was conducted by M. Cadek et al. (2002) to determine the optimal process for the basic MWNT arc process which would allow for maximal yield and purity. The study used a steel chamber 300 mm in length and 100 mm in diameter. The anode was fixed in position and the cathode allowed to move to keep the spark gap constant. Helium was used as the process gas. The voltage between the electrodes was maintained at 23V while current density and helium pressure were varied between 165-195 A/cm^2 and 300-500 Torr respectively. They then employed a rigorous analysis involving electron paramagnetic resonance (EPR) thermogravimetric analysis (TGA) to determine the absolute value of nanotube purity.

Their analysis found that greater current and greater pressure led to increased yield. Specifically, in increasing current from 165 A/cm^2 to 190 A/cm^2, while simultaneously increasing pressure from 300 Torr to 500 Torr, yield increased from 2.6 mg/min to 24 mg/min – roughly by a factor of 10. Not only did the pressure and current increase lead to the formation of more nanotubes, but fewer impurities were found as well. Further analysis indicated that the absolute purity of the high pressure, high current sample was as high as 48%. Although this is still considerably lower than figures for certain other methods of nanotube production, such as laser ablation, the high rate of nanotube generation and simplicity offered by the arc discharge method show that this original and very old method is still one of the most promising for large-scale commercial nanotube production.

6.7.3 Temperature control

One problem with the basic arc process is that temperature differential between the arcing current and associated plasma and the rest of the chamber is extremely high. Carbon atoms and heat can escape from the arc area in every direction into areas of the chamber where overall process conditions are then quite different. This lack of uniformity is certainly at least partly to blame for the large variance in product formed. Typically the distribution of nanotubes is irregular. One tends to see a higher concentration in soot collected from around the cathode and a lower concentration on the wall. In order to make the environment more consistent, Zhao and Liu (2004) encased the entire apparatus in an oven allowing it to be heated from room temperature up to 900°C. The apparatus itself was so successful as to be patented by its designers (Liu and Song, 2002).

This simple change led to an increase in both yield and purity especially on the wall deposit. Since carbon nanotubes possess a highly crystalline structure (as does graphite), it makes sense that purity would be improved with temperature. As temperature increased, it was found that not only did purity increase, but yield increased and average diameter decreased (Zhao and Liu, 2004). It was found that a temperature of 600°C was optimal for SWNT production.

6.7.4 Liquid Nitrogen

Perhaps the most promising addition to the basic arc discharge process involves recent efforts to conduct the entire process inside an atmosphere of liquid nitrogen. The process has been patented by its inventor (Olk, 1998) and more recently garnered considerable interested after it was discovered to increase yield to as much as 70% (Kim et al., 2003). The liquid nitrogen takes the place of the inert gas atmosphere and serves the role of at once cooling the electrodes and preventing electrode contamination. In addition, nanotubes are prevented from depositing on the walls. Perhaps a more significant advantage is that the entire process need not take place in an evacuated environment leading to simpler equipment and cost-savings. Couple this with the already noted simplicity of the basic arc-discharge process, and arc-in-liquid processes start looking very favourable indeed.

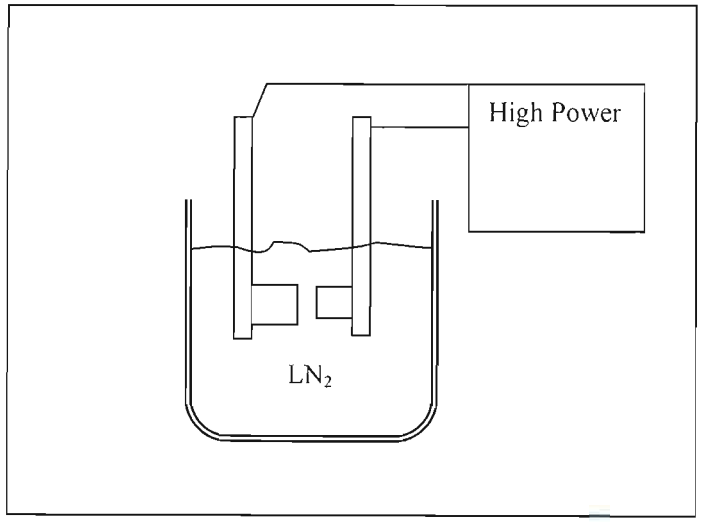

Figure 6-8: Showing arc discharge apparatus in liquid nitrogen atmosphere.

The method has recently been extended to the production of SWNT's by the addition of Ni catalyst to the carbon electrodes (Sano et al., 2004). If the Ni concentration was too high or too

low, the nanotube formation is suppressed. In terms of quality and yield, no numbers were cited in the paper. TEM images seem to suggest, however, that yield is not as impressive as for the MWNT process.

6.7.5 Coal

One of the only expensive aspects of the arc discharge process, is the high purity graphite used to make the anodes. This is a rather specialist form of carbon precursor especially as compared to cheap and abundant CVD reactants such as methane and ethanol. There has been a move in some circles to replace the graphite in these systems with coal in order to lower costs (Pang & Wilson, 1993; Williams et al., 1999; Wilson et al., 2002; Qiu et al., 1998; 2000; 2002a; 2002b, 2003). Qiu et al. (2000, 2002a) established that yield increases with carbon content of the coal. In addition, they discovered that simply adding a wire mesh cage inside the chamber could greatly reduce the quantity of amorphous carbon found contaminating the nanotubes. The wire-mesh screen surrounds the electrodes and serves as a collection net for the nanotubes (whereas, in typical arc setups the product is scraped off the walls).

Since only the anode is consumed in arc-discharge methods, typically only the anode would be made from coal and the cathode would remain graphite. It is possible to either use an anode made completely from coal, or else use a graphite anode hollowed-out and filled with coal. Sometimes both anode and cathode are hollowed out. It is interesting to note that according to the above references, quality need not suffer when using coal as opposed to graphite.

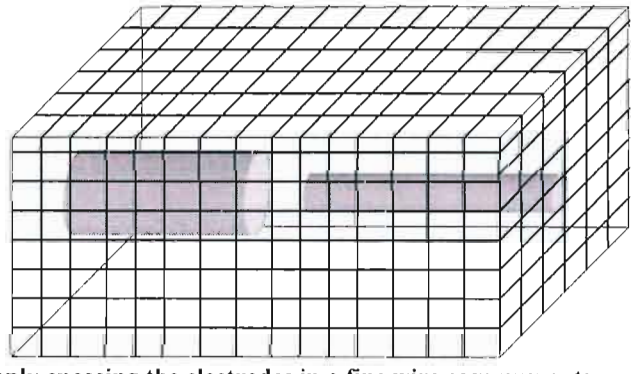

Figure 6-9: Simply encasing the electrodes in a fine wire cage prevents excessive contaminant build-up.

Since coal is not pure carbon, the type of coal used is very important and adds another parameter to the system. Coal also contains elements such as sulphur and iron which are known to alter the nature of nanotubes produced.

6.7.6 Effect of gas environment

It is speculated that the nature of the inert gas affects heat transfer and diffusion in the reactor (Farhat et al., 2001). As noted earlier, temperature and temperature gradients play an important role in synthesis results. Farhat et al. experimented with changing the Helium to Argon ratio in an inert environment containing only those two gases in order to discover more about this effect. It appeared that increasing the argon to helium ratio tended to decrease the average diameter of nanotubes formed.

6.7.7 Arc in water

Although performing the arc discharge in a liquid nitrogen environment is advantageous in terms of simplicity, the cost-saving is not great owing to the eventual high running costs of liquid nitrogen (which naturally vaporizes at a furious rate). To this end, water has been pursued as another environment in which the arc process can take place (Zhu et al., 2002; Sano, 2004). The water may be deionized or an aqueous solution. In the MWNT process (Zhu et al., 2002), the process can only be run for a short period of time (~2 minutes) before the water starts to etch the nanotubes, which may be a drawback when scaling up this method. Purity tended to be low (about 20% at best) and production rate lower than typical arc processes (about 7mg/min) but the utter simplicity of the method and lack of attempt at optimization at this point still makes the method seem promising.

Noriaki Sano has just recently improved the underwater method to allow for production of SWNTs (Sano, 2004). He used a rod doped with 0.8 mol% Gadolinium (Gd) as catalyst and pumped Nitrogen gas through the hollow cathode to create a relatively inert environment. Again, a large number of by-products were created in the process, but the relative simplicity and cost-saving benefits make this an interesting avenue to pursue.

6.7.8 Considerations

This brief overview only begins to cover the sheer mass of literature available on arc discharge nanotube synthesis. Research on this method continues even up to the very week of writing (Sano, 2004). This is partly driven by new angles and ingenuity (such as the arc-in-water) and partly by the great room for experimentation. Catalyst mixture, electrode shape and size, current, gas mixture and pressure, temperature... the list of process parameters goes on. It does not help either that the precise effect of most of these parameters remains unknown and the mechanism of nanotube formation is still the subject of much scrutiny (although, the current theory will be discussed in the section on CVD below).

Arc discharge remains a uniquely simple entry-point to the world of nanotube fabrication. The apparatus is relatively easy to make and the rate of production high. Purity – except in special circumstances – is not exceptional compared to some other methods. However, in terms of nanotubes/hour total yield, the method is still a leader. Should it become possible to improve yield and diameter spread, this would certainly be the method of choice for many applications.

6.8 Chemical Vapour Deposition

Chemical Vapour Deposition (CVD) is also often referred to in the field of carbon nanotubes as catalytic decomposition (although the latter term may be more broadly applied). The basic process is very similar to basic thin-film CVD discussed elsewhere in this dissertation. Since CVD is also a viable route to produce diamond and other carbon films, obviously process parameters play a crucial role. The basic process entails introducing a carbon-containing, gaseous precursor into a reactor vessel. Through the application of energy (such as high temperature or a plasma), the gas is decomposed into its constituent atoms. This is also commonly referred to as 'cracking'. The atoms diffuse towards a substrate which will be coated with a catalytic material. If the process conditions are correct, nanotubes will grow at the catalytic nucleation sites. Note however that for nanotube synthesis from the gas phase via catalytic decomposition, a substrate is not entirely necessary. However, when no substrate is used and the nanotubes precipitate from the gas phase into the reactor or gas stream, the process

is typically termed "Vapour Phase Growth" (VPG), although chemically the processes are one and the same. When a substrate is used, the term "supported catalyst" is often used. It must be further noted that the decomposition typically does not take place merely inside the reactor, but at or neat the catalyst site (Meyyappan et al., 2003). That is to say, the gas will not decompose at any point inside the chamber, but only near or in the presence of the catalyst.

CVD as a route to carbon nanotube growth opens up a host of possibilities. First of all, it allows for the use of cheap and easily-obtainable carbon precursors with a high purity such as methane or ethanol vapour. Secondly, when a substrate is used, it allows for nanotubes to be grown at specific, predetermined sites on a substrate if the catalyst on the substrate is suitably patterned. Thirdly, it can allow for very good control of process conditions in contrast to the arc method. The host of control parameters to be tweaked such as pressure, precursor, gas-mix, flow rate, energy source, temperature and pressure just to name a few means that there is a lot of room for modifications in any given process. It is quite possible to use a particular apparatus and precursor mixture, obtain nothing but amorphous carbon, then change a few parameters and have a nanotube yield. In addition to these basic CVD parameters, preparation of substrate (if any) and catalyst are vitally important and have received much attention in the literature - see for example, McBride, 2001 and Bertoni et al., 2004.

As with the other methods of nanotube fabrication there has been considerable work over the last decade or so to improve upon the basic CVD method. Some of the more important developments in this field will now be considered in further detail.

6.8.1 The basic process

The basic process has already been outlined above but will be expanded upon slightly here for the case of thermal chemical vapour deposition. A reactor of some description – typically a quartz tube or stainless steel vessel – is used to contain a substrate which is coated with fine, nanoscale particles of a catalyst material. The catalyst material is most commonly nickel, cobalt or iron (less variety is seen in the literature than for arc synthesis). The substrate is heated to a suitable temperature which ranges from as low as 550°C (Lee et al., 2001) to as high as 1000°C (Su et al., 2000). With the substrate suitably heated, a carbon containing precursor is introduced. This is typically a hydrocarbon such as acetylene (Zheng et al., 2004, Lee et. al., 2001) or ethylene (Che et al., 1998). Carbon monoxide (Zheng et al., 2002), ethanol vapour (Li et al., 2004), vaporized toluene (Singh et al., 2002a) and a seemingly endless array of carbon sources have been used. Typically a support gas such as argon or hydrogen is used as well.

The carbon-containing precursor will be decomposed near the catalyst material yielding carbon. If conditions are correct, the carbon will attach to the catalyst and nanotubes will form. It is interesting to note, as mentioned previously, that decomposition does not occur merely inside the reactor, but only near the substrate, in the presence of the catalyst (Meyyappan, 2003, pp. 206). That is to say, the temperature within the reactor is maintained *below* the thermal decomposition temperature of the relevant precursor. This reduces the production of amorphous carbon. The catalyst metals are known to show catalytic activity for the decomposition of carbon (Sinnott et al., 1999) specifically.

Nanotubes grown via CVD always grow out of the nanoscale catalyst particles and there is a direct relationship between the size and nature of the particles, and the corresponding nanotubes that form (McBride, 2001; Sinnott et al., 1999). Depending on the strength with which the nanoparticle, or nucleation site is adhered to the substrate (assuming supported catalyst), the tiny metal particle will either remain adhered to the substrate and the nanotube will grow up out of it, or else the nanotube will attach its base directly to the substrate and constantly push the metal particle up so that it remains at the tip (Song et al., 2004). Plasma Enhanced methods,

which will be discussed below, often result in the latter since the plasma bombardment erodes the nucleation site/substrate cohesion.

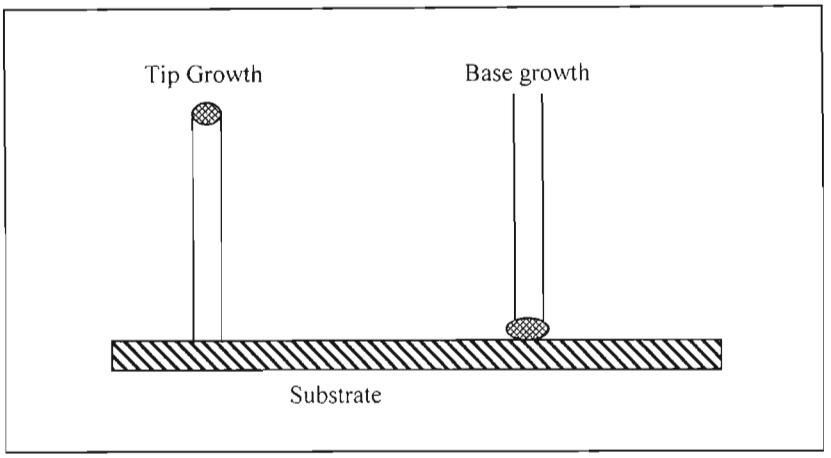

Figure 6-10: Illustrating the two different growth mechanisms of carbon nanotubes via CVD: tip-growth (left) and base-growth (right).

6.8.2 Growth Mechanism

The actual growth mechanism via CVD is not completely understood, but it is speculated that it is quite similar to the more well-understood mechanism of carbon fibre growth via CVD (Meyyappan et al., 2003; Sinnott et al., 1999; Andrews et al., 1999). A molecule of the carbon precursor species first adsorbs onto the catalyst particle and diffuses into it. Eventually, the particle will become saturated and carbon will precipitate out of it in a crystalline form. The catalyst metals tend to not only have strong catalytic ability for decomposing carbon compounds, but also form metastable carbides and allow carbon to rapidly diffuse over and into them (Sinnott, 1999).

Sinnott et al. (1999) consider the growth of nanotubes to be the logical end of a reduction in catalyst particle size. If solid catalyst films are formed on substrates and catalytic decomposition occurs in their presence, sheets of graphite will quickly form with the sheets parallel to the metal plane. If the film is instead made up of large (~0.1 micron) particles (for example, obtained by annealing a starting smooth thin film or sputtering for a very short amount of time), then carbon filaments of a like diameter (~0.1 micron) will be produced. The difference is that in the presence of a particle, the graphite basal planes are tangential to the particle surface, rather than parallel to it as in the former case of a smooth film (Andrews et al., 1999; Sinnott et al., 1999). It is believed that as the particle size decreases even further – to the order of tens of nanometers or less – it becomes energetically favourable for hollow tubes to form due to increased strain on the basal planes. If the particle size is reduced still further, the MWNT diameter will tend to decrease until eventually single-walled nanotubes will form preferentially (Sinnott et al., 1999 statistically showed that the nanotube outer diameter was equal to the particle diameter to within a few nanometers). The tubes are believed to be hollow because carbon does not precipitate from the very apex of the nano-scale particle (recall, the carbon precipitates out of the catalyst particle in a crystalline form after saturation).

6.8.3 Effect of Temperature

It has already been seen that temperature plays a crucial role in the synthesis process. This is quite understandable considering the highly crystalline nature of carbon nanotubes. In CVD, it has been found that temperature of the process is related to diameter of the nanotubes formed insofar as an increase in temperature will increase the diameter. Li, W. et al, 2002, conducted a comprehensive study to analyse this relationship. They found that temperatures higher than 1050°C and lower than 650°C suppressed nanotube growth. Since growth outside of this range has been demonstrated (see, for example, Lee et al., 2001) using different methods and precursors, we can see that temperature alone is hardly the definitive criteria in deciding whether or not nanotubes grow. Nevertheless, the greater than 1000°C, less than 600°C range seems to be quite typical in the literature for CVD.

It was also found by Li, W. et al. (2002) that an increase in temperature increased the nanotube yield – up to a point. Once temperature exceeded 800°C, yield starts to drop off and the nanotubes start to lose their perfect, hollow structure and look more like bamboo. That is, the nanotubes no longer have walls made of concentric, rolled-up cylinders but are made up of stacked parabolic structures. It is unknown at present if such structures will be truly useful but Li, W. et al. suggest they may be useful in various chemical applications. It should be noted that Li, W. et al. are not the only ones to have created such structures (see, for example, Zhang et al., 2002). Average diameter would also tend to increase with temperature.

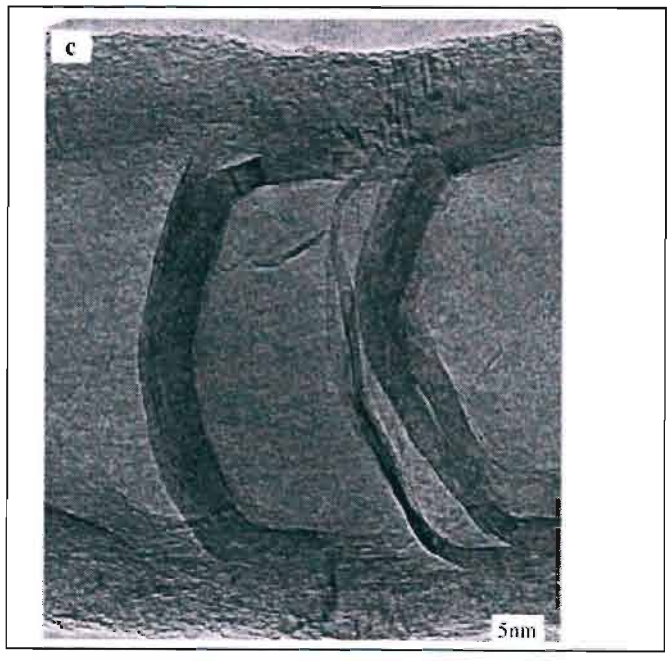

Figure 6-11: Showing high resolution TEM image of "bamboo-like" CNTs (Li, W. et al., 2002).

Apart from this direct study on the affect of temperature on nanotube production, it is quite clear from the literature that temperatures too high or too low would inhibit synthesis or affect yield. In spite of this, we see tremendous variation from author to author. Work conducted at Cambridge achieved consistently good yields of high quality nanotubes working only above 1000°C (Li et al, 2004) and found that going from the 1100°C to 1200°C would assist in changing the nature of the nanotubes from single-walled to multi-walled. In addition Tanaka et al., 2004 showed a reverse trend in their work: increasing temperature led to a *decrease* in average diameter. It has already been noted that Lee et al. (2001) managed a dramatically reduced growing temperature of 550°C for their synthesis process which allowed growth on glass. However, cystallinity was quite poor which one would expect at such reduced

temperatures. It has been shown, however, that post synthesis annealing can improve graphitization to some extent (Che et al., 1998). It should be noted also that this same work illustrated that changing the catalyst from iron to nickel would allow for synthesis at a lower temperature.

Extremely low temperature growth has in fact been achieved using plasma enhanced methods (Hofmann et al., 2003; Boskovic et al., 2002). In fact, Boskovic et al. managed growth as low as room temperature. Plasma additions will be discussed more at a later stage in this review.

These few examples serve to illustrate an important point: each new process by a different group is so different in terms of a vast number of process parameters (pressure, precursors, substrate, reactor, catalyst etc.) that it is difficult to nail-down the effect of any one variable. It is easy to see however that in general, nanotubes will only form well at higher temperatures (greater than 600°C) but that too high a temperature can impair growth – with some notable exceptions. More importantly, one can see that within any given process, the quality and yield of the product can vary greatly with temperature variation by even a hundred degrees either way. It can be said with confidence that for any given process, a subtle variation in temperature can have a dramatic effect on quality and yield, but that temperature alone is hardly the determining factor as to whether the process will be successful or not.

6.8.4 Effect of Pressure

Once again there is a tremendous variety in pressure used for CVD synthesis. Li, W. et al. conducted another study on this effect specifically (Li et al., 2001). Again it was found that an increase in pressure – like an increase in temperature – would improve yield up to a point (noted in this study as 600 torr) after which yield would drop again. At higher pressures the nanotubes would lose their hollow structures and show the "bamboo" structure once again.

It must be noted, however, that again this study is hardly conclusive and many very successful CVD processes take place at atmospheric pressure (such as Li et al. 2004). Indeed, it seems that nanotubes can be grown at just about any pressure, from below a torr (at times, substantially less such as in Bertoni et al., 2004) to atmospheric pressure. Adding to the frustration is the fact that many papers for some reason do not mention reaction pressure (such as Yudasaka et al., 1995; Che et al., 1998; Lupu et al., 2004 and many others). It was assumed in many of these instances that the process was conducted at atmospheric pressure.

In summary it must once again be said that while pressure is a very important parameter, it will hardly be the deciding factor as to whether or not nanotubes form. It will simply control quality and yield within a given process.

6.8.5 Effect of Substrate and supported nanoparticles

Typically in CVD synthesis, the substrate selection is very important since it is desirable for the substrate lattice parameters to match those of the material to be deposited as closely as possible (epitaxy). However, the substrate in nanotube CVD serves a different purpose: it is simply a holder – a place where nucleation can occur. There does not seem to be any theoretical limit on what substrate may be used and this idea is made more obvious by the fact that substrateless growth is quite possible. However, substrate choice can have an effect on whether tip-growth or base-growth occurs since it will affect catalyst-substrate cohesion.

By contrast, the choice of catalyst and method of catalyst preparation is all-important. Typically films of the metal catalyst are applied to the substrate by simple methods such as sputtering

(McBride, 2001) or UHV evaporation (Bertoni et al., 2004; Yudasaka et al., 1995). Often a chemical process may be used instead such as dipping a substrate in a solution of nickel nitrate ethanol and subsequent drying or annealing (Zheng et al., 2004). Regardless of the technique used, one typically ends up with a very thin metal film (typically on the order of nanometers). It is desirous to have instead of a continuous film an array of nanoscale dots or nucleation sites. Typically, separate annealing takes place to force the film to form into tiny droplets (e.g. Yudasaka et al., 1995). However, at higher temperature processes the metal will liquefy in any event. Again, the size of the droplets or nucleation sites has been shown to be critical not only for nanotube growth to occur, but also in determining the diameter and structure of the tubes (for in-depth studies of such effects, Yudasksa et al, 1995; McBride, 2001 and Tanaka et al, 2004 are excellent starting places). This has the advantageous side-effect of allowing one to pattern a substrate using lithography to determine where nanotubes will and will not grow (e.g. Hoffman et al., 2003; Ahlskog et al., 1999; Ren et al., 1999).

Of course, it has been mentioned before that it is possible to simply generate nano-scale catalyst particles *in situ* without the need for a substrate. In such a method, the catalyst may be introduced by means of controlled sublimation of a catalyst-containing precursor. Ferrocene ($Fe(C_5H_5)_2$) has proved popular (Singh et al., 2002a; Lee et al. 2002). The catalyst may also be injected directly as a solid rather than sublimated (Li et al., 2004). In certain plasma processes, the erosion of a metallic electrode provides a convenient point for catalyst introduction (Harbec et al, 2004). Vapour Phase Growth (VPG) has the advantage of allowing the process to be continuous while at the same time obviating the need for tedious substrate preparation. It has also been shown to have high yield.

Much of the richness in the literature of CVD nanotube synthesis surrounds the choice of catalyst and substrate (or lack thereof). This review merely scratches the surface of such great diversity. A group at Duke University, for example, replaced the standard substrate with an alumina aerogel support (Zheng et al., 2002b; Su et al., 2000) resulting in nanotube purity of over 99% with very little amorphous coating. The large surface area of the aerogel base material proved to be very beneficial. In addition, it is believed to enhance the productivity of the catalyst material. The great diversity in choice of catalyst and substrate preparation is another reason why it is difficult to compare results between one group and the next.

6.8.6 Plasma Enhanced Chemical Vapour Deposition

The addition of a plasma to enhance the basic CVD process is well documented. Plasmas are often used in CVD to provide extra energy to the system. This can serve simply to decompose the gaseous precursor, but often has the added advantage of allowing the adsorption and synthesis phase of the CVD reaction to occur at a lower temperature.

Plasma enhancement in nanotube CVD synthesis is very similar in its implementation to general PECVD. Quite simply a plasma is introduced into the basic CVD apparatus and the substrate is either immersed in it or placed near it. The plasma may be created via dc discharge (Hofmann et al., 2003), microwave discharge (Bower et al., 2000; Tsai et al., 1999; Qin et al., 1998; Cui et al., 2000), R.F. (Ho et al., 2001), R.F. with magnetic enhancement (Ishida et al., 2002), Inductively Coupled Plasma (Delzeit et al., 2002) hot-filament assisted dc (Chen et al., 1997; Sugai et al., 2004) and pulsed arc discharge (Sugai et al., 2004).

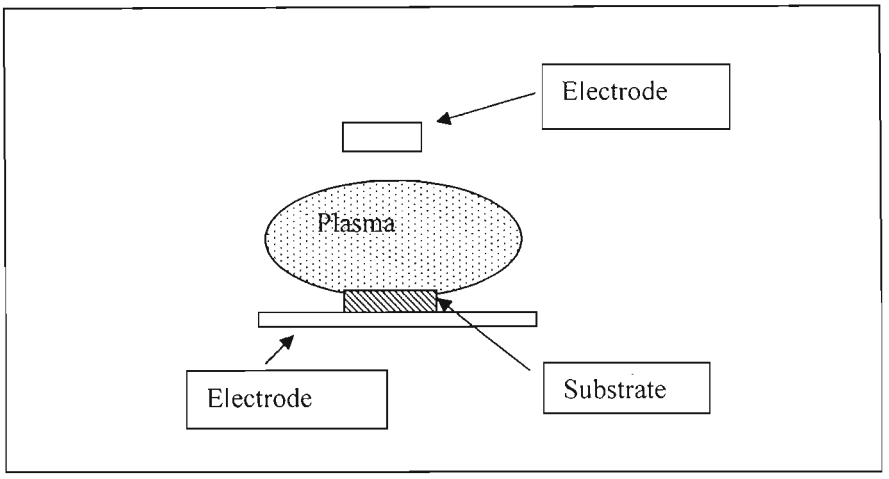

Figure 6-12: Plasma Enhanced CVD apparatus is typically quite similar to thermal CVD apparatus with the exception that a plasma is introduced by some means at or near the substrate.

It was at one stage believed that plasma enhancement would lose its temperature-lowering advantage in the synthesis of carbon nanotubes (Meyyappan et al., 2003). In addition, the ability of a plasma to decompose a gas into its constituent atoms would not be considered advantageous since this would almost certainly lead to the production of amorphous carbon. Recall that in CVD of nanotubes, decomposition should take place only at or near the catalyst surface. To this end, until recently, the single advantage of plasma enhanced processing was in its ability to somewhat remarkably produce fields of vertically aligned nanotubes (Hofmann et al., 2003; Huczko, 2002; Bower et al., 2000; Tsai et al., 1999, Meyyappan et al., 2003; Ho et al., 2001). It is believed that the self-bias potential established on the substrate due to the plasma charging is responsible for this (Bower et al., 2000). This makes sense intuitively since the field lines terminate on the surface perpendicularly and the typically conductive nature of graphitic carbon would allow it to be influenced by the field. In fact, within the same apparatus, Bower et al. (2000) produced nanotubes with and without plasma enhancement by only initiating the plasma after growth had started and it was clearly seen that the nanotubes (which had initially been growing in a typical curly fashion) began to straighten and align.

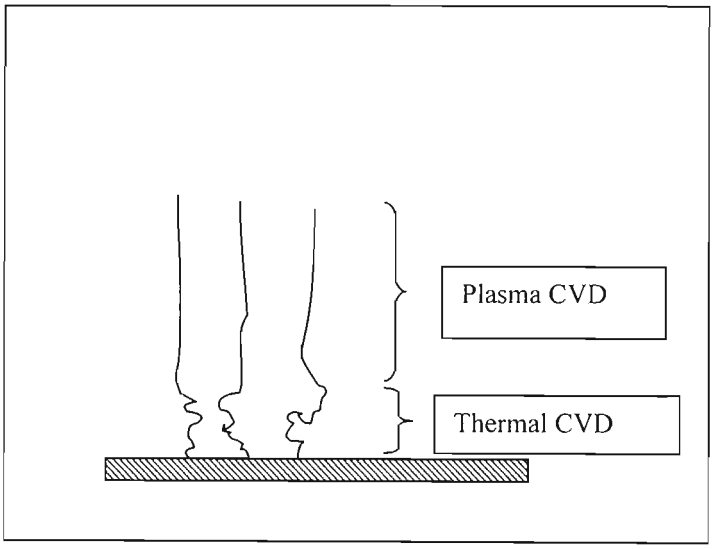

Figure 6-13: Showing how application of plasma leads to straightening and alignment of carbon nanotubes (Bower et al., 2000).

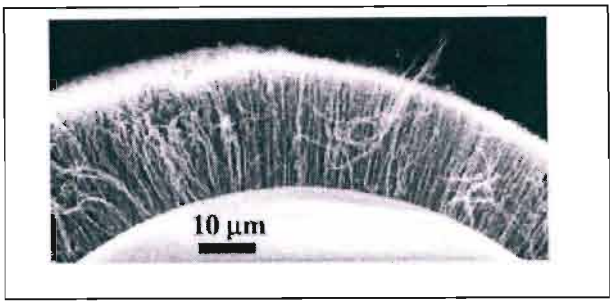

Figure 6-14: Field aligned nanotubes growing perpendicularly to substrate surface (Bower et al., 2000).

The impressive alignment and vertical orientation of plasma synthesized nanotubes was for a time sufficient reason alone to pursue this method of synthesis. It must be noted that the nanotubes need not be in close proximity to be aligned (alignment in thermal CVD is possible as in Zhang et al., 2002 if the nanotubes are densely packed in a "carpet", but this alignment is induced by van der Waals force interaction between the tubes).

However, in recent times it has been shown that the addition of a plasma can indeed lower the temperature at which nanotubes will grow (Hofmann et al., 2003; Boskovic et al., 2002). Nevertheless, while Hofmann et al. were able to grow nanotubes at the low temperature of 120°C in a DC plasma, the degree of crystallinity was extremely poor below 500°C. The authors suggest that the CNT shape depends a great deal on how much of the carbon grows via catalysis at the metal particle and how much is formed by amorphous deposition on the sidewalls. Ammonia was added as a support gas to etch away amorphous carbon and it is possible that further process optimization can achieve higher quality structures at lower temperatures. Growth at low temperature is advantageous since is allows direct deposition onto organic substrates such as Mylar which could be used in capacitors or for hydrogen storage.

The carbon precursor is typically quite diluted in plasma processes to prevent excessive amorphous carbon build-up (Meyyappan et al., 2003). It has also been suggested, as mentioned above, that the addition of ammonia can aid in preferential amorphous carbon etching (Hofmann et al., 2003).

Since it is possible, therefore, to at once prevent excessive amorphous carbon build-up and at the same time achieve the promise of nanotube alignment and lower temperature deposition, plasma-enhanced processing at this point looks a very attractive option.

6.8.7 Thermal plasma torches

In addition, thermal plasma torches have recently been used to synthesize carbon nanotubes (Smiljanic et al., 2002; Hahn et al., 2004; Harbec et al., 2004; Tian et al., 2004; Okuno et al., 2004). The difference in such processes is that the plasma is extremely hot – over 10000 K in some instances (Hahn et al., 2004) and most often operate at atmospheric pressure. Such processes tend not to use a substrate for deposition which makes them really the counterpart of VPG in the plasma domain.

Other than the exceedingly high temperatures used, the methods are quite similar to basic PECVD processes with the exception that it is now possible to introduce solid particle precursors which are quickly vaporized (Okuno et al., 2004; Tian et al., 2004). Some processes, such as that developed by Smiljanic et al. (2002) are more-or-less identical to thermal processes with the exception that the reaction occurs inside a plasma. For example, in the Smiljanic process, a magnetron sustains a thermal plasma inside a quartz tube at atmospheric pressure. A

mixture of ferrocene vapour, argon and ethylene is passed through the plasma resulting in the formation of nanotubes. This is almost identical to the process used by Li et al., (2004) with the exception that in their process ethanol replaced ethylene, there was no argon, and a furnace replaced the plasma.

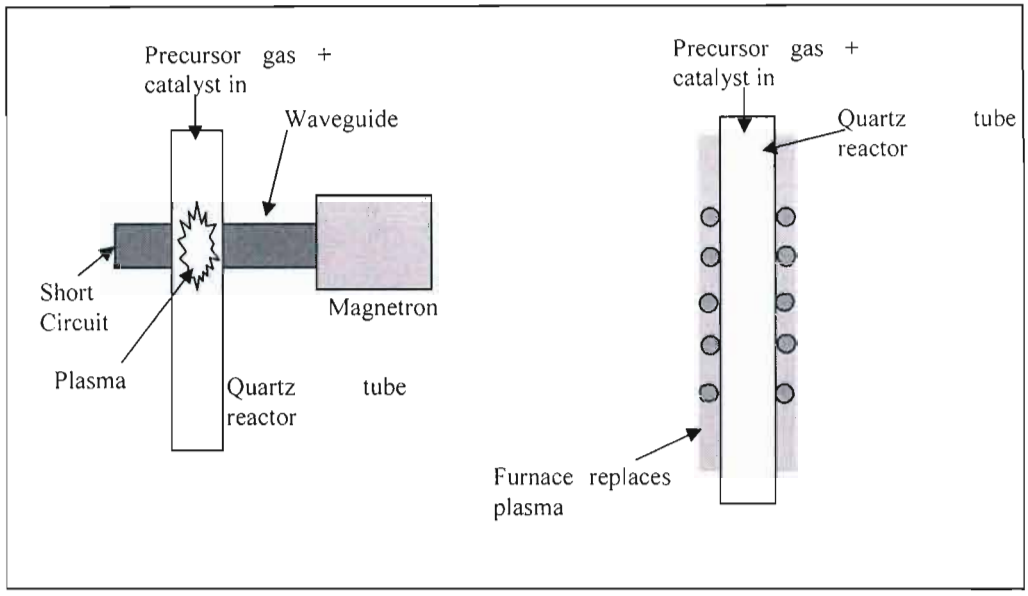

Figure 6-15: Showing how a thermal plasma can, after a fashion, replace heating via a furnace. Of course, the nature of the energy source will affect results, but the processes are remarkable similar and both quite capable of nanotube production.

In addition, these 'torch' processes are truly as much thermal as they are plasma. That is to say, the extreme temperatures would ensure decomposition of the precursors even if the plasma didn't and alignment (as in PECVD) is typically not possible due to lack of substrate. Results using such thermal processes are mixed. Although it is possible to make nanotubes, there is often a large amount of amorphous carbon (Smiljanic et al., 2002) or peculiar nano-structures such as the "stacked-cup" structure or "nano-necklaces" shown below (Okuno et al., 2004). However, it seems that it is possible in most cases to optimize the process to ensure good nanotube yield (Hahn et al, 2004 were very successful with their plasma torch).

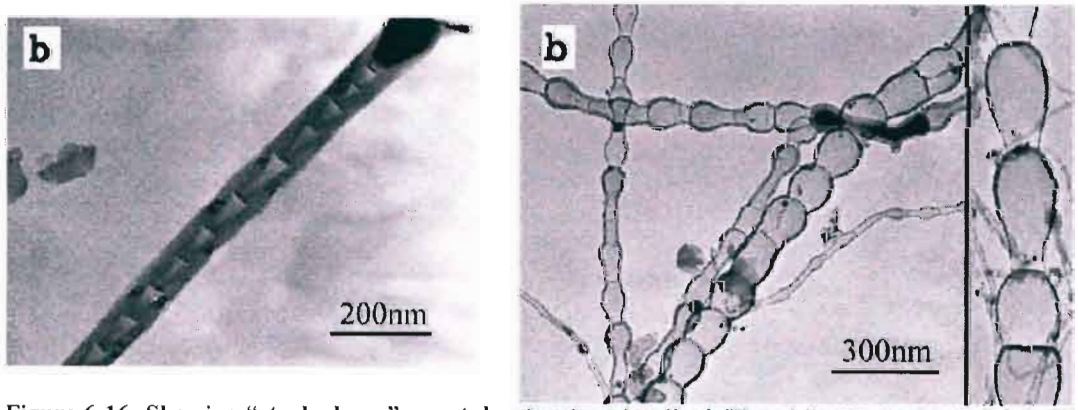

Figure 6-16: Showing "stacked cup" nanotube structure (on the left) and "nano-necklaces" (on the right) (Okuno et al., 2004).

6.8.8 Promoters

It has already been stated that a large variety of carbon precursors and support gases can be used. However, in addition to support gases such as argon, ammonia and hydrogen, other

elements may be added to change the structure of the final nanotubes. Of these, sulphur – most commonly in the form of thiophene (C4H4S) – is often added (Li et al, 2004; Li, X. et al., 2002; Ci et al, 2002; Singh et al., 2002b). However, Bismuth, Yttrium and Lead have also been used (Kiang, 2000a, 2000b). Promoters do not act as catalytic sites, even when they are metals. Instead, they tend to improve yield (Kiang, 2000a; Ci et al., 2002). In addition, thiophene tends to increase the average nanotube diameter (Li, X. et al., 2002) and sulphur has had the odd effect of forcing the preferential production of double-walled nanotubes (Ci et al., 2002), which the authors attribute to its altering of growth dynamics. In some instances, processes would simply not produce nanotubes without the addition of a promoter (Singh et al., 2002b; Kiang, 2000a) which suggests that the promoter can have a co-catalytic role. It has also been found that thiophene may act as both carbon precursor and promoter (Singh et al., 2002b). Changing the concentration of thiophene available can in addition allow for preferential production of single-walled or multi-walled nanotubes (Li et al., 2004). Promoters tend to work particularly well in improving the catalytic ability of iron (Kiang, 2000a; Li et al., 2004) as opposed to other catalysts like cobalt. The precise mechanism by which promoters achieve their ends is not known. Li, X. et al. (2002) suggested that the promoter may prevent large rings from growing into cages and lower the eutectic temperature of iron, but it is uncertain if this is the true benefit. In addition, Ci et al., 2001 found that too much sulfur can suppress nanotube formation. It is suggested (Kim et al., 1993) that in low concentrations, sulphur favours carbon filament precipitation, while in high concentrations, it covers too much metal and destroys the catalytic activity. Typically thiophene/sulphur concentrations are kept very low to a few percent or less than a percent. While the mechanism or promoters may not yet be fully understood, it can be seen the promoters add another layer of control in nanotube synthesis which may be used to alter the results of any given process.

6.8.9 Precursor choice

Precursor choice seems to be far from an exact science. Hydrocarbons are the most common (see, for example, Seo et al., 2003; Li, X. et al., 2002; Lupu et al., 2004; Lee et al., 2001). These include interchangeably methane (CH_4), ethylene (C_2H_4), acetylene (C_2H_2) and so forth. Smiljanic et al. (2002) suggested that those hydrocarbons with a higher hydrogen to carbon ratio achieved better performance (in methane this ratio is 4:1 while in acetylene the ratio is only 1:1). However, since many processes use hydrogen as a support gas, this effect could be muted.

Carbon monoxide (CO) has been used with some considerable success especially in the work of Nikolaev et al. (1999) in their process termed High Pressure CO disproportionation (HiPCO). Disproportionation of CO occurs via the reaction:

$$CO + CO \rightarrow C + CO_2$$

over an iron pentacarbonyl ($Fe(CO)_5$) catalyst. This method allowed for purity in excess of 97% with greater than 70% yields. In addition, nanotubes with diameters as small as 0.7nm could be made (expected to be the smallest chemically stable nanotubes according to Yakobson and Smalley, 1997, although 0.4 nm tubes have since been made by Tang et al., 2001).

Coal has also been used (Tian et. al, 2004) as a solid precursor in plasma processes. A solid precursor would more technically be called catalytic decomposition. Evaporated alcohols have proved useful and were used by the Cambridge group (Li et al., 2004) to create long spun threads of nanotubes. In this process, ethanol, thiophene and ferrocene in a hydrogen flow are introduced by injection into a typical quartz-tube reactor. A thick aerogel of nanotubes forms which have enough cohesion (by way of van der Waals forces) to be spun directly from the furnace hot zone onto a spindle. In this way, threads of arbitrary length can be manufactured. However, since the threads are held together by van der Waals forces, they are quite weak.

The same group tried many oxygen containing precurors such as acetone (CH_3OCH_3) and 1-propanol ($CH_3CH_2CH_2OH$) and found that they would all enable the continuous spin process while aromatic hydrocarbons such as benzene (C_6H_6) would not. However, aromatic hydrocarbons not containing oxygen such as benzene, toluene and xylene have successfully been used in other work (Singh et al., 2003; Hseuh et al., 2003; Andrews et al., 1999). It was suggested that the oxygen component in the alcohol vapour allowed for preferential etching of amorphous carbon. That is, carbon monoxide would tend to form in preference to amorphous carbon in the absence of a catalyst particle.

Alcohol was used previously by Maruyama et al. (2002) in a highly successful process they termed alcohol Catalytic Chemical Vapor Deposition (ACCVD). Again it was noted that much less amorphous carbon was produced than in hydrocarbon methods which the authors attributed to the etching action of the OH radical which will preferentially convert free carbon into CO. In fact, almost no amorphous carbon was produced and furthermore, the nanotubes could be synthesized at temperatures as low as 550°C with methanol.

6.8.10 Hydrogen

One last note involves the importance of hydrogen in nanotube CVD. While noble gases such as Argon or Helium are commonly employed, as in the arc discharge process, many authors report that processes are worse or completely unsuccessful without the addition of hydrogen. In some works (e.g. Smiljanic et al., 2002) the hydrogen is introduced simply as part of the precursor (a hydrocarbon) while in many works it is added directly as a support gas (e.g. Li et al., 2004; Singh et al., 2003). Li et al. 2004 (who used ethanol as a carbon source) report that no nanotubes could form without the addition of hydrogen as a carrier gas and that altering the hydrogen flow rate could aid in preferentially producing SWNTs or MWNTs. In addition, they state that fast-flowing hydrogen would suppress amorphous carbon. Singh et al., 2003, report that increasing the hydrogen to argon ratio slowed the rate of growth of their nanotubes. Recall that as stated above, Smiljanic et al. (2002) also suggested increased hydrogen concentration was beneficial to their process. Ci et al. (2001) also found that lowering the hydrogen flow rate too much would suppress nanotube formation. They suggested that when hydrogen was used as a support gas, its role became quite complicated. The flow rate would at once influence the partial pressures and therefore concentrations of the carbon precursor, while at the same time influencing the morphology of the catalyst particles when these particles were introduced via the floating method. In addition, hydrogen flow rate would affect the growth rate of the nanofibres (as suggested in Singh et al., 2003). On a chemical level, it has been suggested that hydrogen can accelerate carbon fiber formation by decomposing carbides which form from the catalysts (Nishiyama and Tamai, 1976; Yang and Yang, 1986) or by removing any graphite that forms on them (Kim et al., 1991). Slowed growth can be explained by the formation of methane from carbon or hydrogen compounds at the surface (Nishiyama and Tamai, 1976; Yang and Yang, 1986; Kim et al., 1991). It must be noted that these chemical interpretations are based on early studies of carbon fibres. However, as suggested earlier, it is believed that the mechanism of nanotube growth is the same or at least very similar. Hydrogen does indeed play an important role in nanotube growth via CVD.

6.8.11 Considerations

It can be seen once again that, as in the case of the arc discharge method, there is no shortage of variety in CVD synthesis methods. Again, this makes it difficult to track down the effect of certain parameters since there is such large variance in apparatus, carbon precursor, support gas, pressure etc. in just about every study. CVD on the whole is perhaps the most promising of all synthesis methods. It is advantageous insofar as it: 1) allows fabrication from cheap and high

purity precursors which can be introduced in a simple manner (such as ethanol evaporation); 2) it requires little more than a furnace for successful implementation; 3) it can allow for accurate placement of aligned nanotubes and 4) it can allow for continuous processes by using the floating catalyst approach. This combination of advantages will ensure that much research is conducted in this avenue in years to come.

6.9 Laser Ablation

It was Smalley's group (the discoverer of fullerenes) that first discovered SWNTs could be quite easily created via laser ablation of a graphite target (Guo et al., 1995). The process is quite simple: a laser, which may be pulsed (Bower et al., 1998; Guo et al., 1995) or continuous (Gamaly et al., 2000, Munoz et al., 2000) is aimed at a graphite target which may be doped with metal catalyst. The target is typically contained within an air-tight oven to enable the pressure and temperature to be controlled. If no catalyst is added, MWNTs and fullerenes will form. Laser ablation is capable of producing very high purity nanotubes (up to 90% pure) with low amorphous carbon coating.

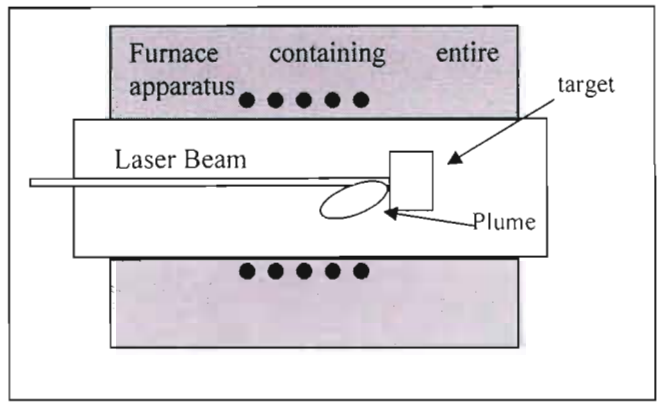

Figure 6-17: Basic laser ablation apparatus.

6.9.1 Basic Process

In earlier work (Guo et al., 1995) the chamber was filled to 500 torr with argon flowing at 50 sccm. Heating the chamber all the way to 1200°C would improve yield. A variety of catalysts were tried of which Nickel and Cobalt produced the greatest and second greatest yields respectively. Copper and Niobium were found to not be conducive to growth. Bi-metal catalysts such as Ni/Co produced orders of magnitude better yields than single-metal catalysts. What is interesting in the SWNT work is that fullerene production is very low (10%) while nanotube yield is very high (50%) indicating that nanotubes will preferentially form. In addition, laser ablation produces some of the highest quality nanotubes possible with very little amorphous carbon coating. Crytallinity is always excellent and the tubes are long, forming "ropes" by van der Waals attraction to other tubes. Co/Pt and Ni/Pt bi-metal catalysts are also found to work well. Since this early work it has been found that adding Yttrium to the catalyst mix, primarily by way of C/Ni/Y mixture (95/4/1 atomic %) also leads to high yield (Gamaly et al., 2000).

6.9.2 Method of growth

It was suggested already in the original work (Guo et al., 1995) that SWNTs form so preferentially because catalyst particles on an atomic scale readily attach themselves to newly formed fullerenes before the fullerenes close and thereafter inhibit closure. It is then more energetically favourable for carbon which collides with the structure to diffuse to the existing

carbon/metal interface and extend the length of the fullerene until nanotubes form. The high temperatures ensure the ability of the carbon atoms to easily diffuse over the metal particles and form a crystalline structure. The presence of carbon, and in particular the growing fullerenes and nanotubes, inhibits the formation of large metal atom clusters. This ensures that SWNTs will form (recall that nanotube diameter is related to catalyst particle diameter). It is believed that although metal clusters may start to increase in size after nanotube formation has begun, the nanotubes will remain thin and single-walled since they have already started growing. In other words, although typically it is more energetically favourable to form larger nanotubes on larger catalyst particles (less strain), in this case the open edges that would result from a sudden widening presents a higher energy barrier.

Many revisions to this basic model have been proposed. Scott et al. (2001) suggest that catalyst particles may even open the rapidly-forming cage structures that have already closed. It is suggested that growth terminates either when catalyst particles become too large, the catalyst becomes too coated with carbon, or temperature cools to a point where diffusion over the metal surface is no longer possible. Scott et al. further suggest that in the pulsed-laser process, fullerenes are continually formed and then themselves laser-ablated to yield up C_2 which feeds nanotube growth. It is believed therefore that keeping the products close to the target and the laser beam can improve quality and yield since non-nanotube products will be re-vaporised and form as nanotubes. This effect was borne out in practice by Smalley's group at Rice University (Thess et al., 1996) where the plume products were spatially confined to stay near the target and the path of the beam. By following the first pulse with a close second, the amount of amorphous carbon was reduced.

6.9.3 Advances

Although laser synthesis gives high purity, high yield nanotubes and is theoretically very interesting, it has fallen out of favour for commercial production. Laser ablation requires expensive apparatus and although yield per vaporized carbon is good, total yield will remain low due to the low rate of carbon vaporization as compared to the arc method or CVD method. In addition, it is prohibitively expensive and difficult to scale the method up. To this extent, advances in this field are limited to attempts to improve rate of vaporization such as by using a Free Electron Laser (FEL) (Eklund et al., 2002).

A Free Electron Laser pulses at a rate of 75 MHz (compared to 10 Hz for a typical Nd:Yag process) and pulse widths are a mere 400 fs (compared to around 10 ns for Nd:Yag). This makes the FEL the "Uzi" of lasers. After focusing, intensity of the pulses reaches an estimated $5x10^{11}$ W/cm^2 which is three orders of magnitude greater than Nd:Yag systems. Such incredible focusing was required to achieve adequate energy per pulse to ablate the target since the pulse duration is so short. Using a FEL laser therefore will allow for much greater rate of SWNT generation. Eklund et al. at Pennsylvania State University suggest rates of greater than 45 g/hr are possible.

Another way to improve yield involves ablating a continuously introduced fine powder as opposed to a graphite target (Bolshakov et al., 2002). This has the advantage of at once making the process continuous and allowing for more efficient use of laser power since there is no heat dissipation into the bulk. Yields for this method with a continuous CO_2 laser were not nearly as impressive as the FEL method, however, at some 5 g/hr and only 20-40% of the soot contained SWNTs. It would be interesting, in this authors opinion, to see if the FEL and continuous feed methods could be combined and optimised.

In addition to attempts to improve yield, there have been some attempts to improve quality such as by using a second pulse and tube to contain the plume as mentioned earlier (Thess et al., 1996). Yudasaka et al. (1997) replaced the single carbon/catalyst mixed ablation target with

dual targets: one of carbon, one of catalyst. By doing this, they prevented surface morphological changes creating an excess of metal.

6.9.4 Considerations

A new review on laser ablation methods has recently been published (Arepalli, 2004), but otherwise, research in this area is far less active than in alternative synthesis methods. The high cost of suitable lasers is in stark contrast to the extremely low setup cost of arc and CVD apparatus. It seems more prudent, in this light, to optimise the latter processes to achieve good yield and quality which is at the moment, a very active research area.

6.10 Alternative Methods

The above three methods of CVD, laser ablation and arc discharge cover the bulk of the work done in the field of nanotube synthesis. However, it would be surprising if researchers were not continuously coming up with new ways to produce nanotubes, with varying success. Some of the more interesting methods are outlined below.

6.10.1 Solar Production

Solar energy has previously been focused onto carbon targets for the production of Fullerenes (Guillard et al., 2001). The method basically involves intense focusing of solar energy onto a crucible containing carbon which will then vaporize. In the production of nanotubes, a 2 kW furnace is used (Laplaze et al., 1998).

Although this method is interesting since it is powered by 'free' energy from the sun, it is certainly no simple task to set up such apparatus. However, after initial setup, this would obviously be the cheapest method of nanotube production. As in many other processes, optimization is needed to improve the ratio of nanotubes to total soot.

6.10.2 Solvothermal Synthesis

A particularly simple chemical process has recently been developed by Zhang et al. (2004). In this process, nanotubes are formed by the chemical reaction of ethanol and transition metal oxides such as NiO and Co_2O_3. The ethanol reduces the oxides to form pure metallic catalysts which then catalyze the ethanol solution at a temperature of 550°C to form nanotubes.

The beauty of this method is in its absolute simplicity. It can be carried out as a high-school practical. Ethanol (15 mL) and the appropriate oxide (0.5g NiO powder) are simply mixed in a small stainless steel container and heated to 550°C for 12 hours. Thereafter, the resulting suspension is allowed to cool to room temperature. At this point, the solution contains nanotubes ready for analysis. Not only is the method simple, but the reactants are cheap and innocuous. The method can also be very easily scaled up. This is a very promising, low-cost route to nanotube synthesis

6.10.3 Catalytic Pyrolysis

CVD is really a subset of a larger synthesis method which could be termed catalytic pyrolysis. Pyrolysis of course refers to the thermal breaking-down of a precursor to yield a desired

product. Typically, however, in the literature when the term pyrolysis is used, it refers to the thermal decomposition of a solid starting precursor.

For example, Wang et al. (2000) managed to grow aligned nanotubes by decomposing nickel-cobalt phthalocyanine (Ni-CoPc) in a quartz tube furnace.

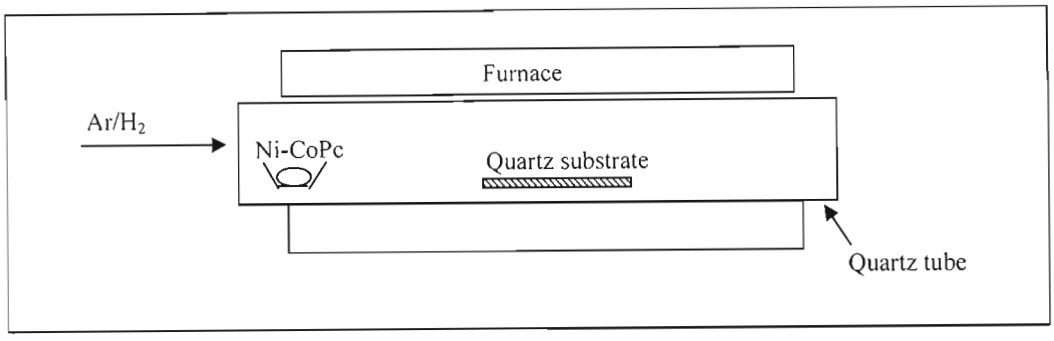

Figure 6-18: Showing Pyrolysis Apparatus.

As can be seen in the above figure, the method is really identical to basic CVD with the exception that all the precursors are placed in the furnace in a solid form. One interesting result of this particular process is that is yielded nanotubes that were aligned and formed into a 'honeycomb'-like structure.

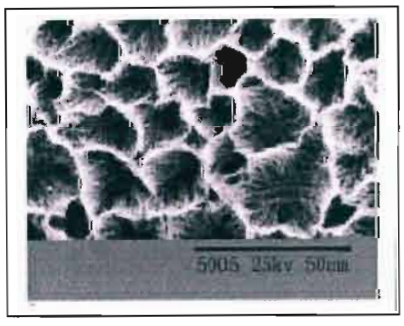

Figure 6-19: Showing honey-comb patterns (Wang et al., 2000).

Note again, however, that CVD is really a subset of pyrolysis.

6.10.4 Annealing

It has also been found that nanotubes will be formed simply by annealing other forms of carbon doped with catalyst at a high temperature. By annealing polyethylene (PET) and diamond-like carbon (DLC) films at a temperature of 1200°C, Sarangi et al. (2001) found that nanotubes would form. The films were mixed with Nickel and Palladium Chloride before annealing. The nanotubes formed showed excellent crystallinity. The process was found to be quite sensitive to the amount of catalyst used and there was considerable unwanted by-product in the unoptimised processes. In addition, various other nanostructures could be produced such as nano-horns. This process is chemically interesting, but does not seem to offer much advantage otherwise.

6.11 Summary

There is certainly no shortage of variety when it comes to nanotube synthesis methods. Even within a particular method, diversity is prevalent with all manner of catalysts, precursors,

pressures, temperatures, equipment and so forth being used to produce nanotubes. On the one hand, this is a very interesting result since it shows that nanotubes form readily for a large variety of process conditions. It is also very inconvenient after a fashion since it makes comparison of methods quite difficult. For example, two methods with the same apparatus may use the same precursors at different temperatures to arrive at different results, and then the effect of temperature can be analysed. However, when the apparatus, pressure and precursors all differ from method to method, it becomes difficult to nail-down the effect of any one parameter.

Certainly nanotube synthesis is attractive for an institution such as ours since it is very current and potentially very cheap materials science research. Materials science is an expensive business often requiring equipment that can cost hundreds of thousands or even millions of rand. However, here is an exciting field within materials science where considerable work can be done with some ethanol and a microwave oven. For this reason alone it is worth pursuing.

It must first be pointed out that the aim of the present work was primarily to grow MgB_2 thin films via the new method explained in previous chapters. It was for this reason that the plasma apparatus was designed and built to its current specification. Interest in producing nanotubes grew out of casual reading on the subject. It was determined that the already produced apparatus would be highly suitable for nanotube fabrication for several reasons:

Firstly, the apparatus was specifically built for CVD reactions. As pointed out above, CVD is perhaps the most promising of the synthesis methods and in addition, very economical. Secondly, the addition of a metallic aerial to the basic APNEP setup provided a convenient means of catalyst introduction. In fact, the apparatus was considered so suitable for nanotube synthesis that at first much time was spent simply deciding which of several possible routes would be most viable. It was known from previous experiments that replacing the metal aerial with a thin graphite rod would result in the graphite arcing and burning up with a plasma at its tip. This alone should be sufficient for fullerene and nanotube synthesis with appropriate environment conditions. Several other routes were also possible: 1) carbon and catalyst (mixed) aerial in inert atmosphere; 2) mixed aerial with carbon precursor gas (such as a hydrocarbon); 3) catalyst only aerial with carbon precursor gas; 4) standard setup (moly aerial) with both catalyst and carbon source introduced externally (such as by injecting a ferrocene/ethanol mixture).

In the end, it was decided that while the fourth choice would almost certainly lead to positive results, the third choice provided the most interesting starting point. This was because: 1) it truly was convenient to introduce the catalyst by way of the slowly evaporating/vaporizing aerial and it would be interesting to see how well this could work; 2) this would mean simple catalyst and aerial preparation, 3) the process was fundamentally similar to the VPG method with the addition of a plasma.

Excellent results had recently been reported by Li et al. (2004) with their VPG method and thus this was considered an exciting avenue. In their work, a mixture of ferrocene, ethanol and thiophene was injected into a furnace operating between 1100°C and 1200°C. A thick aerogel of nanotubes would form which could be pulled out of the furnace hot-zone continuously and spun into a thread. This allowed for a continuous process which produced a high nanotube yield and threads of arbitrary length. In addition, having a continuous, flow-through method is economically advantageous. The basic process to be tried would then be quite similar in many ways to Smiljanic et al. (2002) where methane, ferrocene and argon were introduced into a quartz tube which contained a microwave induced plasma. This was also a flow-through, VPG process which made use of a plasma. The results were certainly not as good as that of Li et al. (2004) (considerably more unwanted byproducts such as amorphous carbon were produced) although the processes differed in terms of precursor, promoter, flow-rate and support gas.

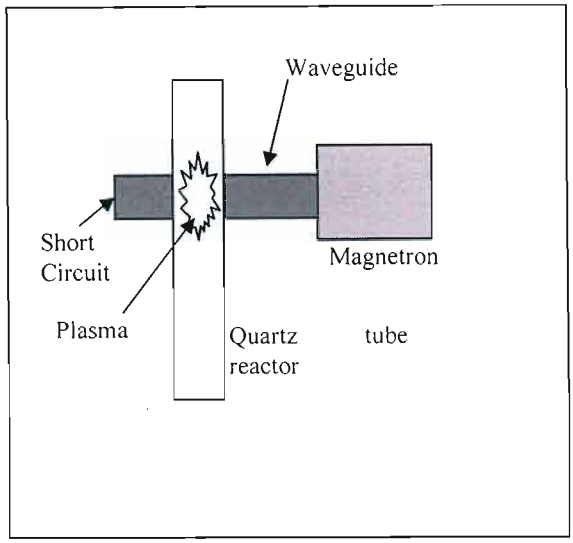

Figure 6-20: The synthesis apparatus of Smiljanic et al. (2002). This differs only from that of Li et al. (2004) insofar as the magnetron and waveguide would be replaced by a tube furnace.

However, our process would differ in the following ways:

1) The apparatus is obviously somewhat different making use of a microwave-oven based APNEP configuration. This is considerably simpler and cheaper to acquire and set up compared to conventional microwave plasma sources – including the tube-in-waveguide method employed by Smiljanic et al. (2002). Waveguide components such as matchers, directional couplers and tuners are extremely costly and even a good tube furnace will cost more than a microwave oven.
2) The catalyst is introduced via the innate evaporation of the plasma-localising aerial. However, it would be interesting at some stage to try using a more traditional ferrocene-injected source
3) The process is not strictly a thermal plasma process (the temperatures of the plasma-in-tube method at atmospheric pressure exceed 5000°C) since there is still some good degree of plasma nonequilibrium at the pressures we intend to use.

In addition, in order to improve yield and purity, it was decided to make use of ethanol as the nanotube source. Since plasmas by their very nature will decompose the precursor gas into its constituents, the probability of amorphous carbon formation increases over the thermal CVD method. It has been noted previously that when an alcohol is used as the vapour source, the OH radical will possibly preferentially etch excess carbon. Inside a plasma, it is reasonable to expect that ozone, active oxygen, and even active hydrogen may do the same. Regardless of the exact chemistry behind its ability to do so, using alcohol should allow for a more pure product. It is expected from the review above that adding hydrogen as a support gas would further improve results. Although Smiljanic et al. (2002) did not make direct use of hydrogen as a support gas, the work noted that increased hydrogen:carbon concentration (by way of moving from acetylene to methane) improved results. In addition, it was decided to try the process with and without thiophene to see what effect this may have.

The process would then be similar on the one hand to the work of Li et al. (2004) with the addition of a plasma, and similar to the work of Smiljanic et al. (2002) with potentially more promising precursors. At the same time, the apparatus used would be cheaper than either source and very simple to set up. The study would potentially provide a simple, low-cost and accessible means of nanotube fabrication. At the same time, it could hopefully provide some insight as to how adding a plasma could affect the work of Li et al. (2004) and how different process conditions and precursors could affect the work of Smiljanic et al. (2002).

7 Experimental: Nanotubes

The goal of this portion of the work, as pointed out in the previous chapter, was not simply to find a different way of making nanotubes. The experimental work would also provide an investigation into the following: 1) the suitability of the modified APNEP apparatus for nanotube synthesis; 2) the effectiveness of introducing the catalyst by way of the slowly-vaporising antenna; 3) if using ethanol and hydrogen could provide a cleaner product than methane/argon as anticipated; 4) if a plasma would be detrimental to the great success of the VPG method employed by Li et al. (2004) mentioned in the previous chapter.

7.1 Apparatus

7.1.1 Plasma Chamber

The apparatus remained unmodified from the final version used in the MgB_2 thin-film experiments with the exception that different aerials were tried. The basic apparatus is shown below for convenience.

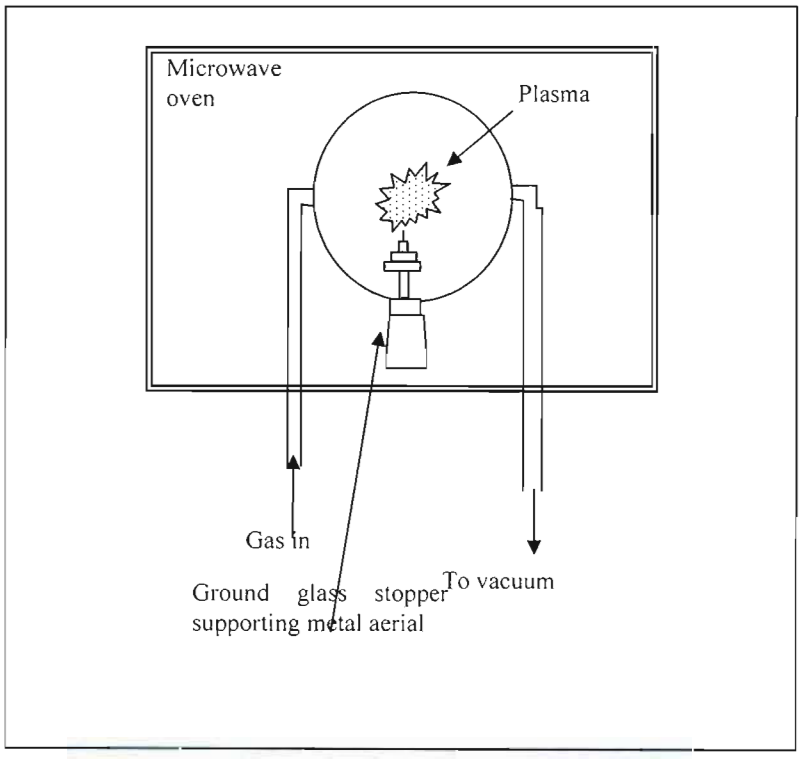

Figure 7-1: Diagram of plasma chamber inside of microwave oven.

The exact details of the system are described earlier in this dissertation. To briefly recap: a spherical, 1 litre, borosilicate, round-bottomed flask is placed upside-down inside a 1000 W commercial microwave oven. The flask is sealed up with a ground-glass stopper which has a glass stand attached to it. The round-bottomed flask has been modified by the addition of two pipes: one to let in gas, and the other to allow for evacuation. A chamber is shown in the images below.

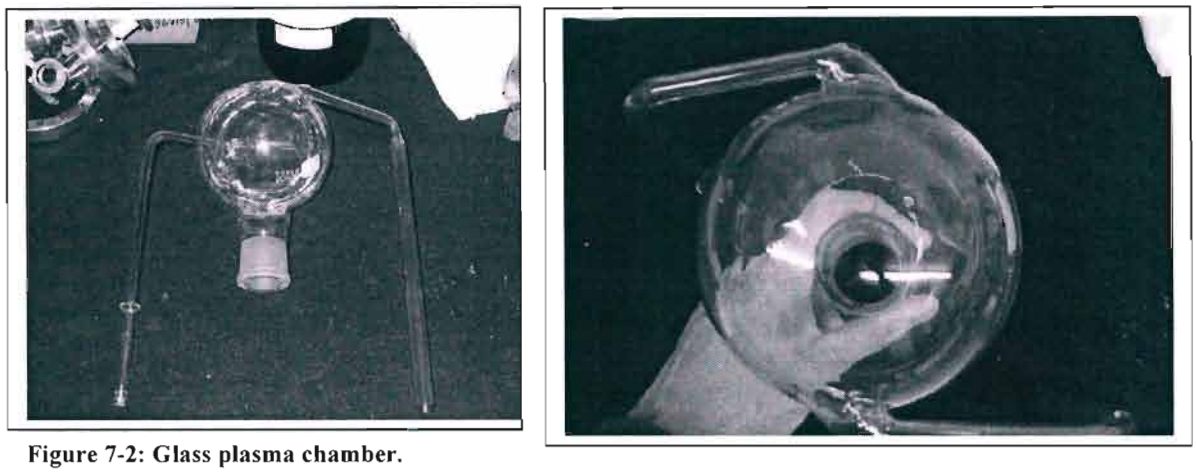

Figure 7-2: Glass plasma chamber.

During all experiments, gases were let into the chamber using the thinner pipe and a vacuum was maintained on the thicker pipe to achieve the desired pressure. The pipes attached to the sphere tangentially to allow the incoming gas to swirl about the glass (when flow rate was high enough).

7.1.2 Aerial

An aerial was placed on the stand which rises out from the ground glass stopper. Several aerials were used which invariably contained two parts: a stainless steel base and a catalyst wire tip. It would be impossible to make the entire aerial out of catalyst, since the standard catalyst metals (Ni, Co and Fe) all melt too easily. Stainless steel was not deemed to be a contamination threat since it is itself a source of catalyst material (iron and nickel), although it will also contain trace quantities of sulphur which is a known promoter. The purpose of the aerial was now two-fold: 1) to contain the plasma by keeping it away from the glass walls; 2) to provide a source of catalyst.

The different aerials tried are shown below:

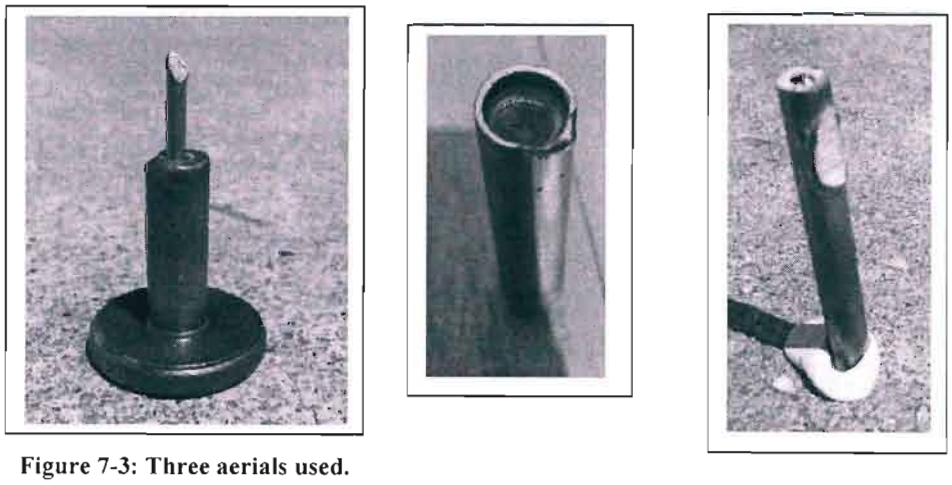

Figure 7-3: Three aerials used.

From left to right, these aerials will henceforth be called 'T-base', 'hollow-top' and 'needle-top'. Such aerials have also been discussed previously in this dissertation. The exception is now that for the T-base aerial, the molybdenum needle tip was replaced by a 1.8 mm diameter wire of mild steel or Kovar (shown in the photo). Similarly, a small coil of 1 mm Kovar wire was

placed in the bowl of the hollow-top aerial, and a short (~15mm) Kovar wire of 1.8 mm diameter was placed in the tip of the needle-top aerial.

Figure 7-4: Small coil of Kovar that would be placed in hollow-top aerial base.

It had been seen from EDS analysis of previous, casual experiments that the stainless steel aerials led to the deposit of small amounts of iron. During one preliminary run, nanotubes were even made using the T-base aerial with a molybdenum tip. It was found that trace iron from 304 grade stainless steel had in fact seeded nanotube growth. To this end, it was believed that mild steel in the form of common nails would yield up even more iron when heated and would make an excellent catalyst (pure iron was unavailable at the time). However, the idea to use mild steel was soon abandoned in favour of Kovar. From previous work in the materials science group, a considerable amount of Kovar wire was available. Kovar alloy fortuitously is made up entirely of the three most successful and common CVD catalysts: Fe (53%), Ni (29%) and Co (17%). Since at this point the primary aim was to see whether or not nanotubes could be formed in abundance, it was thought that using three catalysts at once gave a better percentage chance of success.

The aerials were always placed atop a short cylindrical section of soapstone (10 mm thick by roughly 30 mm in diameter) which was in turn placed atop the borosilicate stopper. The soapstone was necessary to keep the needle-top and hollow-top aerials from falling over and in any event, would preferentially be subjected to the intense heat of the plasma should the plasma happen to attach to the aerial base. This saved many glass stoppers from melting. The soapstone could present a source of contamination, but from previous tests it was known that this contamination was very small so as to be negligible. The exception came during runs where the plasma did truly attach to the bottom of the aerial and consequently the soapstone base for extended periods of time. This would even lead to change in plasma colour. Every effort was made to avoid such an occurrence, however.

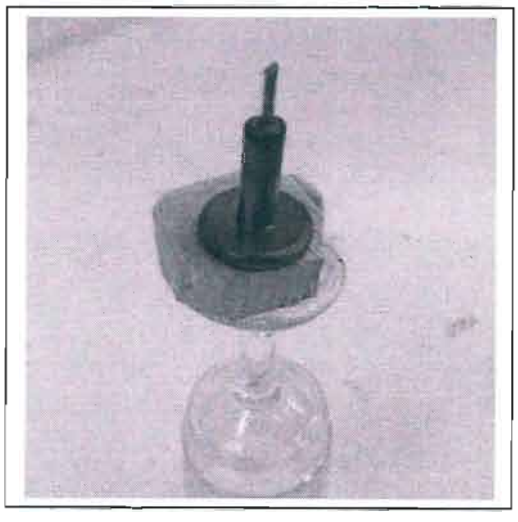

Figure 7-5: Stopper, soapstone spacer and aerial combination.

7.1.3 Gases and vacuum system

Hydrogen and argon, both 99.999% purity (Afrox UHP grade) were used as support gases. Standard PVC hose was attached to the regulator of each cylinder to pipe the gases to the main chamber. The gases were mixed via a simple copper T-piece. A second T-piece allowed the attachment of a third hose which was connected to a filter flask sealed with a bung. The filter flask contained variably ethanol and ethanol mixed with thiophene. Each PVC hose was fitted with a tap to control the flow rate of the various gases. The final output was attached to the thin input pipe of the plasma chamber via high temperature hose.

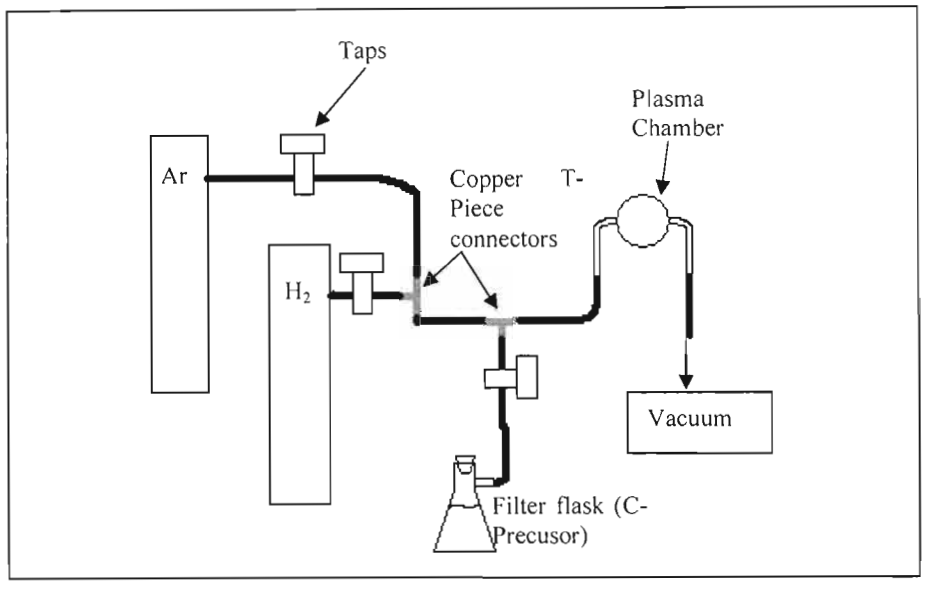

Figure 7-6: Support gases and carbon precursor vapour were attached to plasma chamber using PVC hose.

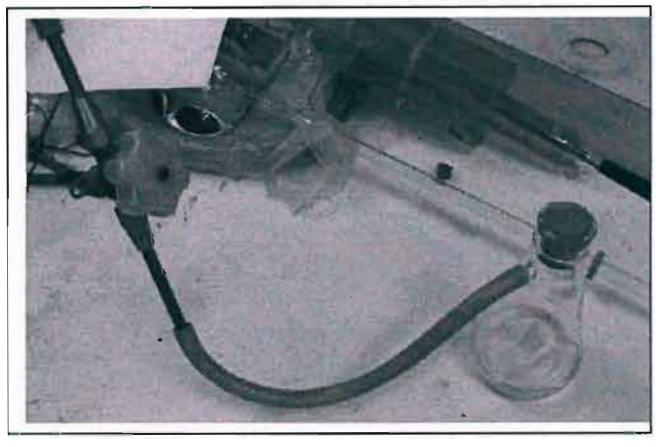

Figure 7-7: Showing photo of filter flask and tap.

The taps provided unfortunately only primitive flow rate control. Since flow-rate could not be measured, this was sufficient. A further tap was placed between the chamber output pipe and the rotary pump (Edwards "18" two-stage) to provide control over the rate at which the chamber was evacuated. Again the system suffers from the flaw that flow-rate could not be measured since no apparatus to perform such measurement was available.

To the vacuum side of the plasma chamber, a cold-trap was fitted. The cold trap was connected to the plasma chamber output via a silicone bush and to the rotary pump via simple PVC hose. The output of the trap was also connected to a mercury manometer for pressure measurement.

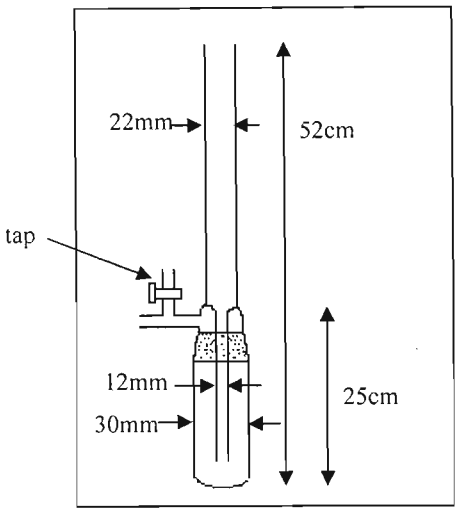

Figure 7-8: Rough schematic of cold trap with relevant dimensions.

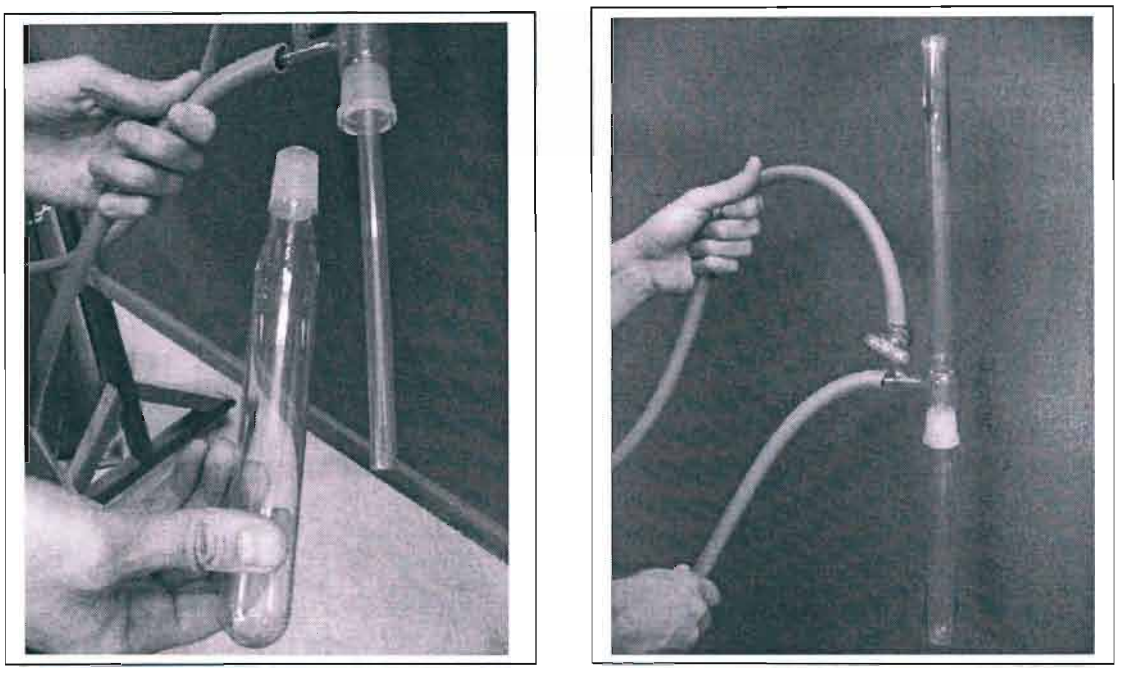

Figure 7-9: Cold trap. The glass tap visible allows connection to the manometer.

The idea was to immerse the trap in liquid nitrogen to catch nanotubes out of the air stream in flow-through experiments. However, this proved a foolish idea since the trap was far too efficient at precipitating ethanol from the air stream and then freezing it. A dry-ice/alcohol slurry would do better.

7.1.4 Soot Collection

It was decided that it would be best in these tests to place an alumina rod inside the plasma chamber to act as a collection point for any deposit. A fresh, clean, unpolished 0.8 mm diameter

alumina rod was therefore fixed to the aerial holder for each experiment. The alumina rod was fixed to the aerial-holder using Fire Cement - a local product something akin to coarse clay that is useable up to temperatures of around 1200°C. Like the soap-stone, this could present a potential source of contamination. However, the cement was always baked thoroughly and realistically would not introduce any more contamination than the borosilicate glass chamber itself. Certainly, so long as the plasma was kept from directly touching the base and fire-cement, its effect was negligible.

The alumina rod was always angled as in the photo below so as to pass through the plasma and extend some distance beyond it. In this way, it could be seen whether deposition would occur within the plasma, near the plasma, or relatively far away from it. The length of the rod was typically 7 to 10 cm. The plasma itself was usually around 3 to 4cm high and similar in lateral extent, situated at the tip of the aerial (these dimensions are for a hydrogen plasma. Argon mixes could be arbitrarily large depending on how much argon was added). Not only were the different rod sections either exposed to the plasma or not, but placing the rods in this way meant that certain parts of the rod were considerably hotter than others.

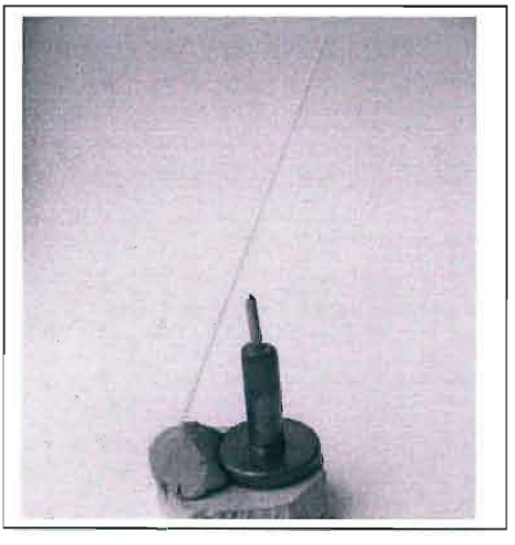

Figure 7-10: Aerial thin alumina rod angled over the steel aerial.

Technically then, all the experiments conducted were CVD with floating catalyst or rather, VPG. Although the soot was collected close to the aerial, this needn't be the case. It would be interesting to collect soot further downstream at some stage and compare results.

7.2 Experiments

Once again it must be stressed that the nanotube section of this work was very much an investigation, and thus it was decided to try several sets of parameters, even those less likely to be successful, and observe the results. Ultimately, ten final runs were conducted. Ethanol was used exclusively as the carbon source owing to the belief that the presence of active oxygen, OH radicals and possibly even ozone in the plasma would reduce amorphous deposits. The ethanol was at times mixed with thiophene to see what effect, if any, this had. 2.5% vol. of thiophene was added to the ethanol in the filter flask for these experiments. Of course, since the ethanol was introduced via evaporation, this does not mean that 2.5% mol of thiophene was present as vapour.

The experiments involve changing the support gases, pressures (and consequently temperatures) and ethanol concentration (achieved by heating the filter flask containing the liquid ethanol). All experiments were run with the microwave oven set to full power (1000 W). The following is a list of the different experiments that were run together with pertinent parameters. In each case, pressure was typically adjusted until the plasma stabilised at the aerial tip. Thus final pressure was often dictated by aerial configuration, not whim. For most aerials, particularly with hydrogen flow, the plasma would stabilise in the area of 80-100 torr which is termed 'moderate pressure' below. For certain configurations and particularly with an argon/hydrogen mix, higher pressures (at times, all the way to atmosphere) could be achieved. Special note will be made in such circumstances. The following is a list of the ten experiments conducted (E1 through E10):

E1) Room temperature ethanol with argon as support gas. Pressure was maintained at 80-100 torr. No hydrogen was introduced. This experiment used the hollow-top aerial with a Kovar wire coil at its tip.

E2) Room temperature ethanol with hydrogen support gas. No argon. Used T-base aerial with Kovar tip. The low hydrogen flow rate led to a few brief periods of stopped hydrogen flow but these were very brief in duration. Again a moderate pressure of 80-100 torr.

E3) Similar to E2 but with needle-top aerial. Pressure was higher (about 140 torr).

E4) Pure ethanol with no support gases. The ethanol was heated to raise its vapour pressure in order to create a good, stabilised plasma. Hollow top aerial at typical 80-100 torr window.

E5) Room temperature ethanol + thiophene with hydrogen as support gas. Hollow-top aerial. Moderate pressure again.

E6) E5 with T-base aerial

E7) Hydrogen + argon + ethanol/thiophene mix. Higher pressure of 150 to 200 torr.

E8) E7 without thiophene. Note that due to the lingering effect of thiophene in the pipes, it is unlikely that the thiophene was eliminated completely, but concentration was certainly greatly reduced.

E9) Ethanol only at moderate pressure (in the region of 100 to 120 torr). Experiment followed a high pressure hydrogen-only run to pre-vaporise aerial and deposit metal on alumina

E10) Re-run of E6 at higher pressure (140 to 160 torr)

These experiments are summarised in the table overleaf

	E1	E2	E3	E4	E5	E6	E7	E8	E9	E10
Ethanol Pressure	L	L	L	H	L	L	L	L	M	L
Support Gas	Ar	H_2	H_2	None	H_2	H_2	H_2 Ar	H_2 Ar	None	H_2
Thiophene	No	No	No	No	Yes	Yes	Yes	No	No	Yes
Aerial	HT	TB	NT	HT	HT	TB	NT	NT	TB	TB
Pressure	M	M	MH	M	M	M	H	H	M	MH

Table 7-1: List of Nanotube experiments

Key:

H	High	L	Low
M	Moderate	MH	Moderately high
HT	hollow-top	NT	needle-top
TB	T-base		

The results in each case were analysed using a JEOL JSM 6000F field emission scanning microscope operated at 20 kV. Observations for each experiment and the results obtained are discussed in the next chapter.

8 Results: Nanotubes

This chapter details observations made during the runs of experiments E1 through E10 listed in the previous chapter. SEM images of resultant products are presented and considered in detail.

8.1 E1

This experiment made use of ethanol vapour and argon with no hydrogen as a support gas. No thiophene was added, and the hollow-top aerial, tipped with Kovar was used to stabilise the plasma and provide catalyst particles. The pressure was kept at around 100 torr.

Firstly, recall that as hydrogen gas is added to the plasma chamber, the plasma will begin to shrink until it is a small, purple wisp located at the tip of the aerial. The aerial in turn becomes extremely hot and will typically melt unless it is made from a refractory metal such as molybdenum or stainless steel.

Without hydrogen, however, it can be difficult to stabilise the plasma. If the plasma were made entirely of Argon, it will not shrink as pressure is increased. This is considered a major problem for our apparatus since in this case the plasma exists primarily near the glass where it can easily cause melting (although melting has been avoided from such a plasma thus far). It would be interesting to simply run a high pressure argon plasma for a significant time and see if the chamber did indeed melt, but this was considered too costly an experiment. In addition, if the plasma is large, its effect on the aerial (in terms of heating) would be limited since it exists primarily on the walls and not in the centre of the chamber. This is not true of Argon/H_2 mixes, however.

With ethanol added, it is possible to shrink the plasma to a small ball on the aerial tip. Nevertheless, stabilisation remains a problem and frequently during this run the plasma would move about. This meant that the antenna would at times stop glowing from local heating by the plasma.

A pure argon plasma is a brilliant, shimmering turquoise – quite spectacular. A pure ethanol plasma is only slightly less spectacular as it forms a brilliant white ball at the aerial tip – something like a mini sun and reminiscent in its colour of burning magnesium. During this experiment, the plasma would vary between purple and brilliant white/orange. The orange is often indicative of the plasma eating the stopper or base and could have been a result of the occasional bad containment of the plasma.

The entire run lasted for some three minutes after which the alumina rod was coated with significant carbon deposit.

Under analysis with the JEOL 6000F, no nanotubes were discovered. This was at least partly to be expected since the plasma was largely ethanol based (argon dilution was quite low) which would expectantly lead to large amorphous carbon deposits. Considering the importance placed on hydrogen presence in the literature, this was never expected to be a good run.

However, previously, during a test run, nanotubes had in fact been made using an almost ethanol-only plasma (very low argon level). The yield was low, and the nanotube quality was poor, but nevertheless, nanotubes were produced.

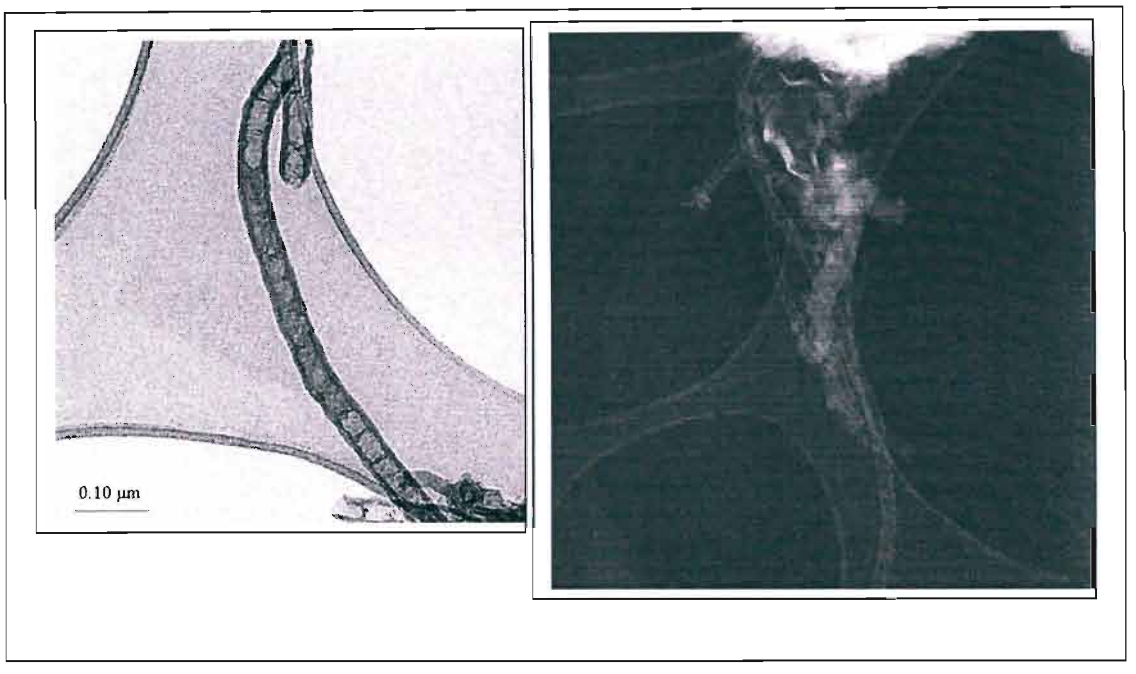

Figure 8-1: Showing TEM images taken from early nanotube synthesis work. Images taken at 200kV on a CM200 TEM. The nanotubes on the right are growing from an iron particle and seem to have the "bamboo" structure.

It is therefore not unreasonable to expect that some sporadic nanotubes may have been created in this process. However, it is safe to say that an ethanol/argon mixture is not particularly promising. The following images were taken using the JEOL JSM 6000F of the E1 samples.

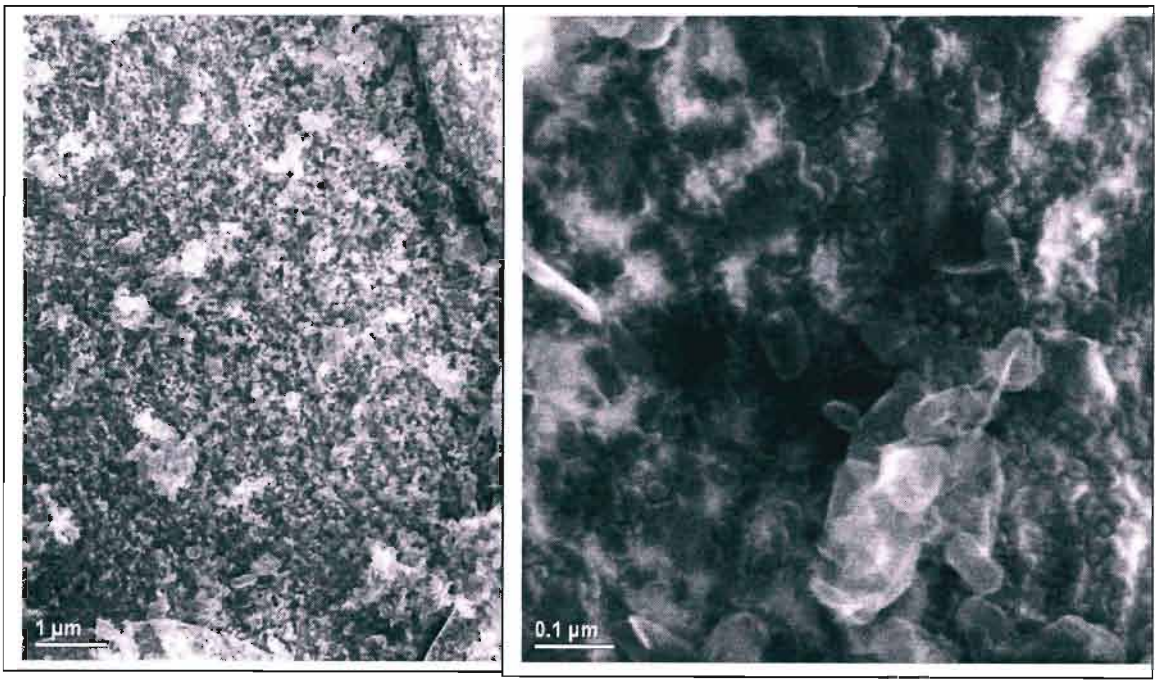

Figure 8-2: Deposit on alumina surface following E1 experiment.

No nanotubes were visible at any resolution. The method remains a fancy way of making carbon soot. Again, this is not unexpected.

8.2 E2

This experiment differed from E1 insofar as hydrogen replaced argon as the carrier gas. From the literature review, a good flow of hydrogen is considered crucial. At times it is necessary for nanotube growth to occur at all, and at other times it may at least suppress amorphous carbon formation. A switch was made to the T-base for this experiment, which tended to work better.

It was observed that, as usual with hydrogen gas, the plasma quickly shrank with increasing pressure until is formed a small, purple wisp at the top of the aerial tip. The aerial tip melted rapidly, but as the molten ball became bigger, eventually a point was reached where melting ceased. This all occurred over a very brief period of time, before the introduction of ethanol. As usual, ethanol was introduced by opening a flask of ethanol to the vacuum chamber.

The small plasma is, of course, extremely hot (capable of rapidly eating its way through the borosilicate were it not contained). As such it would cause both the aerial tip and alumina substrate to glow bright orange/white. This was considered advantageous since higher temperature – even beyond a thousand degrees – encourages crystallinity of the nanotubes.

Carbon deposition occurred gradually and primarily in and around the hot zone of the alumina. The low rate of deposition was also considered conducive to nanotube growth since a low concentration of carbon precursor should lead to less amorphous carbon deposit. An experiment such as this could take up to 10 minutes to form suitable, visible carbon deposit. However, since the alumina glowed brightly during the experiment, it is not actually known how long it took before any visible carbon deposit at all was formed. Various experiments showed that this depended on pressure (and hence temperature) and could take only a few minutes – perhaps less.

Adding ethanol would not change the colour of the plasma at suitably high pressures (100 torr was sufficient). For a very low flow rate of hydrogen and very low hydrogen pressure (lower than in this experiment), the addition of ethanol could turn the purple hydrogen plasma to a faint, pale blue colour.

Upon analysis, nanotubes were indeed found to populate the surface of the alumina.

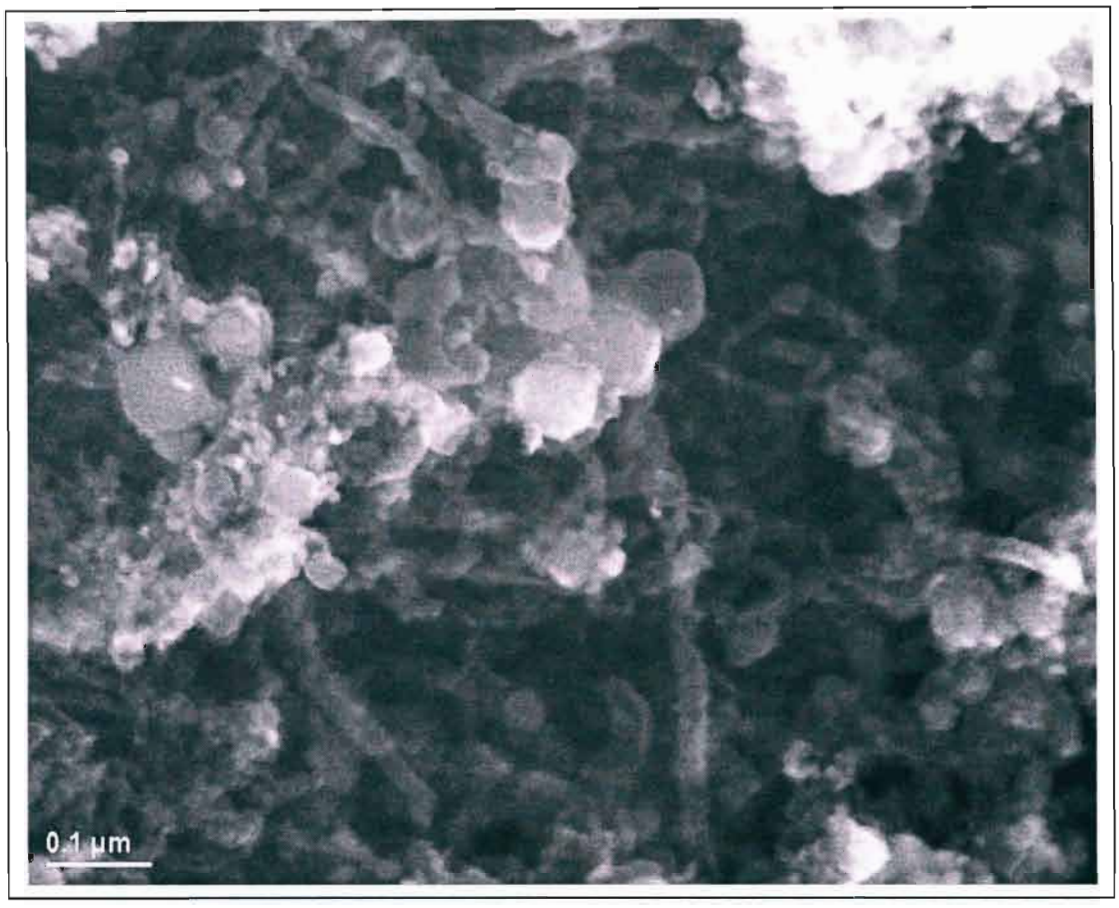

Figure 8-3: Nanotubes on surface of E2 sample. Some sporadic coating shows up as white clumps.

This was a very promising result. The replacement of Argon with Hydrogen had indeed ensured the deposition of a large number of nanotubes on the alumina surface. There is considerable variance in the diameter of the nanotubes. The thickest is around 27 nm and the thinnest roughly 10 nm. Large clumps are clearly visible on the surface of the deposit. Lack of EDX prevented identification of these lumps, but it is expected that they are clumps of metal catalyst, perhaps with some amorphous carbon as well. Amorphous carbon is likely to be present given that most methods for nanotube production do produce amorphous carbon in some quantity. However, metal catalyst fragments are almost certainly present as well, or else nanotube growth could not have occurred. It must be noted that due to the low hydrogen flow rate, the hydrogen flow did accidentally stop very briefly a few times which could have caused some small amorphous deposit. It is difficult to gauge the extent of the deposit from the images, but there are definitely more nanotubes than useless deposit and the unwanted 'white clumps' seem to be located primarily at the surface. A scan from another area of the sample is shown below.

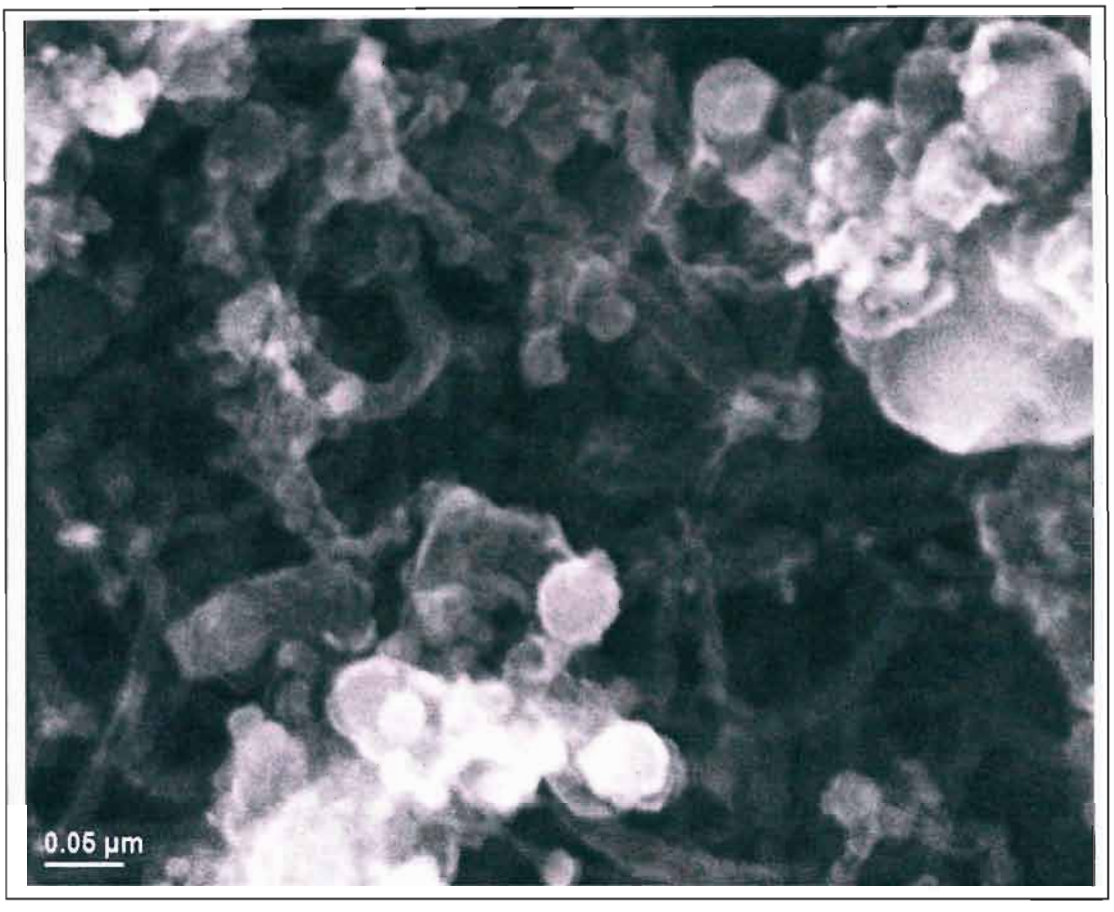

Figure 8-4: Nanotubes from another area of E2 sample.

This pattern of clumps of white metal/carbon surrounded by and covering a sea of nanotubes is consistent throughout the sample. The following image shows successively closer zooms of the surface.

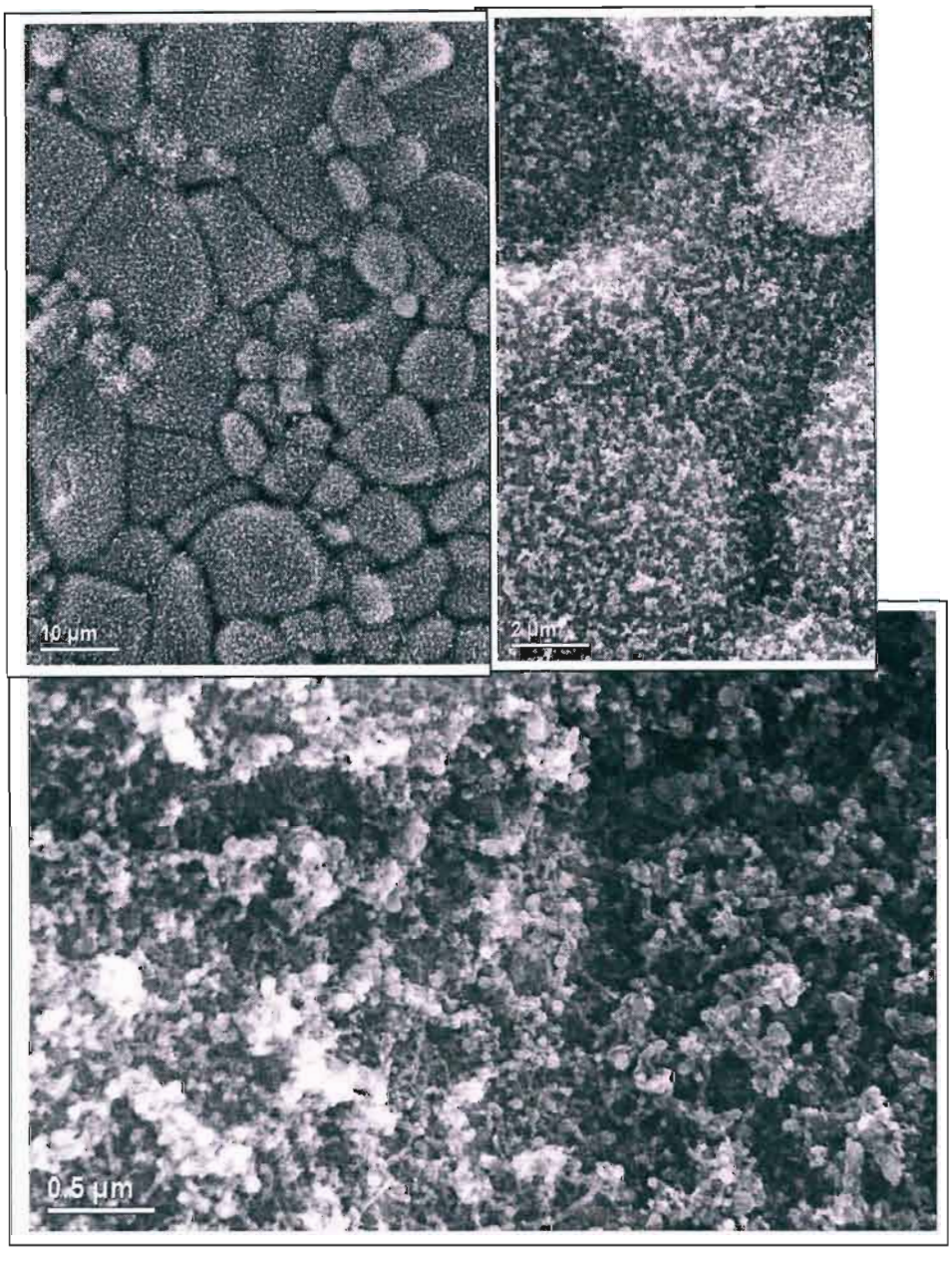

Figure 8-5: Successively closer zooms of E2 sample.

Apart from the clumps of unidentified matter and lack of uniformity in nanotube diameter, this is a very promising result. The process has not been optimised at all. Pressure was arbitrarily set by way of watching when the hydrogen plasma shrank to a suitable size and stabilised. Flow rate was arbitrarily set as it could not be measured (but was on the low side to preserve gas). Temperature was dictated by pressure and flow-rate. We can quite confidently predict that with further optimisation, the process could achieve consistently good results. In particular, a swifter hydrogen flow rate may already reduce unwanted deposits (Li et al., 2004). Addition of ammonia could also be beneficial as discussed in the literature review.

8.3 E3

This was an interesting experiment primarily for its lack of result. The parameters remained the same as those used in the E2 run, with the exception of the aerial. Switching to the needle-top antenna allowed higher pressures to be reached. However, the pressure increase was not considered to be particularly significant (about 40 extra torr). Nonetheless, by the end of this run, (total time roughly 10 minutes) no significant deposit had been formed on the alumina. Attempts to scan the surface lead to excessive charging indicating that indeed, even microscopically the surface was more or less barren.

At first it was uncertain as to exactly why no deposit formed. It seems, however, from later experiments that the increase in temperature simply made the alumina too hot. A shorter-than-usual alumina rod was used in this experiment and as such was more-or-less exclusively a hot-zone. Later experiments at significantly increased pressure continually showed no deposition in the hot zone. This is in contrast to 'cooler' experiments at lower pressures, such as E2, where deposition will always occur in the brightest part of the rod.

Fortunately, the alumina is not the only surface that tends to catch soot in these experiments. The aerial itself is covered with black powder during most runs. The aerial was sonicated in ethanol and the resulting solution was applied to a carbon stub. After drying, the carbon stub was viewed at 20 kV.

Indeed, nanotubes had formed on the aerial tip. Many of them appeared of poor quality, however, especially compared to the E2 sample. Some results are shown below.

Figure 8-6: Some carbon nanotubes amidst other carbon formations.

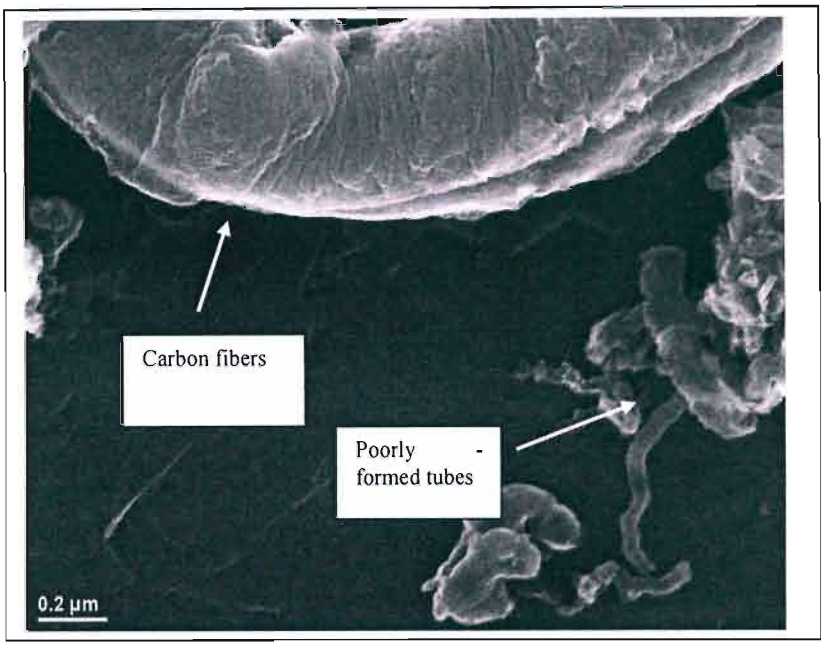

Figure 8-7: Carbon fibres and poorly formed nanotubes from the aerial tip.

It can clearly be seen that while some nanotubes did form, there is also an assortment of carbon fibres and other structures that look as if they are full of defects. This is possibly due to the influence of the higher temperature, higher pressure plasma. Although high temperatures are conducive to good crystallinity (such as in the arc discharge process), most of the CVD literature reports excessive temperatures frustrating good growth.

It is interesting, in a way, that nanotubes would form at all on the antenna itself, since nanoscale particulate catalyst, not bulk catalyst, is needed to precipitate nanotube growth. There are two explanations for this: 1) It is possible that microbeading of a fashion occurs at the tip of the aerial. Plasma bombardment of the atomic surface combined with high heat could result in a very nonuniform surface that is particularly 'bumpy' or containing many sites conducive to nanotube growth. 2) It is also quite possible that nanotubes are formed very close to the surface of the aerial and then simply drift towards and adhere to it by virtue of the fairly chaotic flow dynamics around the aerial. If nanotubes did move quite close to the aerial, it would be simple for them to adhere to it by virtue of their strong van der Waals forces. The latter seems to be the more reasonable of the two explanations. Coatings were often seen on the aerial holder as well, and carbon deposits tended to form in many places (such as on the soapstone spacer). This lends credence to this explanation.

Looking at these results alone, we could conclude that nanotube growth at or very near the antenna surface is poor at best and corrupted by the intense heat and plasma bombardment. However, later results show that high quality nanotubes are quite capable of forming on, or attaching themselves to, the aerial tip. Rather, it is believed that the excessive heat around the aerial in this run was the primary problem.

8.4 E4

This experiment used ethanol only without support gases. From earlier results, and even theoretically, it is easy to predict that amorphous coating would be the primary product. Considering the plasma effect, diamond-like carbon (DLC) could also possibly form, but that is unimportant.

From afar, the surface resembles to some extent the surface of the E2 sample, with speckles of white:

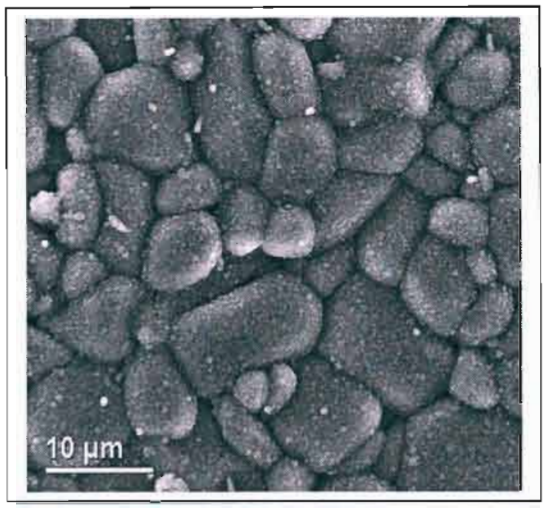

Figure 8-8: Low magnification view of alumina surface for sample E4.

A closer look reveals no nanotubes whatsoever, and merely jagged looking carbon surfaces. The form of carbon was not considered important and so not considered further.

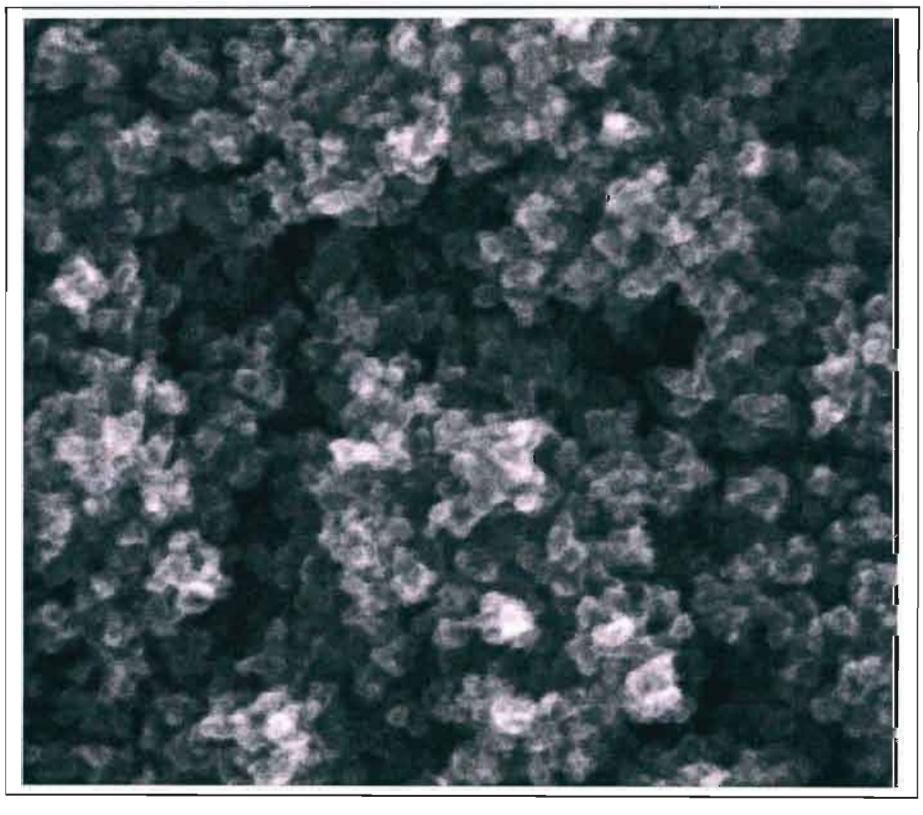

Figure 8-9: Closer view of E4 surface.

8.5 E5

The hollow-top aerial did not work particularly well during this run, which was intended to emulate the E2 run (ethanol and hydrogen, no argon) but with the addition of thiophene. It is thought that the poorly functioning aerial was the reason very little carbon deposit was seen. The plasma was incredibly small (barely a glow) and good pressures (considered as 80-100 torr) could barely be reached without extinguishing it. This sample was considered a failure. Again the aerial tip was sonicated and the results are displayed below.

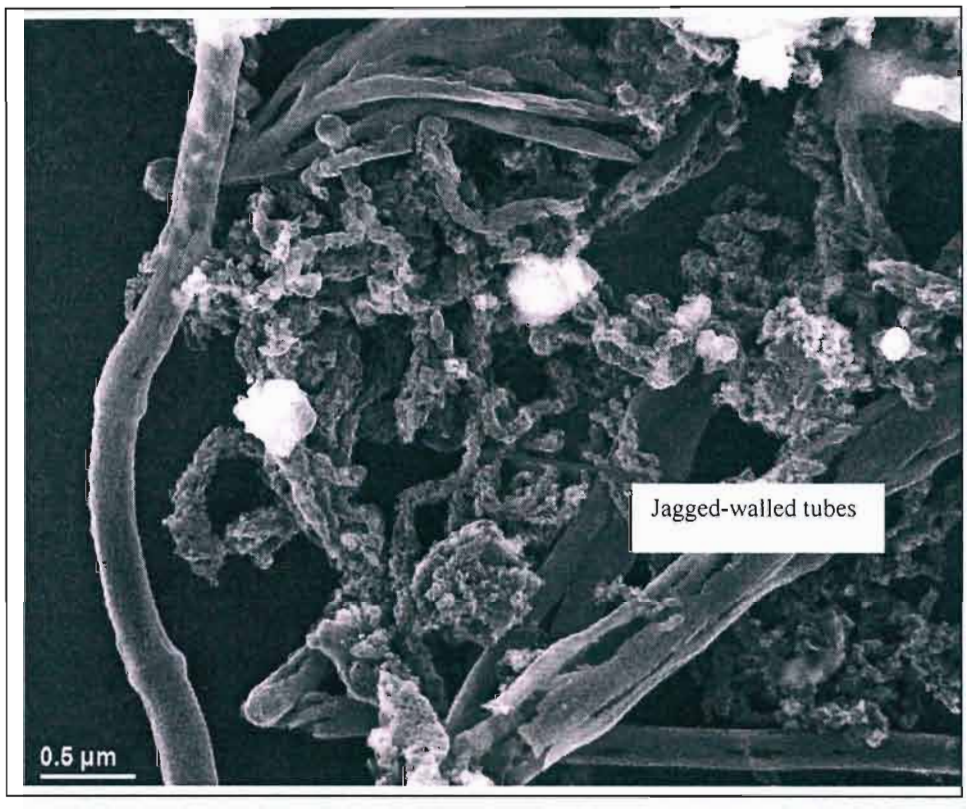

Figure 8-10: Jagged-walled tubes were seen to form amongst larger carbon fibres.

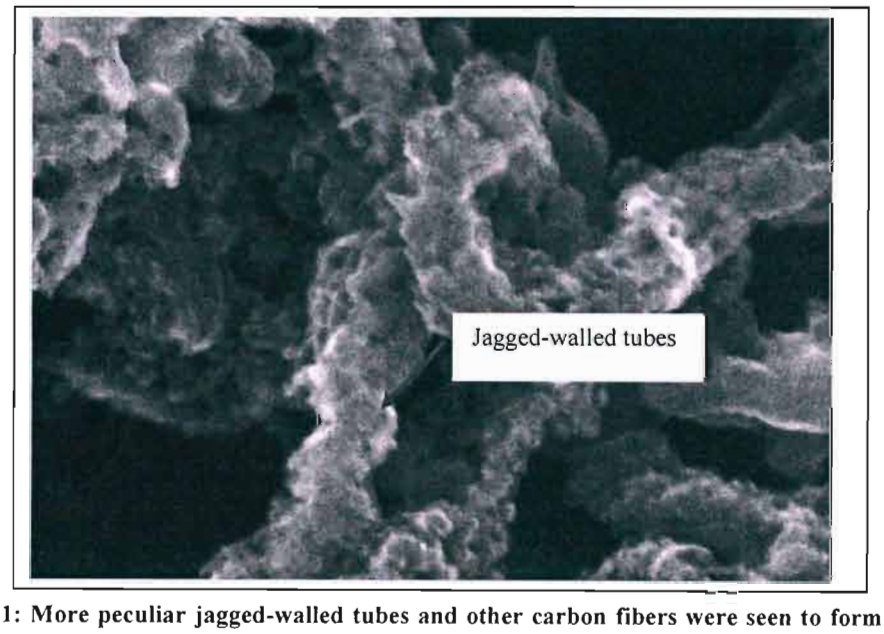

Figure 8-11: More peculiar jagged-walled tubes and other carbon fibers were seen to form on the aerial tip.

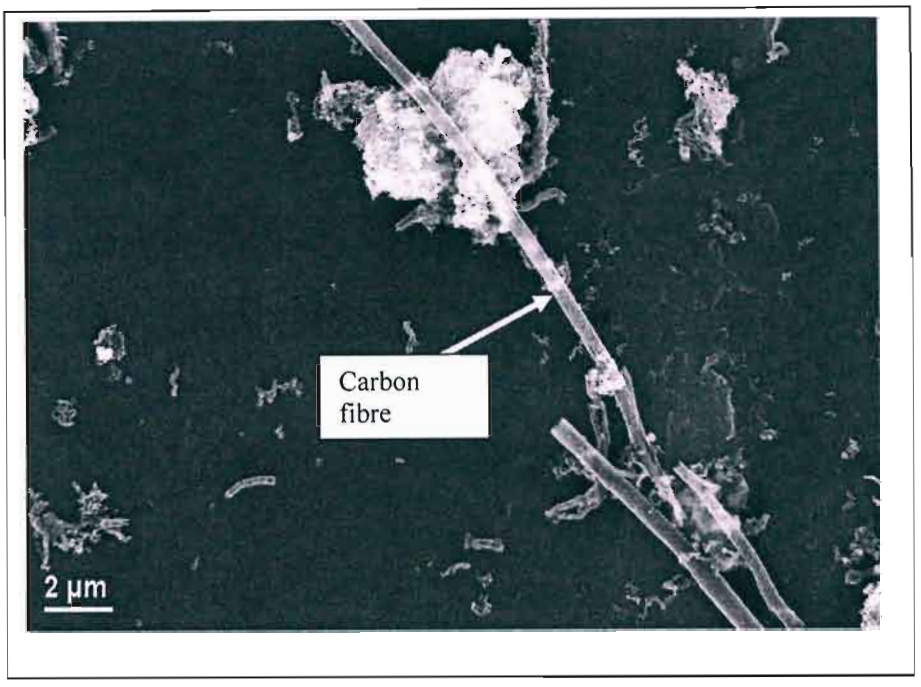

Figure 8-12: Large carbon fibers were also created.

The results show structures which cannot really be called nanotubes. There are some rather thick carbon fibres (figure 8-12) and many structures that look like jagged, very rough-walled tubes (figure 8-10 and 8-11). We can offer no insight as to what these structures may be. It is interesting, however, that they do take the form of tubes, but with walls that are completely damaged or amorphous. Certainly, amorphous carbon would be unlikely to form itself into such structures. At the same time, had nanotubes actually formed, the author knows of no precedent for their walls being damaged in such a peculiar way. Thus it seems more likely that carbon did form into these structures originally. To this end, it is reasonable to say that nanotubes may well form in this process, but for different process parameters (temperature and pressure primarily). Access to HRTEM would be invaluable in assessing the nature of such structures.

The bad results are deemed to be indicative of the poorly working plasma during this run and poor parameter choice. The very small plasma does not generate a great deal of heat at any area other than the very tip of the aerial (it is more of a glow, like a corona). This experiment was repeated with a different, more capable aerial next.

8.6 E6

This experiment used the same parameters as E5 but with the T-base aerial which worked considerably better. Unfortunately, there was a problem with the alumina rod substrate analysis. However, the aerial was once again covered in a black powder. This was sonicated in ethanol and applied to a carbon stub for better viewing. The following are images of nanotube deposit on the aerial:

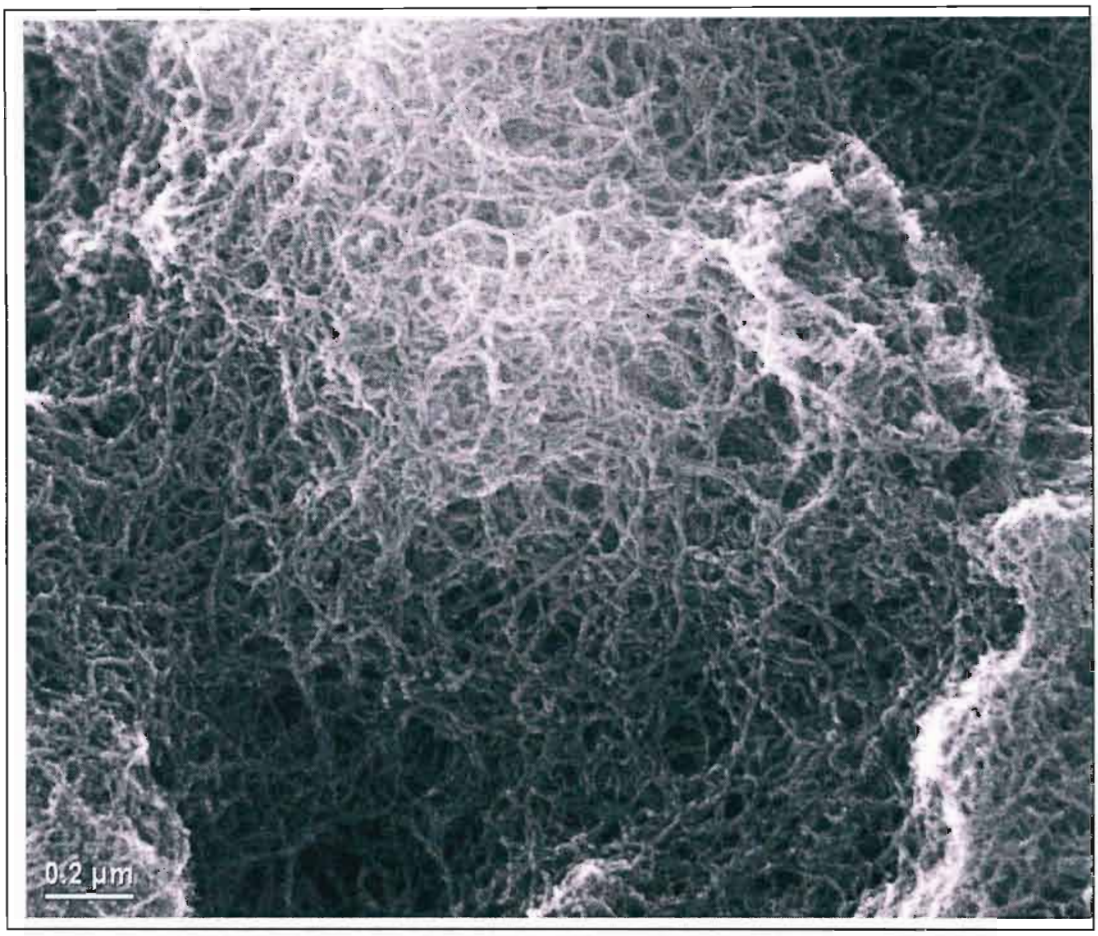

Figure 8-13: Sea of nanotubes from aerial tip. The diameters are seen to be quite uniform.

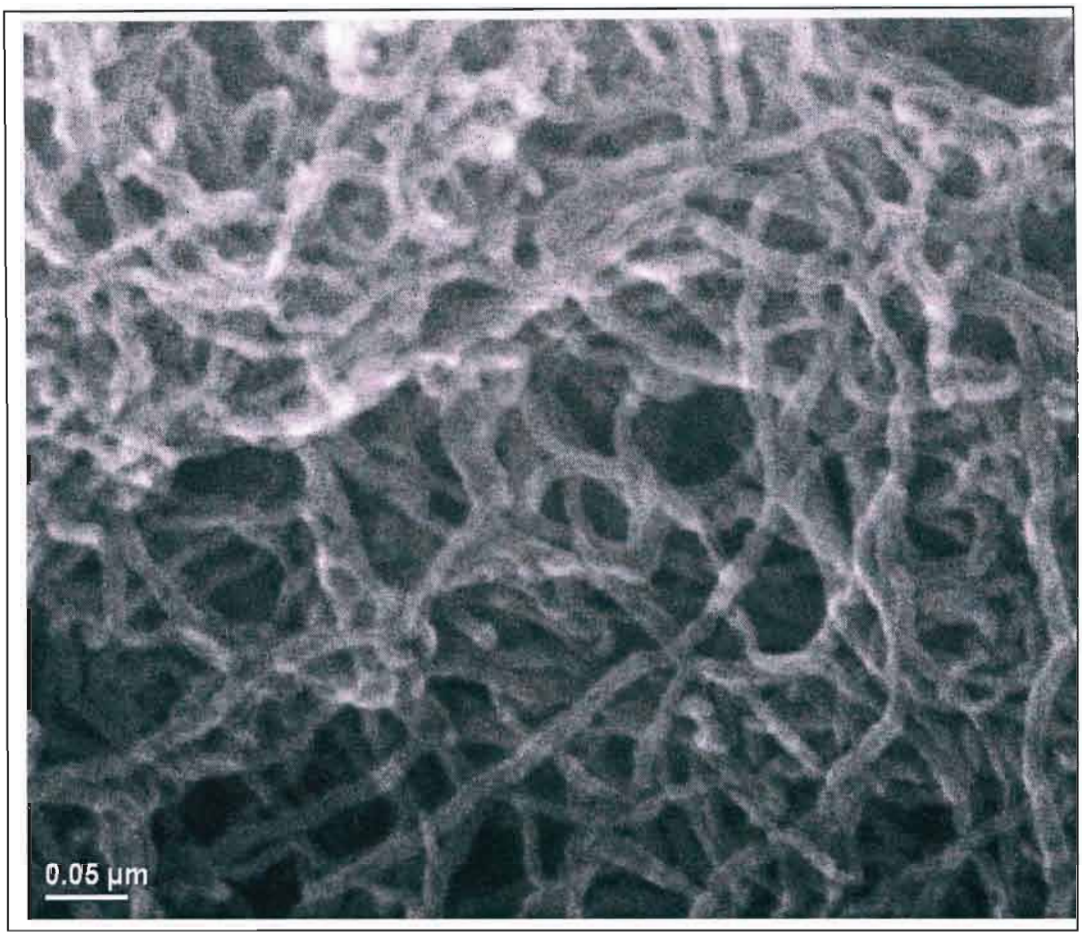

Figure 8-14:Closer view of nanotubes. Again, a great consistency in diameter is seen.

The results are exceedingly promising. Large clusters of similarly-sized nanotubes have formed on the aerial surface. The nanotubes appear of good quality, although it is difficult to make out the structure of the walls without better resolution. It is possible at this magnification that some 'bumpiness' of the walls may exist, but they do appear reasonably well-crystallised. No amorphous deposit is seen in these images.

Looking around the carbon stub onto which the aerial soot had been sonicated, some other, less spectacular results could be seen:

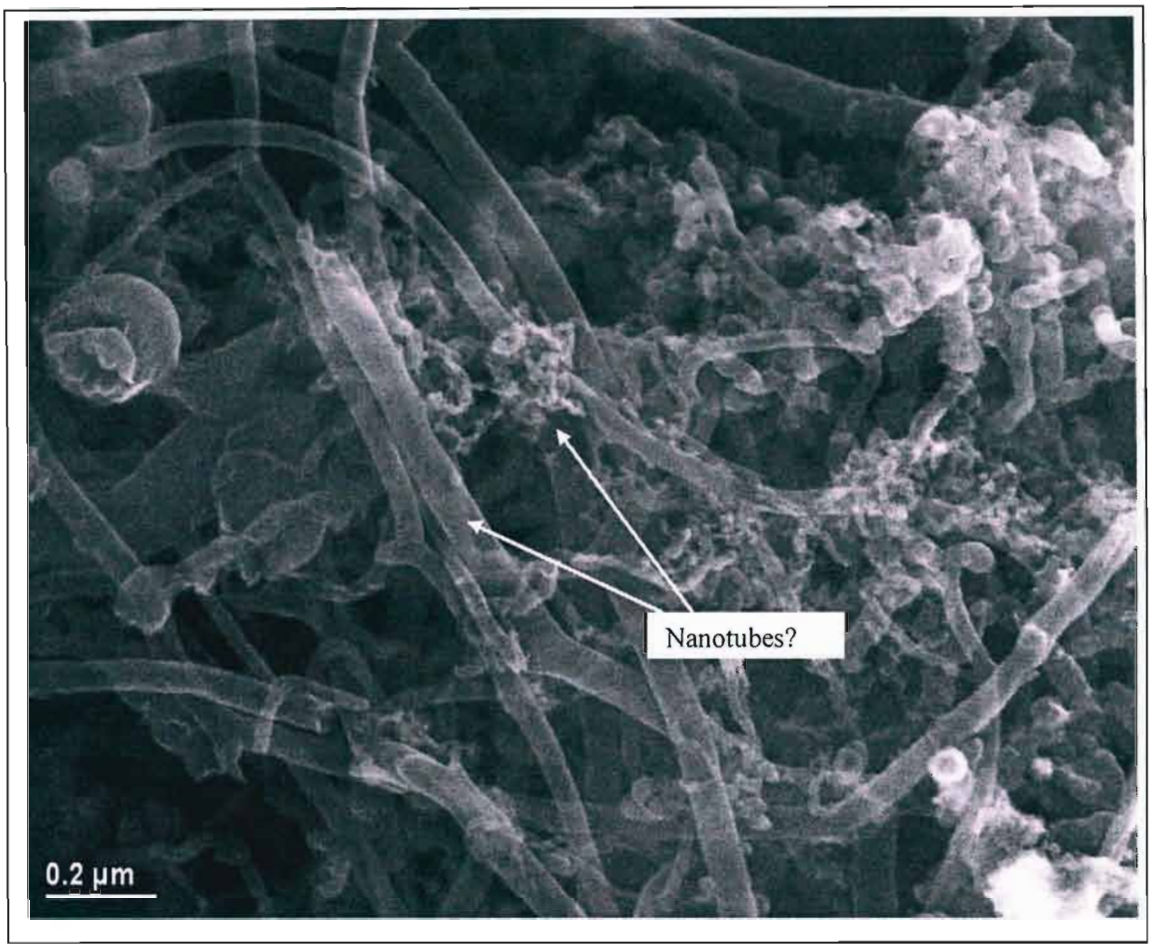

Figure 8-15: Nanotubes from a different section. Here there is more variety in diameter seen along with a few structures that may not be nanotubes.

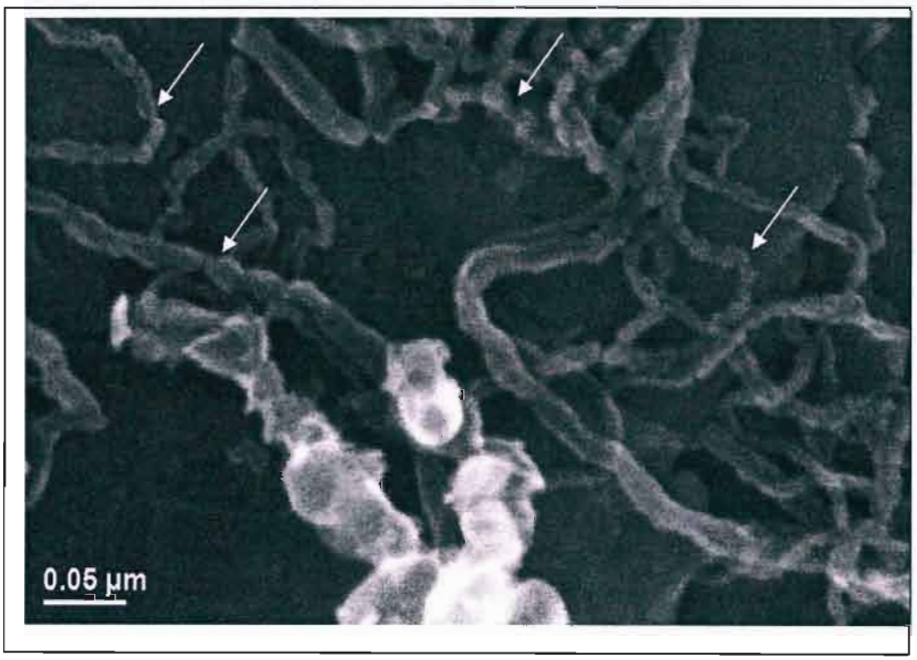

Figure 8-16: Results from yet another area of the same sample. Some tubes with jagged, or perhaps 'necklace-like' structures are seen (marked with white arrows).

These images indicate that the good results shown earlier were not consistent throughout the whole sample. In some areas, there was considerably less uniformity, and apparently lower yield. In figure 8-16 above can be seen tubes with surfaces that appear jagged, or possibly having the appearance of chains of bulbs stuck together. These are reminiscent of the "nano-necklaces" reported by Okuno et al. (2004) as shown in the following figure:

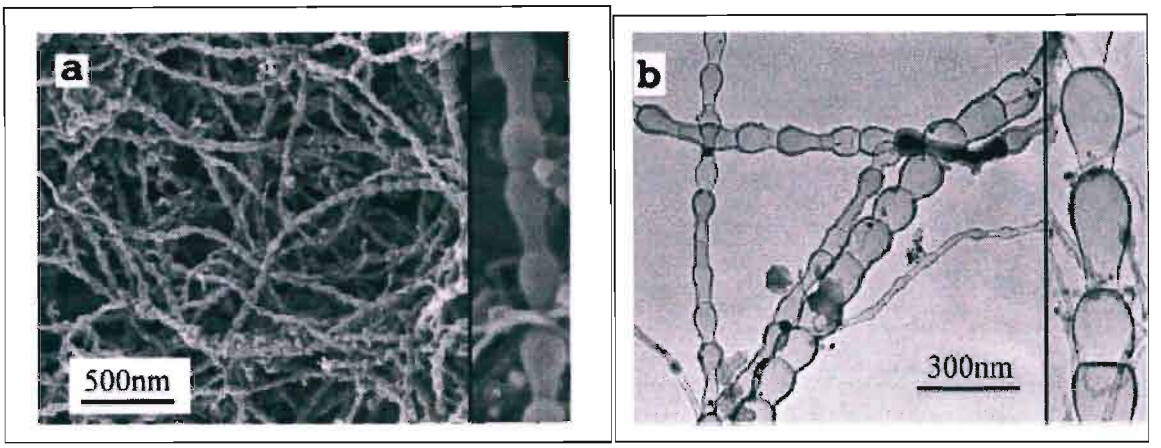

Figure 8-17:Nano-necklaces as reported by Okuno et al. (2004) (SEM image left and TEM right).

The SEM used, however, was not capable of resolving these structures any further.

It is safe to say that the addition of thiophene seemed to improve the results generally. Nanotube diameter was more consistent, and the yield was impressive. There were areas on the aerial which contained less impressive results, but by and large it seems that further optimisation of this process could produce high yields of quality nanotubes. Once again, there was no attempt at optimisation and most parameters were picked rather arbitrarily. In addition, it is possible that using three-catalysts in one is responsible for some of the variance seen. It could be the iron, for example, led to good uniform deposits under these conditions, while nickel or cobalt created peculiar structures and nanotubes of different diameter.

8.7 E7

Experiment E7 made use of the same mix as E6, but with the addition of argon which allowed much higher pressures (and consequently temperatures) to be reached.

It was found that carbon deposition did not occur to a reasonable extent on the rod. This was probably again due to temperature being too high which seems to suppress formation of any carbon deposit whatsoever.

8.8 E8

Another attempt at a high temperature run was still made, however. This time without the thiophene. Temperatures reached incredible levels. Although temperature could not be measured, the thin alumina rod used in this experiment actually bent from the heat. It is a wonder that the glass did not melt.

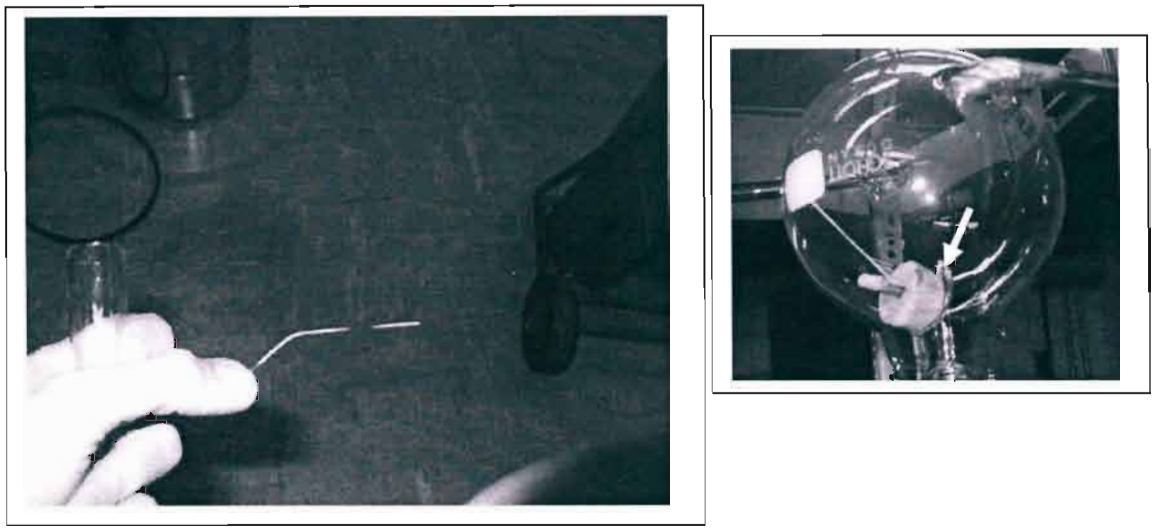

Figure 8-18: Bent alumina (left) and another high temperature run where the entire stand melted and bent over (right). This is indicative of the very high temperatures the centre of the plasma can reach. Alumina melts at around 2000°C.

In the above figures, one can observe how deposition occurred out of the hottest zone only (there is no deposit around the section where the alumina bent). This is further proof that these high temperatures suppress deposition.

The plasma, in addition, is larger with the Argon/Hydrogen mix than with Hydrogen alone. Once stable, it forms a purple/deep orange glowing ball that fills about 50% of the volume of the chamber. Were it not for the swirling gas and separation from the walls, the chamber would surely have melted. During such experiments, the entire aerial and at times even the top of the glass stopper is seen to glow a brilliant orange. It is not desirable to have the glass stopper so hot in order to both prevent damage and reduce contamination.

There was deposition that could be examined in this run showing that it should be possible to make the E7 run work better. Nevertheless, the deposit was not promising. However, other work in the literature with high temperature plasmas (such as all the plasma torch work) has shown that nanotubes will still form after or away from the plasma itself (reassembling from dissociated carbon after the hottest zone) so there is no reason to suspect such a process may not work better in a flow-through type of setup. It may be that if the collection point (the alumina rod) were placed further downstream, nanotubes would be detected. In fact, based on the literature, this is reasonably probable.

Below are two images that seem to indicate it may be possible for nanotubes to form under these conditions:

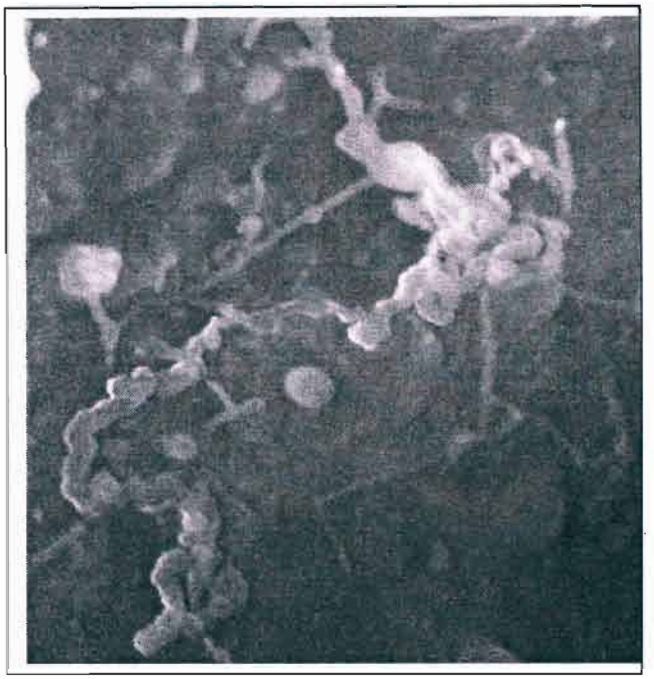

Figure 8-19: Some tube-like structures from the sample.

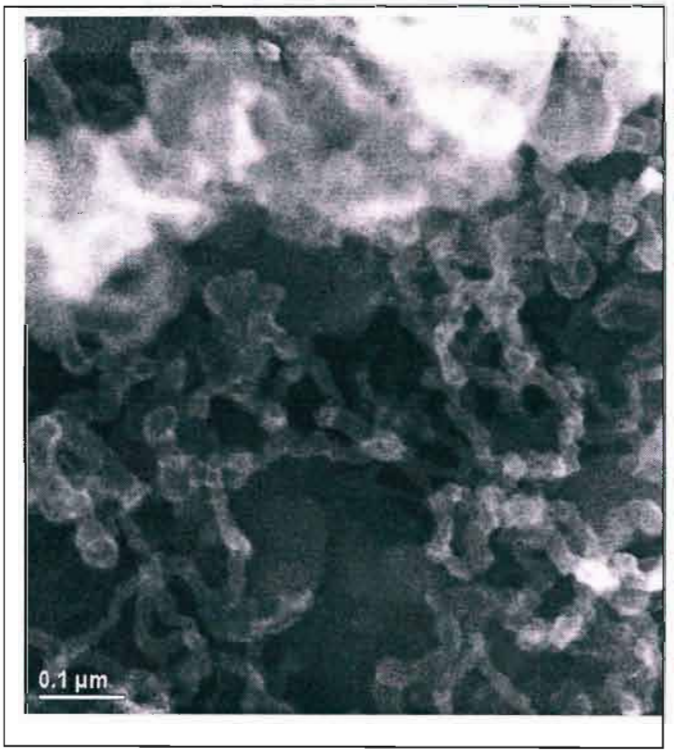

Figure 8-20: 'Bumpy' tubes.

The bumpy-looking tube-like structures above are again marginally reminiscent of the "nano-necklaces", although this is not necessarily what they are.

8.9 E9

This experiment ran once again without support gases, but this time a hydrogen plasma was run prior to ethanol introduction. This could theoretically have pre-coated the alumina rod with kovar material. However, the pure-ethanol plasma did not stabilise well. It can be very difficult to get an ethanol-only plasma to stabilise since it is difficult to change pressure without support gases. Once again, this experiment resulted in nanotubeless carbon deposit. This result can be expected with hindsight.

8.10 E10

Experiment E10 was meant to duplicate experiment E6 in order to analyse the alumina rod deposit. However, the T-base aerial had recently been modified simply by reforming the tip and re-drilling its hole (high temperatures had fused a previous Kovar tip to the stainless steel). This subtle change caused the same aerial to work at a higher temperature of around 160 torr. This is quite high for a hydrogen-only plasma in this apparatus and caused the entire aerial (not just the tip) and the alumina rod to glow intensely.

Figure 8-21: The aerial gave off an intense glow and the plasma was immensely hot in this final run.

The alumina rod bent in the middle once again. This time, however, the rod was quite long and part of it extended sufficiently far beyond the hot region (near the outlet pipe) so that there was some considerable deposit. The results were once again quite peculiar.

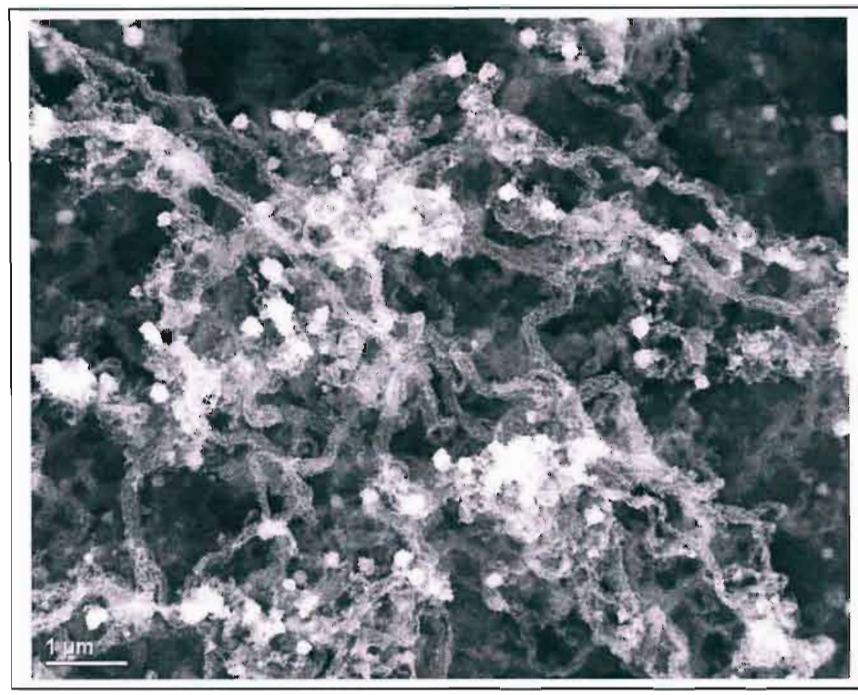

Figure 8-22: Tendrils of carbon having a tube-like appearance.

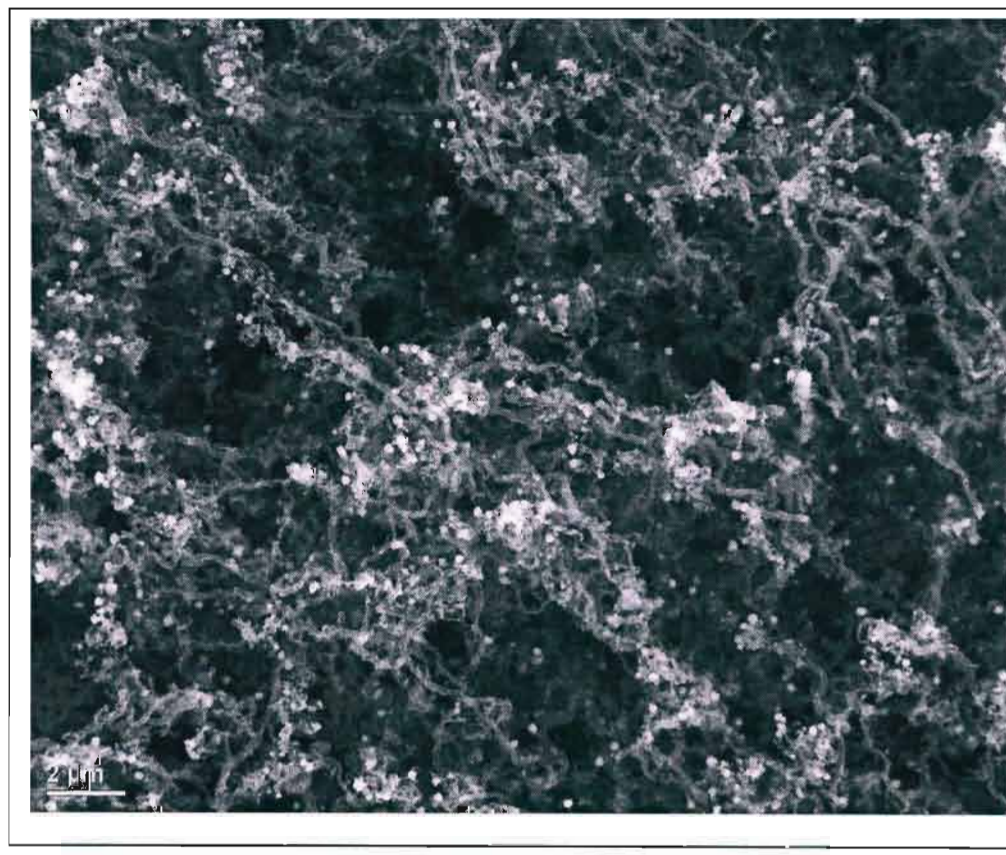

Figure 8-23: A lower magnification view of the carbon tendrils.

At first glance one might be inclined to believe nanotubes had formed. But in fact, the surfaces of these 'tendrils' are quite strange.

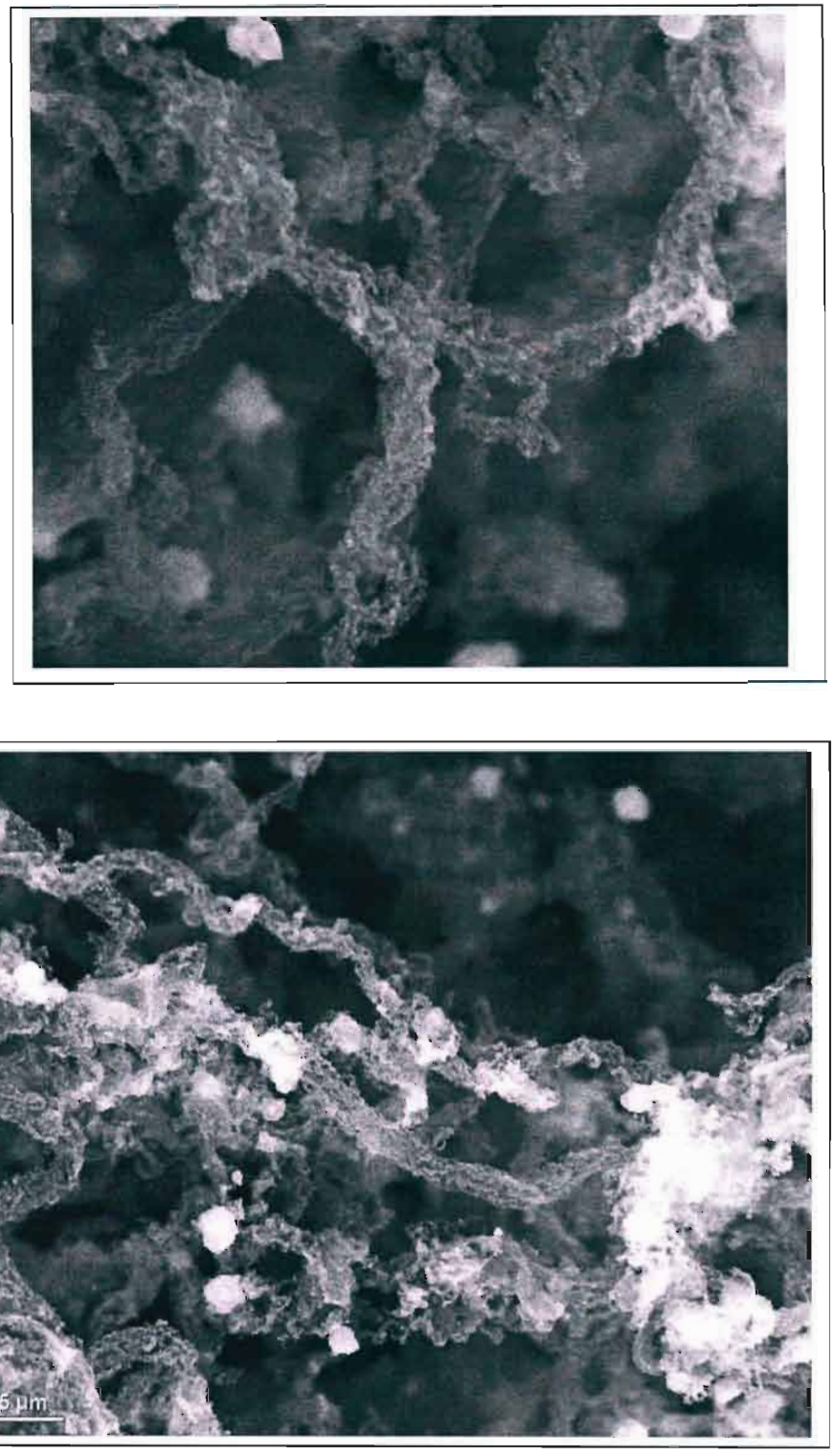

Figure 8-24: The tendril surfaces are rough and amorphous.

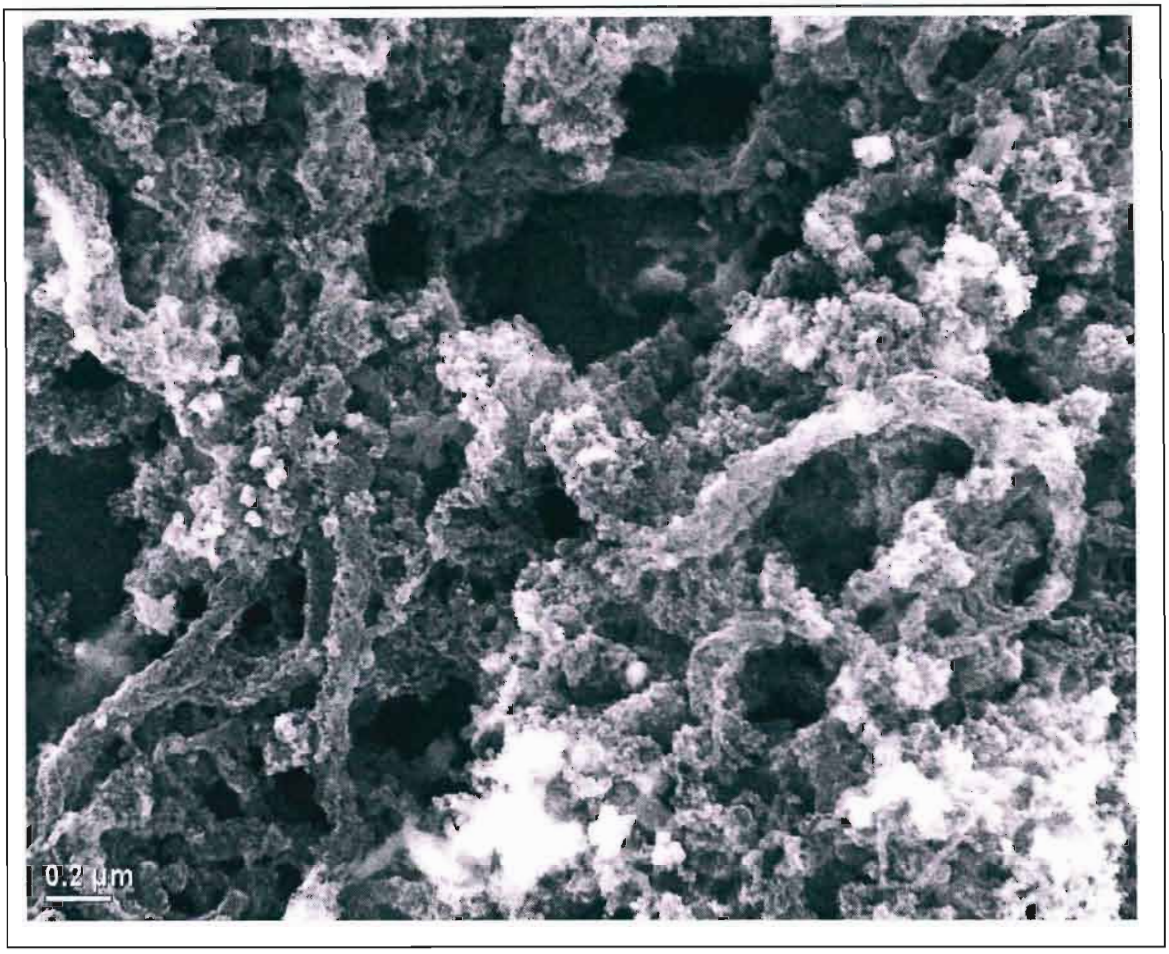

Figure 8-25: Jagged, damaged tubes are also visible.

Once again we see surfaces that are highly damaged. Certainly, these are not rolled up graphene sheets. And yet, once again, the structures form into tubes on a nanometer scale. The structures are actually quite thick for nanotubes (around 200 nm) and therefore would possibly be classified as carbon fibres. This could be the reason why their walls are so peculiar. That is to say, it is possible that these tubes grew from larger catalyst particles. Perhaps large catalyst particles formed because of the higher catalyst vapour pressure in these experiments. It is even possible that nanotubes did form and were successively coated by layers of carbon until the fibres resulted. The tube-like nature of the results is certainly unmistakable.

Nevertheless, it is seen once again that too high a pressure makes the process less useful. Since these samples were collected slightly more downstream than usual, this suggests that perhaps even farther downstream the product is essentially useless in these sorts of high temperature experiments.

At the same time, it could be that the thiophene concentration is all wrong for these parameters. As noted in the literature review, thiophene concentration can hamper results as well as help them.

8.11 Summary

Considering that at least two runs were capable of producing a good yield of uniform multi-walled nanotubes without optimisation of any kind, it seems that the apparatus is indeed useful

for making nanotubes. On successful runs, extra deposit was seen in the form of bright "clumps" (possibly amorphous carbon or metal), but concentration of such deposit is quite low and should be easy to filter out (for a good overview of filtering techniques, the reader is referred to Daenen et al., 2003).

It seems that the addition of hydrogen is quite necessary for the formation of nanotubes. Although nanotubes have been formed in this apparatus without hydrogen in the past, these were few in number and poor in quality. The comparison between the results of E1 and E2 make this quite plain. The theoretical importance of hydrogen was discussed at length in the literature review and thus such results should come as no surprise. Further increasing the hydrogen flow rate could even improve results as suggested in Li et al. (2004). The results also indicate that a pure argon environment is quite unsuitable for nanotube growth.

The amount of extraneous deposit appears to be quite low and the use of ethanol as a carbon source is no doubt at least partially to thank for this. Hydrogen etching of amorphous carbon could also be contributing to the effect. The use of low levels of ethanol is also certainly beneficial since excess carbon will be easily dissociated and deposited as amorphous carbon. We had access to no apparatus capable of identifying the white 'clumps' seen in some of the nanotube images, but these may well be metal. In any event, extra amorphous carbon deposit is either low or virtually nonexistent.

At the same time, the low concentration of ethanol vapour used makes the process less useful in a 'through-flow' type of mode since the quantity of nanotubes in the air is incredibly small. This is in stark contrast to the work of Li et al. (2004) where by injecting ethanol directly, a thick 'aerogel' of nanotubes could be seen to form. This makes our setup considerably less valuable for such a process.

The addition of thiophene seems to be unnecessary for nanotube formation. However, adding thiophene does seem to affect both yield and diameter consistency in a positive fashion.

Too high a pressure and temperature seems to have a detrimental impact on results. The temperature inside the plasma at higher pressures reaches thousands of degrees and thus would realistically vaporise any carbon formation in that zone. However, since the sample was collected only near the aerial (the hottest region), it is not unreasonable to expect that results may be better further downstream since thermal plasma nanotube synthesis has been performed many times before (e.g. Okuno et al., 2004 or Smiljanic et al., 2002) with plasmas still hotter than this one. The E10 result seems to suggest, however, that at least for the parameters used in that experiment, this is not the case. However, given how reasonably common high temperature plasma synthesis is, there should be a set of precursors and parameters for which growth downstream would be better. Nevertheless this does not seem to be a promising way to use the apparatus.

Again it must be stressed just how much room for optimisation there is. In fact, there is too much room and it was difficult for this author to decide to stop trying different things (though the decision was aided in part by monumental equipment failure). It would make an interesting study to discover the effect of altering various variables. For example:

1) **Concentration of thiophene**. It would be advantageous to not simply mix the thiophene in with the ethanol, but have it attached to the chamber by way of a separate filter flask. The vapour pressures of the two liquids could then be individually controlled (through temperature control of the liquids). As seen in the literature review, yield and quality can be quite sensitive to actual thiophene concentration.
2) **Replacement of hydrogen with ammonia**. Hofmann et al. (2003) suggested that adding ammonia to plasma systems caused the etching away of amorphous carbon and it would be interesting to see if this could improve results further.

3) **Different catalysts.** The use of Kovar as a catalyst seemed expedient. However, it would be beneficial to try in turn iron, cobalt and nickel and see how results were affected. EDX scans of some samples indicated a very low presence of Ni and Co (typically only a few atomic %) indicating that iron was the primary catalyst in these experiments. It was unfortunate these scans could not be saved or printed as they were performed on malfunctioning apparatus at the University of Kwazulu-Natal Westville campus electron microscope laboratory. It is also possible that the different catalysts used simultaneously caused some of the large variation in diameter and structure seen in certain results. It would be a very good idea to try pure iron alone.
4) **Flow-through.** All results in these tests were collected inside the chamber, near the aerial. Since the technique is actually a variation on VPG, it would be a good idea to catch soot outside the plasma chamber (using a filter or cold-trap) and see what the results are like. In order to make the apparatus truly useful in a flow-through type of arrangement, the concentration of introduced ethanol should probably be increased. The amount of introduced catalyst may need to be increased in turn to prevent excessive amorphous carbon formation. It may be then that the most promising manner in which to achieve this is to use an external catalyst source such as ferrocene. Injection of a ferrocene/ethanol cocktail is a distinct possibility. In fact, in the very hot plasmas, fine iron powder could even be used. Nevertheless, once again it must be stressed that this does not seem to be the apparatus' strong suit.
5) **Replacement of ethanol with a hydrocarbon.** Ethanol is almost certainly a better choice if for no other reason than its low cost and ease of use. However, there is only one way to find out if it truly does achieve better results than a standard hydrocarbon source.
6) **Replacement of the aerial with a more controlled means of catalyst introduction.** Using a catalyst aerial seemed at once expedient and convenient and there was a need to know if it would work at all. However, there is no doubt that a more controlled process such as injection of ferrocene or controlled sublimation may be beneficial. At the very least, it would make an interesting study.

From the literature review it is known that even subtle variations in pressure and temperature can have a notable impact and so it seems quite plausible that results can still be improved a great deal. In particular, it seems in the literature that there is a temperature/pressure window for which good quality tubes will form. In our own experiments, it is clear that lower temperatures and pressures of about 100 torr (as in the successful E2 and E6 runs) are most appropriate. Re-running the same experiments at higher pressure (and consequently temperature) would ruin the experiment. This is not to say that it is impossible to form tubes under such conditions.

In all nanotube synthesis methods in the literature, parameter control proved vital in optimising both yield and quality of the product. This is one area that must be looked at as a priority. There is a decided lack of control available in this system – as in most high pressure plasma systems. The primary problem is that pressure and temperature are interlinked in this system and not independent variables. In addition, the plasma may only be stabilised and confined over certain pressure windows which precludes the use of just any temperature/pressure combination. The window itself is strongly influenced by the aerial design, but for the T-base aerial in a hydrogen plasma it is typically 80 to 160 torr.

Nevertheless, there is some good room to tweak and improve results, and it is believed that this is indeed a viable method for nanotube synthesis.

9 Conclusions and Future work

9.1 Nanotubes

There is no doubt that the plasma reactor can be used to produce nanotubes quite successfully, but is it useful for such a task? The method has in its favour the fact that it is low-cost and simple to set up. In fact, even a simple tube furnace would cost considerably more. This makes the method accessible to even the casual researcher, which was one of the primary aims. The results achieved with the apparatus appear good, even without optimisation. Nevertheless, further optimisation is certainly needed.

In terms of commercial applicability, it is the author's opinion that this apparatus holds no advantage whatsoever. There are many simple and cheap methods of high quality nanotube production that are easy to scale up and seem to provide better yield. For example, the work of Li et al. (2004) often cited throughout this dissertation is a model example of a recently developed process that holds much promise. Nevertheless, the apparatus would certainly make a useful nanotube research tool. It could even be used for PECVD of nanotubes, since traditional PECVD apparatus is often beyond the means of many small research groups. Strict PECVD was not attempted with this apparatus, but there is no good reason to suspect it would not be successful given all the good work that has been done with microwave CVD in the past (see, e.g. Bower et al., 2000) and considering our own results with this vapour phase growth variant.

This work can also be considered as something of a study. Recall that it was of interest to see if different precursor use and a less thermal plasma could improve on the results of Smiljanic et al. (2002) and if the addition of a plasma would negatively impact on the good results of Li et al. (2004). At this point both questions can safely be answered in the affirmative. The better runs appeared to give a cleaner product than Smiljanic, but yield and quality are lacking as compared to Li et al. In addition, the importance of hydrogen has been confirmed for this process and some investigation into the role of thiophene conducted. Various studies may yet be conducted by changing the reactor conditions and the precursor mix. This serves to illustrate that the process and apparatus can be quite useful for the purpose of scientific investigation.

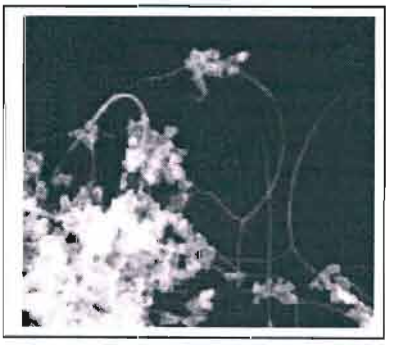

Figure 9-1: Results of nanotube fabrication in a quartz-tube plasma torch using a hydrocarbon precursor appeared to give a result with more unwanted by-product (Smiljanic et al., 2002).

There is much room for process tweaking and parameter variation and there is good reason to believe, considering the promise of such unrefined results, that it is possible to obtain good yields of high quality nanotubes using the apparatus. This would then become an easy way to quickly make nanotubes for other research such as nanotube application work.

In summary, this area of the work has been quite successful and shows much promise for the future.

9.2 The Apparatus

The apparatus itself is - or at least can be - quite useful. There are many laboratories (such as our own) that could make use of a cheap, easy-to-make plasma source. The equipment is perfectly useful for a number of applications including etching, surface treatment and PECVD. It could even be used for spectroscopy and any number of creative applications. At lower pressures, the aerial need not be used, allowing for less possibility of contamination. Of course, the aerial need not necessarily be a source of contamination, as in our nanotube work, but that would depend very much on how the equipment was used. The simplicity of the device and the ease with which it can be used – at least at lower pressures – could also make it a valuable training or teaching device.

At the same time, certain limitations of this rather cheap device are easily apparent and can limit the extent of the work done. Firstly, temperature and pressure are interrelated and cannot be altered independently. Changing the input power can alter temperature at a given pressure, but only at the expense of shrinking and possibly extinguishing the plasma, as well as lowering plasma density. In addition, the plasma will only stabilise away from the glass over certain pressure windows which means that not every desirable or conceivable pressure may be attempted. The useable window is related to antenna design and gas used. The addition of argon allows much higher pressures to be reached. Certain gases will not allow the plasma to shrink with increasing pressure (such as pure argon). This is potentially dangerous, since the plasma remains close to the glass. The glass reactor might not melt under such circumstances (we have run "plasmoid"-type experiments with atmospheric-pressure air plasmoids close the glass without causing melting). This remains to be seen.

On the present setup, flow rate and temperature could not be measured, but this need not necessarily be the case. Temperature measurement can be tricky because of the microwaves present in the chamber.

With regard to using the apparatus for PECVD, because the entire chamber is enclosed within a microwave oven, it is difficult to independently heat or cool a substrate placed in the oven. The substrate may be heated by the plasma or else a coil antenna can be designed to absorb microwaves and heat up. Unfortunately, this would potentially ruin the confining effect, and the heater may support its own plasma unless, perhaps, it were outside a hot-spot. In any event, independent substrate heating is very difficult. Independent substrate heating is not always necessary, but it is desirable.

The apparatus in its current form is difficult to use and most people in the laboratory grow a little afraid when the author switches it on. Minor mercury spills have occurred and, on rare occasion, overzealous flow rates of hydrogen would result in the vacuum breaking and a nice, small, hydrogen 'pop' complete with shattering glass. It can also be exceedingly difficult to confine the plasma properly at times as there may be a strong tendency for plasma to form at the aerial base. This can be overcome with better aerial designs and better location of the aerial tip near a hot-spot (a few centimetres can make a big difference). A clean aerial is seen to help as well. Nevertheless, the sheer number of chambers that have had holes melted in them is testimony to the fact that stabilisation can still be tricky. This is not the kind of apparatus one would leave running unattended overnight - or even for five minutes. That said, with a good aerial, in a good spot, stabilisation and confinement does indeed work with reasonable consistency. Care, and perhaps some aerial design/placement refinement is all that is needed.

In fact, most of the problems with the apparatus can be ironed out and the apparatus should make a useful addition to the laboratory. Though not the ideal plasma system, it certainly has many merits and could be used for both research and education were the kinks ironed out.

9.3 MgB_2

The MgB_2 experiments were an unfortunate failure. There simply did not seem to be sufficient etching of the Boron occurring to make the process useful. We can think of no way around this problem except to increase pressure and temperature and make the process more thermal. For example, fine boron powder introduced into a plasma torch would vaporise immediately. But is there any advantage in going such a route over the HPCVD method which gives such impressive results? It may be worth a try nevertheless.

It is still believed that the basic premise for the idea behind this deposition method is quite sound: use a plasma to etch a substance into a gas stream, and then use that gas stream to re-deposit the substance as a film. The trick is to find a substance that will etch easily enough in the presence of a gas that will not contaminate the deposition portion of the experiment.

The 'heat-pipe' idea for MgB_2 thin film fabrication may actually work very well. It does after all, allow for precise control over temperature and the respective Mg and B vapour pressures. In retrospect, it is disappointing this option was not pursued. However, fabrication of the dual-element heat pipe would be quite expensive especially owing to the high temperatures to which boron would need to be heated. A highly refractory substance such as tantalum would need to be used to contain the boron for heating because of boron's very low vapour pressure.

9.4 Future work

It remains to be seen if the nanotube process can be improved. Some additional nanotube experimental ideas were given in the previous chapter: 1) independently controlling thiophene concentration, 2) using ammonia, 3) using iron, nickel and cobalt separately, 4) trying to capture samples further downstream, 5) using a hydrocarbon for the sake of comparison and 6) using an *ex situ* catalyst. However, there is no end to the number of experiments that may be conducted and there is certainly much room for experimentation. It is of primary concern to improve the window over which a good plasma will form. By changing the aerial, it is possible to work over different pressure/temperature windows and this may lead to more optimal process conditions. Gas mix, flow rate and ethanol concentration are also untapped variables that may be used to perfect the process. In summary, what is needed is a brute-force approach using different parameters and processes. The results would certainly be very interesting and it is quite possible that yield, quality and consistency can be improved considerably. It would also be interesting to see if it were possible to form single-walled nanotubes.

With regard to the apparatus itself, it is necessary as a first step to swap the mercury manometer for a capacitive or electronic one. Then, better refinement of aerial design and placement, possibly with the addition of some modelling should be conducted. Given how well certain runs proceed, it seems that it is quite possible to make the apparatus significantly more stable over greater windows (possibly achieved by using different aerials for each window). The trouble right now is that it is easy to have ten very good, stable runs at similar pressure, then have endless trouble stabilising the plasma for another five runs. Work is needed to make the equipment more easy to use, and to make results more repeatable. This done, the apparatus should make a very good research tool. Somebody also needs to have the courage (and budget) to run a high pressure argon plasma for a significant amount of time to see if the chamber will indeed melt.

On the MgB_2 front, there is not much that can be done to rescue this idea. It would be interesting to see if one of the other MgB_2 deposition ideas could bear fruit: perhaps the heat-pipe design or plasma torch with boron powder spray. Or perhaps it would be worthwhile to

attempt to generate the Boron flux simply via evaporation or through the reaction of MgB_2 and HCl (which yields diborane gas). In addition to thermal torches, arc sublimation of boron is feasible. It would be more interesting, however, to see if the basic premise behind this idea (re-using the etch product in the gas stream) could be successful with some other material.

There remains also the possibility of attempting the activated reactive evaporation (ARE) variant suggested in chapter 5. In this version of the deposition experiment, the substrate would be placed inside the plasma reactor, above the aerial (which would preferentially be made of MgB_2), under condition of zero or low flow rate. The trouble with this is that the substrate temperature cannot be independently controlled. In addition, there is no guarantee that sufficient boron flux would reach it in any event given the high ambient pressure.

The plasma apparatus could still be used to attempt plasma enhanced chemical vapour deposition (PECVD) of MgB_2. In this scheme, the HPCVD apparatus and method would be used as is (with diborane gas), with the exception that the substrate would be immersed in a plasma, or just downstream of one. PECVD has not been attempted with MgB_2. The addition of such a plasma is used in many processes to artificially change the thermodynamic state that the substrate surface experiences. For example, typically substrate temperature may be lowered in PECVD experiments compared to their CVD counterparts since the more energetic reactants will readily form products without the same level of heating. The actual physics of such things and the explanation as to how and why plasma enhancement is advantageous is beyond the scope of this dissertation (Rossnagel, Cuomo and Westwood, 1990 is a good starting place), but there does not seem to be a reason why MgB_2 synthesis cannot benefit in some way.

9.5 Closing thoughts

Considerable time and effort has been expended in this project and yet it can be seen that there remains much work to do. In the end, success was mixed. However, the nature of the work pursued meant that quite possibly none of the schemes attempted would have ever worked: the plasma needn't have stabilised, and nanotubes need never have formed for the process conditions tried. To this end, the results are certainly most pleasing, if not perfect. We have succeeded in modifying the APNEP apparatus to make a plasma chamber that is at once cheap and accessible. We have succeeded in creating quality nanotubes in good yield in a very simple, and low-cost manner – potentially opening the door to such research for many similarly cash-strapped research groups. We have succeeded also in assessing the effect of several parameters on the fabrication of these nanotubes. In addition, a fully functioning 16-bit data acquisition board was designed and built which may yet prove useful. This is described in the Appendix.

Improvement is needed and there is much scope for future work in this project. The author has no doubt that something good may yet come of what has been done here. On the whole, the project is considered a success.

Appendix

1 : Design of 16-bit data acquisition board for lithography

When this work began, the first goal was to convert an old JEOL JSM 35C scanning electron microscope (SEM) into an electron beam lithography station. The work described in the body of this thesis actually evolved out of a sideline project that was begun simply as a way to fill in gaps frequently encountered while we were waiting for parts to be delivered, PCB's to be manufactured and so forth. In the end, the JEOL microscope had developed a fault with one of its valves and the entire lithography project was scrapped in favour of the work with the plasma chamber which had become, in the author's mind at least, considerably more interesting. Nevertheless, considerable effort and time was expended on designing and building a circuit to control the SEM and writing the firmware and software for this application. In fact, all that remains to be done is to plug the circuit into the SEM (which can be repaired) and perfect the process of lithography.

Since the design and build of this hardware and software may yet be useful, this appendix serves to document the design and features of this electronic equipment. The conversion of an electron beam microscope for the purpose of lithography and the general processes involved in electron beam lithography are not covered in any detail. As a good starting point for any interested parties, the websites of the two major SEM conversion manufacturers are great starting points ((Raith) and (Nabity) in the bibliography).

Unfortunately, there is simply no way to make hardware design sound interesting unless one has a passion for it and this appendix is of necessity full of detail. Any reader not primarily interested in electronic design is advised to skip it entirely. At the same time, the full circuit diagrams, PCB images and bill of materials for this board would occupy an extra 30 to 40 pages. To this end, the complete circuit is rather included in the attached CD in Protel 99SE format. Some particular images are added at the end of the Appendix to give the more casual reader an idea of the circuit.

A.1 Electron-beam lithography

Lithography is the industry standard process for patterning fine lines, dots and other shapes onto a surface. Currently, semiconductor manufacturers fabricate lines smaller than 130nm wide in their advanced IC's.

The famous "Moore's Law" states that the number of transistors per integrated circuit will increase exponentially with time. Intel in particular seems to have made it their goal to keep up with Moore's Law ever since the 1970's. In order to cram more and more transistors onto an integrated circuit (without increasing the overall size of the IC), it is necessary of course to make the transistors smaller and smaller. Specifically, Intel's website states that their goal is to allow for a 30% reduction in the size of printed features every two years (Intel, web). To say that this is a challenge is a tragic understatement. Some of the best engineers in the world have managed to virtually defy physics for many decades already and this is done primarily by way of improving the lithography techniques used in IC fabrication.

However, at the time of writing it really does seem as though present light-based lithography is rapidly reaching its limits and this is brought home by the recent development of many promising alternatives. Extreme UV lithography, nano-imprint lithography and e-beam lithography are among the next-generation technologies at this point in time. Even so, there are groups that believe Moore's Law is finally reaching an end due primarily to surging costs involved in keeping up with it. Moore's fourth (unofficial) law was apparently that the cost of fabrication plants would double every two years. Indeed, chip manufacturers are now beset by

the problem that new fabrication plants cost many billions of dollars while the sale price of chips continues to shrink. It seems as if there is an increasing likelihood that instead of making transistors smaller and smaller in the future, there will be a switch to a new technology. This will sooner or later be necessary in any event to prevent tunnelling effects from becoming a problem.

Electron beam lithography, or e-beam lithography, does not actually position itself as a strong contender to replace light lithography. It faces the seemingly insurmountable problem of very low throughput making it less useful for high volume commercial IC production. Some high throughput electron beam techniques exist (such as SCALPEL, being developed by Bell Labs (Liddle et al., 1999)), but these are not yet prominent or popular. In spite of this, e-beam lithography has become an invaluable research and mask-making tool and has already found fairly widespread use in the universities of this world.

Essentially, electron beam lithography is a very similar process to traditional photo-lighography with two notable exceptions: no mask is used in the process, and attainable line widths are shrunk to under 20nm.

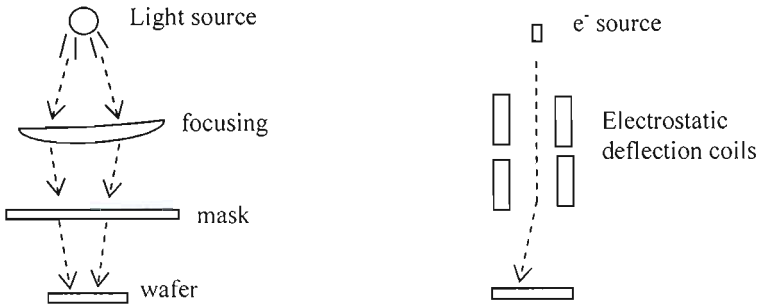

Figure 1-1: Showing optical lithography system (left) compared to electron beam system (right).

In an optical lithography system, a light source is focused through a mask (which blocks out part of the light) to form patterns on a wafer that has been coated with a light-sensitive resist. The chemical nature of the resist is altered where the light falls and by suitable processing it then becomes possible to remove those areas where light fell (or leave only those areas where light fell, depending on the resist used). Thus fine lines can be created.

In electron beam lithography, the light source is replaced with an electron beam and the mask is absent. The beam is simply traced about in the desired pattern on the resist surface directly. Movement is achieved by electrostatic deflection.

Electron beam lithography allows for considerably finer lithography work to be done since the wavelength of an electron is so exceedingly small (0.006nm). The wavelength of course determines the ultimate spot size to which a beam may be focused. It is impossible to focus any electromagnetic wave to a true point as an airy disc will always form instead (the diameter of which is determined by wavelength). Electron focusing systems are quite poor compared to optical lenses, however, and thus electrons cannot be focused to near their diffraction limit. However, it is still possible to fabricate lines down to around 10nm (but more commonly 20nm) in width. The ultimate limitation is primarily imposed by the resist and processing, not the electron beam spot size. Field Emission electron beams do allow for smaller line widths as well.

Thus, to achieve electron beam lithography, all that is needed is a highly focused electron beam that can be suitably deflected, and a resist capable of having its structure chemically modified when struck by electron beams. Such resists are common although polymethylmethacrylate (PMMA) is the most common choice and the resist selected for this work. A scanning electron microscope (SEM) provides a convenient and accessible source of a highly focused electron beam. Thus it is easily possible to achieve electron beam lithography simply by taking control of the scan coils of an electron beam microscope (the coils that determine x and y deflection) and tracing the desired pattern over a resist-coated substrate. Suitable processing after such patterning will allow patterns to be formed.

Subsequent lithography steps such as lift-off and rinsing will not be discussed in this appendix since its purpose is primarily to describe the hardware designed for the purposes of controlling the SEM scan coils.

A.2 Hardware Design: circuitry

In order to suitably control the beam of an electron microscope, a voltage must be applied to its scan coils. Most microscopes have plugs that allow external voltage sources to be applied. So, for example, for the JEOL JSM 35C we planned to use, the voltage input for each coil (one for x deflection, one for y deflection) is varied between -0.5V and +15V. To trace a horizontal line, one would keep the y-voltage constant, and slowly increase the x-voltage from one limit to the other at a predetermined rate (the rate is determined by the beam current, spot size, and resist). Thus it can be seen that in order to adequately control the beam so as to trace out arbitrary patterns, all that is needed is a two-channel digital to analogue converter (DAC).

To build a circuit that would be truly useful for lithography, one must add two analogue to digital converters (ADCs) as well. These will be used to receive feedback from the SEM. One channel reads the output of the secondary electron detector. The intensity of secondary electron emission is what generates an image on an SEM. Thus with the simple addition of this ADC channel, the hardware can be used to read images from the SEM as well as write patterns for lithography. The second ADC channel is used to read beam current which is an important parameter in the lithography process.

Thus it was desired to produce a board that has two 16-bit DAC channels and two 16-bit ADC channels. The ADC channels need not actually be 16-bit, however. Typically 8-bit grayscale and at best 12-bit deep images are formed from the secondary electron (SE) detector images. 16 bit ADCs were simply used for the sake of convenience. First of all, if higher resolution is ever needed, it is available. Secondly, using 16-bit ADCs when all that is required is 8-bit resolution allows for software scaling. That is to say, if the output of an SEM's SE detector varies between 0 volts for lowest intensity and 5V for maximum intensity, and the 16 bit ADC has an input range of 0 to 5 volts, the lower 8 bits may simply be discarded. If the output of the SE detector varies between 0 and 1V, then 8 bits resolution can still be maintained without the need for any hardware amplification or changing of the ADC input range. In fact, a 16 bit ADC with a 0 to 5V span can measure a range of 0 to 0.0195V with 8 bits of accuracy (although, at such a low level noise will probably prevent this). This simplifies the hardware design and in addition the board is made more versatile.

The DACs, however, need to be 16 bits in resolution. Whether all 16 bits are needed or not is dependent on the line widths desired and the magnification of the SEM during writing. For example, if the SEM is magnified such that the full extent of its deflection covers an area 0.1mm by 0.1mm, then the 16^{th} bit of either channel covers 1/65536 of 0.1mm which is 1.5nm. As a rule of thumb, J.C Nabity (the manufacturer of a popular SEM to lithography conversion system) suggests that this minimum step size should be roughly ¼ of the width of the line desired (personal communication). Thus in this example, 16 bits of resolution are sufficient for

10nm lines and even 15 bits will probably work. For larger fields of view with larger line widths, 14 bits may even be acceptable. In fact, private correspondence from J.C. Nabity indicated that 16 bits is seldom used. However, all commercial SEM conversion kits do have 16 bit accurate deflectors. This is quite important since one would find that if a system is designed for 14 bit accuracy, it may well be quite noisy or inaccurate in the 14^{th} or even 13^{th} bits. By designing to 16 bits of accuracy, the system should be noise free up to the 15^{th} bit in a good design (15 bits being a resolution that may be required for very fine lines). Keeping noise levels down was the most challenging aspect of this mixed-signal design.

In addition to two DAC channels and two ADC channels, a controller would be needed to feed data to the DACs and retrieve data from the ADCs. There were two approaches that could be adopted here: the controller could itself generate and process all the pattern data and feed it to the DACs, or the PC could generate this data and then simply feed it to the controller which would distribute it to the DACs at the desired rate. The first option allows for a faster system. If the pattern data is generated onboard, throughput is higher since less data needs to be transmitted between the PC and hardware. For example, if it is desired that a circle should be traced, the PC need only tell the controller to trace out a circle with diameter x and radius r at a rate of s steps per second. This would constitute very few bytes. The controller would then take this information and calculate all x,y coordinate pairs to be fed to the DACs, subsequently feeding this data at the desired rate.

In the latter method, the PC would rasterise all the data into x,y points beforehand and then transmit these coordinates one-by-one to the controller. The controller would then simply clock the data into the DACs at the required rate. This allows for a simpler processor to be used since rasterisation of vector data is quite an intensive process for an 8 bit microcontroller at the rates required.

Thus the choice would be primarily dictated by the controller used. It was decided that it would be more cost effective to go with the latter route and use a simple PIC18F8520 microcontroller. This is a simple and cheap device which is quite easy to program. Initially some work was done with a TI DSP that would have been quite capable of generating the raster data sufficiently quickly, but this was abandoned in favour of the cheaper solution. In retrospect, this may have been an unwise decision as although TI development kits are quite pricey, the actual chips are not. The lower data transfer rates required could have translated into quieter data transfers and less noise overall. In spite of this, the present solution works adequately.

Other than the ADCs, DACs and central controller, the rest of the circuit was comprised of first-in-first-out buffers (FIFOs), opamps, power supplies and some digital circuitry. The full circuit diagram can be found at the end of this Appendix. The more interesting aspects will be described below.

A.3 USB

A high data throughput was needed since the PC would be generating all the coordinate pairs. We were aiming for 100kHz DAC output rates (to match commercial hardware used for this purpose) which translates to 3,2 Mbps. USB is unmatched in performance and data integrity at these speeds and is realistically the only option available. Parallel ports are prone to data errors and have difficulty reaching such speeds. More exotic options such as Firewire are simply too much work for little profit. By contrast, USB may be simply implemented using commercially available USB chips which take care of all the handshaking and data decoding. A DLP-USB245M USB adapter (component labelled 'USB' on the board) was used for this purpose. This module contains a USB to parallel converter (FT-245BM from FTDI) that will convert data sent via a USB stream into parallel bytes which can be clocked out from the small on-chip FIFO. Likewise, data can be clocked into the device one byte at a time and then transmitted to

the PC via USB. The device is capable of a full 8Mbps bandwidth. Brute testing was performed transferring large sections of data without a single bit error (~39Megs at a time). It is important that the device is capable of speeds in excess of the required 3,2Mbps. Ideally, a speed of twice that is desired. This is because it is desirable to provide data to the board at a rate higher than it can clock the data out. That way, buffer underruns cannot occur. Buffer overruns are far easier to manage in software.

A.4 Bus Structure

The following diagram gives a basic overview of the bus structure employed in the circuit.

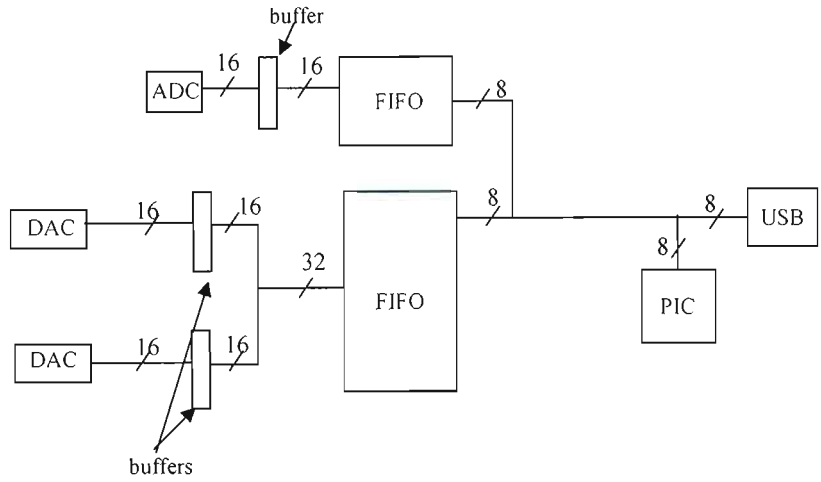

Figure 1-2: Bus structure of the circuit.

It can be seen that the PIC had access to the USB bus. This allowed the PIC to receive data from, and send data to the PC directly. In addition, the PIC could send data straight to the DAC FIFO and hence to the DACs. Similarly, the PIC could read data directly from the ADC through its FIFO. This was useful when performing reads from the SEM (grabbing an image) rather than when writing patterns. In this case, the waveforms outputted on the DACs were generated by the PIC, not the PC. Thus it was essential that the PIC could access the DAC FIFO directly.

A.5 FIFOs

The PC was going to generate massive numbers of x,y coordinate pairs and then transfer these to the hardware at a rate different to that at which the board used them. The PC also had to receive large quantities of data from the hardware during reads, again with a data rate mismatch. It was necessary therefore to place FIFO buffers between the PC and the DACs/ADCs – the deeper the better.

A 36 bit wide (2 words and one parity bit per byte) 32 768 level deep SN74V3690 FIFO (component U25 on the board) from Texas Instruments (TI) was placed between the PC and the DACs. Data was streamed from the PC through the USB module directly into the FIFO, one-byte at a time. The FIFO performed automatic 8 bit to 32 bit widening of the input data and then output the 32 bit x,y coordinate pairs directly to the DACs, one pair at a time. The parity bits were not used.

Similarly, a 16 bit wide, 65536 level deep SN74V293 FIFO (component U2) was placed between the ADC output and USB module input. This FIFO performed the necessary 16 bit to 8 bit conversion since the USB module has an 8-bit wide bus.

Thus the onboard microcontroller simply had to keep all the relevant clocks running at the correct rates and toggle buses on and off as needed. Data did not actually pass through the controller itself, which saves processing time.

There are very few manufacturers of such deep, high speed FIFOs of which TI at the time was the cheapest. The depth of the DAC FIFO chosen was very important since it needed to be as deep as possible to give the computer sufficient time to generate points. That is, it is inefficient for the PC to generate raster data one point at a time and then feed them to the hardware. Rather, efficiency is improved as the packet length of data generated and transferred increases. There is also a minimum time required for the software to generate even one point due to various latencies. The DAC FIFO was typically filled to half way before emptying. This provided 163ms of buffer latency at 100kHz which proved sufficient time for data generation and transfer. Note that this proved only just sufficient and a smaller FIFO would not have sufficed without software changes. As it was, efficiency of the code needed to be improved to manage with the 163ms buffer. Half-the buffer was used primarily to simplify code although it is possible to use the whole buffer should the need arise.

A.6 DAC Output

The DAC chosen was Linear Technology's (LT) LT1597 16-bit current out DACs. In picking a DAC we were primarily interested in accuracy. Differential nonlinearity (DNL) was the most important specification since the DACs would typically be stepped in small increments. DNL refers to the error in change in analog output for a 1LSB change in input. So if the DNL were specified as max 0.5LSB, then increasing the digital input by 1LSB could result in the analogue output voltage increasing by 1/65536 to 1.5/655366 of full scale. Integral nonlinearity (INL) is also quite important as it refers to the maximum deviation of the DAC output from the ideal transfer function. Gain error and offset error were less of a concern since variable scaling and offset of the output had been added. The LT1597 has the best integral nonlinearity (INL) and differential nonlinearity (DNL) in its class on the market at 0.25LSB and 0.2LSB respectively. In fact, across the board a more accurate 16 bit DAC cannot be found with the exception of very expensive calibration DACs. It must be noted that significant time was spent hunting for parts in this project. The DAC has a parallel input and a current output. Using a parallel input DAC for the main deflector DAC was a tough choice. A parallel bus as opposed to a serial bus meant more noise generated each time a new data point was clocked in. This was because obviously 16 lines toggling would create much more noise than just two. However, with a parallel bus, the bus changed only once per data point, just before a data point was loaded and any noise would appear as a small glitch at that point. With a serial bus, the noise is continuous, and not necessarily much smaller. Indeed, in the present application, it is not often that all 16 bits will toggle simultaneously since the DAC is stepped one, two or maybe four bits at a time in sequence. Private communication with Linear Technology tech support revealed that digital feedthrough noise should be less than the DACs own glitch in any event and to this end, parallel DACs make for more efficient data transfer.

Because the DAC has a current output, it is necessary to perform I-V conversion of this output. This is accomplished using the LT1468CS8 opamp. Opamp selection posed quite a problem in this design since there really is no perfect opamp. Ultimately a compromise was needed to be reached between speed, noise and bandwidth. The LT1468 was found to provide the optimal blend of these parameters. It will settle to 16 bits in 900 microseconds with an input noise voltage of only 5nV/ $\sqrt{Hz}$ and an input current noise of only 0.6pA/ $\sqrt{Hz}$. Note that only dc noise specs such as input noise voltage and input current noise are important since the application essentially uses the DACs in a dc mode due to the relatively long time between

steps. In addition, the LT1468 allows for supplies all the way up to +/-18V which is rare in an opamp of such specifications.

A.7 Scale and Offset

It was desired that the DAC card should be flexible in the range of outputs it could provide. To this end, circuitry was added to allow for software-variable scale and offset of the output voltage. This would allow the board to be used for other microscopes, whose input voltage range would typically be different to that of the JEOL JSM 35C (the 35C was quite unique in its input ranges). Voltage offsetting also allowed for fine shifting of the beam and was useful for alignment purposes.

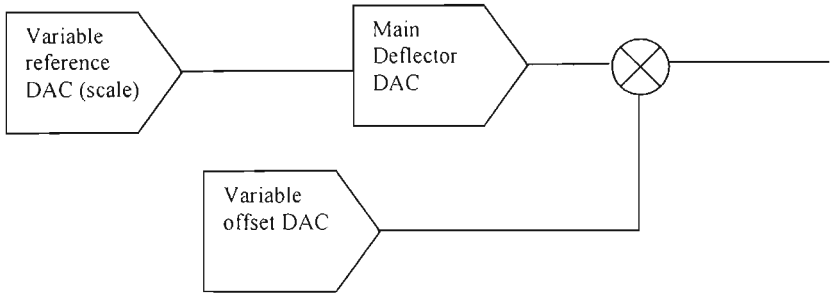

Figure 1-3: One DAC channel actually was comprised of three DACs: one for scale, one for offset, and one to provide deflection of the beam.

To accomplish this, two extra DACs per channel provided a variable offset voltage (components R21 and R23), and a variable scale or reference voltage (components R22 and R20). The offset voltage was added to the output voltage of the main deflector DAC by way of a summer. An LT1595CS8 was used to create this variable offset voltage. The LT1595 is essentially the same as the LT1597 in its performance and specifications with the exception that its input data is fed serially. Having multiple 16 bit buses on the board is very undesirable for noise performance and a terrible nuisance when tracking the PCB.

Another LT1595 was used to provide a variable input to the reference input of the main deflector DAC for each channel. By digitally varying the reference seen by the LT1597 main deflector DAC – which was actually a multiplying DAC – the output span it covered was altered.

To ensure a clean reference was supplied to the main deflector DACs, the output from the scale DAC was filtered heavily using a triple pole RC filter. Technically RC filters should not be cascaded this way, but in this case it is fine since there is no real current load and the position of the poles need not be accurate. Using three poles (low frequency, mid frequency and high frequency) is important since RC filters tend to lose effectiveness after a few decades due to parasitic effects in the components.

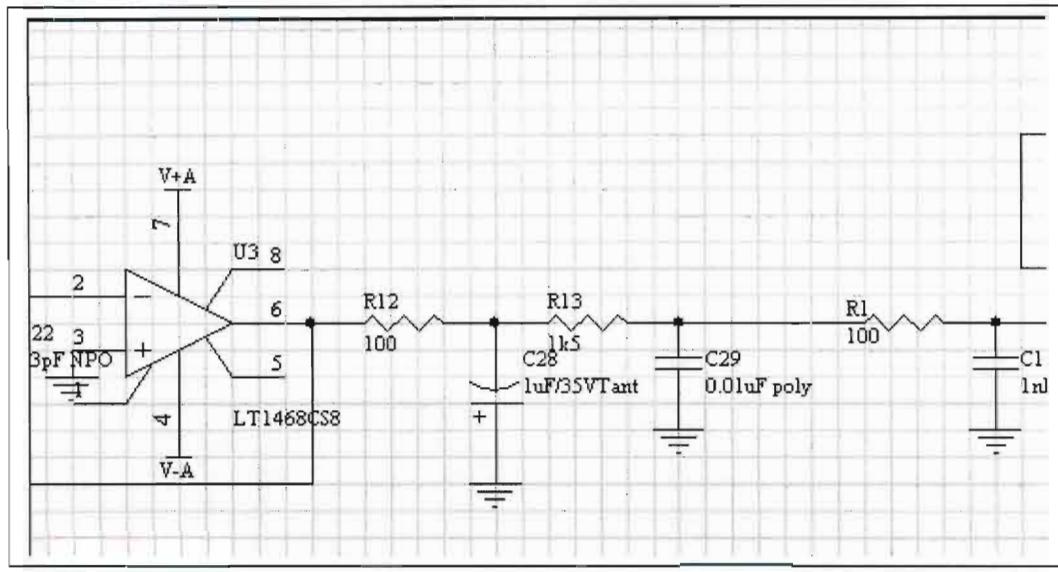

Figure 1-4: Showing triple output filter after scale DAC.

As for the output of the offset DAC, this was filtered by adding a capacitor to the weighted summer on its output (capacitors C36 and C37).

In all cases it was considered important to use ceramic COG dielectric capacitors or polypropylene/polystyrene capacitors for the high frequency filters. COG capacitors do suffer from the problem that they are mildly piezoelectric, and as such sensitive to vibrational noise or tapping, but this was not seen as a problem in the application. The high frequency performance of such capacitors is very impressive.

A.8 Output filtering

The summed output was passed through a three pole, active Bessel filter for further noise removal. The filter had a cutoff of 500 kHz. Filter design was somewhat tricky since bandwidth should be restricted as much as possible for minimal noise, but bandwidth restriction would slow down the step response. Using freely available software, "Filter Free", it was possible to vary the cutoff frequency, number of poles and filter class and see the effect on step response. Bessel filters provide minimal overshoot (typically less than 10%) for a slight trade-off in settling time. The freely available program FilterPro from Texas Instruments was also invaluable in filter design insofar as it can give standard range capacitance values and resistance values. A multiple feedback (MFB) topology was used since it is less sensitive to component variation and we had access only to the E12 resistor series range and the E6 capacitor range.

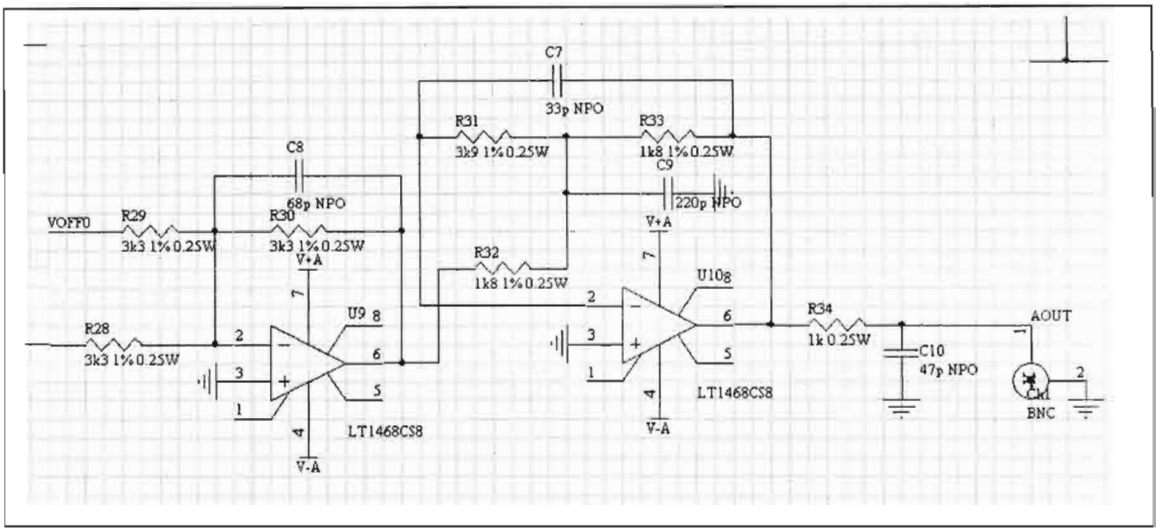

Figure 1-5: The output stage. The weighted summer (U9) also forms the first pole of the filter.

It was possible to use only two opamps to implement the three pole filter by adding a capacitor (C8) to the weighted summer (U9) as shown in the above figure. That way, the summer formed the first pole. Using as few opamps as possible was important since each one had its own noise contribution. In addition, resistor values needed to be kept as low as possible since resistors add considerable noise (a 1kΩ resistor generates 4nV/ √Hz of Johnson noise at room temperature). However, if the resistor value is too low then excessive current is drawn. The values in the above figure were designed as a tradeoff between these two constraints.

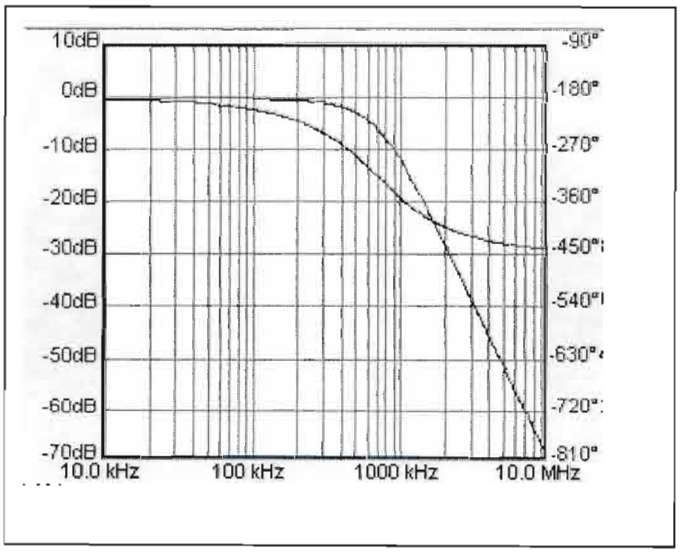

Figure 1-6: Transfer function of designed filter.

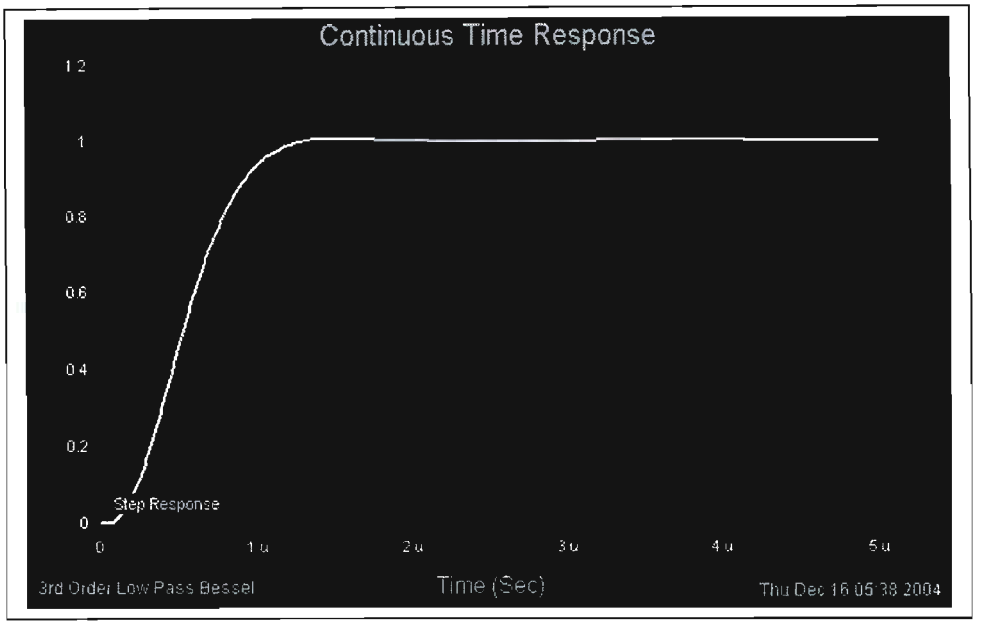

Figure 1-7: Filter step response.

The decision to use three poles was not taken lightly. Obviously, the higher the filter order the better for noise attenuation, however, adding more poles will again adversely affect step response.

It will be noted that again LT1468 opamps were used. These opamps make excellent filters with their wide bandwidths (90MHz), high slew rates (22V/μs) and low distortion (-96.5dB at 100kHz). In addition, as had been mentioned previously they are low noise devices capable of high rail operation. Actually, 22V/μs is not sufficient for full power response (slew rate = π x V_{pp} x corner frequency). At 20V peak to peak voltage with a 500kHz cutoff frequency, 31,4V/μs slew rate is needed. However, the application made this unimportant since the DACs were not used to produce large AC waveforms in this manner. Indeed, step response was the important parameter.

A.9 General Noise Precautions

A.9.1 Circuit level precautions

Many precautions against noise were taken in the design of both the circuit itself and its PCB. Though many of these precautions may seem somewhat excessive, it must be remembered that we were aiming for noise only in the 16^{th} bit which translates to 150μV in 10V. This is truly difficult to achieve even on paper. With regard to the circuit design, the following precautions were taken:

1) Regulators were placed locally on the board. This as opposed to providing regulated power to the board through wires. By having the regulators onboard, connected to the various components using power planes, the inductance between power supply and component is greatly reduced, very much improving noise performance. Feedback is improved and current spikes are far less of an issue.

In order to further improve noise performance, multiple rails were used. The digital section had its own 5V and 3.3V rails, while the analog section had a quiet 5V rail, and separate +/-20V rails for each DAC channel. The ADC input also had its own power supply (although, it did not have regulators onboard since ADC noise was not an issue). This made 9 separate rails onboard. Separating analog and digital power supplies is quite advantageous from a noise separation perspective. Furthermore, using a separate +/-16V rail pair for each output channel allowed us to keep their grounds isolated from each other. Much care was taken in the grounding of the system, but that is discussed later on in this appendix. Each regulator was fed with its own external regulator meaning power was essentially double-regulated. It was intended that the offboard regulators would be connected to the onboard regulators using shielded twisted pair, the shield of which would be connected to the chassis. The onboard analog regulators all had rms noise levels of under 30μV.

Note that the power supply rejection ratio (PSRR) of the operational amplifiers (80dB at 100kHz) actually makes such exceedingly quiet power supplies as were used redundant (the analogue regulators had less than 30μV of rms noise). However, the PSRR of the DACs is worse, falling off rapidly with frequency to become essentially nonexistent at higher frequencies (personal communication, LT tech support). To this end, quiet power is essential.

2) All long digital lines and digital lines connecting to analog components were series (source) terminated with 100 ohm 0603 surface mount resistors. Although this is useful for preventing unwanted reflections, reflection should not be a real problem at the speeds being used. However, series termination resistors have a host of benefits. First of all, they provide termination without adversely affecting the balancing or loading of the line. Secondly, they provide current limiting in case of a fault. Thirdly, because of intrinsic capacitances in shunt with the transmission lines, the resistors actually form the basis for RC filters on the line and thus offer some degree of noise reduction. In fact, for all sensitive and long digital lines, a 100pF 0603 ceramic capacitor was placed in front of the series termination resistor, shunting the line to ground. Thus all these digital lines were RC filtered. RC filtering is possibly the best way to reduce noise in digital lines (except at very high speeds) and many commercial filter companies (such as Murata) sell discrete RC filters for this purpose. However, RC filters will naturally slow down the wave rise and fall times (unlike chokes). If rise/fall times become too slow, they cause oscillations (TI,1998a). With AHC logic this is less of a problem, but with the LT1597s it could be an issue (private communication, LT tech support). Nevertheless, the 100 ohm, 100pF combination used provided good filtering without compromising stability. The 100 ohm value is not necessarily the correct matching value. However, matching is not a big issue for the speeds and distances used – especially since the edge it filtered. The characteristic impedance of microstrip lines is typically slightly less than this value (suggested as between 50 and 80 ohms by various sources such as (Ott,2000)).

3) AHC (advanced high speed CMOS) logic from Texas Instruments was selected as the logic family of choice. AHC provides the low noise of high speed CMOS (HC) devices while offering much higher speeds and half the static power consumption (TI,1998b). They are characterized by lower switching noise (such as ground bounce) and smaller current spikes than most logic families due to more slowly rising/falling waveforms (slew rate it limited). This is accomplished without compromising propagation delay. In addition, care was taken to use low profile surface mount components where possible. This reduces the loop area created by IC pins (the substrate is closer to the ground plane and the pins are shorter), reduces the amount of high K dielectric surrounding the pins, and allows for tighter placement of components. Surface mount components are universally recommended for better noise performance.

4) Considerable decoupling of power pins was provided to further reduce any noise created by line switching. This was considered very important considering that digital and analog lines would switch quickly and frequently. Decoupling is a fairly in-depth topic and was considered

at length. The results of this review can be found elsewhere (Coetsee, 2003) but are summarized here briefly.

At high speed, the parasitic effects of decoupling capacitors must be considered. Every capacitor can be considered as having an effective series resistance (ESR) and effective series inductance (ESL), effectively making them RLC series circuits. Thus capacitors all show the characteristic v-shaped impedance curve of RLC circuits.

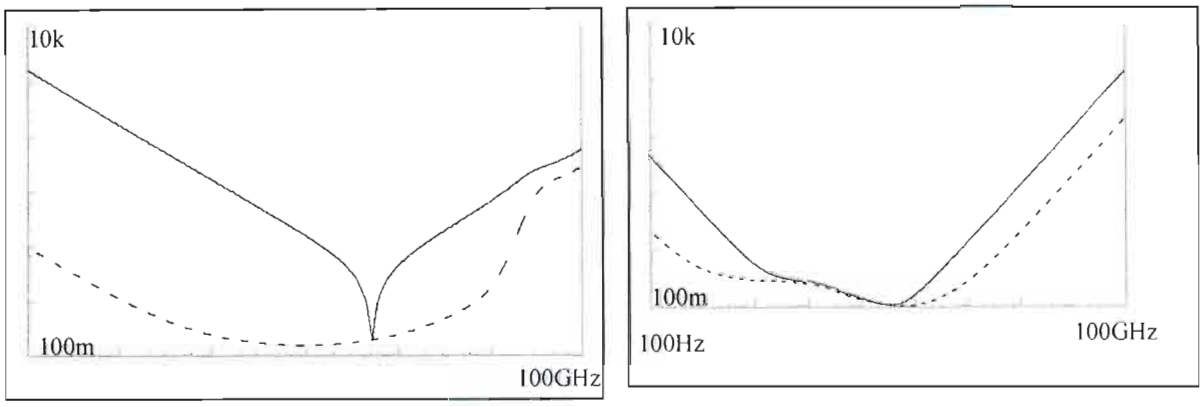

Figure 1-8: Impedance curves for a tantalum (top) and ceramic COG (bottom) capacitor. Impedance values are in ohms. Impedance is shown by the solid line.

A capacitor therefore becomes less useful after its self-resonant frequency. It can be seen from the above figure that this frequency is typically higher for a small ceramic capacitor (100pF COG 0603 is shown in the figure) than for a larger tantalum (33μF C case shown in figure). Typically, smaller packages and smaller capactitances mean a higher resonant frequency and ceramics resonate at higher frequencies than electrolytics.

Although this would seem to suggest that placing a few small, low capacitance ceramics at the IC of every pin is advantageous, in fact much literature suggests this is counter-productive (Pattavina and Jeffrey, 1998; Hubing et al., 1995a). The high Q of such capacitors (as evidenced in the figure above) can cause terrible resonance effects. For example, if one is using only a small 100pF capacitor to decouple each IC, then typically large electrolytics will be required at the power supply to provide sufficient total capacitance for adequate decoupling. These electrolytics will reach the inductive portion of their RLC curves (the positive slope after self-resonance) much sooner than the local 100pF capacitors. This means that at these higher frequencies we really have a capacitance (the 100pF) in parallel with an inductance (the electrolytic that is on the inductive region of its curve): a parallel LC circuit. Should the two values become equal, resonance would result causing in 'infinite' impedance spike in the total rail-to-ground impedance of the board. This is called anti-resonance in the literature. This is obviously very bad for decoupling since the amount of voltage noise produced is proportional to impedance at a given frequency.

One possible solution is to use many different capacitance values (100pF, 500pF, 1000pF etc.) in parallel at each IC. This keeps the anti-resonant spikes to a minimum as anti-resonance will always occur between the RLC resonant frequencies of two capacitors in parallel (Smith et al., 1999). However, a better solution is to use low Q capacitors such as tantalums for decoupling purposes. The low Q and typically higher ESR of these capacitors will provide damping against such anti-resonant effects (Pattavina and Jeffrey, 1998). This effect can also be gained by using a small resistance in series with a ceramic capacitor (Hubing et al., 1995a), but this can unnecessarily raise total impedance.

Indeed, however, in the end it is good to simply do the design from a frequency analysis perspective. Placing many capacitors in parallel has the effect of pushing these anti-resonant spikes to ever higher frequencies (Hubing et al., 1995a) and thus enough ceramics (at least 100) will work well. Also, in our system it is not necessary to decouple all the way to 100MHz since there is a finite noise bandwidth associated with our output filtering and the scan coils of the microscope itself. Thus this feature becomes less critical, but it is good to bear in mind. Using SPICE analysis, it was decided to use a combination of tantalum and high frequency COG ceramics for decoupling. The ceramics are absent from the analog section, however, where decoupling needs to be performed to lower frequencies only.

Typically two to four ceramics (more for big ICs like the FIFOs) were placed about the ICs near their power and ground pins, while one or two tantalums were placed near each IC. This resulted in both a large number of total capacitors and both high Q and low Q capacitors being used. This contributed to a lowering of decoupling impedance (the impedance of each capacitor is of course in parallel) with useful decoupling ability at higher frequencies without anti-resonant effects.

Note also that for decoupling capacitors to be effective, they must be placed close to the ICs they decouple, typically using well designed pads. Larger pads with vias placed within their boundaries are better than smaller pads connected to ICs through wires (Smith et al., 1999; Drewniak et al., 1994). Such designs minimize inductance between capacitor and IC. For single-layer boards (no vias), the track length must be minimized.

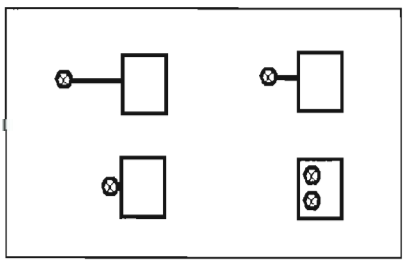

Figure 1-9: Various pad designs. It is important to keep inductance to a minimum. Keeping vias in or very near pads is imperative. For single-layer boards, track length to IC must be reduced.

Minimising the distance between capacitor and IC power pin is very important, even on multilayer boards (Hubing et al., 1995b; Fan et al., 2000). Doing so can increase mutual inductance between capacitor via and power pin via which will further improve coupling. This, while at the same time minimizing series inductance in the interconnect and the total area of the current flow loop. Every effort was made to keep small (100pF) 0603 ceramic COG capacitors as close to IC pins as possible in this design, with vias typically touching their pads directly.

It must be stressed that the decoupling solution is largely based on theory – both by way of literature reviewing and some SPICE modeling. To this end the actual effectiveness of such recommendations on the circuit built was never measured.

A.9.2 Printed Circuit Board Precautions

a) Grounding

There is no point in designing a circuit to theoretically low noise levels if the design is not executed well via good PCB design. It is well known that using multiple layers in a PCB has significant noise-reducing benefits. First of all, it allows for entire planes to be used to provide ground and power connections to the various ICs. Using a plane instead of a track to supply

power and ground means lower impedance and inductance seen by the circulating current which translates into lower switching noise. In addition, lower voltage is created by current traveling from the regulators to supply all the decoupling ICs (the decoupling ICs provide most of the fast switching current to the ICs and are constantly replenished by the regulators). Loop area of current flow is also minimized. Current need only flow along a track, through an IC pin, and out the IC to the return plane (power or ground) and can then travel back to the source directly underneath the track that brought it there.

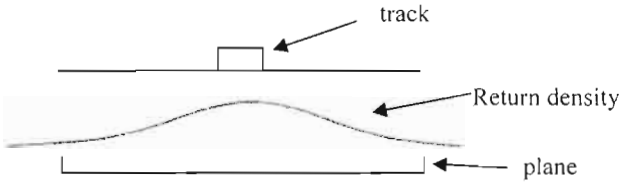

Figure 1-10: Current (AC) returns via a plane directly below the track that brought it to the IC. The charge density (or voltage density) is shown by the curved line (Brooks, 2000).

In addition, if spacing between power and ground planes is very small (less than 0.254mm) there can be significant capacitive coupling between the planes (Hubing et al., 1995a). However, this effect is typically only noticeable at very high frequencies. Using power planes also turns all surface tracks into microstrip lines and thus their characteristic impedances are easier to calculate. This was less important for our relatively low speed application, however.

The question remains as to how many planes to use and how to arrange them (referred to as 'stackup'). Stackup is a reasonably complex issue. A very good guide can be found on the internet site of Henry Ott, an electromagnetic compatability consultant (Ott, 2004). Ott suggests it is a good idea to always have a power and ground planes adjacent in a stackup, and to have signal planes adjacent to a power or ground plane (either can act as a return for ac signals). This provides for effective coupling between power and ground planes and minimizes loop area for return signals. In addition, multiple ground planes are a good idea since ground impedance is further lowered. These sorts of recommendations are not uncommon.

In the end, it was decided to use 6 PCB layers (four internal) owing to the large number of power supplies the board used and the need for very low noise levels.

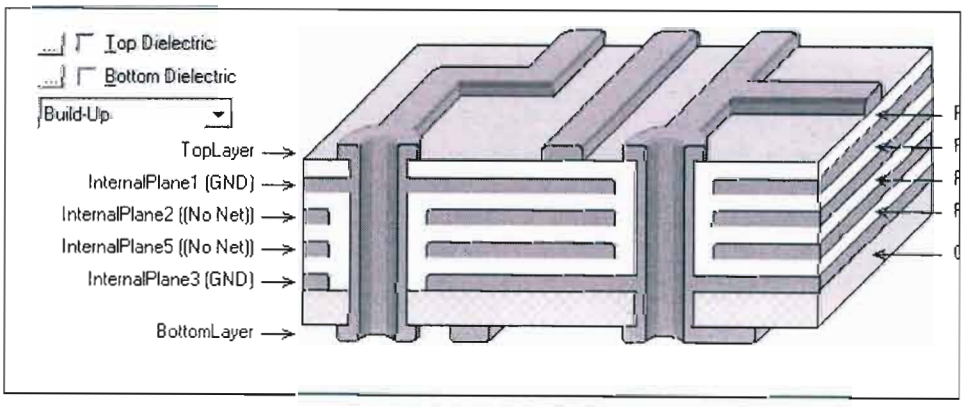

Figure 1-11: Stackup of final PCB.

Two ground planes were used, one adjacent to the top signal layer and the other adjacent to the bottom signal layer. The middle two planes were power planes. The power planes were further split internally such that power zones were created

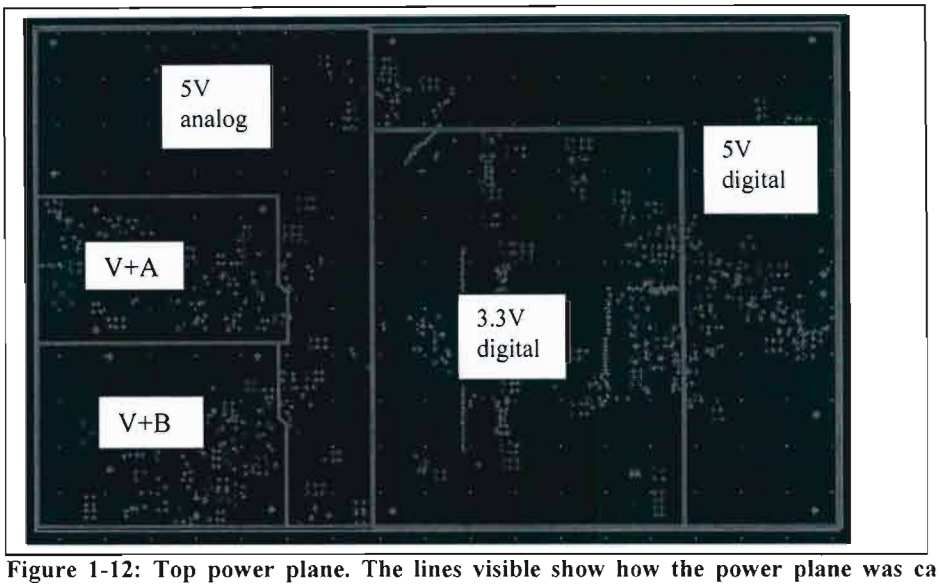

Figure 1-12: Top power plane. The lines visible show how the power plane was carved up into sections.

The top power plane provided power to the 3.3V digital section, the 5V digital section, the quiet, 5V analog section, and the high rail of each of the output stages (V+A and V+B in the figure). The lower power plane provided power to the negative rail of the output stages, and the rest was ground.

This brings up the topic of board zoning which is equally important for low noise performance. It is vital to separate analog from digital sections. This was accomplished by keeping all digital ICs on the right side of the board and all analog sections on the left side. Adequate separation between zones prevents noise coupling via radiation and ground spikes.

However, zoning is not enough. It is necessary to adequately isolate the ground planes of all the digital and analogue sections. Essentially, digital switching causes voltage spikes not only on the digital supply rail, but on the digital ground plane as well (commonly referred to as ground bounce). This is due to the circulating digital currents in the ground plane. As shown in figure A-10, these currents tend to be located beneath the microstrip lines on multilayer boards, and thus it is vital to keep digital lines from impinging on analogue zones.

Ground separation can be achieved simply by zoning for most systems. However, complications arise for low noise mixed-signal circuits. Here it is desirous to have separate analog and digital grounds and this is recommended on most precision ADC and DAC data sheets (see, for example, the AD768 data sheet). However, the two grounds must necessarily connect at some point. Data sheets such as that for the AD768 tend to recommend this connection take place directly beneath the mixed signal IC. Henry Ott, cited above (Ott, 2003) recommends the following scheme:

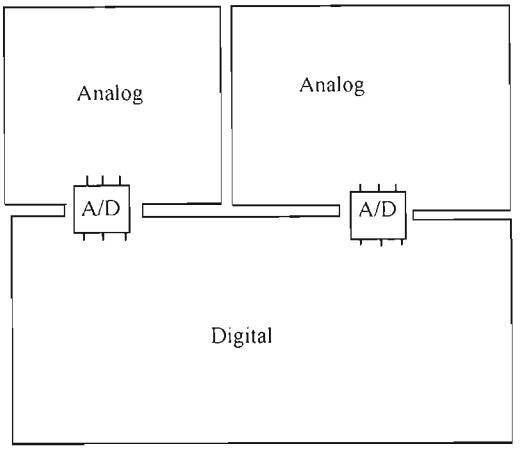

Figure 1-13: Optimal mixed-signal grounding. The ground plane is separated into three sections.

Dr. Howard Johnson, a notable author in the field of high speed design, recommends the same system (Johnson, 2001). In this system, not only is the digital ground separated from the analog grounds, but the analog grounds are separated from each other (for systems with multiple mixed-signal devices such as ours). This is important since otherwise ground loops may form. In this system, digital currents will have no 'desire' to travel into analogue regions since there is no way back. Our design employed this approach as shown in the following figure

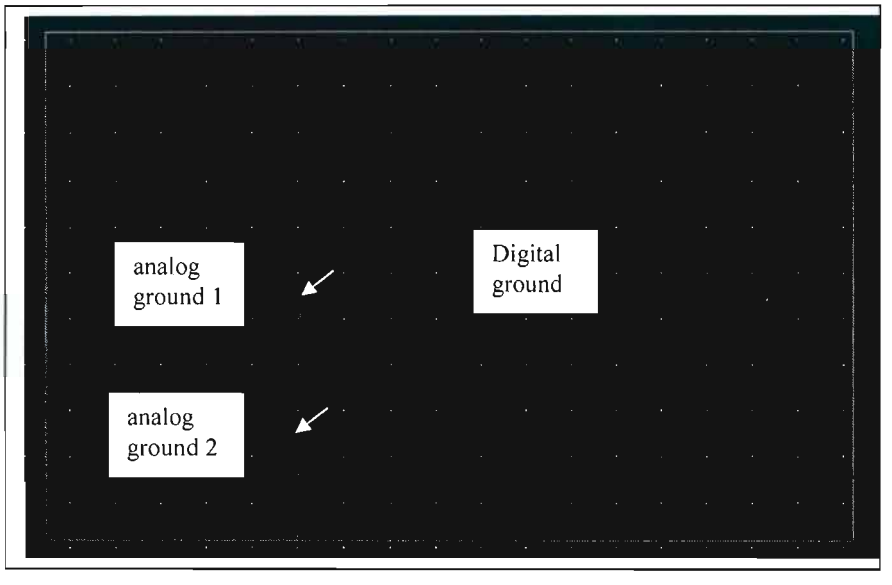

Figure 1-14: Upper ground plane of PCB. The position of the DACs is shown by white arrows.

To maintain this ground separation, it was necessary that the grounds of the DACs did not reconnect off the board when attaching to the SEM. This was accomplished by feeding the DAC outputs first to an offboard daughtercard which had differential inputs. The daughtercard simply performed differential-to-single ended conversion and applied the buffered DAC output signals to the scope. Since the inputs to the daughtercard were differential, the grounds of the DAC output signal did not actually ever interface directly with the SEM ground. In this way, separation of all grounds was maintained.

Similarly, the external regulators powering the PCB made use of their own transformers and were isolated from the mains earth. Thus each regulator did not share a common ground.

The PCB was further enclosed in a metal box, which would act as a shield from outside noise. The chassis of the box connected to the PCB ground at only one point.

b) Tracking

It is also important in minimizing noise to keep digital tracking away from sensitive analog areas. Furthermore, tracks should not cross barriers in ground/power planes (since this would interrupt their return paths). This is reasonably easy to accomplish for the present board since it is simple to zone. The only sensitive area is again the region where digital and analog lines come together at the precision DACs.

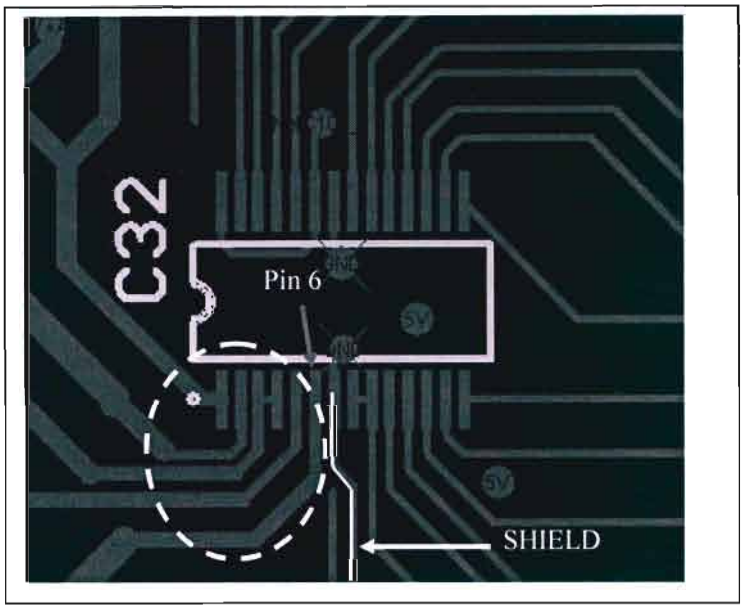

Figure 1-15: Tracking around DAC C32 (an LT1597). Analog tracks are ringed in white.

In the above figure, the barriers in the ground plane are shown in green. The analog tracks are ringed in white. It can be seen that care was taken to ensure that digital tracks were on one side of the invisible line separating analog and digital regions, while analog tracks were on the other. A ground track was further laid between the two sections to provide some shielding effect (indicated by white writing and white marking on the track). This was considered important since the pin next to this is the current out pin (pin 6, marked in the figure). Coupling from digital lines to the Iout pin is potentially the worst source of noise in this DAC. For example, just 0.1 pF coupling from a 5V digital line to Iout 1, will result in a step of 15 mV (personal communication, LT tech support).

Other than this area, tracking was fairly routine. It will be seen that in most areas, components were placed close together and tracking kept to a minimum. There is considerable separation between the various zones, however. In fact, this was possibly overdone in the prototype, particularly in the FIFO to DAC distance.

A.10 Dual Digital Rails

It will be noticed that a 3.3V and 5V digital supply were used. This was primarily because the FIFOs selected could only operate at 3.3V, while the microcontroller needed to operate at 5V to reach maximum speed. In addition, using 3.3V as opposed to 5V logic reduces switching noise (TI, 1998b). However, the DACs were designed to take 5V inputs and using 3.3V actually increases their power consumption (private communication, LT tech support). This was considered a negligible impact, however, since power supply should still only be a few milliamps. The ADCs were able to interface easily with both 5V and 3.3V logic. In addition, the FIFOs were quite versatile and their inputs could tolerate 5V signals even though they were 3.3V devices. When AHC logic runs off a 3.3V rail its inputs can similarly handle 5V levels. This made interfacing the 3.3V to 5V rails quite simple. The USB was left running at 5V.

Interfacing was no problem then, so long as 5V device outputs fed to 3.3V device inputs, since such inputs were universally tolerant of 5V levels. However, level translation buffers (SN74LVC4245A components UT1 and UT2) were needed in those areas where 3.3V device outputs fed into 5V device inputs. Although for CMOS logic, 3.3V is technically above the minimum input voltage needed to signal a high for 5V logic ($V_{ih(min)}$), using translators ensured data integrity and made power supply sequencing easier.

Power supply sequencing was an issue since when multiple rails are used, latch-up is a possibility if the supply rail for one digital section comes up before the other. By using level translators, it becomes safe to power up the 3.3V section before the 5V sections. This is because the 3.3V outputs that feed into the 5V section are blocked by the level translators until the 5V rail comes up.

Unfortunately, the only error of the circuit was made in this area. The outputs of the FIFOs are not 5V tolerant, as the inputs are. The trouble arises since the output of the ADC FIFO connects to the same bus as the inputs of the DAC FIFO. This means that it is quite possible for the USB module (a 5V device) or PIC (also connected to the bus) to apply 5V to the outputs of the ADC FIFO. The addition of a level translator between USB bus and ADC FIFO solved this problem

A.11 In Circuit Debugger (ICD)

The circuit can be programmed and debugged while in operation using Microchip's ICD 2 device. The device connects to the board via JP1.

A.12 Clock Matching (Interfacing)

It was possible to interface the USB to the FIFOs and the FIFOs to the DACs without any 'glue' logic. These devices functioned quite similarly and thus the PIC could clock the USB module and FIFOs simultaneously, using a single line, latching data from the USB into the FIFO directly (or from FIFO to USB). Similarly, the same signal that was used to latch data out of a FIFO could latch the data directly into the DAC. This allowed for speedy operating since the PIC would not need to, for example, pull the USB clock low to latch data out of the USB device, then pull the FIFO clock high to latch this same data into the FIFO. Rather, a single clock pulse on one line tied to both the USB and FIFO clocks would latch data out of the USB device into the FIFO seamlessly. This could be done similarly in transferring data from the FIFO to the DACs. This allowed for fast operation. It was possible, however, to disconnect the various clocks (by means of buffers). This was necessary for when it was not desired that data should flow directly from one device to the other (such as when the PIC should send data to the

FIFO, not the USB module). The exception was the ADC module. It was necessary to clock data out of the ADC module, and then clock that same data into the ADC FIFO using a separate clock line.

A.13 Daughtercard

It has been mentioned that a daughtercard was designed to go between this analog hardware and the SEM. Part of the circuit diagram is available at the end of this appendix. The daughtercard was a very simple device that essentially acted as a buffer. DAC outputs from the main board were accepted by the daughtercard through differential intputs, converted to single-ended signals, and then applied to the scope. SEM outputs were buffered and sent to the main board where they were again accepted by differential inputs (UDIFF0 and UDIFF1). The precision AMP03 differential amplifiers from analog devices were used for the differential input buffering. The daughtercard was only employed for further ground isolation. This way, the grounds of the ADC inputs and the two DAC outputs never had to connect to each other.

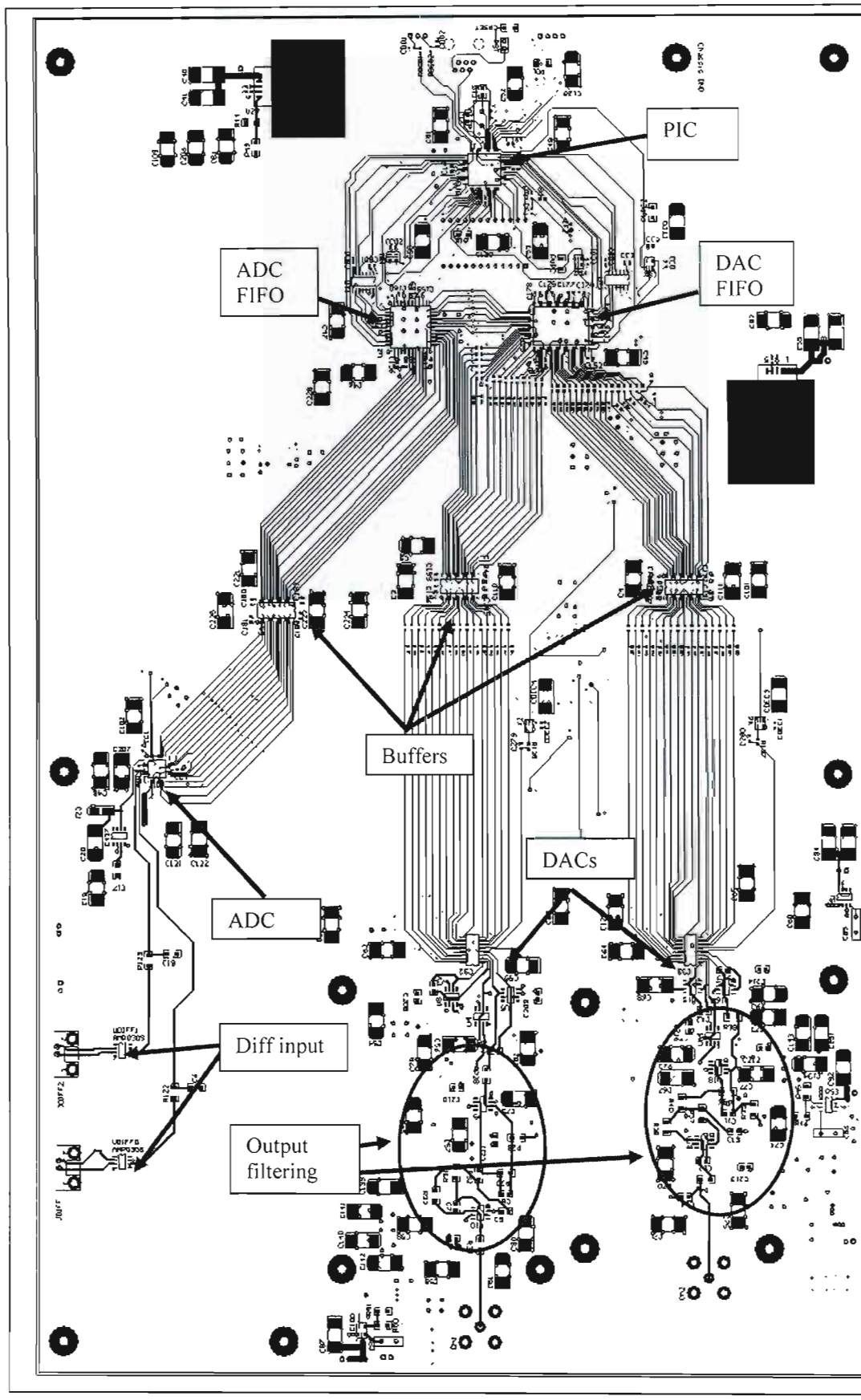

Figure 1-16: PCB Top layer overview.

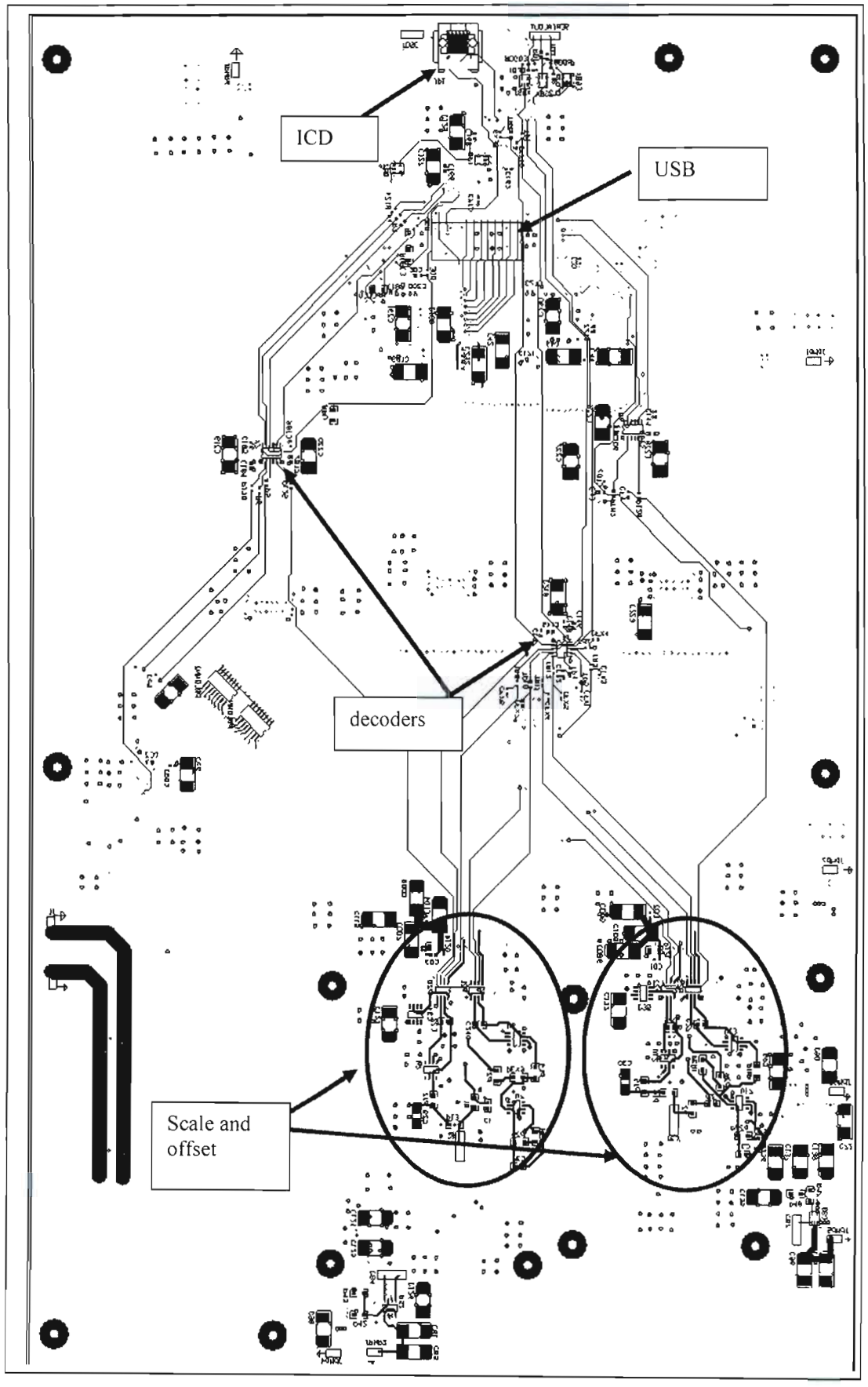

Figure 1-17: Bottom layer PCB overview.

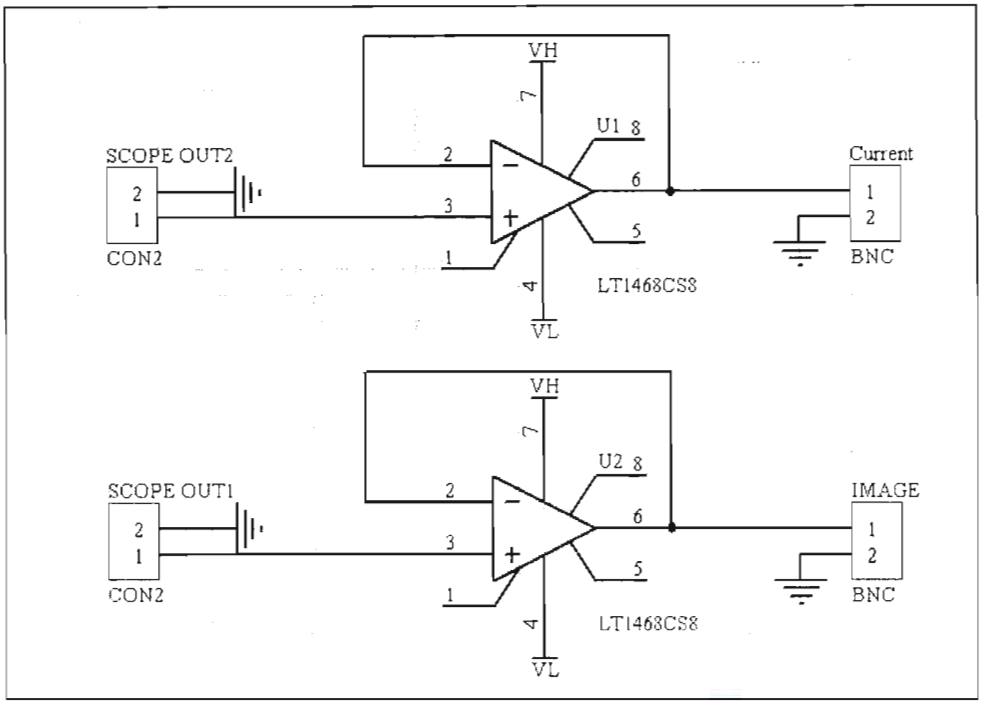

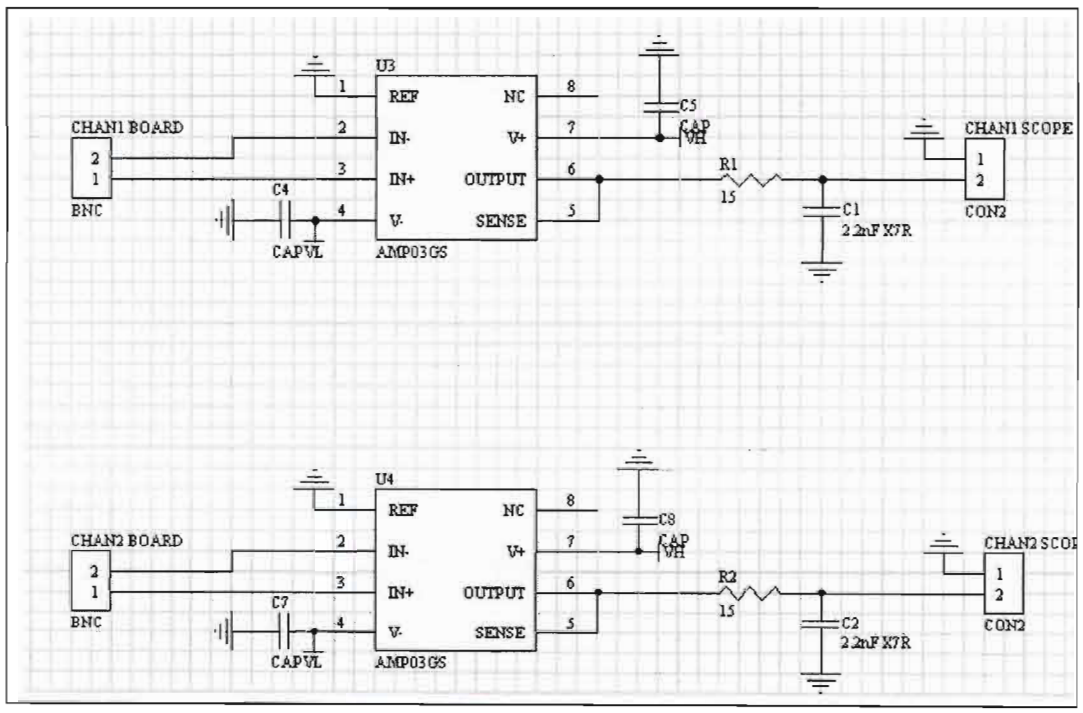

Figure 1-18: The daughtercard is simply a series of buffers.

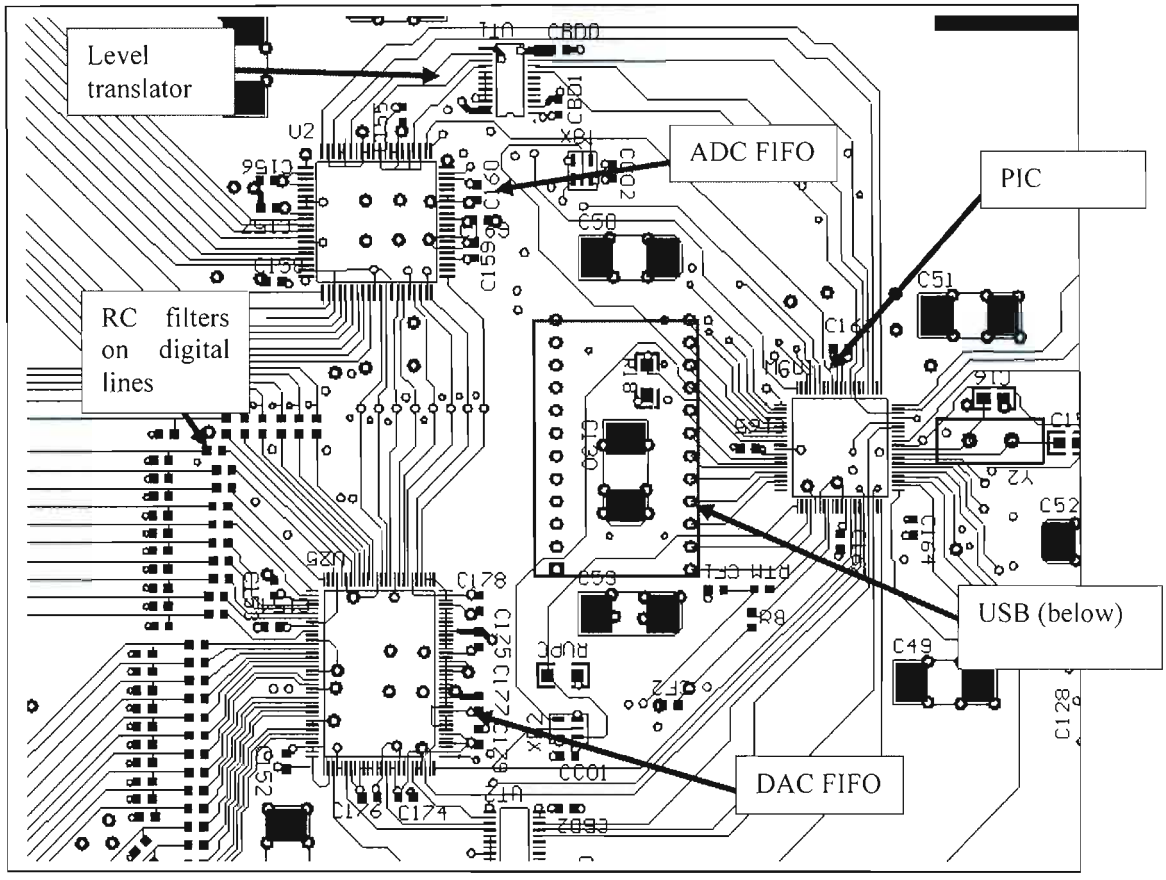

Figure 1-19: The digital area is tightly integrated.

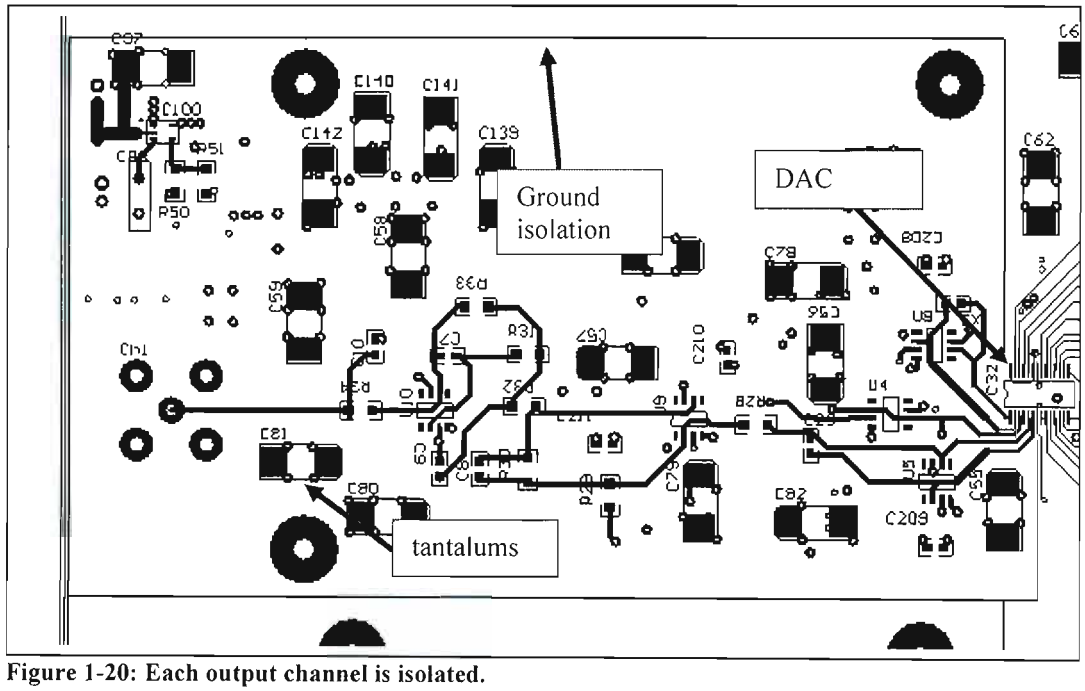

Figure 1-20: Each output channel is isolated.

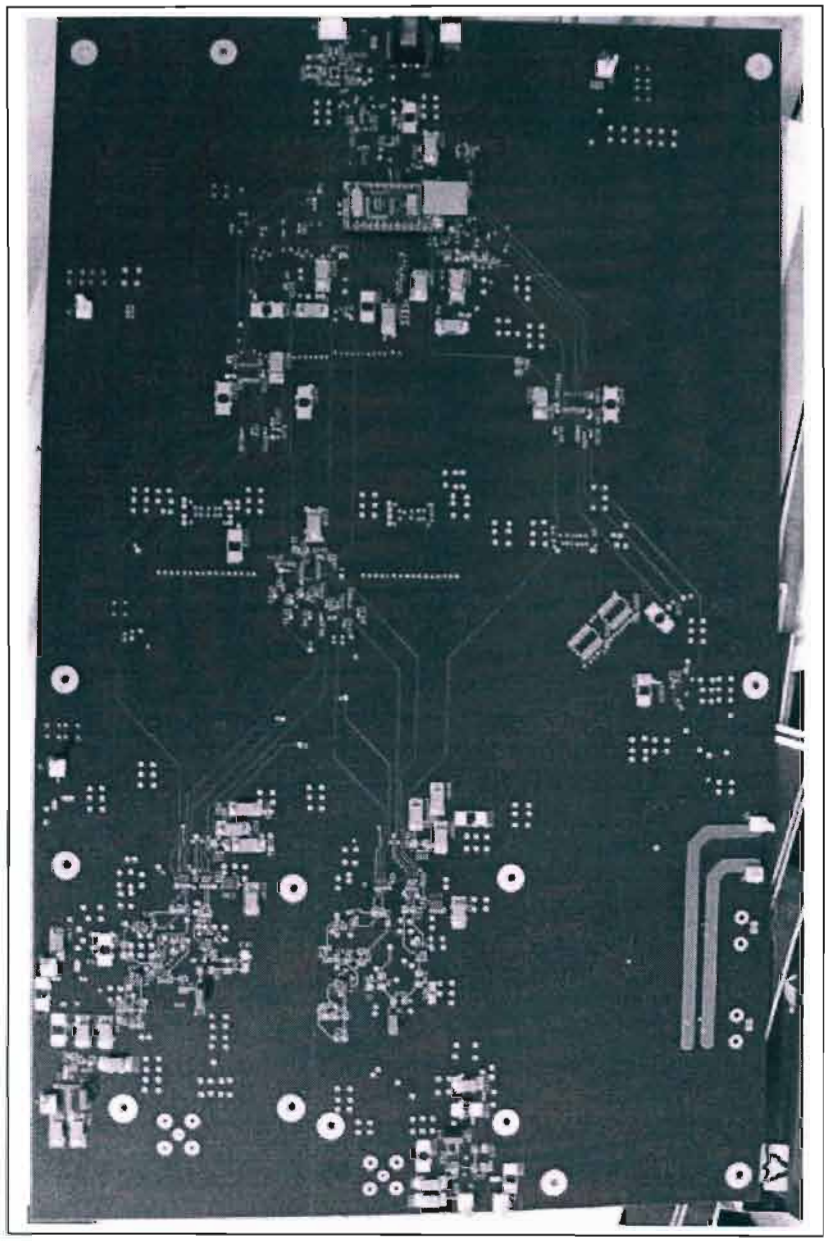

Figure 1-21: PCB Bottom.

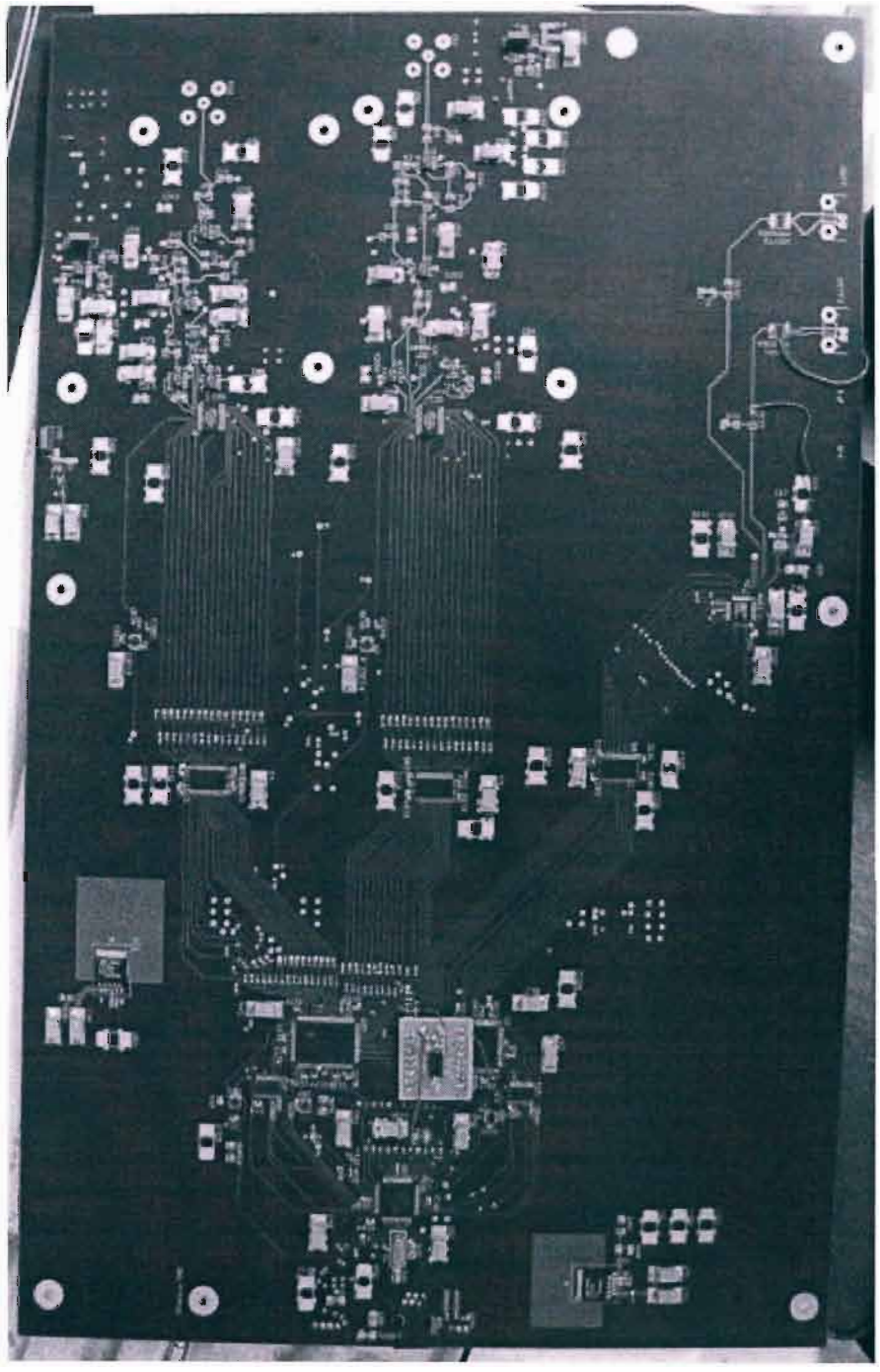

Figure 1-22: PCB Top.

2 : Software Design

The software and firmware for this project constitutes many thousands of lines of code. It is thus not possible to describe all this code in detail and this overview will rather concentrate on the basic functionality and purpose of the software as well as any notable algorithms employed.

B.1 PC Software

The PC software was designed to be able to carry out the following processes:

1) Load a CAD file containing pattern to be written via lithography
2) Generate *x,y* coordinate pairs for the data in the CAD file
3) Transmit *x,y* data to hardware
4) Receive secondary electron intensity values from hardware
5) Communicate with hardware to set output voltage span and offset

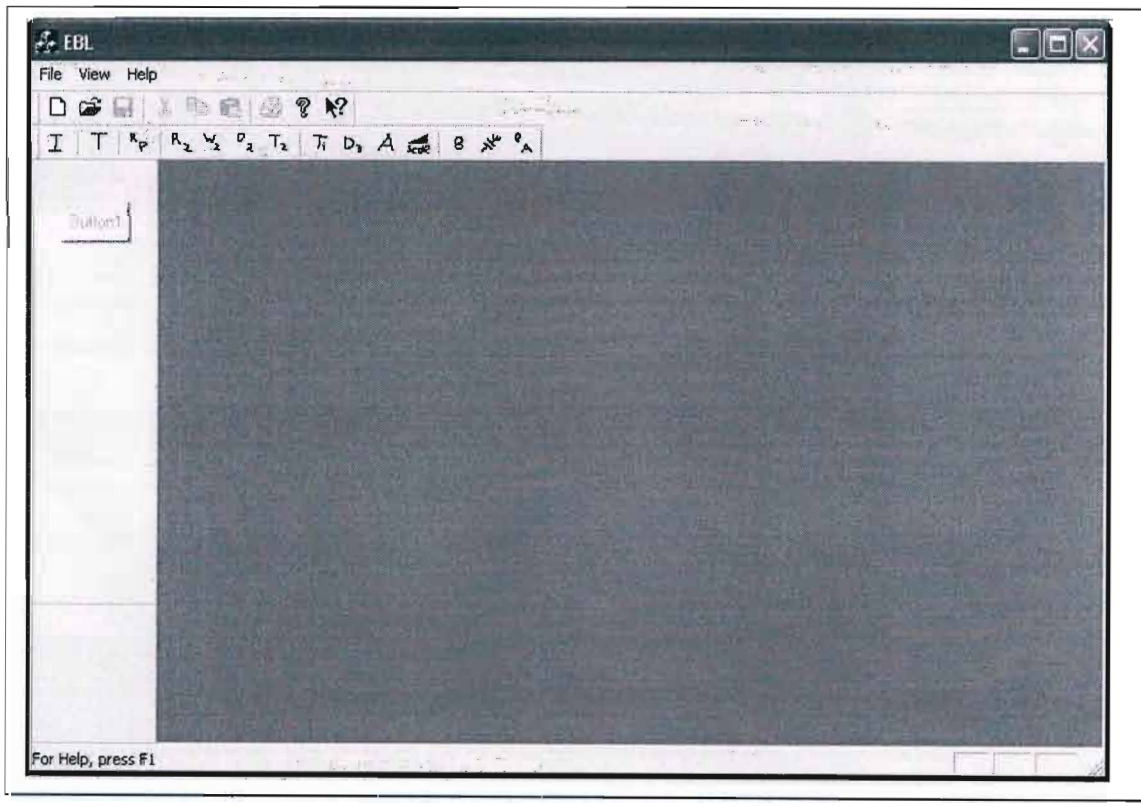

Figure 2-1: Image of the software as it is first run.

The software was written in Visual C++ using the Microsoft Foundation Classes (MFC).
It is possible to open (or create) three types of files with the software: 1) CAD files (*.dc3) generated by the program "DesignCAD Express", 2) Scope files (*.scp) generated by the software itself and 3) Grayscale bitmap image files (*.bmp). Although general bmp's can be opened, it is intended that bitmaps generated by the program itself will be saved and opened.

B.2 CAD file reading

The software could read files generated by the CAD program "DesignCAD Express version 12" manufactured by IMSI. In fact, version 14 files were compatible. This CAD program is quite standard as drawing programs go, allowing the user to generate a number of arcs, circles, lines, etc. as desired. It is versatile enough to create any desirable 2D pattern to be fabricated.

The CAD program has the advantage that it is possible to save files in ascii form. So, for example, the saved file for a drawn circle may look as follows:

```
480.0000 200.0000 400.0000 400.0000 0 -0.0000 0.0000
20 0 0 0 0 0
8.000000, 0.800000
8.000000
*
21 1 0 0 0 0
16 4 16 0 0 1 0 1 0 0 0 0 0 0
680 400 0
480 400 0
480 400 0
680 200 0
```

The details of this file format will not be covered here, but are freely available from IMSI. Essentially, the file contains the radius and centre of the circle so that it may be reconstructed. That is, the information is stored in vector form. Similarly, lines are stored by noting their endpoints and so forth.

The ascii nature of the files makes it simple to write software to read these files and decode their data, once the file format is understood. Currently, the software can read and decode information for lines, arcs and circles which should be sufficient for most purposes. When a CAD file is loaded by the software, it immediately breaks the data up into 'entities'. An entity is one of the following: line, circle or arc. Entities are then stored internally in a linked list such that vector data can be easily retrieved. Because the data is stored in vector form, it is easy to rescale.
Polygons (made out of multiple lines) or the interior of circles may be filled. If shapes are not filled, then the software will understand that the outline of the shapes must be drawn by the hardware. If the shapes are filled, then every point within their boundaries is traced from left to right and then right to left in a raster fashion.

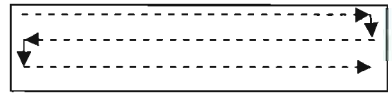

Figure 2-2: Shapes may be filled in allowing solid objects to be patterned on a substrate.

Filled objects are internally stored in a separate linked list and are identified by having a group number assigned to them in the CAD program.

B.3 Generating data points

The program takes the vector data and turns it into raster data points that can be sent directly to the hardware. Objects are traced out in a vector fashion, however. This means that, for example,

when tracing out a circle, the hardware will force the beam to actually move around in a circular pattern of the correct diameter. This as opposed to sweeping the beam left to right and right to left and simply switching it on at the correct times. This is supposedly advantageous for pattern writing according to J.C. Nabity (Nabity).

In order to generate data points, the program makes use of the traditional Bresenham line algorithm and Bresenham circle algorithms in converting vector data to a series of points. The algorithms themselves will not be discussed in depth since this is primarily a functionality review. Essentially, the Brsenham algorithms reduce the generation of data points to simple additions done in loops. The line algorithm works on the premise that when rasterising a line, after plotting a point, there are only two possible places where the next point may be plotted. Say, for example, the line exists in the first quadrant. If the x coordinate is incremented by one point at a time, then the next y coordinate can either be directly adjacent to the previous y coordinate, or directly above it. In other words, if at $x=x_0$, $y=y_o$, then at $x=x_0+1$, $y=y_0$ or $y=y_0+1$. This is because the gradient it less than or equal to one, and greater than or equal to zero.

Figure 2-3: A line (in white) is rasterised into pixels (black squares). In moving from left to right, the value of y can only stay the same, or increment by one for each step.

Thus Bresenham's algorithm is a simple, small loop that checks for whether y should be incremented or not for each increment in x. It is an integer-only algorithm with no multiplications, one branch and some addition. This is a very fast algorithm. Lines in other quadrants are handled by the same algorithm.

The Bresenham circle algorithm works on a similar principle. Here, it is necessary only to calculate the pixel values for the first octant of the circle, and then these can be suitably translated to the other quadrants.

One setback with the Bresenham circle algorithm is that it tends to create duplicate points for certain radii of circle. Such points are coloured in gray in the following image.

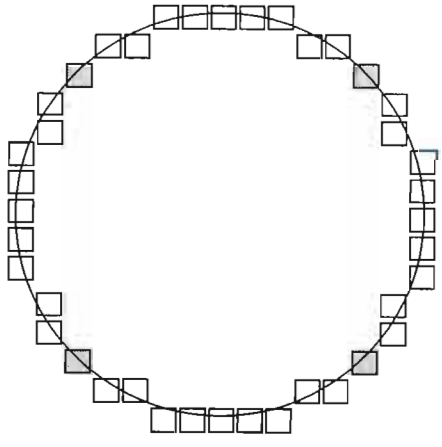

Figure 2-4: Rasterisation of a circle. For some radii, certain points would be drawn twice.

These points tended to be on areas of quadrant overlap. In fact, it turned out there were three kinds of circles and the difference was based on whether there was an odd or even number of pixels between 0 and 45°. In fact, the solution is a little complex and will not be entered into in this discussion. Documentation is available with the software itself that covers this. One side-effect of this problem is that the work-around made the algorithm considerably slower than it would otherwise have been. It would be interesting, once the hardware is hooked up to a microscope, to see if these duplicate points really matter. Although much effort was put into solving this problem, it is the author's present view that this time was actually wasted and that these few duplicate points per circle will not be noticeable in a final write.

Arc generation used the Bresenham circle algorithm. Because different quadrants would need to be calculated for different arcs, and some quadrants should not be filled with points, the arc algorithm necessarily executes more slowly than the pure circle algorithm due to more decision trees.

Points in filled polygons were generated using the traditional scan-line fill algorithm. Since this is also a widely used algorithm its details will not be provided here. Filling polygons is relatively easy since the process really involves finding the left-most limit of the polygon (for example, the left edge of a circle) and the right-most limit of the polygon at a given y-value, and then just filling all the points between. For example, in filling a square that is 10 pixels by 10 pixels, centered on the origin, one first finds the left limit of the top row (x= -5, y=5), then the right limit of the top row (x=5, y=5). The fill is simply all the points in between. Then one moves to the next row and goes back from right to left. The algorithm is complicated by allowing for hollow fills and irregular polygons, but remains relatively straightforward and fast.

All data point generation is accomplished in a separate thread. The use of multithreading is more important to ensure that the USB device never waits on the PC. It does not provide considerable improvement in data generation times, unless thread priority is massively increased. This was found to not be necessary.

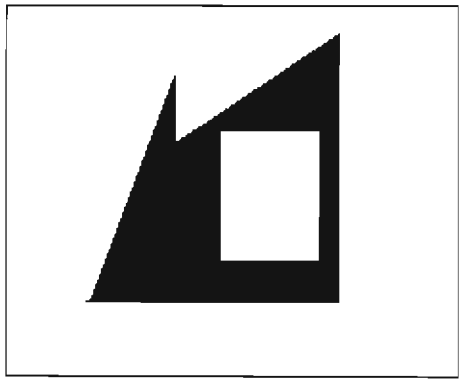

Figure 2-5: The algorithm is complicated by allowing for hollow and irregular fills.

B.4 Reading Images

The software and hardware are capable of grabbing images from the microscope. To do this, the DACs sweep the electron beam along the sample, one row at a time. At each step, the ADC will read the secondary electron intensity (available on most scopes as a voltage output). These values are stored in a grayscale bitmap which the software can save. It is also possible to load arbitrary bitmaps if desired.

During scanning, the x deflector DAC will increment from left to right. When it reaches its right limit, it will reset and the y-deflector DAC will increment. Thus the x-deflector DAC traces a saw-tooth pattern while the y-deflector DAC traces a slowly rising line.

B.5 Configuring the Microscope

Recall from Appendix A that it was desired to make the hardware flexible by allowing it to span variable output ranges. In addition, variable input ranges are also possible by virtue of the fact that the ADC is 16 bits in resolution while only 8 are needed.

The software needed to control how the board would be configured for any given microscope. To accomplish this, it was possible to create, open and save Scope (*.scp) files that contained all the necessary data. In switching between microscopes, the user could simply open a new Scope file.

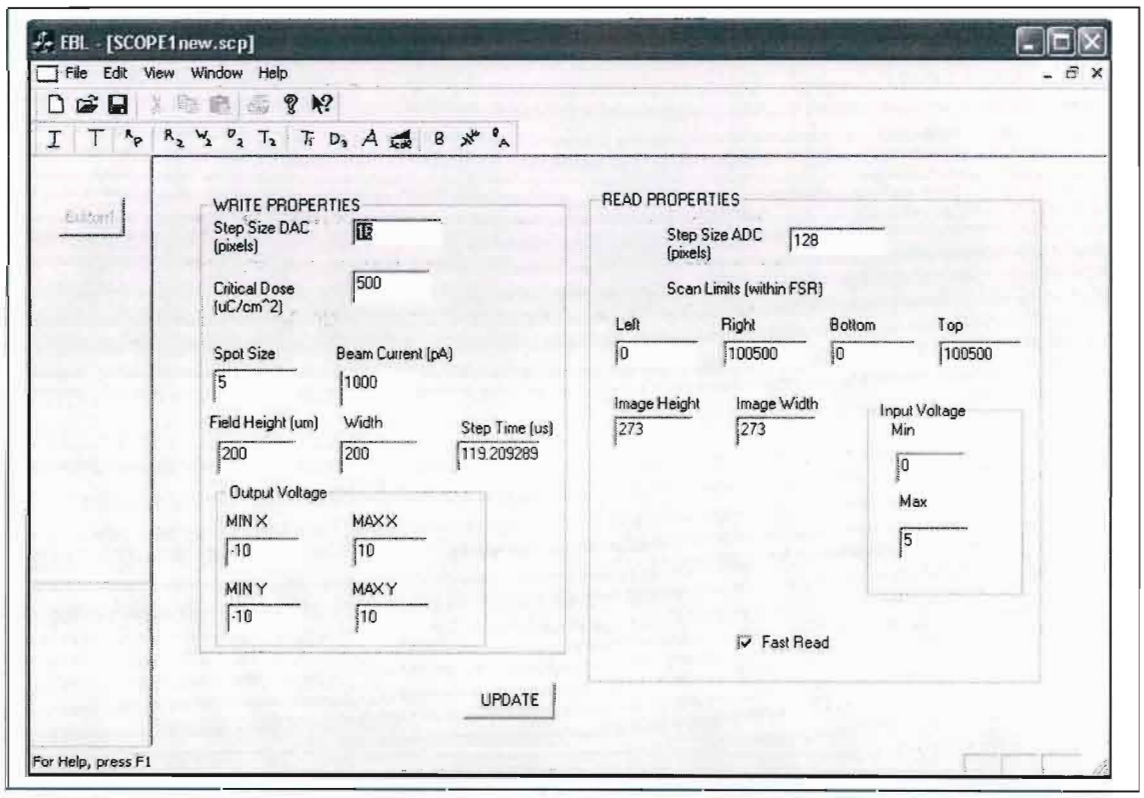

Figure 2-6: An open Scope file.

The Scope file allowed for the storage of many parameters. In fact, the current scope files are a little user-unfriendly and are designed more for developers and engineers. The following is a list of parameters that could be stored and altered:

Write Properties

Step Size DAC (pixels): This is the number of pixels that are moved in each step of the beam. So, for 16-bit resolution, this value would be 1 meaning that the DACs are incremented 1 bit at a time.

Critical Dose ($\mu C/cm^2$): The critical dose is a parameter that determines how many Coulombs of charge must be delivered to a unit area of resist (Rai-Choudhury, 1997). This is dependent on the resist itself (molecular weight, chemical structure) and on post-lithography processing conditions. It is also dependent on accelerating voltage. Typical values for PMMA (the resist we were to use) range from 50 to 500 $\mu C/cm^2$

Spot Size: This variable is entered here for the purpose of calculations. The hardware does not actually control spot size

Beam current: Beam current is important in determining the step rate required to deliver the correct critical dose. The hardware is capable of measuring beam current through an onboard DAC, if the scope allows for this current to be measured (which is necessary).

Field Height and Width: These parameters affect how a CAD document is interpreted and are related to zoom. Field height and width as entered give the physical size of the current field of view. These values must be entered by the user. So, for example, if a CAD drawing is created of a circle with a 100 unit diameter (extending from x=0 to x=100), and the user enters here that field width is 100 microns and field height is 100 microns, then the software will interpret this as meaning that the circle extends from pixel 0 to pixel 65536 in width. Thus this value is used in the interpretation of CAD files only

Step Time: This value is not entered by the user, but is calculated internally by the program. It determines the step rate of the beam and is designed to achieve the critical dose.

Output voltage: Here the user can enter the minimum and maximum x and y voltage values that will be output by the DAC. Note that these need not be symmetrical about zero. The hardware is capable of spanning any 20V range with a maximum of +15V or minimum of -15V per channel.

Read Properties:

Step Size ADC: Similar to step size DAC, this determines how many LSBs the DACs are incremented by during a read operation. This, together with the scan limits, determines the resolution of the resulting image.

Scan limits (within FSR): These four entries determine the extent of the area swept by the DACs during a read. That is to say, the DACs need not increment from 0 to 65536 (full scale range or FSR). It is possible to capture an image using only part of the range. The actual DAC code is entered here. Thus to scan the upper left quadrant of the field, the user would enter left limit as 0, right limit as 32768, upper limit as 0 and lower limit as 32 768. This effectively provides zooming.

Image Height and Width: These are calculated from the step size and scan limits and are not entered by the user

Input voltage: The maximum and minimum voltage generated by the microscope can be entered here for flexibility. The maximum level is interpreted as white in the image, and the minimum level is black. This allows the board to be used with many different microscopes.

Fast Read: The hardware generates all the DAC data during reads and also has two preset scan rates built in. Reading will either be conducted at 10μs per step, or 100μs per step.

B.6 Toolbar

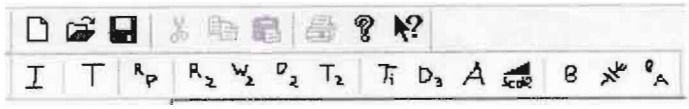

Figure 2-7: The toolbar used by the program.

All functionality of the program is controlled via the toolbar. Apart from the windows-standard functions (new, open, save, help, etc.), there are 14 buttons that provide access to the software routines.

The button graphics are currently placeholders, as are the buttons themselves. Not all of them are actually useful and some are there primarily for testing and debugging purposes. The buttons perform the following functions, from left to right:

I : Initialise. This button will initialise the board. Initialisation involves opening a USB channel and sending one byte to the board, receiving a confirmation from the board upon data reception

T : Test. This button is used for testing purposes during debugging and provides an easy way to execute random sections of code

R_2 : Read in second thread. This button allows for reading of an SEM image

W_2 : Write in second thread. This button generates patterns on the hardware

D_2 : Draw in second thread. This was a testing button used to draw a bitmap of the loaded CAD file to check that the data was interpreted and drawn correctly. It must be used by setting field width and height to 65536 to ensure the bitmap is of a reasonable size

T_2 : Time in second thread. This was a testing button used to time how long point generation took when the generation occurred in the separate work thread

T_i : Time in main thread. This is the same function as T_2 with the exception that data generation occurred in the foreground

D_3 : Draw 3. This button like D_2 will draw a bitmap of the loaded CAD file. The difference is that this button uses the same code to generate patterns as the W_2 function and as such objects are drawn in packets. Thus this button must be clicked multiple times to finish drawing one entity.

A : Abort. Clicking this button will halt the writing process. Reading cannot be interrupted. Since the entire reading process only takes a few seconds (depending on image size), the ability to abort the reading process was not considered important.

 : Scale and offset. This button will configure the DAC output range of the hardware to the value currently specified in the open *.scp file

B : Test Board. This is a hardware tester function used for debugging purposes. It provides a convenient way to execute separate chunks of code. Currently it was used to test scale and offset code.

: Disconnect USB. This will sever a USB connection. It is necessary to do this manually quite often during debugging if the firmware and software lose syncronisation (for example, by resetting the microcontroller).

$\mathbf{B_A}$: Test Board A/D. This button is used to test ADC functionality on the board. Right now is actually does not interface with the current firmware, but uses a separate "tester" assembler block.

As can be seen from above, not only are the icons placeholders, but many of the testing and debug features have been left in. These are very useful in further expansion of functionality of the board and it is intended that future users will build on the code as it stands. For example, it would be a good idea to add zoom code, automatic alignment and calibration code and so forth to make the program truly feature-rich.

At the present moment, the code is fully functioning. It can write arbitrary pattern to the hardware, which will generate the desired patterns. In addition, it can grab images from the onboard ADC (in which case, the DACs will generate patterns to sweep the beam along the sample surface). Unpolished, and lacking some advanced features, the code is very much a prototype, "engineer's" build. Work on refining it and adding features was abandoned after it became apparent that this line of work would be scrapped.

B.7 Firmware

The firmware was written in assembler in MPLAB, Microchip's PIC development tool. The decision to use assembler was based on the fact that timing was quite crucial and it would be beneficial in addition to have the code execute as fast as possible. Because of the nature of assembly code, the program itself is a little confusing to follow and thus again the code itself will not be discussed here, only the basic functionality.

The firmware is essentially split into four sections: 1) a loop that downloads 'info' packets (called IDpackets internally) and stores them in the on-chip RAM, 2) a loop that downloads data points and clocks them into the DAC FIFO, 3) a loop that transmits ADC data to the PC and 4) a loop that generates point data for the DACs during reading (a sweep pattern) and feeds it to the DAC FIFOs. In addition, there are small sections of code to take care of such things as offset and scaling of the DAC output ranges and aborting the writing process.

All communication and synchronisation between PC and PIC is accomplished via ID packets and some initial handshaking. Upon startup, the PIC waits for a particular code from the PC and then sends 0xDC back to confirm communication. After this, the PC will send ID packets followed by large (59520 byte) packets of data to be written to the DAC. The ID packets are 11 bytes long and dictate the flow of the code. An ID packet ensures synchronisation and in addition tells the firmware: 1) whether to write data to the DACs, change the scale and offset, execute a read (grab an image from the SEM), or abort; 2) In the case of writes, how many data points are being transmitted in the next data packet and what the time interval is between points, 3) in the case of scaling and offsetting, the ID packets also contain the values to be written to the scale and offset DACs.

IDpackets are stored in a circular buffer in the onboard RAM. The code, for the most part, alternates between downloading an IDpacket from the PC, and then downloading the associated data points (raster data for the DACs). Once all the data points for an ID packet have been downloaded, a new ID packet is downloaded and so forth. A timer interrupt will periodically halt these loops to clock out the next data point from the FIFOs to the DACs.

When grabbing and image from the SEM (performing a read), a second 'info' packet is sent to the firmware detailing the image size and extent. After receiving this packet, the code similarly settles into two loops: one where data is dumped to the DACs to generate the reading pattern, and one that transmits data from the ADC FIFO to the PC. Again, the operation of these loops is punctuated periodically by timer interrupts which clock data in and out of the FIFOs.

B.8 Conclusion

The hardware and software created for the lithography aspect of this work are in perfect working order. It remains for somebody to fix the old JEOL JSM 35-C SEM and attach the hardware. The process of creating fine lines using e-beam lithography is well documented and with some practice and patience it could be simply achieved. This would make an incredibly useful tool for research in the Materials Science laboratory.

3 Bibliography

Adams,2004: Open access and useful index of various carbon nanotube properties. Accessible online at http://www.pa.msu.edu/cmp/csc/ntproperties/

Ahlskog, M., Seynaeve, E., Vullers, R. J. M., Van Haesendonck, C. 1999, "A microdeposition technique for carbon nanotubes based on electron beam lithography", *Journal of Applied Physics*, vol. 85, issue 12, pp. 8432-8435

Akimitsu, J. and Muranaka, T. 2003 "Superconductivity in MgB_2", *Physica C: Superconductivity*, vol. 388-389, pp. 98-102

Akinaga, M., Umeda, S., Hasegawa, H., Shirasawa, T. 2003 "A simple preparation of superconducting MgB2 thin films by composite—target sputtering system", *Physica C: Superconductivity*, vols. 388-389, pp. 119-120

Al-Shamma'a, A. I., Wylie, S. R., Lucas, J., Pau, C. F., 2001 "Design and construction of a 2.45 GHz waveguide-based microwave plasma jet at atmospheric pressure for material processing", *Journal of Physics D: Applied Physics*, vol. 34, pp. 2734-2741

Ames, 2004 "AMES LAB PHYSICISTS "PERTURB" SUPERCONDUCTOR TO NEW HEIGHTS", Press release on AMES website at http://www.external.ameslab.gov/news/release/2004rel/mgboride.htm last accessed on 7/12/2004

Andrews, R., Jacques, D., Rao, A.M., Derbyshire, F., Qian, D., Fan, X., Dickey, E.C., Chen, J. 1999 "Continuous production of aligned carbon nanotubes: a step closer to commercial realization", *Chemical Physics Letters,* vol. 303, pp. 467-474

Arepalli, S. 2004 "Laser Ablation Process for Single-Walled Carbon Nanotube Production", *Journal of Nanoscience and Nanotechnology,* vol. 4, no. 4, pp. 317-325

Azom, 2003, News article on recent work done at Los Alamos laboratory, accessible at http://www.azom.com/details.asp?ArticleID=2370 last accessed 8/12/2003

Ball, P. 2004 : News report on Materials Update. *Nature*, vol. 431, pp. 259. Accessible at http://www.nature.com/cgi-taf/Gateway.taf?g=3&file=/materials/nanozone/news/040916/journal/431259a.html&filetype=&_UserReference=

Barankova, H., and Bardos, L. 2000a, "Fused hollow cathode cold atmospheric plasma", *Applied Physics Letters*, vol. 76, no. 3, pp. 285-287

Barankova, H., and Bardos, L. 2000b, "Fused Hollow Cathode for Cold Atmospheric Plasma Processing", *Society of Vacuum Coaters*, 43rd Annual Conference Proceedings, pp. 113-115 Denver, April 15-20

Bardos, L., Barankova, H. and Berg, S., 1998 "PECVD by hollow cathodes", *Society of Vacuum Coaters*, 41st annual conference proceedings

Bednarska, V., Jackowska, I., Jastrzebski, W., Kowalczyk, P. 1996 "A three-section heat-pipe oven for heteronuclear alkali molecules", *Measurement Science and Technology*, vol. 7, pp. 1291-1293

Benito, A. M., Maniette, Y., MuGoza, E. Martinez, M. T. 1998 "Carbon Nanotubes production by catalytic pyrolysis of benzene", *Carbon,* vol. 36, no. 5-6, pp. 681-683

Berenov, A., Lockman, Z., Qi, X., MacManus-Driscoll, J. L., Bugoslavskya, Y., Cohen, L. F., Jo, M.H., Stelmashenko, N. A., Tsaneva, V. N., Kambara, M., Hari Babu, N., Cardwell, D. A., Blamire, M. G. 2001 "Growth of strongly biaxially aligned MgB2 thin films on

sapphire by postannealing of amorphous precursors", *Applied Physics Letters*, vol. 79, no. 24, pp. 4001-4003

Berkeley, 2003: Reported on Berkeley news, accessed online at http://www.berkeley.edu/news/media/releases/2003/07/23_motor.shtml on 30/11/2004

Bertoni, G., Cepek, C., Romanato, F., Casari, C., Bassi, A., Bottani, C., Sancrotti, M., 2004 "Growth of multi-wall and single-wall carbon nanotubes with in situ high vacuum catalyst deposition", *Carbon,* vol. 42, pp. 423-460

Bilgic, A.M., Prokisch, C., Broekaert, J.A.C., Voges, E. 1998 "Design and modelling of a modified 2.45 GHz coaxial plasma torch for atomic spectrometry", *Spectrochimica Acta*, Part B, vol. 53, pp. 773-777

Bolshakov, A.P., Uglov, S.A., Saveliev, A.V., Konov, V.I., Gorbunov, A.A., Pompe, W., Graff, A. 2002 "A novel CW laser–powder method of carbon single-wall nanotubes production", *Diamond and Related Materials,* vol. 11, issues 3-6, pp. 927-930

Boskovic, B., Stolojan, V., Khan, R., Haq, S., Ravi, S., Silva, P. 2002 "Large-area synthesis of carbon nanofibres at room temperature", *Nature Materials*, vol. 1, pp. 165-168

Bower, C., Suzuki, S., Tanigaki, K., Zhou, O. 1998 "Synthesis and structure of pristine and alkali-metal-intercalated single-walled carbon nanotubes", *Applied Physics A: Materials Science and Processing*, vol. 67, pp. 47-52

Bower, C., Zhu, W., Jin, S., Zhou, O. 2000 "Plasma-induced alignment of carbon nanotubes", *Applied Physics Letters,* vol. 77, no. 6, pp. 830-832

Braccini, V., Gurevich, A., Giencke, J.E., Jewell, M.C., Eom, C.B., Larbalestier, D.C., Pogrebnyakov, A., Cui, Y., Liu, B. T., Hu, Y. F., Redwing, J. M., Li, Q., Xi, X.X., Singh, R.K., Gandikota, R., Kim, J., Wilkens, B., Newman, N. Rowell, J. Moeckly, B., Ferrando, V., Tarantini, C., Marre, D., Putti, M., Ferdeghini, C., Vaglio, R., Haanappel, E. 2004 "High-field superconductivity in alloyed MgB2 thin films", available on arxiv.org, condensed matter at http://arxiv.org/abs/cond-mat/0402001

Brandenburg, J., and Kline, J. 1998 "Experimental investigation of large-volume PIA plasmas at atmospheric pressure", *IEEE Transactions on Plasma Science*, vol. 26, no. 2, pp. 145-149

Bretz, E. 2004 "Superconductors on the high seas", *Spectrum*, January 2004, pp. 53

Brinkman, A., Mijatovic, D., Hilgenkamp, H., Rijnders, G., Oomen, I., Veldhuis, D., Roesthuis, F., Rogalla,H. and Blank, D. 2003 "The road to magnesium diboride thin films, Josephson junctions and SQUIDs", *Superconductor Science and Technology*, vol. 16, pp. 246-253

Brooks, D. 2000 "Splitting planes for speed and power", *Printed Circuit Design*, December issue. Available online at http://www.ultracad.com/planesplits.pdf last accessed 15/12/2004

Bu, S. D., Kim, D. M., Choi, J. H., Giencke, J., Hellstrom, E. E., Larbalestier, D. C., Patnaik, S., Cooley, L., Eoma, C. B. 2002 "Synthesis and properties of c-axis oriented epitaxial MgB2 thin films", *Applied Physics Letters*, vol. 81, no. 10, pp. 1851-1853

Bud'ko, S., Lapertot, G., Petrovic, C., Cunningham, C., Anderson, N., Canfield, P., 2001 "Boron Isotope Effect in Superconducting MgB_2", *Physical Review Letters*, vol. 86, no. 9, pp. 1877-1880

Bunshah, R.F. (editor) 1994 "Handbook of deposition technologies for films and coatings: Science, Technology and Applications", 2nd Edition, Noyes Publications, New Jersey USA

Burnell, G., Kang, D. J., Lee, H. N., Moon, S. H., Oh, B., Blamire, M. G. 2001 "Planar Superconductor-Normal-Superconductor Josephson Junctions in MgB2", arxiv.org preprint cond-mat/0106562, available at http://arxiv.org/abs/cond-mat/0106562 last accessed 7/12/2004

Buzea, C. and Yamashita, T. 2001 "Review of Superconducting Properties of MgB2

Cadek M., Murphy R., McCarthy, B., Drury, A., Lahr, B., Barklie, R.C., in het Panhuis, M., Coleman, J.N., Blau, W.J. 2002, "Optimisation of the arc-discharge production of multi-walled carbon nanotubes", *Carbon,* vol. 40, pp. 923-928

Canfield, P. and Bud'ko, S. 2002 "Magnesium diboride: one year on", *Physics World*, January 2002, pp. 29-34, downloadable at http://cmp.ameslab.gov/personnel/canfield/pub/pw0201.pdf last accessed 10/12/2004

Canfield, P. C. , Finnemore, D. K., Bud'ko, S. L., Ostenson, J. E., Lapertot, G., Cunningham, C. E., Petrovic, C. 2001 "Superconductivity in Dense MgB2 Wires", *Physical Review Letters*, vol. 86, issue 11, pp. 2423-2426

Che, G., Lakshmi, B., Martin, C., Fisher, E., 1998 "Chemical Vapor Deposition Based Synthesis of Carbon Nanotubes and Nanofibers Using a Template Method", *Chemical of Materials,* vol. 10, pp. 260-267

Chen, Y., Wang, Z., Yin, J., Johnson, D., Prince, R. H. 1997 "Well-aligned graphitic nanofibers synthesized by plasma-assisted chemical vapor deposition", *Chemical Physics Letters*, vol. 272, pp. 178-182

Ci, L., Rao, Z., Zhou, Z., Tang, D., Yan, X., Liang, Y., Liu, D., Yuan, H., Zhou, W., Wang, G., Liu, W., Xie, S. 2002 "Double wall carbon nanotubes promoted by sulfur in a floating iron catalyst CVD system", *Chemical Physics Letters*, vol. 359, pp. 63-67

Ci, L., Wei, J., Wei, B., Liang, J., Xu, C., Wu, D. 2001 "Carbon nanofibers and single-walled carbon nanotubes prepared by the floating catalyst method", *Carbon,* vol. 39, pp. 329-335

Coetsee, D.C. and Jarvis, A.L.L 2003 "Decoupling in high speed 16-bit systems", *Elektron Journal*, September issue, pp. 25-27

Cui, H., Zhou, O., Stoner, B. R. 2000 "Deposition of aligned bamboo-like carbon nanotubes via microwave plasma enhanced chemical vapor deposition", *Journal of Applied Physics,* vol. 88, no. 10, pp. 6072-6074

Daenen, M., de Fouw, R.D., Hamers, B., Janssen, P., Schouteden, K., Veld, M., 2003, "The Wondrous World of Carbon Nanotubes", Interfaculty Project for Eindhoven University of Technology, Retrieved 23/8/2004 from http://students.chem.tue.nl/ifp03/Wondrous%20World%20of%20Carbon%20Nanotubes_Final.pdf

Dalton, A.B., Collins, S., Munoz, E., Razal, J., Ebron, V., Ferraris, J., Coleman, J., Kim, B., Baughman, R. 2003 "Super-tough carbon-nanotube fibres", *Nature*, vol. 423, pp. 703

Delzeit, L., McAninch, I., Cruden, B., Hash, D., Chen, B., Han, J., Meyyappan, M. 2002 "Growth of multiwall carbon nanotubes in an inductively coupled plasma reactor", *Journal of Applied Physics,* vol. 91, no. 9, pp. 6027-6033

Diamond, 2004: Information accessed on P1 Diamond's website at http://www.p1diamond.com/engine.html on 30/11/2004

Dijkkamp, D., Venkatesan, T., Wu, X. D., Shaheen, S. A., Jisrawi, N., Min-Lee, Y. H., McLean, W. L., Croft, M. 1987 "Preparation of Y-Ba-Cu oxide superconductor thin films using pulsed laser evaporation from high Tc bulk material", *Applied Physics Letters,* vol. 51, issue 8, pp. 619-621

Dresselhaus, M., Dresselhaus, G., Saito, R., 1995 "Physics of Carbon Nanotubes" *Carbon*, vol. 33, no. 7, pp. 883-891

Dresselhaus, M., Dresselhaus, G., Eklund, P., Saito, R., 1998 "Carbon Nanotubes", *Physicsweb,* January 1998, available at http://physicsweb.org/articles/world/11/1/9

Drewniak, J. L., Hubing, T. H., Van Doren, T. P., Baudendistal, P. 1994 "Modeling power bus decoupling on multilayer printed circuit boards," *IEEE Electromagnetic Compatibility Symposium Proceedings*, Chicago, IL, pp. 456-461

Duan, X., 1999, USA patent number 5,874,705

Dume, B. 2004 "Nanotube transistors speed up", physicsweb report at http://physicsweb.org/articles/news/8/4/15/1 last accessed 15/12/2004

Ebbesen T.W. and Ajayan, P.M. 1992, "Large-scale synthesis of carbon nanotubes", *Nature,* vol. 358,pp. 220–2

Eklund, P. C., Pradhan, B. K., Kim, U. J. and Xiong, Q. 2002 "Large-Scale Production of Single-Walled Carbon Nanotubes Using Ultrafast Pulses from a Free Electron Laser", *Nano Letters*, vol. 2, no. 6, pp. 561-566

El-Habachi, A., and Schoenbach, K., 1998 "Emission of excimer radiation from direct current, high-pressure hollow cathode discharges", *Applied Physics Letters*, vol. 72, no. 1, pp. 22-24

England, G. 2004 "Plasma Flame theory": website accessible at http://www.gordonengland.co.uk/xpft.htm last accessed 14/12/2004

Fan, J., Knighten, J., Orlandi, A., Smith, N., Drewniak, J. 2000 "Quantifying Decoupling Capacitor Location", *Proc. of the 2000 IEEE International Symposium on Electromagnetic Compatibility* Washington D.C., pp. 757-762

Fan, Z. Y., Hinks, D. G., Newman, N., Rowell, J. M. 2001 "Experimental study of MgB_2 decomposition", *Applied Physics Letters*, vol. 79, no. 1, pp. 87-89

Farhata, S., de La Chapelle, M., Loiseau, A., Scott, C., Lefrant, S., Journet, C., Bernier, P. 2001, "Diameter control of single-walled carbon nanotubes using argon–helium mixture gases", *Journal of Chemical Physics,* vol. 115 (14), pp. 6752-6759

Fennimore, A. M. , Yuzvinky, T. D., Han, W., Fuhrer, M. S., Cumings, J. and Zettl, A. 2003 "Rotational actuators based on carbon nanotubes", *Nature*, vol. 424, pp. 408-410

Ferdeghini, C., Ferrando, V., Grassano, G., Ramadan, W., Bellingeri, E., Braccini, V., Marre, D., Manfrinetti, P., Palenzona, A., Borgatti, F., Felici, R. Lee, T. L. 2001 "Growth of c-oriented MgB2 thin films by pulsed laser deposition: structural characterization and electronic anisotropy", *Superconducting Science and Technology*, vol. 14, pp. 952-957

Ferrando, V. Amoruso, S., Bellingeri, E., Bruzzese, R., Manfrinetti, P., Marre, D., Velotta, R., Wang, X., Ferdeghini, C. 2003 "Growth methods of *c*-axis oriented MgB2 thin films by pulsed laser deposition", *Superconducting Science and Technology*, vol. 16, pp. 241-245

Feynman, R. 1959, reported on *There's Plenty of Room at the Bottom,* retrieved on 27 October 2004 from http://www.zyvex.com/nanotech/feynman.html

FTDI, 2003: "Optimising data throughput over USB", AN232-03 available from FTDI

Fu, X.H., Wang , D.S., Zhang, Z.P., Yang, J. 2002 "Superconducting MgB2 thin films prepared by chemical vapor deposition from diborane", *Physica C: Superconductivity*, vol. 377, pp. 407-410

Gamaly, E.G., Rode, A.V., Maser, W.K., Munoz, E., Benito, A.M., Martinez, M.T., de la Fuente, G.F. 2000 "Single-walled carbon nanotubes formation with a continuous CO2-laser: experiments and theory", *Applied Physics A: Materials Science and Processing*, vol. 70, pp. 161-168

Grassano, G., Ramadan, W., Ferrando, V., Bellingeri, E., Marre, D., Ferdeghini, C., Grasso, G., Putti, M., Manfrinetti, P., Palenzona,A., Chincarini, A., 2001 "As-grown magnesium Diboride superconducting thin films deposited by pulsed laser deposition", *Superconducting Science and Technology*, vol. 14, pp. 762-764

Guay, P., Stansfield, B., Rochefort, A. 2004 "On the control of carbon nanostructures for hydrogen storage applications", *Carbon*, vol. 42, pp. 2187-2193

Guillard, T., Flamant, G., Laplaze, D., Robert, J., Rivoire, B., Giral, J. 2001 "Laser Ablation Process for Single-Walled Carbon Nanotube Production", *Proceeding of Solar Forum 2001: Solar Energy the Power to Choose*, April 2001, Washington DC

Guo, T., Nikolaev, P., Thess, A., Colbert, D.T., and Smalley, R.E., 1995 "Catalytic growth of single-walled nanotubes by laser vaporization", *Chemical Physics Letters,* vol. 243, pp. 49-54

Hadidi, K., Woskov, P. 1999, "Efficient, modular microwave plasma torch for thermal treatment", internal paper from MIT accessible at http://www.psfc.mit.edu/library/99ja/99ja008/99ja008_full.pdf last accessed on 04/12/2004

Hahn, J., Han, J., Yoo, J., Jung, H., Suh, J. 2004 "New continuous gas-phase synthesis of high purity carbon nanotubes by a thermal plasma jet", *Carbon,* vol. 42, pp. 877-883

Hamada, N., Sawada, S., Oshiyama, A., 1992 "New One-Dimensional Conductors: Graphitic Microtubules", *Physical Review Letters*, vol. 68, no. 10, pp. 1579-1581

Harbec, D., Meunier, J., Guol, L., Gauvin, R., Mallah, N. 2004 "Carbon nanotubes from the dissociation of C2Cl4 using a dc thermal plasma torch", *Journal of Physics D: Applied Physics*, vol. 37, pp. 2121-2126

Harris, S., Doll, G., Chance, D., Weiner, A., 1995 "A gas phase chemical etchant for boron nitride films", *Applied Physics Letters*, vol. 67, no. 16, pp. 2314-2317

Ho, G. W., Wee, A. T. S., Lin, J., Tjiu, W. C. 2001 "Synthesis of well-aligned multiwalled carbon nanotubes on Ni catalyst using radio frequency plasma-enhanced chemical vapor deposition", *Thin Solid Films*, vol. 388, pp. 73-77

Hofmann, S ., Kleinsorge, B., Ducati, C., Robertson, J., 2003 "Controlled low-temperature growth of carbon nanofibres by plasma deposition", *New Journal of Physics,* vol. 5, pp. 153.1-153.13

Hseuh, H., Tai, N., Perng, T., Chyou, S., 2003, "Fabrication and Characterisation of nanocomposites reinforced by carbon nanotubes – (1) Sythesis of Carbon nanotubes", *Key Engineering Materials*, vol. 249, pp. 65-68

Hsu, W.K., Terrones, M., Hare, J. P., Terrones, H., Kroto, H. W., Walton, D. R. M. 1996, "Electrolytic Formation of Carbon Nanostructures", *Chemical Physics Letters,* vol. 262, pp. 161-166

Hubert, J., Moisan, M., Richard, A. 1978 "A new microwave plasma at atmospheric pressure", *Spectrochimica Acta*, Part B, vol. 33, pp. 1-10

Hubing, T.H., Drewniak, J.L., Van Doren, T.P., Hockanson, D. 1995a "Power bus decoupling on multilayer printed circuit boards", *IEEE Transactions on Electromagnetic Compatability*, vol. 37, pp. 155-166

Hubing, T. H., Drewniak, J. L., Van Doren, T. P., Sha, F., Wilhelm, M. 1995b "An experimental investigation of 4-layer printed circuit board decoupling" *IEEE Electromagnetic Compatibility Symposium Proceedings*, Atlanta, GA, pp. 308-312,

Huczko, A. 2002 "Synthesis of aligned carbon nanotubes", *Applied Physics A: Materials Science and Processing*, vol. 74, pp. 617-638

Ijima, S. 1991, "Helical Microtubules of Graphitic Carbon", *Nature*, vol. 354, pp. 56-58

Intel, web – website giving overview of lithography at Intel http://www.intel.com/research/silicon/lithography.htm last accessed on 12/12/2004

Ishida, H., Satake, N., Jeong, G.H., Abe, Y., Hirata, T., Hatakeyama, R., Tohji, K., Motomiya, K. 2002 "Experimental study of fullerene-family formation using radio-frequency-discharge reactive plasmas", *Thin Solid Films,* vol. 407, issues 1-2, pp. 26-31

Jadhav, A.B. and Pawar, S.H. 2003 "Electrochemical synthesis of superconducting magnesium diboride films: a novel potential technique", *Superconducting Science and Technology*, vol. 16, pp. 752-759

Jeong, J. Y., Babayan, S. E., Tu, V. J., Park, J., Henins, I., Hicks, R. F., Selwyn, G. S. 1998 "Etching materials with an atmospheric-pressure plasma jet", *Plasma Sources Science and Technology*, vol. 7, pp. 282-285

Johnson, H., 2001 "Multiple ADC grounding", *EDN* magazine, available online at http://www.edn.com/article/CA61859.html last accessed 15/12/2001

Kalaugher, L. 2003. Reported on nanotechweb.org. Accessed at http://nanotechweb.org/articles/news/2/4/4/1 on 30/11/2004

Kalaugher, L. 2004. Reported on nanotechweb.org. Accessed at http://nanotechweb.org/articles/news/3/7/7/1 on 30/11/2004

Kang, W.N., Kim, H., Choi, E., Jung, C. U., Lee, S. 2001a "Epitaxial MgB2 superconducting thin films with a transition temperature of 39 Kelvin", cond-mat/ 0103179v2 available at http://arxiv.org/abs/cond-mat/0103179%20v2 last accessed on 8/12/2004

Kang, W. N., Kim, H., Choi, E., Jung, C. U., Lee, S. 2001b "MgB2 Superconducting Thin Films with a Transition Temperature of 39 Kelvin", *Science*, vol. 292, pp. 1521-1523

Kang, W. N., Kim, H., Choi, E., Kim, K., U., Lee, S. 2002 "Growth and transport properties of c-axis-oriented MgB2 thin films", *Physica C,* vols 378-381, pp. 1246-1251

Kester, W. "High Sped Operational Amplifiers", part of Analog devices "High Speed Design Techniques" series, available online at www.analog.com/UploadedFiles/Associated_Docs/527255193532939544363701451.pdf last accessed 16/12/2004

Kiang, C. 2000a "Growth of Large-Diameter Single-Walled Carbon Nanotubes", *Journal of Physical Chemistry A*, vol. 104, pp. 2454-2456

Kiang, C. 2000b "Carbon rings and cages in the growth of single-walled carbon nanotubes", *Journal of Chemical Physics,* vol. 113, no. 11, pp. 4763-4766

Kim M.S., Rodriguez N.M., Baker R.T.K, 1993 "The Interplay Between Sulfur Adsorption and Carbon Deposition on Cobalt Catalysts", *Journal of Catalysis,* vol. 143, issue 2, pp. 449-463

Kim M.S., Rodriguez N.M., Baker R.T.K. 1991, "The interaction of hydrocarbons with copper---nickel and nickel in the formation of carbon filaments", *Journal of Catalysis,* vol. 131, pp.60–73

Kim, M.R., Jung, S.H., Jeong, S.H., Kim, S.U., Lee, O.J., Lee, K.H., Suh, J.H., Park, C.K. 2003, "High-yield synthesis of multi-walled carbon nanotubes by arc discharge in liquid nitrogen", *Applied Physics A,* vol. 76, pp. 285-286

Kim, Y., Park, M., Yeltepe, E., Altay, A., 2002 "Weak Link Problem in MgB2 SIS Josephson Junctions", *American Physical Society*, Annual APS meeting, March 2002, Indiana, abstract #G14.007

Klages, C., Hopfner, K., Klake, N., Thyen, R., 2000 "Plasma-Assisted Deposition at Atmospheric Pressure Using Dielectric Barrier Discharges", *Society of Vacuum Coaters*, 43rd Annual Technical Conference Proceedings, Denver, April 15-20

Kumakura, H., Matsumoto, A., Fujii, H., Togano, K. 2001 "High transport critical current density obtained for powder-in-tube-processed MgB_2 tapes and wires using stainless steel and Cu–Ni tubes", *Applied Physics Letters,* vol. 79, issue 15, pp. 2435-2437

Laplaze, D., Bernier, P., Maser, W. K., Flamantt, G., Guillard, T., Loiseau, A. 1998 "Carbon Nanotubes: The Solar Approach", *Carbon,* vol. 36, pp. 685-688

Lee, C., Lyu, S., Kim, H., Park, C., Yang, C., 2002 "Large-scale production of aligned carbon nanotubes by the vapor phase growth method", *Chemical Physics Letters*, vol. 359, Issues 1-2, pp. 109-114

Lee, C., Park, J., Han, S. and Ihm, J. 2001, "Growth and field emission of carbon nanotubes on sodalime glass at 550°C using thermal chemical vapor deposition", *Chemical Physics Letters,* vol. 337, pp. 398-402

Lee, S., Ahn, J., Kim, Y., Moon, S., Lee, K., Kim, I., Park, Y., 2003 "Properties of MgB2 thin films made by radio frequency magnetron co-sputtering", *Superconducting Science and Technology,* vol. 16, pp. 1550-1553

Li, L., Kinloch, I., Windle, A., 2004 "Direct Spinning of Carbon Nanotube Fibers from Chemical Vapor Deposition Synthesis", *Science,* vol. 304, pp. 276-278

Li, W. Z., Wen, J.G., Ren, Z.F. 2001, "Effect of gas pressure on the growth and structure of carbon nanotubes by chemical vapor deposition", *Applied Physics A: Materials Science and Processing*, vol. 73, pp. 259-264

Li, W., Wen, J.G., Ren, Z.F. 2002, "Effect of temperature on growth and structure of carbon nanotubes by chemical vapor deposition", *Applied Physics A: Materials Science & Processing,* vol. 74, pp. 397-402

Li, X., Zhang, J., Li, H., Liu, Z. 2002 "Growth of Single-Walled Carbon nanotubes with Controlled Length and Diameter by Chemical Vapor Deposition", Presented at the 8th International Conference on Electronic Materials, China, 2002

Liddle, J.A., Harriott, L., Novembre, A.E., Waskiewicz, W.K., 1999, "SCALPEL: A projection electron beam approach to sub-optical lithpgraphy", White Paper on SCALPEL technology downloaded from http://www.bell-labs.com/project/SCALPEL/ available on attached CD

Liu, Y. and Song, X. 2002, "An electric arc furnace for producing carbon nanotube", Patent No. 01240373.3 2002 (China).

Liu, Z., Schlom, D., Li, Q. and Xi, X. X. 2001 "Thermodynamics of the Mg-B system: Implications for the deposition of MgB_2 thin films", *Applied Physics Letters*, vol. 78, no. 23, pp. 3678-3681

LRI, 2001: Website at Stellenbosch University describing use of heat pipe oven in laser spectroscopy: http://www.physics.sun.ac.za/lasers/institute/index last accessed 10/12/2004

Lupu, D., Biris, A.R., Jianu, A., Bunescu, C., Burkel, E., Indrea, E., Mihailescu, G., Pruneanu, S., Olenic, L., Misan, I., 2004 "Carbon nanostructures produced by CCVD with induction heating", *Carbon,* vol. 42, pp. 503-507

Madison, 2003: website of UW-Madison MRSEC, "Superconducting Magnesium Diboride Wire", available at http://mrsec.wisc.edu/nuggets/magnesium_diboride_wire.php last accessed on 7/12/2004

Malisa, A., Valkeapaa, M., Johansson, L.G., Ivanov, Z., 2004 "Josephson junctions fabricated by focused ion beam from ex situ grown MgB2 thin films", *Physica C: Superconductivity*, vol. 405, pp. 84-88

Maruyama, S., Kojima, R., Miyauchi, Y., Chiashi, S., Kohno, M., 2002 "Low-temperature synthesis of high-purity single-walled carbon nanotubes from alcohol", *Chemical Physics Letters*, vol. 360, no. 3-4, pp. 229-234

McBride, W. 2001, "Synthesis of Carbon Nanotubes by Chemical Vapor Deposition (CVD)", Thesis Submitted to College of William and Mary in Virginia, accessed at : http://physics.wm.edu/physicsnew/undergrad/2001/Will_McBride.pdf on 21/11/2004

Metaxas, A.C. and Meredith, R.J. 1983 *"Industrial Microwave heating"*, IEE Power Engineering Series 4, Peter Peregrinus Ltd., London UK

Meyyappan, M., Delzeit, L., Cassell, A. and Hash, D. 2003, "Carbon nanotube growth by PECVD: a review", *Plasma Sources Science and Technology,* vol. 12, pp. 205-216

Meyyappan, M., Delzeit, L., Cassell, A. and Hash, D., 2003 "Carbon nanotube growth by PECVD: a review", *Plasma Sources Science and Technology,* vol. 12, pp. 205-216

Mijatovic, D., 2004 "MgB_2 thin films and Josephson devices", PhD thesis submitted at the University of Twente, Enschede, The Netherlands

Mijatovic, D., Brinkman, A., Rijnders, G., Hilgenkamp,H., Rogalla, H., Blank, D. 2002 "Superconducting thin films of MgB2 by pulsed-laser deposition", *Physica C*, vols 372-376, pp. 1258-1261

Moisan, M., Sauve, G., Zakrzewski, Z., Hubert, J., 1994 "An atmospheric pressure waveguide-fed microwave plasma torch: the TIA design", *Plasma Sources Science and Technology*, vol. 3, pp. 584-592

Moon, S. H., Yun, J. H., Lee, H. N., Kye, J. I., Kim, H. G., Chung, W., Oh, B., 2001 "High critical current densities in superconducting MgB2 thin films", *Applied Physics Letters*, vol. 79, no. 15, pp. 2429-2431

Moon, S., Choe, W., Uhm, H., Hwang, Y.S., Choi, J.J. 2002 "Characteristics of an atmospheric microwave-induced plasma generated in ambient air by an argon discharge excited in an open-ended dielectric discharge tube", *Physics of Plasmas*, vol. 9, no. 9, pp. 4045-4051

Munoz, E., Maser, W.K., Benitol, A.M., Martinez, M.T., de la Fuente, G.F., Righi, A., Sauvajol, J.L., Anglaret, E., Maniette, Y., 2000, "Single-walled carbon nanotubes produced by cwCO2-laser ablation: study of parameters important for their formation", *Applied Physics A: Materials Science and Processing*, vol. 70, pp. 145-151

Nabity, website for NPGS e-beam lithography system at http://www.jcnabity.com/ last accessed 12/12/2004

Nagamatsu, J., Nakagawa, N., Muranaka, T., Zenitani, Y. and Akimitsu, J. 2001 "Superconductivity at 39K in magnesium Diboride", *Nature,* vol. 410, pp. 63-64

Naito, M., Ueda, K. 2004 "Growth and Properties of Superconducting MgB2 Thin Films", cond-mat/0402333 elecronic preprint available at http://arxiv.org/abs/cond-mat/0402333 last accessed 9/12/2004

Napartovich, A., 2001 "Overview of Atmospheric Pressure Discharges Producing Nonthermal Plasma", *Plasmas and Polymers*, vol. 6, nos. 1/2, pp. 1-14

Naudin, 2000: "How to build yourself a One Atmosphere Plasmoid", accessed at http://jnaudin.free.fr/html/oa_plasmoid.htm on 4/12/2004

Naudin, 2004: "Plasmoid (Ball Lightning) generation with microwaves: tests and analysis, web page accessed at http://jlnlabs.online.fr/plasma/gmrtst/ last on 5/12/2004

Nguyen, D. and Doan, Q. 2004 "Superconductivity in MgB2", Internal document available at http://garnet.acns.fsu.edu/~dnn9636/hw15.pdf last accessed on 6/12/2004

Nishiyama Y., Tamai Y. 1976 "Effect of hydrogen on carbon deposition catalyzed by copper-nickel alloys", *Journal of Catalysis*, vol. 45, issue 1, pp. 1-5

Ohkubo, H., Akinaga, M. 2004 "Fabrication of as-grown superconducting MgB2 thin films", *Physica C: Superconductivity*, vols. 408-410, pp. 898- 899

Okuno, H., Grivei,l E., Fabry, F., Gruenberger, T., Gonzalez-Aguilar, J., Palnichenko, A., Fulcheri, L., Probst, N., Charlier, J. 2004 "Synthesis of carbon nanotubes and nano-necklaces by thermal plasma process", *Carbon*, vol 42, pp. 2543-2549

Olk, C.H. 1998, U.S. Patent No. 5 753 088

Ott, H. 2000 "Transmission Line Rules of Thumb", available online at http://www.hottconsultants.com/techtips/rulesofthumb.html last accessed 15/12/2004

Ott, H. 2003 "Grounding of mixed signal PCBs", available online at http://www.hottconsultants.com/techtips/split-gnd-plane.html last accessed on 15/12/2004

Ott, H. 2004 *Tech tips* available online at http://www.hottconsultants.com/tips.html last accessed 15/12/2004

Pang L.S.K. and Wilson, M.A. 1993, "Nanotubes from Coal", *Energy and Fuels,* vol. 7, pp. 436-437

Paranthaman, M.P., Christen, D.K., Christen, H.M., Thompson, J.R., Kerchner, H.R., Cantoni C., Zhai, H.Y., 2001 "Growth of high current density MgB2 films using ex-situ precursor approach", *Physica C*: *Superconductivity*, vols 378-381, pp. 1252-1255

Pattavina, J. 1998 "Bypassing PC Boards: Thumb your nose at rules of thumb", *EDN*, (www.edn.com) October 22 issue

Pawar, S. H., Jadhav, A. B., Shirage, P. M., Shivagan, D. D. 2002 "Electrochemical synthesis of superconducting MgB2 thin films: a novel potential technique", cond-mat/0207406 preprint available on arxiv.org at http://arxiv.org/abs/cond-mat/0207406 last accessed at 8/12/2004

Peng, N., Shao, G., Jeynes, C., Webb, R. P., Gwilliam, R. M., Boudreault, G., Astill, D. M., Liang, W. Y., 2003 "Ion beam synthesis of superconducting MgB2 thin films", *Applied Physics Letters*, vol. 82, no. 2, pp. 236-238

Pierson, H., 1999 "Handbook of Chemical Vapour Deposition (CVD) : Principles, Technology and Applications", 2nd Edition, Noyes Publications, New Jersey, USA

Plecenik, A., Satrapinsky, L., Kus, P., Gazi, S., Benacka, S., Vavra, I., Kostic I. 2001 "MgB2 superconductor thin films on Si and Al2O3 substrates", cond-mat/0105612 preprint available online at http://arxiv.org/abs/cond-mat/0105612 last accessed 9/12/2004

Pogrebnyakova, A. V., Redwing, J. M., Jones, J. E., Xi, X. X., Xu, S. Y., Li, Q., Vaithyanathan, V., Schlom, D. G. 2003 "Thickness dependence of the properties of epitaxial MgB2 thin films grown by hybrid physical-chemical vapor deposition", *Applied Physics Letters*, vol. 84, no. 2, pp. 4319-4321

Popov, O. (Editor) 1995, *High Density Plasma Sources*: *Design, Physics and Performance,* Noyes Publications, New Jersey USA

Qin, L. C., Zhou, D., Krauss, A. R., Gruen, D. M. 1998 "Growing carbon nanotubes by microwave plasma-enhanced chemical vapor deposition", *Applied Physics Letters,* vol. 72, no. 26, pp. 3437-3439

Qiu J.S., Zhang F, Zhou Y, Han HM, Hu DS, Tsang SC, 2002, "Carbon nanomaterials from eleven caking coals", *Fuel,* vol. 81, pp.1509-1514

Qiu J.S., Zhao ZB, Wang TH, Wang YP, Li W. 2002b, "Bamboo-shaped carbon tubes from coal" *Chemical Physics Letters,* vol. 366, pp. 544-550

Qiu J.S., Zhou Y, Wang LN, Tsang SC, 1998 "Formation of carbon nanotubes and encapsulated nanoparticles from coals with moderate ash contents", *Carbon,* vol. 36(4), pp. 465-467

Qiu J.S., Zhou Y, Yang ZG, Wang DK, Guo SC, Tsang SC 2000, "Preparation of fullerenes using carbon rods manufactured from Chinese hard coals", *Fuel,* vol. 79, pp.1303-1308

Qiu, J.S., Li, Y., Wang, Y., Wang, T., Zhao, Z., Zhou, Y., Li, F., Cheng, H. 2003, "High-purity single-wall carbon nanotubes synthesized from coal by arc discharge", *Carbon,* vol. 41, pp. 2170-2173

Rai-Choudhury, P. (Editor) 1997 "Handbook of Microlithography, Micromachining, and Microfabrication, volume 1: Microlithography", *SPIE* publishers, also available online at http://www.nnf.cornell.edu/spiebook/toc.htm last accessed 15/12/2004

Raith, website of e-beam SEM conversion manufacturer available at http://www.raith.com/WWW_RAITH/nanolithography/nano_overview.html last accessed 12/12/2004

Reinke, P., and Oelhafen, P., Feldermann, H., Ronning, C., Hofsass, H. 2000 "Hydrogen-plasma etching of ion beam deposited c-BN films: An in situ investigation of the surface with electron spectroscopy", *Journal of Applied Physics*, vol. 88, no. 10, pp 5597-5603

Rembar, metals: Technical data on refractory metals available at http://www.rembar.com/tech2.htm last accessed 5/12/2004

Ren, Z. F., Huang, Z. P., Wang, D. Z., Wen, J. G., Xu, J. W., Wang, J. H., Calvet, L. E., Chen, J., Klemic, J. F., Reed, M. A. 1999 "Growth of a single reestanding multiwall carbon nanotube on each nanonickel dot", *Applied Physics Letters,* vol. 75, number 8, pp. 1086-1088

Rinaldi, F. 2002 "Basics of Molecular Beam Epitaxy", available online at http://www-opto.e-technik.uni-ulm.de/forschung/jahresbericht/2002/ar2002_fr.pdf last accessed 13/12/2004

Rossnagel, S., Cuomo, J., Westwood, W. (Editors) 1990, *"Handbook of plasma processing technology: Fundamentals, Etching, Deposition and Surface Interactions"*, Noyes Publications, New Jersey USA

Rowell, J., 2001 "A View of the Potential of MgB_2 in Superconducting Digital Electronics", comment on high Tc update available at http://www.iitap.iastate.edu/htcu/rowellcomment.html last accessed on 7/12/2004

Rowell, J., Xu, S. Y., Zeng, X. H., Pogrebnyakov, A. V., Li, Q., Xi, X. X., Redwing, J., Tian, W., and Pan, X., 2003 "Critical Current Density and Resistivity of MgB2 Films", available from arxiv.org cond-mat/0302017, online at http://arxiv.org/abs/cond-mat/0302017

Ruoff, R. and Lorents, C., 1995 "Mechanical and Thermal Properties of Carbon Nanotubes", *Carbon*, vol. 33, no. 7, pp. 925-930

Saito, A., Kawakami, A., Shimakage, H., Wang, Z., 2002 "As-grown MgB2 thin films deposited on Al2O3 substrates with different crystal planes", *Superconducting Science and Technology*, vol. 15, pp. 1325-1329

Saito, Y. and Uemura, S., 2000 "Field emission from carbon nanotubes and its application to electron sources", *Carbon,* vol. 38, pp. 169-182

Sano, N. 2004, "Separated syntheses of Gd-hybridized single-wall carbon nanohorns, single-wall nanotubes and multi-wall nanostructures by arc discharge in water with support of gas injection", *Carbon,* In Press

Sano, N., Nakano, J., Tatsuo, K. 2004, "Synthesis of single-walled carbon nanotubes with nanohorns by arc in liquid nitrogen", *Carbon,* vol. 42, pp. 667-691

Sarangi, D., Godon, C., Granier, A., Moalic, R., Goullet, A., Turban, G., Chauvet, O. 2001 "Carbon nanotubes and nanostructures grown fromdiamond-like carbon and polyethylene", *Applied Physics A: Materials Science and Processing*, vol. 73, pp. 765-768

Schewe, P., and Stein, B., 1996 reported on *Physics News Update*. Accessed online at: http://www.aip.org/enews/physnews/1996/split/pnu279-2.htm on 30/11/2004

Schewe, P., and Stein, B., 2004 reported on *Physics News Update*. Accessed online at: http://www.aip.org/pnu/2004/split/701-1.html

Schutze, A., Jeong, J., Babayan, S., Park, J., Selwyn, G., Hicks, R. 1998 "The Atmospheric-Pressure Plasma Jet: A Review and Comparison to Other Plasma Sources", *IEEE Transactions on plasma science*, vol. 26, no. 6, pp. 1685-1693

Scott, C.D., Arepalli, S., Nikolaev, P., Smalley, R.E. 2001 "Growth mechanisms for single-wall carbon nanotubes in a laser-ablation process", *Applied Physics A: Materials Science and Processing*, vol. 72, pp. 573-580

Seo, J. W., Couteau, E., Umek, P., Hernadi, K., Marcoux, P., Luki, B., Miko, C., Milas, M., Gaal, R., Forro, L., 2003, "Synthesis and manipulation of carbon nanotubes", *New Journal Of Physics,* vol. 5, 120.1-120.22

Shenton, M., and Stevens, G., 1999 "Investigating the effect of the thermal component of atmospheric plasmas on commodity polymers", *Thermochimica acta*, vol. 332, pp. 151-160

Shenton, M., Stevens, G., Wright, N., Duan, X., 2002 "Chemical-surface modification of polymers using atmospheric pressure nonequilibrium plasmas and comparisons with vacuum plasmas", *Journal of Polymer Science: Part A: Polymer Chemistry*, vol. 40, pp. 95-109

Shimakage, H., Saito, A., Kawakami,A., Wang, Z. 2003 "Optimizing preparation of as-grown MgB2 thin films made using the co-evaporation method", *Physica C: Superconductivity*, vols. 392-396, pp. 1291-1295

Shimakage, H., Saito, A., Kawakami,A., Wang, Z. 2004 "Fabrication condition dependence of as-grown MgB2 thin films by co-evaporation method", *Physica C: Superconductivity*, vols. 408-410, pp. 891-893

Singh, C. , Shaffer, M., Windle, A., 2002a, "Production of controlled architectures of aligned carbon nanotubes by an injection chemical vapour deposition method", *Carbon,* vol. 41, pp. 359-368

Singh, C., Quested, T., Boothroyd, C., Thomas, P., Kinloch, A., Abou-Kandil, A., Windle, A., 2002b "Synthesis and Characterization of Carbon Nanofibers Produced by the Floating Catalyst Method", *Journal of Physical Chemistry B,* vol. 106, pp. 10915-10922

Sinnott, S.B., Andrews, R., Qian, D., Rao, A.M., Mao, Z., Dickey, E.C., Derbyshire, F. 1999 "Model of carbon nanotube growth through chemical vapor deposition", *Chemical Physics Letters*, vol. 315, pp. 25-30

Smalley, R. E., Kroto H.W., Heath J.R., O'Brien S.C., Curl 1985 R.F., 'C60: Buckminsterfullerene,' *Nature,* 318, 162

Smiljanic, O.,, Stansfield, B.L., Dodelet, J.-P., Serventi, A., Desilets, S. 2002 "Gas-phase synthesis of SWNT by an atmospheric pressure plasma jet", *Chemical Physics Letters,* vol. 356, pp. 189-193

Smith, D. L., Anderson, R. E., Forehand, D. W., Pelc, T. J., Roy, T. 1999 "Power Distribution System Design Methodology and Capacitor Selection for Modern CMOS Technology", *IEEE Transactions on Advanced Packaging*, Volume 22, No. 3, pp. 284

Song, I., Yu, W., Cho, Y., Choi, G. and Kim, D. 2004, "The determining factors for the growth mode of carbon nanotubes in the chemical vapour deposition process", *Nanotechnology,* vol. 15, pp. S590–S595

Souma, S., Machida, Y., Sato T., Takahashi, T., Matsui, H., Wang, S.C., Ding, H., Kaminski, A., Campuzano, J.C., Sasaki, S., Kadowaki, K. 2004 "Direct observation of superconducting gaps in MgB2 by angle-resolved photoemission spectroscopy", *Physica C: Superconductivity*, vols. 408-410, pp. 102-103

SpaceDaily, 2004: Article accessed at http://www.spacedaily.com/news/nanotech-04o.html on 30/11/2004

Stark, R., and Schoenbach, K., 1999 "Direct current glowdischarges inatmospheric air", *Applied Physics Letters*, vol. 74, no. 25, pp. 3770-3772

Su, M., Zheng, B., Liu, J., 2000, "A scalable CVD method for the synthesis of single-walled carbon nanotubes with high catalyst productivity", *Chemical Physics Letters,* vol. 322, pp. 321-326

Sugai, T., Okazaki, T., Yoshida, H., Shinohara, H., 2004 "Syntheses of single- and double-wall carbon nanotubes by the HTPAD and HFCVD methods", *New Journal of Physics,* vol. 6, article 21

Tajima, S., Masui, T., Quilty , J., Lee, S., Yamamoto , A., Yamanaka, A., 2003 "Experimental study of electron–phonon interaction in MgB2", *Physica C: Superconductivity*, vols. 388-389, pp. 103-104

Tanaka, A., Yoon, S., Mochida, I., 2004 "Formation of fine Fe–Ni particles for the non-supported catalytic synthesis of uniform carbon nanofibers", *Carbon*, vol. 42, pp. 1291-1298

Tang, D.S., Xie, S.S., Liu, W., Chang, B.H., Sun, L.F., Liu, Z.Q., Wan, G., Zhou, W.Y. 2000, "Evidence for an open-ended nanotube growth model in arc Discharge", *Carbon,* vol. 38, pp. 480-483

Tang, Z. K., Zhang, L., Wang, N., Zhang, X. X., Wen, G. H., Li, G. D., Wang, J. N., Chan, C. T., Sheng, P. 2001 "Superconductivity in 4 Angstrom Single-Walled Carbon Nanotubes", *Science*, vol. 292, issue 5526, pp. 2462-2465

Tao, H.J., Li, Z.Z., Xuan, Y., Ren, Z.A., Che, G.C., Zhao, B.R., Zhao Z.X. 2003 "Josephson effects in MgB2 break junctions and MgB2/Nb point contacts", *Physica C: Superconductivity*, vol. 386, pp. 569-574

TechWorld, 2004: Article on NRAM accessed at http://www.techworld.com/storage/news/index.cfm?newsid=1846&page=1&pagepos=0 on 30/11/2004

Thess, A., Lee, R., Nikolaev, P., Dai, H., Petit, P., Robert, J., Xu, C., Lee, Y. H., Kim, S. G., Rinzler, A. G., Colbert, D. T., Scuseria, G. E., Tománek, D., Fischer, J. E., Smalley, R. E., 1996 "Crystalline Ropes of Metallic Carbon Nanotubes", *Science*, vol. 273, pp. 483-487

Thomas, R. 2001 "A Beginner's Guide to ICP-MS Part III: The Plasma Source", *Spectroscopy*, vol. 16, pp. 26-30, accessed online at http://www.spectroscopymag.com/spectroscopy/data/articlestandard/spectroscopy/452001/1096/article.pdf on 3/12/2004

TI, 1998 "Implications of Slow of Floating CMOS inputs", Document SCBA004C published by Texas instruments online at http://focus.ti.com/docs/apps/catalog/resources/appnoteabstract.jhtml?abstractName=scba004c last accessed 15/12/2004

TI, 1998b "AHC/AHCT designer's guide", TI design document SCLAO13D

Tian, Y., Zhang, Y., Wang, B., Ji, W., Zhang, Y., Xie, K., 2004 "Coal-derived carbon nanotubes by thermal plasma jet", *Carbon,* vol. 42, pp. 2597-2601

Timmermans, E., and can der Mullen, J., 2003 "Microwave induced plasma torches for on-line combustion gas analysis", *Spectroscopy Europe,* issue 15/5, pp. 14-21

Tsai, S. H., Chao, C. W., Lee, C. L., Shiha, H. C. 1999 "Bias-enhanced nucleation and growth of the aligned carbon nanotubes with open ends under microwave plasma synthesis", *Applied Physics Letters,* vol. 74, no. 23, pp. 3462-3464

Uchiyama, T., Koga, H., Iguchi, I., 2004 "Novel preparation method for superconducting magnesium-diboride thin films with high-Tc", *Physica C*, vols. 412-414, pp. 1362-1365

Ueda, K. and Naito, M. 2001 "As-grown superconducting MgB_2 thin films prepared by molecular beam epitaxy", *Applied Physics Letters*, vol. 29, no. 13

Ueda, K. and Naito, M. 2002 "Growth of Superconducting MgB_2 films", cond-mat/0203181 electronic preprint. Available at http://arxiv.org/abs/cond-mat/0203181 last accessed 9/12/2004

USC, 2004 : Vapor pressure data obtained on USC website at http://heliumclub.usc.edu/Refs/Vapor.htm last accessed 14/12/2004

van Erven, A. J. M, Kim, T. H., Muenzenberg, M., Mooderab, J. S., 2002 "Highly crystallized as-grown smooth and superconducting MgB2 films by molecular-beam epitaxy", *Applied Physics Letters,* vol. 81, no. 26, pp. 4982-4984

Venkatesan, T. and Green S., 1996 "Pulsed Laser Deposition: Thin Films in a Flash", *The Industrial Physicist,* vol. 2, no. 3

Vidal, C. R., and Hessel, M.M. 1972 "Heat-Pipe Oven for Homogeneous Mixtures of Saturated and Unsaturated Vapors: Application to NaLi", *Journal of Applied Physics,* vol. 43, pp. 2776-2780

Wang, S. F., Dai, S. Y., Zhou, Y. L., Chen, Z. H., Cui, D. F., Xu, J. D., He, M., Lu, H. B., Yang, G. Z., Fu, G. S., Han, L. 2001 "Superconducting MgB2 thin films grown by pulsed laser deposition on Al2O3(0001) and MgO(100) substrates", *Superconducting Science and Technology*, vol. 14, pp. 885-887

Wang, S., Zhou, Y., Zhu, Y., Liu, Z., Zhang, Q., Chen, Z., Lu, H., Dai, S., Yang, G., 2003 "Preparation and properties of MgB2 thin films on LaAlO3 substrates by chemical vapour deposition", *Superconducting Science and Technology*, vol. 16, pp. 748-751

Wang, X.B., Liu, Y.Q., Zhu, D.B. 2000 "Honeycomb-like alignments of carbon nanotubes synthesized by pyrolysis of a metal phthalocyanine", *Applied Physics A: Materials Science and Processing,* vol. 71, pp. 347-348

Wang, Y. , Kempa, K., Kimball, B., Carlson, J. B., Benham, G.,, Li, W. Z., Kempa, T., Rybczynski, J., Herczynski, A., Ren, Z. F., 2004 "Receiving and transmitting light-like radio waves: Antenna effect in arrays of aligned carbon nanotubes", *Applied Physics Letters,* vol. 85, issue 13, pp. 2607-2609

Wikipedia, Nanotubes: Data taken from online encyclopedia accessed at http://en.wikipedia.org/wiki/Carbon_nanotube on 30/11/2004

Wikipedia, Plasma : Information available from online encyclopedia accessed at http://en.wikipedia.org/wiki/Plasma on 3/12/2004

Williams K.A., Tachibana M., Allen J.L., Grigorian L., Cheng S.C., Fang S.L., Sumanasekera G.U., Loper A.L., Williams J.H., Eklund P.C. 1999, "Single-wall carbon nanotubes from coal", *Chemical Physics Letters,* vol. 310, pp.31-37

Wilson M.A., Patney H.K., Kalman J. 2002, "New developments in the formation of nanotubes from coal", *Fuel,* vol. 81(1), pp.5-14

Woskov, P., and Hadidi, K., 2002 "Large Electrodless Plasmas at Atmospheric Pressure Sustained by a Microwave Waveguide", *IEEE Transactions on Plasma Science*, vol. 30, issue 1, pp. 156-157

Xi, X. X., Zeng, X. H., Pogrebnyakov, A. V., Xu, S. Y., Li, Q., Zhong, Y., Brubaker, C. O., Liu, Z., Lysczek, E. M. J. M. Redwing, J. Lettieri, D. G. Schlom, W. Tian, and X. Q. Pan 2003 "*In Situ* Growth of MgB2 Thin Films by Hybrid Physical-Chemical Vapor Deposition", *IEEE Transactions on Applied Superconductivity,* vol. 13, no. 2, pp. 3233-3237

Xi, X. X., Zeng, X. H., Soukiassian, A., Jones, J., Hotchkiss, J., Zhong, Y., Brubaker, C. O., Liu, Z., Lettieri, J. Schlom, D. G., Hu, Y. F., Wertz, E., Li, Q., Tian, W., Sun, H. P., Pan, X. Q. 2002 "Thermodynamics and thin film deposition of MgB2 superconductors", *Superconducting Science and Technology*, vol. 15, pp. 451-457

Yakobson, B., and Smalley, R., 1997 "Fullerene Nanotubes: C1,000,000 and Beyond", *American Scientist,* July-August Issue, pp. 324-327

Yang K.L., Yang R.T. 1986 "The accelerating and retarding effects of hydrogen on carbon deposition on metal surfaces", *Carbon,* vol. 24, issue 6, pp. 687-693

Yudasaka, M., Kikuchi, R., Matsui, T., Ohki, Y., Yoshimura, S., 1995, "Specific conditions for Ni catalyzed carbon nanotube growth by chemical vapor deposition", *Applied Physics Letters,* vol 67, issue 17, pp. 2477-2479

Yudasaka, M., Komatsu, T., Ichihashi, T. and Iijima, S. 1997 "Single-wall Carbon nanotube formation by laser ablation using double-targets of carbon and metal", *Chemical Physics Letters,* vol. 278, issues 1-3, pp. 102-106

Zeng, X. H., Sukiasyan, A., Xi, X. X., Hu, Y. F., Wertz, E., Li, Q., Tian, W., Sun, H. P., Pan, X. Q., Lettieri, J., Schlom, D. G., Brubaker, C. O., Liu, Z., Li, Q. 2001 "Superconducting properties of nanocrystalline MgB2 thin films made by an in situannealing process", *Applied Physics Letters,* vol. 79, no. 12, pp. 1840-1842

Zeng, X., Pogrebnyakov, A., Kotcharov, A., Jones, J., Xi, X., Lysczek, E., Redwing, J., Xu, S., Li, Q., Lettieri, J., Schlom, D., Tian, W., Pan, X., Liu, Z. 2002 "In situ epitaxial MgB_2 thin films for superconducting electronics", *Nature Materials*, vol. 1, pp. 1-4

Zhang, W., Dekun, M., Jianwei, L., Lingfen, K., Weichao, Y., Yitai, Q. 2004, "Solvothermal synthesis of carbon nanotubes by metal oxide and ethanol at mild temperature", *Carbon,* vol. 42, issue 11, pp. 2341-2343

Zhang, W.D., Wen, Y., Tjiu1, W.C., Xu, G.Q., Gan, L.M. 2002, "Growth of vertically aligned carbon-nanotube array on large area of quartz plates by chemical vapor deposition", *Applied Physics A: Materials Science and Processing*, vol. 74, pp. 419-422

Zhao, T. and Liu, Y. 2004, "Large scale and high purity synthesis of single-walled carbon nanotubes by arc discharge at controlled temperatures", *Carbon,* vol. 42, pp. 2765-2768

Zhao, T. and Liu, Y. 2004, "Large scale and high purity synthesis of single-walled carbon nanotubes by arc discharge at controlled temperatures", *Carbon,* vol. 42, pp. 2765-2768

Zhao, Y., Ionescu, M., Pan, A., Dou, S., Collings, E. 2003 "In situ annealing of superconducting MgB2 films prepared by pulsed laser deposition", *Superconducting Science and Technology*, vol. 16, pp. 1487-1492

Zhao, Y., Ionescu, M., Horvat, J., Dou, S. X. 2003b "Comparative study of in situ and ex situ MgB2 films deposited by pulsed laser deposition", cond-mat/0311556 preprint available at http://arxiv.org/abs/cond-mat/0311556 last accessed on 9/12/2004

Zheng, B., Lu, C., Gu, G., Makarovski, A., Finkelstein, G. and Liu, J., 2002a, "Efficient CVD Growth of Single-Walled Carbon Nanotubes on Surface Using Carbon Monoxide Precursor", *Nano Letters*, vol. 2, issue 8, pp. 895-898

Zheng, B., Li, Y., Liu, J., 2002b "CVD synthesis and purification of single-walled carbon nanotubes on aerogel-supported catalyst", *Applied Physics A: Materials Science and Processing,* vol. 74, pp. 345-348

Zheng, G., Kouda, K., Sano, H., Uchiyama, Y., Shi, Y., Quan, H., 2004 "A model for the structure and growth of carbon nanofibers synthesized by the CVD method using nickel as a catalyst", *Carbon*, vol. 42, pp. 635-640

Zhu, H.W., Li, X.S., Jiang, B., Xu, C.L., Zhu, Y.F., Wu D.H., Chen, X.H. 2002, "Formation of carbon nanotubes in water by the electric-arc technique", *Chemical Physics Letters,* vol. 366, pp. 664-669